The Gran Sasso National Laboratory

The INFN Gran Sasso National Laboratory (LNGS) is the largest underground laboratory in the world for experiments in particle and astroparticle physics. It is one of the four INFN national laboratories and it is a worldwide facility used by scientists (presently 900 in number) from 24 countries.

Its location is near the town of L'Aquila, about 120 km from Rome. The underground facilities are located on a side of the ten kilometres long freeway tunnel crossing the Gran Sasso d'Italia Mountain. They consist of three large experimental halls, each about 100 m long, 20 m wide and 15 m high and service tunnels for a total volume of about 180,000 cubic metres.

The average 1400 m rock coverage gives a reduction factor of one million in the cosmic ray flux; moreover, the neutron flux is thousand times less than on the surface, thanks to the smallness of the Uranium and Thorium content of the dolomite rocks of the mountain.

The headquarters and the support facilities including the general electric and safety service, library and meeting halls, canteen, computing and networking services, mechanical, electronic and chemical shops, low radioactivity service, assembly halls, offices and administration department are located on the surface.

The mission of the Laboratory is to host experiments that require a low background environment in the field of astroparticle physics and nuclear astrophysics and other disciplines that can profit of its characteristics and of its infrastructures.

The geographical location (inside the National Park of Gran Sasso - Monti della Laga) and the special operating conditions (underground, near a highway tunnel and in close proximity to a large water basin) demand that special attention is paid to the safety and environmental aspects of the activities.

Main research topics of the present scientific programme are: neutrino physics with neutrinos naturally produced in the Sun and in Supernova explosion and neutrino oscillations with a beam from CERN (CNGS program), search for neutrino mass in neutrinoless double beta decays, dark matter search, nuclear reactions of astrophysical interest.
Let me summarize the activity of the main research lines in 2007.

A very important event characterising 2007 was the start of the data taking of the Borexino solar neutrino experiment. Solar neutrino physics is one of the traditional research sectors of the laboratory. After the glorious life of GALLEX and GNO, the focus is now on Borexino, which is dedicated mainly to the measurement of the Be line component of the solar neutrino spectrum. The experiment started the data taking in May.
One of the major commitments of the Gran Sasso laboratory in the next five years will be the search of τ neutrino appearance on the artificial μ neutrino beam built at CERN in Geneva, the CERN Neutrinos to Gran Sasso (CNGS) project. The beam, directed through the Earth crust to Gran Sasso at 732 km distance, started sending neutrinos in the summer of 2006 but its operation was seriously reduced in 2007.

The OPERA experiment is designed for the direct observation of τ neutrinos resulting from oscillations of the μ neutrino of the beam. This search requires both micrometer scale resolution, obtained with modern emulsion techniques and large (kton) sensitive mass obtained with 150,000 bricks consisting in Pb sheets interleaved by emulsion layers. In 2007 the production of the bricks with the brick assembly machine has continued.

ICARUS is a general-purpose detector, with a broad physics programme, based on the novel concept of the liquid Argon time-projection chamber. During 2007 the completion of the installation of the T600 in Hall B and of the needed infrastructure have continued intensely. The detector will be ready for operation in 2008.

The detection of low energy neutrinos from the gravitational collapse of galactic objects is the major purpose of the LVD (Large Volume Detector) experiment. The experiment is continuosly monitoring the galaxies with its 1000 tons of liquid scintillator and is able to detect the events induced by the CNGS neutrino beam. LVD participates to the Supernovae Early Warning System of detectors.

Elementary particles are different from their antiparticles because their charges - not only the electric one, but all of them - are opposite. The standard model assumes that neutrinos have only one charge, the lepton number. But, if this charge is not conserved, neutrinos and antineutrinos can be two states of the same particle. In this case well-specified nuclides would decay through the neutrino-less double beta channel. The Laboratory hosts today experiments searching for these very rare decays, employing different and complementary techniques, and is preparing new important activities.

CUORICINO, which employs TeO_2 bolometers for a total of 42 kg and started taking data data in 2003, has continuously operated in 2007. It is the most sensitive running experiment today.

In this field the Laboratory approved two new experiments representing the state of the art: GERDA planning to employ 500 kg of enriched ^{76}Ge, and CUORE bringing the CUORICINO technique to a mass of more than 400 kg of TeO_2 bolometers. The works for the installation of these experiments are in progress, and are already in the advanced installation phase for GERDA.

From astronomical observations, we know that most of the matter in the Universe is not made of nuclei and electrons as normal matter. It is called dark matter, because it does not emit light, and its nature is unknown. Its likely constituents, elementary particles that interact only very weakly with the rest (they are called WIMPs), have not been discovered yet. But maybe we are near. The search for WIMPs is very difficult and requires a very low background environment and the development of advanced background reduction techniques. The search is going on in many experiments worldwide. At Gran Sasso several experiments, using different techniques, are active and new experiments have been approved and started operating.

DAMA/LIBRA employs NaI crystals to detect the WIMPs by means of the flash of light produced in the detector by a Iodine nucleus recoiling after having been hit by a WIMP, a very rare phenomenon. To distinguish these events from the background, DAMA searches for an annual modulation of the rate, a behaviour that has several aspects that are peculiar of the searched effect and not of the main backgrounds. With its about 100 kg sensitive mass DAMA was the only experiment world wide sensitive to the annual modulation signature. After the conclusion of the experiment, results were published confirming a signal of annual modulation.

The larger experiment LIBRA, with 250 kg sensitive mass, started taking data in 2003 and continued regularly to take data along all the year 2007.

CRESST searches for WIMPs with a cryogenic technique, looking for a very tiny temperature increase in the detector, due to the energy deposited by nuclei hit by the WIMPs. Activity of the new CRESST2 $CaWO_2$ detector has continued.

Two new dark matter experiments, WARP and XENON are active underground. They are based on the simultaneous detection of the ionization and scintillation signals in, respectively,

liquid argon and liquid xenon. WARP and XENON performed interesting measurements underground with a 2.3 l and a 10 l prototype, respectively. In 2007 the WARP Collaboration started the installation of the 100 litres experiment and the Xenon Collaboration started the modification of their apparatus to host a 50 litres experiment.

The solar models are based on data and extrapolations; in particular the thermonuclear cross sections of the involved reactions are not measured in the relevant energy range but rather extrapolated from higher energies. The direct measurements are made very difficult by the very low values of the cross sections. Using the 400 kV accelerator, LUNA continued its activity for the measurements of the cross section of nuclear reaction of astrophysical interest.

The main activity of the theory group, staff and visitor scientists, has been focused on astroparticle physics, including solar and Supernova neutrinos, massive neutrinos, ultra high energy cosmic rays, topological defects and relativistic astrophysics. Important activity took place also in particle phenomenology and computer simulations of Lattice Field Theories.

Intense programs of Training and Outreach are being carried out in the last years. About the Outreach, let me put the emphasis here on the preparation activity during 2007 for the new Museum of Physics and Astrophysics in Teramo and on the continuation of the Gran Sasso–Princeton Summer School for Abruzzo Region secondary school students. About the Training, I want to mention the Agreement in 2007 between INFN-LNGS, Abruzzo Region and local firms giving twenty1-year fellowships to young graduate and undergraduate people of this region and the e-learning original training program set in motion by our Lab.

The Gran Sasso laboratory is recognized by Europe as a large scientific infrastructure. An EU contract is involving LNGS as one of the leader participants in the Integrated Infrastructure Initiative (I3) called ILIAS within Framework Program 6 (contract RII3-CT-2003-505818).

The main goal of ILIAS (Integrated Large Infrastructures for Astroparticle Physics) is to pull together all of Europe's leading infrastructures in Astroparticle Physics to produce a focused, coherent and integrated project to improve the existing infrastructures and their operation as well as to organise and structure the scientific community to prepare the best infrastructures for the future.

Gran Sasso, May 2008

The Director of the Laboratory
Prof. Eugenio Coccia

BOREXINO. Solar Neutrino Physics

G. Bellini[a], J. Benziger[c], S. Bonetti[a], R. Boraso[t], A. Brigatti[a], M. Buizza Avanzini[a],
B. Caccianiga[a], L. Cadonati[b], F.P. Calaprice[d], C. Carraro[i], A. Chavarria[d],
F. Dalnoki-Veress[d], D. D'Angelo[h], A. de Bellefono, E. de Haas[d], H. de Kerret[o], A. Derbin[m],
A. di Cienzo[b], G. di Pietro[a], A. Etenko[s], G. Fernandez[i], K. Fomenko[m], R. Ford[b], D. Franco[a],
C. Galbiati[d], S. Gazzana[b], M.G. Giammarchi[a], M. Goeger-Neff[h], A. Goretti[d], C. Grieb[n],
S. Hardy[n], G. Heusser[j], A. Ianni,[d], A.M. Ianni[c], M. Joyce[n], S. Kidner[n], V. Kobychev[b],
G. Korga[a], Y. Kozlov[s], D. Kryn[o], M. Laubenstein[b], M. Leung[d], T. Lewke[h], E. Litvinovich[s],
P. Lombardi[a], I. Machulin[s], W. Maneschg[j], G. Manuzio[i], F. Masetti[g], U. Mazzucato[g],
K. McCarty[d], Q. Meindl[h], E. Meroni[a], L. Miramonti[a], M. Misiaszek[q], D. Montanari[b],
V. Muratova[m], A. Nelson[d], Y. Nikitenko[s], S. Nisi[b], L. Oberauer[h], M. Obolensky[o],
M. Orsini[b], F. Ortica[g], M. Pallavicini[i], L. Papp[a], S. Parmeggiano[a], L. Perasso[a], S. Perasso[i],
A. Pocar[d], R.S. Raghavan[n], G. Ranucci[a], A. Razeto[i], P. Risso[i], A. Romani[g], A. Sabelnikov[s],
P. Saggese[a], C. Salvo[i], S. Schönert[j], H. Simgen[j], M. Skorokhvatov[s], O. Smirnov[m],
A. Sotnikov[m], S. Sukhotin[s], Y. Suvorov[s], V. Tarasenkov[s], R. Tartaglia,[b], G. Testera[i],
D. Vignaud[o], B. Vogelaar[n], F. von Feilitzsch[h], V. Vyrodov[s], B. Williams[n], J. Winter[h],
W. Wojcik[q], M. Wurm[h], S. Zavatarelli[i], O. Zaimidoroga[m], G. Zuzel[j]

[a]Dip. di Fisica dell'Università and Infn Milano - Italy
[b]Laboratori Nazionali del Gras Sasso, Assergi (Aq) - Italy
[c]Dept. of Chemical Engineering, Princeton University - NJ USA
[d]Dept. of Physics, Princeton University - NJ USA
[g]Dip. di Chimica dell'Università and Infn Perugia - Italy
[h]Technische Universität München - Germany
[i]Dip. di Fisica dell'Università and Infn Genova - Italy
[j]Max Planck Inst. für Kernphysik, Heidelberg - Germany
[m]J.I.N.R. Dubna - Russia
[n]Dept. of Physics, Virginia Polytechnic Institute - VA USA
[o]Laboratoire de Physique Corpusculaire et Cosmologie, Paris - France
[q]Institute of Physics, Jagellonian University, Kracov - Poland
[s]RRC Kurchatov Institute, Moscow - Russia
[t]Infn Ferrara - Italy

Abstract

Borexino is a solar neutrino detector fully operational in the Hall C of LNGS. The data taking with the complete detector has started in May 2007, leading during the course of last year to the first real time measurement of ^{7}Be solar neutrinos. We summarize here the status of the project and briefly outline the essentials of the Be-7 measurement performed in 2007. We also discuss the perspectives for future measurements.

1

1 Introduction

Solar neutrino physics is a topic that originally started from the perspective of studying the basic working principle of the core of the Sun, nuclear fusion reactions producing energy and emitting neutrinos.

The pioneer Davis experiment [1] was the first one to measure (with radiochemical methods) the neutrino solar flux as predicted by solar models and to detect a significant deficit in the predicted flux.

New experiments were performed starting from the end of the 80's, both in radiochemical mode [2, 3, 4] and in real-time mode [5, 6] while the most widely accepted model of the Sun evolved into what is now known as the Standard Solar Model [7].

As a general statement, the real-time experiments have been performed with large water Cerenkov detectors with an energy threshold of about 5 MeV, mainly due to natural radioactivity. This implies that only $\sim 0.001\%$ of the total neutrino flux has been observed in real time prior to 2007.

The issue of directly measuring low energy solar neutrinos has been the subject of an intensive research study carried out in the frame of the Borexino development and starting from the very beginning of the 90's. Borexino is a real time experiment to study low energy (sub-MeV) solar neutrinos [10] having as the main experimental goal the detection of the 0.862 MeV ^{7}Be solar neutrino line through the neutrino-electron elastic scattering reaction. The maximum energy of the recoiling electron is 664 KeV and the experimental design threshold is of 50 keV. The detection reaction is observed in a large mass (100 tons fiducial volume) of well shielded liquid scintillator.

The prediction of the ^{7} solar flux depends both on the Standard Solar Model and the value of the parameters of the LMA solution of neutrino oscillations [8] [9]. The Borexino experimental program makes it possible to specifically test this prediction in a direct way as well as opening up the unexplored territory of real time sub-MeV solar neutrino spectroscopy.

The main problem of a real time experiment with such a low energy threshold is the background coming from natural sources such as cosmic rays or radioactivity.

This problem has been addressed by means of an intense R&D program carried out in the last ten years to develop methods for selecting low radioactivity materials and/or purify them. An effort in this field has to be complemented by a comparably thorough research in the field of detection and measurement of very low radioactivity levels [11].

As a part of this program, a prototype of the Borexino detector, called Counting Test Facility [12], was built and operated at LNGS to demonstrate very low radioactive contamination levels (10^{-16} g/g of U-238 equivalent or less [13]) in a ton scale scintillator detector.

These research and development culminated into the construction, filling and operation of the Borexino detector that has performed, during year 2007, the first real time measurement of solar ^{7}Be neutrinos.

2 The Borexino Detector

Borexino is an unsegmented scintillation detector featuring 300 tonnes of well shielded liquid ultrapure scintillator viewed by 2200 photomultipliers (fig. 1). The detector core is a transparent spherical vessel (Nylon Sphere, $100\mu m$ thick), 8.5 m of diameter, filled with 300 tonnes of liquid scintillator and surrounded by 1000 tonnes of high-purity buffer liquid. The scintillator mixture is PC and PPO (1.5 g/l) as a fluor, while the buffer liquid will be PC alone (with the addition of DMP as light quencher). The photomultipliers are supported by a Stainless Steel Sphere, which also separates the inner part of the detector from the external shielding, provided by 2400 tonnes of pure water (water buffer).

An additional containment vessel (Nylon film Radon barrier) is interposed between the Scintillator Nylon Sphere and the photomultipliers, with the goal of reducing Radon diffusion towards the internal part of the detector.

The outer water shield is instrumented with 200 outward-pointing photomultipliers serving as a veto for penetrating muons, the only significant remaining cosmic ray background at the Gran Sasso depth (about 3500 meters of water equivalent). The innermost 2200 photomultipliers are divided into a set of 1800 photomultipliers equipped with light cones (so that they see light only from the Nylon Sphere region) and a set of 400 PMT's without light cones, sensitive to light originated in the whole Stainless Steel Sphere volume. This design greatly increases the capability of the system to identify muons crossing the PC buffer (and not the scintillator).

The BOREXINO design is based on the concept of a graded shield of progressively lower intrinsic radioactivity as one approaches the sensitive volume of the detector; this culminates in the use of 200 tonnes of the low background scintillator to shield the 100 tonnes innermost Fiducial Volume. In these conditions, the ultimate background will be dominated by the intrinsic contamination of the scintillator, while all backgrounds from the construction materials and external shieldings will be negligible.

BOREXINO also features several external systems and conceived to purify the experimental fluids (water, nitrogen and scintillator) used by the experiment.

3 Status of the project

The Borexino filling started in January 2007, with scintillator displacing the purified water from inside the detector volumes. Data taking started and the detector was completely filled and operational by May 2007.

The radiopurity of the detector has been found in general to be better than the specifications, as roughly detailed in the following list:

1. C-14 contamination of the scintillator was found to be at $\sim 2 \times 10^{-18}$ $^{14}C/^{12}C$ which is a value well within specification.

2. The general level of Th-232 contamination - as measured by means of $^{212}Bi/^{212}Po$ delayed coincidences was found to be at $\sim 6 \times 10^{-18}$ g/g.

3. The U-238 family contamination - assessed by studying the $^{214}Bi/^{214}Po$ delayed coincidence rate, was measured to be less than 7×10^{-18} g/g.

4. Kr-85 contamination, of considerable importance due to the spectral shape similar to the one of the signal searched for was found (by means of the ^{85m}Rb decay and the related β/γ tagging) to be at the tolerable level of less than 35 count/day in the 100 tons fiducial volume.

This general level of radiopurity, together with the use of mild cuts and the α/β discrimination technique has allowed a sensitive study of the Be-7 solar signal inside the 100 tons of fiducial volume.

The result of this study, published at the end of 2007, concerns the first 47 days of data taking of the detector.

4   Measurement of Be-7 solar neutrino component

While we refer the interested reader to the published paper for the description of the analysis, fig. 2 shows an illustrative spectrum of the singles rate obtained after mild cuts (including veto of external muons and Rn activity) in the Borexino fiducial volume of 100 tons.

The main background component in the observed spectrum is the ^{210}Po alpha peak at ~ 420 keV of equivalent energy. This background is out of equilibrium with respect to the ^{222}Rn decay sequence. It amounts to ~ 60 counts/day/ton and appears to be decaying away with the expected lifetime.

The presence of this background does not prevent the possibility of fitting the recoil spectrum (Compton-like shoulder) of electron coming from B-7 neutrinos through the reaction $\nu e^- \rightarrow \nu e^-$. This feature is clearly visible in fig. 2 where also the other main fit components are shown.

The published measurement of $47 \pm 7_{stat} \pm 12_{syst}$ counts/(day·100 ton) has to be compared to the expected Standard Solar Model without oscillations of 75 ± 4 or to the expected number of 49 ± 4 when LMA oscillations of solar neutrinos are taken into account [9].

5   Future perspectives

The Borexino experimental program is continuing with the short-term goal of improving the understanding of the detector and reducing the error on the Be-7 measurement (dominated by the knowledge of the fiducial volume mass, a systematic error).

In addition, the following additional physics topics are being considered for the future investigation, depending on the background conditions and on the refinement of the ongoing analysis:

1. Reduce the background in the region above the Be-7 shoulder, to the goal of measuring the CNO solar neutrinos and possibly the pep component as well.

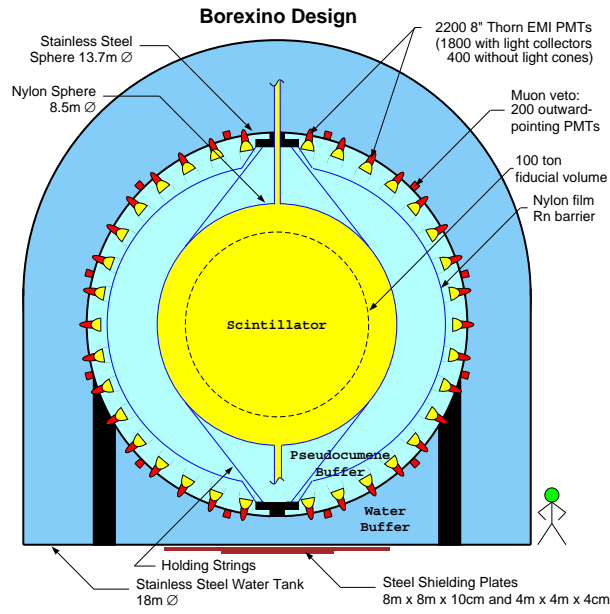2. Search for terrestrial antineutrino interactions

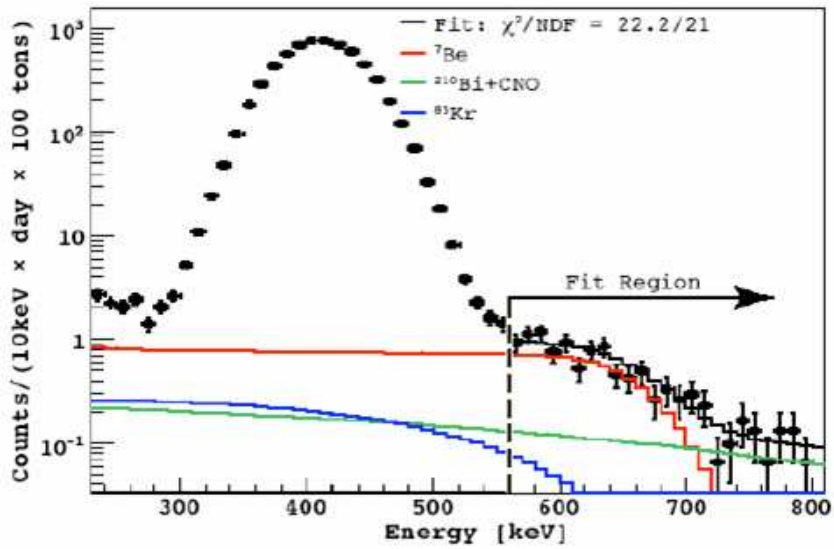Figure 1: Schematic view of the Borexino detector.

Figure 2: The observed Borexino spectrum after mild cuts, showing the shoulder due to solar Be-7 neutrino events (red line). The other main fit components in this energy region are also shown. The copious peak at the left of the Be-7 shoulder is due to quenched Po-210 alphas.

3. Study the very low energy part of the spectrum to the goal of looking for pp neutrinos.

4. Watch for neutrino bursts from Supernovae events

In addition, neutrino source calibrations (with a ^{51}Cr source) are being considered, both to the goal of a final calibration and to the study of neutrino magnetic moment.

6   List of articles published in year 2007

1. C. Arpesella et al., *First real time detection of ^{7}Be solar neutrinos by Borexino*, Accepted for publication on Phys. Lett. B. Also, arXiv:0708.2251v2.

References

[1] R. Davis, Nobel Prize Lecture 2002.

[2] W. Hampel et al., Phys. Lett. B 447 (1999) 127.

[3] J.N. Abdurashitov et al., Phys. Rev. Lett. 83 (1999) 4686.

[4] M. Altmann et al., Phys. Lett. B 616 (2005) 174.

[5] S. Fukuda et al., Phys. Rev. Lett. 86 (2001) 5651; Phys. Lett. B 539 (2002) 179.

[6] Q.R. Ahmad et al., Phys. Rev. Lett. 87 (2001) 071301.

[7] J.N. Bahcall and M.H. Pinsonneault, Phys. Rev. Lett. 92 (2004) 121301.

[8] J.N. Bahcall et al., JHEP 0408 (2004) 016.

[9] G.L. Fogli et al., Progr. Nucl. Phys., 57 (2006) 742.

[10] G. Alimonti et al., Astroparticle Physics 16 (2002) 205.

[11] C. Arpesella et al., Astroparticle Physics 18 (2002) 1.

[12] G. Alimonti et al., Nucl. Instr, & Methods A406 (1998) 411.

[13] G. Alimonti et al., Astroparticle Physics 8 (1998) 141.

COBRA

T. Bloxham[a], V. Bocarov[b], A. Boston[c], P. Cermak[b], O. Civitarese[d], J.V. Dawson[e],
N. Devenish[e], S.P. Fox[f], M. Freer[a], B. Fulton[f], C. Gößling[g], P.F. Harrison[h], M. Junker[i],
T. Köttig[g], H. Krawczynski[j], Q. Li[j], J. McGrath[f], B. Morgan[h], D. Münstermann[g],
P. Nolan[c], S. Oehl[g], S. Rajek[g], Y. Ramachers[h], C. Reeve[e], O. Schulz[g], F. Simkovic[k],
I. Stekl[b], D. Stewart[h], J. Suhonen[l], R. Wadsworth[f], J.R. Wilson[e], K. Zuber[e,*]

[a] *University of Birmingham*- UK
[b] *Technical University of Prague*- Czech Republic
[c] *University of Liverpool* - UK
[d] *University of La Plata*- Argentina
[e] *University of Sussex*- UK
[f] *University of York*- UK
[g] *Universität Dortmund*- Germany
[h] *University of Warwick*- UK
[i] *Laboratori Nazionali del Gran Sasso* - Italy
[j] *Washington University in St. Louis*- USA
[k] *University of Bratislava*- Slovakia
[l] *University of Jyvaskyla*- Finnland
(* Spokesperson)

Abstract

The aim of COBRA is to search for neutrino-less double beta decay events in
a large array of Cadmium Zinc Telluride (CZT) semiconductor detectors. As a
semiconductor, CZT offers the low radioactivity levels and good energy resolution
required for a rare decay search, with the added advantage that it can be operated
at room temperature. It contains a number of double beta decay candidates, the
most promising of which is ^{116}Cd, which has a high Q-value (2.8 MeV) above many
of the possible background contributions from natural radioactivity. Currently, a
proto-type apparatus consisting out of 64 detectors is being established in LNGS to
investigate the major experimental issues of operating CZT detectors in low back-
ground mode, whilst additional studies into the detector technology are proceeding
in surface laboratories.

1 Introduction

Over the last 10 years various neutrino experiments have proved that neutrinos oscillate between flavour states and therefore have a non-vanishing rest mass. However, as neutrino oscillation experiments probe the difference between neutrino mass states, the absolute mass scale is still unknown. Another important unknown is the fundamental nature of the neutrino which could be either Dirac or Majorana. A golden channel for answering both the question of neutrino nature and neutrino mass is neutrinoless double beta decay. The COBRA experiment aims to provide answers to these fundamental questions by searching for these rare decays of ^{116}Cd isotopes in a large array of Cadmium Zinc Telluride (CZT) semiconductor detectors. An extensive discussion of the double beta decay modes detectable with COBRA is given in the LNGS Annual Report 2006.

2 COBRA

The idea of COBRA is to use a large quantity of CdZnTe (CZT) semiconductor material which contains a number of isotopes that can undergo double beta decay[1]. The main focus will be on ^{116}Cd and ^{130}Te, which are well suited for a double beta search due to their high Q-values (2809 and 2529 keV respectively). Calculations show that the theoretical rates of $0\nu\beta\beta$–decay for ^{116}Cd and ^{130}Te are favourably high. First shell model calculations for nuclei heavier than ^{48}Ca make ^{116}Cd the most sensitive isotope from the theoretical point of view [2].

COBRA follows the strategy that source and detector are identical, a method proven to be successful in various other double beta decay approaches. As a semiconductor, CZT crystals can be produced with good energy resolution and low levels of intrinsic radioactivity. Due to a large bandgap the detectors can be operated at room temperature avoiding extensive cooling operations. More details can be found in the LNGS Annual Report 2006.

3 R&D Activities

The experiment is currently in an R&D phase, operating a proto-type low-background apparatus in the LNGS laboratory in order to investigate the instrumentation and background issues critical to the rare decay search. Studies into detector properties, especially pixelated CZT detectors, are being performed simultaneously at a number of member institutions. Details of the experimental set-up and recent progress are given in this section.

3.1 Low Background Proto-type

A proto-type COBRA detector, consisting of 64 1 cm^3 CZT crystals is being installed in LNGS. This small array will provide valuable information on the background levels of various components of the set-up and will be used to test methods of instrumentation and construction that would also be applicable to a larger array. It will also allow studies

using coincidences among the detector and its potential to reduce background, as double beta decay is considered to be a single detector event.

The crystals currently used in the low background experiment are $1\,cm \times 1\,cm \times 1\,cm$ CZT semiconductor detectors, each of mass $\sim 6.5\,g$, provided by eV-PRODUCTS. The detectors are mounted in four 4×4 layers, held in a Delrin support. The first layer of 16 detectors operating since april 2006 is surrounded by $10\,cm$ of pure copper shielding and $20\,cm$ of low radioactivity lead. Supply of bias voltages, and signal readout occurs via copper traces on kapton foils which feed through this shielding. The custom built preamplifier electronics are $\sim 25\,cm$ from the crystals. This apparatus is all mounted inside a copper Faraday cage, surrounded by $5\,cm$ of polypropylene and $20\,cm$ of borated paraffin to shield the apparatus from neutrons. Location in the Gran Sasso laboratory provides a further $\sim 3500\,mwe$ of shielding against cosmic ray sources. The setup was moved in spring 2007 within LNGS into a more convenient location between hall A and B.

Physics results based on the 4 detector array used before with an exposure of 4.34 kg days have been published in [3]. With the first layer of 16 detectors more than 12 kg days of data have been accumulated. A sum spectrum of all detectors is shown in Fig. 1. Besides the shoulder at low energy coming from the 4-fold forbidden non-unique beta decay of ^{113}Cd two lines at 351 and 609 keV can be seen. They result from the red passivation paint on the surface of the detectors and the radon in the air. A background model containing the paint contaminations, radon and the ^{113}Cd describes the observed spectrum pretty well (Fig. 2). The radon contents could be estimated by running 4 detectors with an colourless passivation, which has three orders of magnitude less contaminations and hence are dominated by the radon contribution.
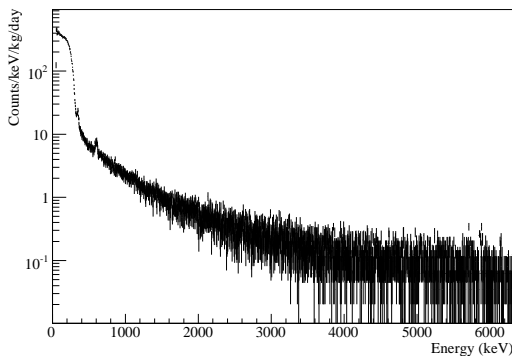

Figure 1: Sum spectrum of the first layer with an exposure of 11.9 kg days. Besides the low energy shoulder of ^{113}Cd beta decay two lines at 351 and 609 keV are visible.
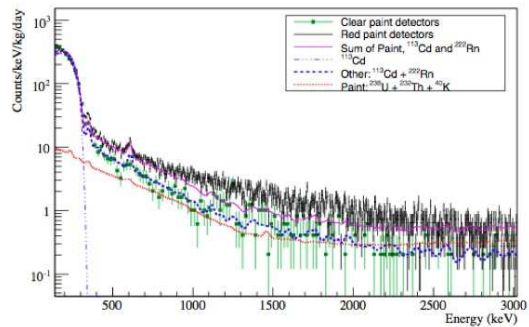

Figure 2: Simulated background model consisting of ^{113}Cd, red passivation paint and radon. Shown are the data from the first layer and the one from the colourless detectors (green).

3.2 Analysis

A total of 7.9 kg·days out of more than 12 kg·days of data were analysed with the first layer of 16 detectors.

3.2.1 $\beta\beta$-Decay Half-life Limits

A search was performed for rare decays of all the double beta candidate isotopes in CdZnTe that produce peaks above 600 keV. A maximum likelihood analysis was used to determine the most likely number of signal and background events in the data sample, taking into account variations in background levels and resolution functions between the different crystals and data-collecting periods. An exponential parameterisation of the form,

$$y = A + B\exp(-C.x) \tag{1}$$

was selected to describe the background based on studies of the simulated background components.

The 90% upper confidence limit on half-life is derived from the fitted number of signal events, $\theta_s \pm \delta_s$:

$$T_{\text{half}} \geq \frac{N_{\text{iso}} \ln 2\epsilon}{\theta_s + 1.28\delta_s} \tag{2}$$

where N_{iso} is the number of candidate nuclei for the given decay per crystal and ϵ is the efficiency for observing the peak, as determined from Monte Carlo simulations of the decay in question. The factor 1.28 is for one-sided 90% confidence limits.

A limit calculated with equation 2 only includes the statistical uncertainty from the likelihood fit. A comprehensive review of possible systematic effects identified two dominant uncertainties. An uncertainty in the size of the active volume of each crystal could be as much as 10% and the zinc content in the CdZnTe material could vary between 7 and 11%.[1] Therefore, to account for these possible systematic effects the limiting parameters which give the least candidate isotopes for each decay were used in calculating the half-life limits.[2]

Where possible, each conceivable signal peak was fitted separately, however, in some cases the proximity of peak energies required multiple peaks to be treated together in the likelihood function.

For each double beta fit performed, the fitted number of events was found to be consistent with zero. Therefore, the 90% C.L. upper limit on the number of signal events was used to calculate a minimum half-life for each decay process. A comparison of the new preliminary results with the one published in [3] is summarised in table 1. Note that new world-best limits are achieved for the neutrinoless double electron captures decays of ^{64}Zn and ^{106}Cd.

---

[1]These are conservative limits provided by eV-PRODUCTS.

[2]Work is underway to measure both the zinc content and crystal active volumes more accurately in the near future.

Isotope	Decay	T$_{1/2}$ limit (years)	
		4-detector	First layer
$\beta^-\beta^-$ decays			
^{116}Cd	to g.s	3.14×10^{19}	6.05×10^{20}
^{130}Te	to g.s	9.92×10^{19}	3.44×10^{20}
^{130}Te	to 536 keV	3.73×10^{19}	2.49×10^{20}
^{116}Cd	to 1294 keV	4.92×10^{18}	2.8×10^{19}
^{116}Cd	to 1757 keV	9.13×10^{18}	3.03×10^{19}
^{114}Cd	to g.s	-	4.71×10^{20}
$\beta^+\beta^+$ decays			
^{64}Zn	$0\nu\beta^+$EC to g.s.	2.78×10^{17}	1.18×10^{18}
^{64}Zn	0νECEC to g.s.	1.19×10^{17}	**7.43×10^{18}**
^{120}Te	0νECEC to g.s.	2.68×10^{15}	1.13×10^{17}
^{120}Te	0νECEC to 1171keV	9.72×10^{15}	3.43×10^{16}
^{106}Cd	$0\nu\beta^+\beta^+$ to g.s.	4.50×10^{17}	5.48×10^{18}
^{106}Cd	0νECEC to g.s.	5.70×10^{16}	**5.48×10^{18}**
^{106}Cd	$0\nu\beta^+\beta^+$ to 512keV	1.81×10^{17}	7.17×10^{17}

Table 1: Comparison of obtained 90% confidence limits with the original prototype of 4 detectors as published in [3] together with preliminary limits from the first layer of the 64 array. New world best values from COBRA are shown in bold.

3.3 Pixellated Detector Studies

The development of pixellated detectors offers the possibility for enhancing the performance of COBRA in two key areas; (i) background suppression, and (ii) providing a unique signal for double beta-decay. It is the different characters of beta, alpha and gamma-radiation compared to that of double beta decay, within the CZT material, which provides the potential for event identification. For example, an electron of energy 1.4 MeV (half of the Q-value of ^{116}Cd) will travel 1–1.5 mm in CZT, whilst an alpha of a similar energy has a range of only $\sim$15 μm. A detector with pixellization of the order of 200 μm would yield a sample of 5–10 points along the track of the electrons (Fig. 3), but the alpha-decay would be largely confined to single-pixel. In this way, combined with timing criteria, pixellization would allow the elimination of all background processes which precede, or follow, alpha decay. This includes many of the beta-decay components of the natural thorium and uranium chains which can be problematic for low-background experiments. Simulations of the response of a 200 μm pixel detector indicate that it is possible to suppress such background by almost three orders of magnitude[4].

Further background reduction can be achieved by discriminating against events in which non-adjacent pixels are activated. This occurs for Compton scattering of gamma-rays, or pair-production where the produced gamma-rays propagate through the crystal, where they re-interact.

The second strand is that it is highly desirable to uniquely identify the double-beta decay as opposed to the single beta events, or high energy electrons from photoelectric

gamma-ray interactions. This provides a signal enhancement which potentially via track reconstruction could permit the characteristics of the decay process to be determined, e.g. angular distributions, etc. The present simulations indicate that the distributions of the single and double-electron events are characteristically different and these may be used to substantially enhance the sensitivity to the decay mode of interest. The present simulations suggest that for a $200\,\mu$m pixel detector it is possible to uniquely identify double-beta events (as opposed to single electrons) with a 70% efficiency.

While two detectors with 16 pixels (conventional electronics) and 256 pixels (ASIC readout) have been operated at surface, activities have been spent to reduce the pixel size. In this way a 2x2x0.5 cm^3 detector was built with 1024 pixels, resulting in a pixel size of 625 μm (Fig. 4).
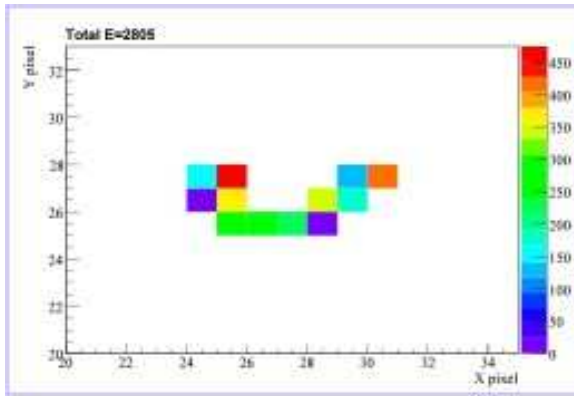

Figure 3: Simulated double beta decay event. The double beta decay occured in the middle. The colour coding describes the energy deposition in the pixels.
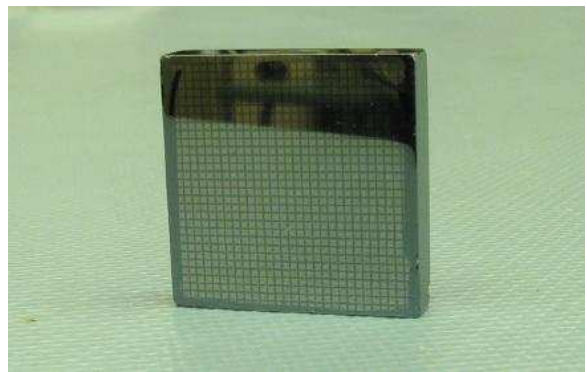

Figure 4: Photograph of a 1024 pixel CZT detector of 5 mm thickness. It has a 32 × 32 electrode structure on it.

4   Conclusions

The COBRA experiment aims to search for neutrinoless double beta decay of ^{116}Cd with a sensitivity to half-lives greater than 10^{26} years with a large array of CdZnTe crystals. The background in the signal region will be minimised through careful selection of materials, a comprehensive shielding with active veto, and the use of timing and spatial coincidences to reject radioactive decay events. A proto-type experiment is operating in the Gran Sasso laboratory to investigate the experimental requirements, in particular the low background issues for a large array. In this way half-life limits for several decay modes beyond 10^{20} yrs could be achieved. The work on pixellated detectors continued and first detectors are at hand with sub-mm pixel size.

5   List of Publications

1. *First Results on Double Beta Decay Modes of Cd, Te and Zn Isotopes with the COBRA Experiment*, T. Bloxham *et al*, Phys. Rev. C. 76, 025501 (2007)

2. *Radiation Shielding for Underground Low-background Experiments*, D.Y. Stewart *et al*, Nucl. Inst. Meth. A 571,651 (2007)

3. *Evaluation of Pixellated CZT Detectors for Neutrinoless Double Beta-decay Measurements*, T.R. Bloxham, M. Freer, Nucl. Inst. Meth. A 572,722 (2007)

4. *Energy resolution improvement in room temperature CZT detectors*, Y. Ramachers, D. Y. Stewart, JINST 2:P12003 (2007)

5. *Updates on activities since the Durham meeting and status of COBRA*, K. Zuber, AIP Conf.Proc.942:96 (2007)

References

[1] K. Zuber, *Physics Letters B* **519** (2001) 1

[2] E. Caurier et al., *Phys. Rev. Lett.***100** (2008) 052503

[3] T. Bloxham et al., *Phys. Rev. C* **76** (2007) 025501

[4] T. Bloxham, M. Freer, *Nucl. Inst. Meth. A***572** (2007) 722

CRESST. Dark Matter Search

G. Angloher [a], M. Bauer [b], I. Bavykina [a], A. Bento [a], A. Brown [c], C. Bucci [d],
C. Ciemniak [e], C. Coppi [e], G. Deuter [b], F. von Feilitzsch [e], D. Hauff [a], S. Henry [c],
P. Huff [a], J. Imber [c], S. Ingleby [c], C. Isaila [e], J. Jochum [b], M. Kiefer [a], M. Kimmerle [b],
H. Kraus [c], J. Lanfranchi [e], R. F. Lang [a], M. Malek [c], R. McGowan [c], V. Mikhailik [c],
E. Pantic [a], F. Petricca [a], S. Pfister [e], W. Potzel [e], F. Pröbst [a], S. Roth [e], K. Rottler [b],
C. Sailer [b], K. Schäffner [a], J. Schmaler [a], S. Scholl [b], W. Seidel [a], M. Stark [e],
L. Stodolsky [a], A. J. B. Tolhurst [c], I. Usherov [b], W. Westphal [e]

[a] Max-Planck-Institut für Physik, Föhringer Ring 6, D-80805 München, Germany
[b] Eberhard-Karls-Universität Tübingen, D-72076 Tübingen, Germany
[c] Department of Physics, University of Oxford,
Oxford OX1 3RH, United Kingdom
[d] Laboratori Nazionali del Gran Sasso, I-67010 Assergi, Italy
[e] Physik Department, Technische Universität München,
D-85747 Garching, Germany

Abstract

The aim of CRESST experiment (**C**ryogenic **R**are **E**vent **S**earch with **S**uperconducting **T**hermometers) is to search for particle dark matter and to contribute to the elucidation of its nature. The experiment is located at the Laboratori Nazionali del Gran Sasso (LNGS), Italy, and it uses low-background cryogenic detectors with superconducting phase-transition thermometers for the direct detection of WIMP–nucleus scattering events.

1 Dark Matter

There is strong evidence for the existence of dark matter on all astronomical scales, ranging from dwarf galaxies, through spiral galaxies like our own, to large-scale structures. The history of the universe is difficult to reconstruct without dark matter, be it Big Bang Nucleosynthesis or structure formation.

Despite this persuasive indirect evidence for its existence, the direct detection of dark matter remains one of the outstanding experimental challenges of present-day physics and cosmology.

A plausible candidate for the dark matter is the Weakly Interacting Massive Particle (WIMP) and it is possible that it can be detected by laboratory experiments, particularly using cryogenic methods, which are well adapted to the small energy deposit anticipated. Supersymmetry provides a well-motivated WIMP candidate in the form of the Lightest

Supersymmetric Particle. WIMPs are expected to be gravitationally bound in a roughly isothermal halo around the visible part of our galaxy with a density of about $0.3\,\mathrm{GeV/cm^3}$ at the position of the Earth.

Interaction with ordinary matter is expected via elastic scattering on nuclei. This elastic scattering can occur via coherent ("spin-independent") and spin-dependent interactions. For the coherent case, a factor A^2 is expected in the cross-section, favouring heavy nuclei.

Conventional methods for direct detection rely on the ionisation or scintillation caused by the recoiling nucleus. This leads to certain limitations connected with the low ionisation or scintillation efficiency of the slow recoil nuclei. The cryogenic detectors developed for CRESST measure the deposited energy calorimetrically, independent of the type of interaction, and allow for the detection of much smaller recoil energies. When such a calorimetric measurement of the deposited energy is combined with a measurement of scintillation light, an extremely efficient discrimination of the nuclear recoil signals from radioactive background signals can be obtained. These type of detectors are being used in the present phase CRESST-II.
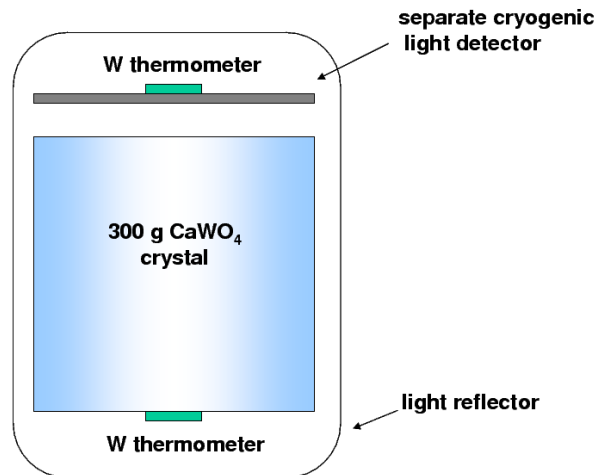
2 Detection Principle

Figure 1: Schematic representation of the detector for simultaneous phonon and light measurement. It consists of two separate cryogenic detectors enclosed in a highly reflective housing, read out by tungsten superconducting phase-transition thermometers. This concept, developed by scientists of the institute, is used in CRESST-II. It allows a very efficient discrimination of the searched nuclear recoil signals from the dominant radioactive β- and γ-backgrounds.

The low-temperature calorimeters consist of a target crystal with an extremely sensitive superconducting phase transition thermometer on its surface. A weak thermal cou-

pling to a heat bath restores again the equilibrium temperature after an interaction. The thermometer is made of a tungsten film evaporated onto the target crystal. Its temperature is stabilised within the transition from the superconducting to the normal conducting state, which occurs at temperatures of about 10 mK. A typical width of the transition is about 1 mK. A small temperature rise e.g. from a WIMP–nucleus scattering event (typically some μK), leads to an increase of resistance, which is measured with a SQUID (**S**uperconducting **Qu**antum **I**nterference **D**evice). For the first phase of CRESST, which ended in 2001, 262 g sapphire detectors had been developed. These detectors provided an excellent energy resolution of 133 eV at 6 keV and a very low energy threshold of 600 eV.

In the second phase, CRESST-II, we are using 300 g scintillating $CaWO_4$ target crystals. The scintillating crystal is equipped with a superconducting tungsten phase-transition thermometer for the detection of the phonons created by a particle interaction in the scintillating crystal. A small fraction of $\sim 1\%$ of the deposited energy is emitted as scintillation light, which is measured with a separate cryogenic detector, optimised for
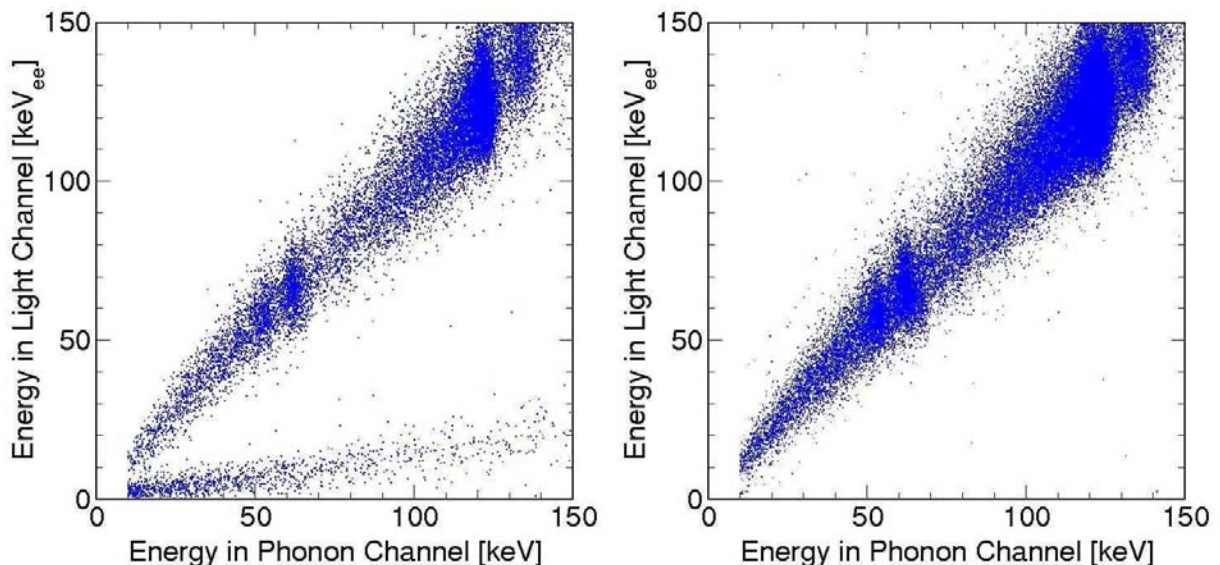

Figure 2: Coincident detection of phonons and scintillation light with a $CaWO_4$ detector. Left: The upper band of events is due to irradiation of the $CaWO_4$ crystal with electrons and gammas, whereas the lower band with lower light yield, is from nuclear recoils caused by a neutron source. Right: Removing the neutron source confirms that there is no leakage of ionising events into the nuclear recoil region.

Starting with a proof-of-principle experiment in 1998, the technique of simultaneous measurement of phonons and scintillation light has been developed at the institute. The important advantage of this technique is that it offers an extremely efficient suppression of the radioactive background down to very low recoil energies of about 10 keV. While the phonon signal measures the deposited energy, the amplitude of the corresponding light signal depends on the type of interaction. Nuclear recoils, such as WIMP or neutron scattering events, emit substantially less scintillation light than fully ionising interactions, e.g. γ or β interactions, do. As the overwhelming part of the background consists of β and

γ interactions, this phonon/light technique provides a very effective method of background suppression. Fig. 2 illustrates this detection method.

Compared with the alternative approach of simultaneous measurement of phonons and charge in a semiconductor crystal, which is applied in the experiments CDMS-II and Edelweiss-II, the method developed for CRESST-II has the important advantage that it does not suffer from dead layers at the surface. A reduced charge collection for ionising events occurring close to the surface in semiconducting crystals may lead to a false identification of low energetic γ's and β's as nuclear recoils. The result in Fig. 2, which was obtained with a gamma and beta source, confirms that the suppression also works for low-energy electrons impinging onto the crystal surface.

3 The CRESST Setup in Gran Sasso

The central part of the CRESST installation at Gran Sasso is the cryostat, sketched in Fig. 3. The low temperature which is generated in the mixing chamber of the dilution refrigerator is transferred into the radio-pure cold box, via a 1.5 m long cold finger. The cold finger is protected by thermal radiation shields, all fabricated of low-background copper. The detectors are mounted inside the cold box at the end of the cold finger. Two internal cold shields consisting of low-level lead are attached to the mixing chamber and to a thermal radiation shield at liquid N_2 temperature, respectively, in order to block any line-of-sight from the non-radio-pure parts of the dilution refrigerator to the detectors inside the cold box. The design completely avoids potentially contaminated cryogenic liquids inside the cold box.

An extensive passive shielding of low-background copper and lead surrounds the cold box and serves to shield radioactivity from the surrounding rock. The entire shielding is enclosed inside a gas-tight radon box that is flushed with boil of N_2 gas and maintained at a small overpressure. Special care was taken to minimise above-ground exposure of the construction materials of the cold box and the shielding to cosmic rays, in order to avoid activation.

This setup has been upgraded for the experimental program of CRESST-II, to allow the operation of 33 phonon/light detector modules. The upgrade included the installation of a 66-channel SQUID readout in the existing cryostat, a system for the integration of the 33 detectors in the cold box, the installation of a passive neutron shield, a muon veto, and a new multichannel electronics and DAQ. The cryostat with the upgraded shielding is shown schematically in Fig. 4. In this upgrade the institute was responsible for the neutron shield, the wiring of the cryostat from the mixing chamber down to the detectors, the detector integration system and the DAQ. The upgrade began in 2004 after a 52-day run with two 300 g prototype phonon/light detector modules in the old setup. With this short run a competitive sensitivity of 1.6×10^{-6} pb for the WIMP nucleon scattering cross section was reached despite the absence of any neutron shield.
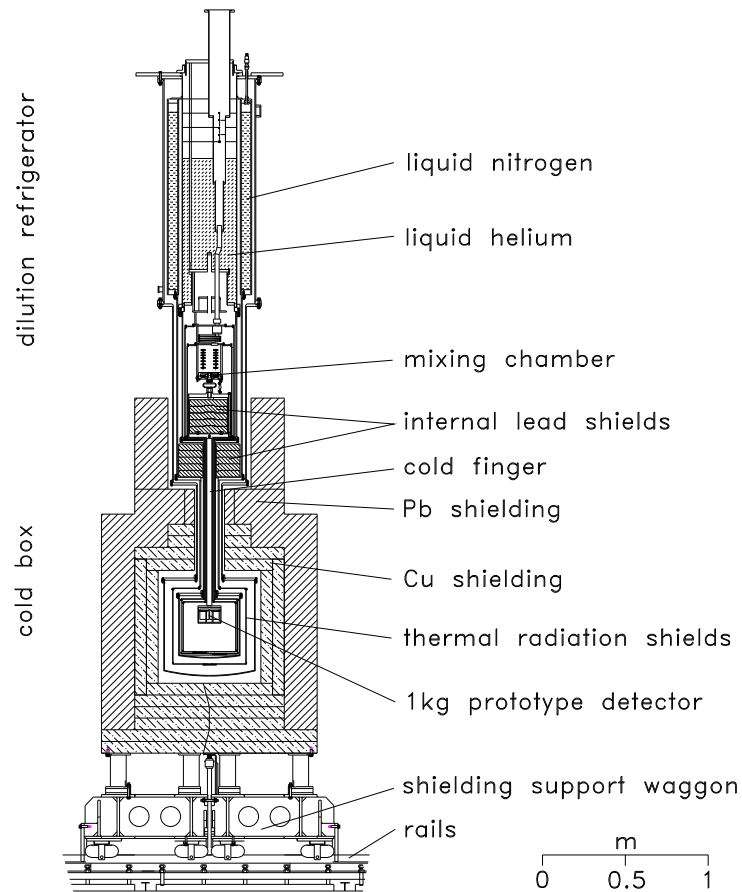
Figure 3: Layout of the CRESST ^{3}He/^{4}He dilution refrigerator and low-background cold box with its shielding.
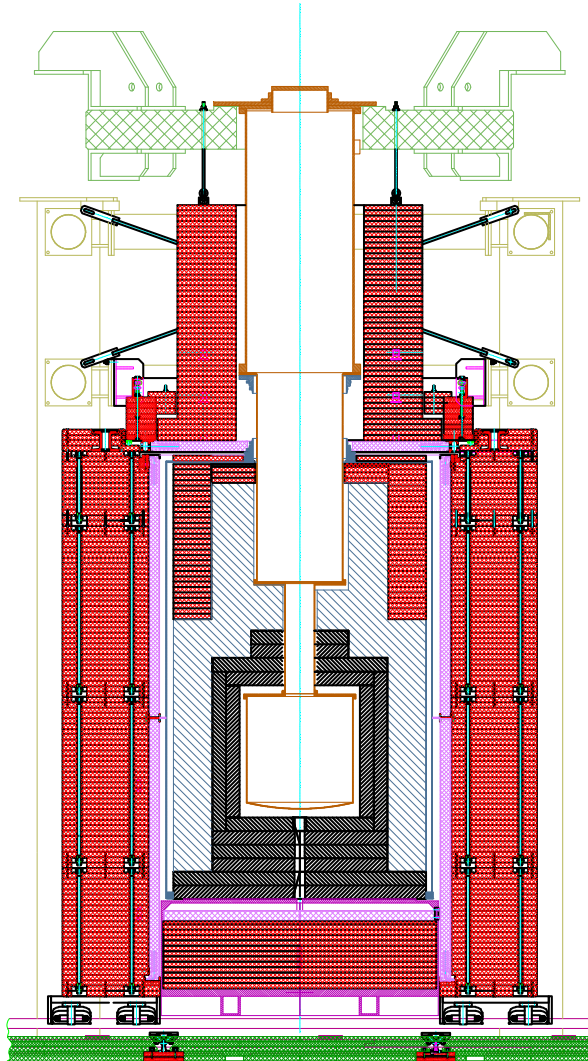
Figure 4: Dilution refrigerator and low-background cold box with its shielding upgraded for CRESST-II. The gas-tight radon box enclosing the Cu (shown in gray) and Pb (blue) shielding is completely covered by a plastic scintillator μ-veto (pink) and 40 cm of polyethylene (red).

4 Results from the commissioning run

After completion of the upgrade, nine detector modules were mounted in October 2006. Fig. 5 shows the mounted detectors before closing the cold box.
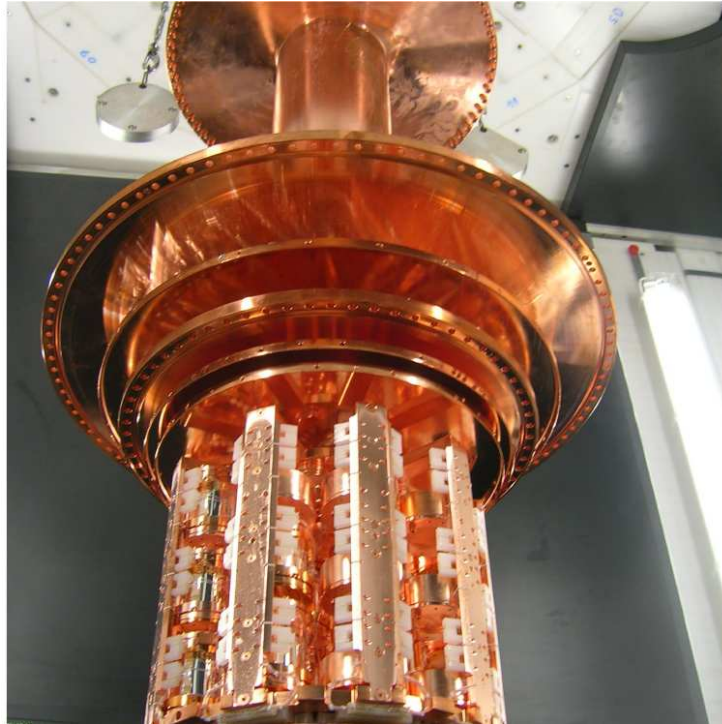

Figure 5: Detector modules mounted at the end of the cold finger, before closing the cold box in October 2006. The spring suspended platform provides additional vibration decoupling of the detectors from the cryostat. The mounting system was fabricated from low background, low heat leak Cu and low background CuSn2 springs.

An extended commissioning run followed the cool down in November 2006. A number of issues with the biasing electronics and SQUID system had to be settled during this commissioning run. A series of modifications has finally improved the interferences originally seen in the light detectors to an acceptable level. Seven phonon channels were working perfectly, delivering sub keV energy resolutions. Due to problems with some light detectors and SQUID channels, only three complete modules were working. Towards the end of this commissioning run, the 50 kg days of dark matter data shown in Fig. 6 were collected with two detector modules. Form-factor effects effectively limit the energy transfer to the heavy tungsten nuclei in elastic WIMP nucleus scattering to energies below 40 keV for all WIMP masses. In the energy region below 40 keV and above the background separation threshold of 11 keV, three tungsten recoil events were observed in the data of Fig. 6.

The light signal, which varies with the recoiling nucleus, can be used to determine which nucleus, in a compound material like $CaWO_4$, is recoiling. This would have significant consequences in verifying a possible positive dark matter signal. For these reasons it is important to understand the light output (or 'quenching factor') and the CRESST
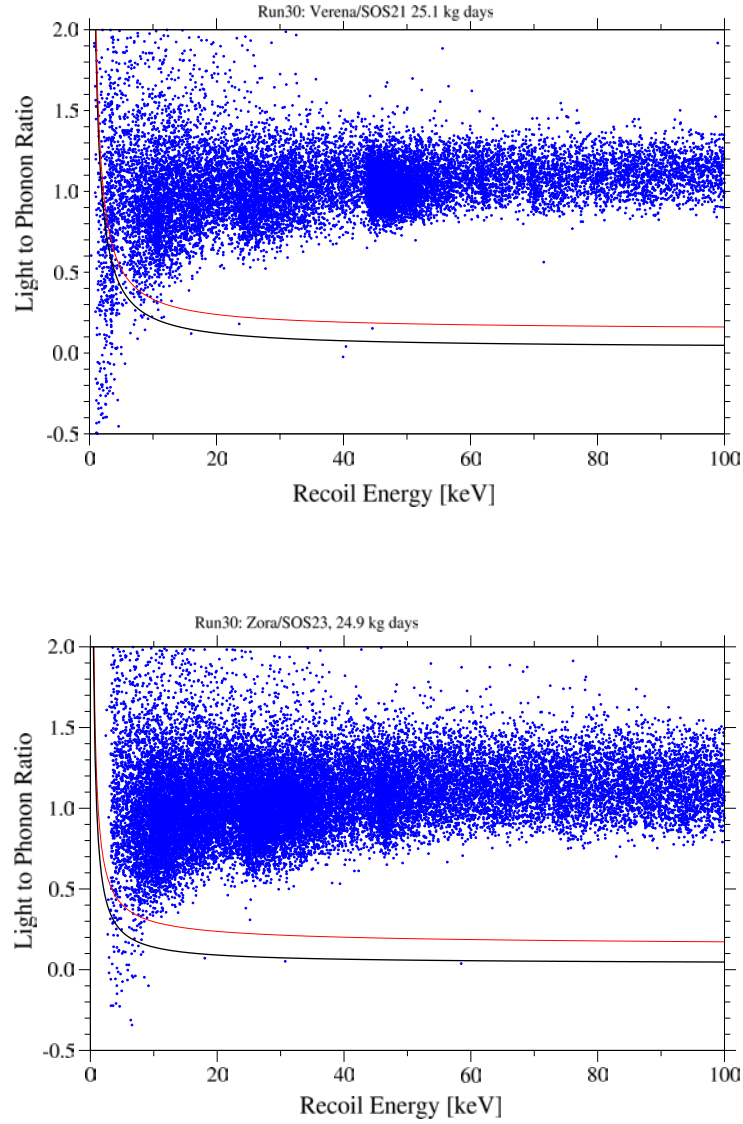
Figure 6: Low energy event distribution measured with two 300g $CaWO_4$ detector modules during the commissioning run. The vertical axis represents the light yield expressed as the ratio (energy from the light channel/energy from the phonon channel), the horizontal axis is the total energy measured by the phonon channel. Below the red curve 90% of all nuclear recoils, and below the black curve 90% of the tungsten recoils are expected.
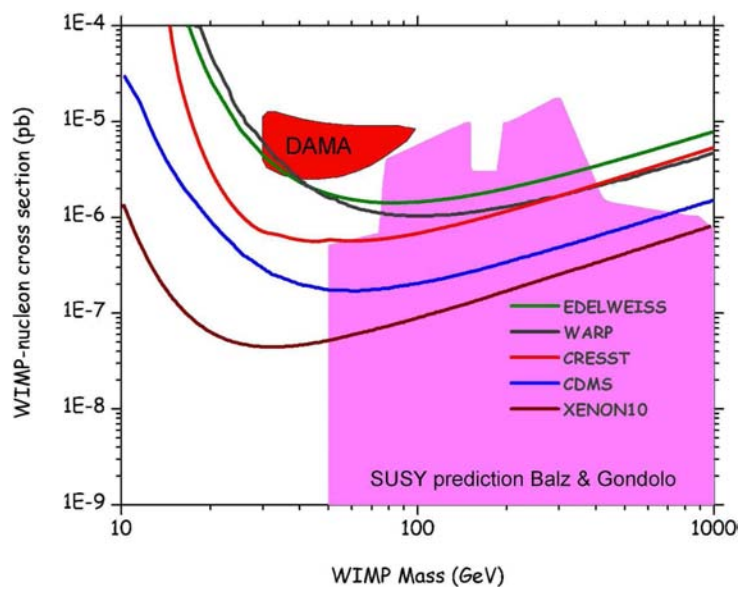
Figure 7: Spin independent or coherent scattering cross section exclusion limit derived from the 50 kg days of data of Fig. 6, collected with two detector modules during the commission run. For comparison the limits from other experiments and the range predicted by Supersymmetry are also shown.

collaboration has undertaken a series of investigations of light emission with different projectiles and particles. An interesting and simple explanation of the pattern of results was found by means of the assumption that the light output is simply proportional to the length of the light-producing track (and not the energy for example). In addition it was noted that this assumption leads to a simple model for the intrinsic fluctuations in light output at low energy. These turn out to be rather large and could be of significance in limiting noble gas detector projects.

If we attribute all tungsten recoils below the black lines in Fig. 6 to WIMP interactions, we can set the upper limit for the WIMP scattering cross-section shown in Fig. 7. The minimum of the curve is at about 5.5×10^{-7} pb, which is about a factor of 3 improvement over the previous run in 2004 before the upgrade.

During the commissioning run, the recoil acceptance region of the detectors has been calibrated in situ by applying a neutron source. Fig. 8 shows the result of this calibration for one of the two detectors. Due to kinematic reasons, the spectrum is dominated by oxygen recoils above 10 keV. The red line in Fig. 8, below which 90% of the oxygen recoils are expected, was calculated from a previously measured quenching factor and the measured energy dependence of the energy resolution of the light detector. The neutron calibration data agree very well with this prediction of the acceptance region. This justifies the calculation of the acceptance region for tungsten recoils based on the same principle.
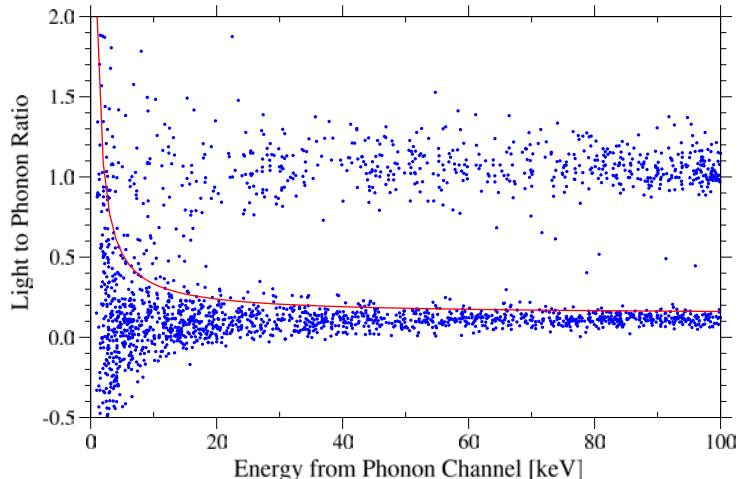
Figure 8: Low energy event distribution measured with a neutron source during the commissioning run. The axis are the same as in Fig. 6. The red curve, below which 90% of the oxygen recoils are expected, is calculated from a previously measured quenching factor and the measured energy resolution of the light detector.

5   Near term plans for CRESST-II

To get interferences likely caused by the multi channel SQUID electronics under control, the Oxford group made a strong effort to build a replacement for that part of the commercial SQUID electronics, which was very likely the origin of the interference problems

in the commissioning run. A new set of detectors has been fabricated at MPI, and 17 detectors will be installed in spring 2008. With some of them, design variations have been implemented to address the question of the origin of our very small residual background observed in the commissioning run. With this next run we hope to increase the recorded data volume by a factor of 10. This could allow us to reach a sensitivity for the scattering cross section below 10^{-7} pb and touch the region favoured by a larger class of Supersymmetric model predictions.

Publications

H. Kraus et al., Nuc. Phys. B (Proc. Suppl.), **173** (2007) 104–107
W. Seidel et al., J. Physics (Conf. Proc.), to be published
S. Henry et al., J. Inst., **2** (2007) P11003
I. Bavykina et al., Astropart. Phys., **28** (2007) 489–493

CUORICINO and CUORE

F. Alessandria[b], E. Andreotti[i], R. Ardito[a,c], C. Arnaboldi[a], F. T. Avignone III[d], M. Balata[e], I. Bandac[d], M. Barucci[f], J.W. Beeman[s], F. Bellini[p], B. Berger[g,l], C. Brofferio[a], A. Bryant[g,l], C. Bucci[c], S. Capelli[a], L. Carbone[a], M. Clemenza[a], C. Cosmelli[p], O. Cremonesi[a], I. Dafinei[p], M.P. Decowski[g,l], A. Dewaard[z], S. Di Domizio[j,k], M.J, Dolinski[g,l,o], L. Ejzak[r], R. Faccini[p], F. Ferroni[p], E. Fiorini[a], L. Foggetta[i], S.J. Freedman[g,l], C. Gargiulo[p], A. Giachero[e,j], L. Gironi[a], A. Giuliani[i], P. Gorla[e], E. Guardincerri[g], T.D. Gutierrez[q], E. E. Haller[m,s], K.M. Heeger[r], R. Kadel[g], K. Kazkaz[o], L.Koogler[g,l], Yu.G.Kolomensky[g,l], E. Longo[p], G. Maier[c], R.H. Maruyama[r], C. Martinez[a], S. Morganti[p], S. Nisi[e], C. Nones[i], E. B. Norman[o], A. Nucciotti[a], M. Olcese[j,k], P. Ottonello[j,k], M. Pallavicini[j,k], V. Palmieri[n], M. Pavan[a], M. Pedretti[i], G. Pessina[a], S. Pirro[a], E. Previtali[a], L. Risegari[f], C. Rosenfeld[d], S. Sangiorgio[r], N.D. Scielzo[o], M. Sisti[a], A. R. Smith[g], L. Tatananni[c] C. Tomei[p], G. Ventura[f], M. Vignati[p], N. Xu[g], L. Zanotti[a] and C. Zarra[e].

[a] Dip. di Fisica dell'Univ. di Milano-Bicocca e Sez. INFN di Mi-Bicocca, Milano I-20126 -Italy
[b] INFN - Sez. di Milano, Milano I-20133 - Italy
[c] Dip. di Ingegneria Strutturale del Politecnico di Milano, Milano I-20133 - Italy
[d] Dept.of Phys. and Astron., Univ. of South Carolina, Columbia, South Carolina 29208 - USA
[e] Laboratori Nazionali del Gran Sasso, I-67010, Assergi (L'Aquila) - Italy
[f] Dip. di Fisica dell'Univ. di Firenze e Sez. INFN di Firenze, Firenze I-50125 - Italy
[g] Nuclear Science Division, Lawrence Berkeley National Lab., Berkeley, CA 94720 - USA
[h] Lab. de Fisica Nuclear y Altas Energias, Univ. de Zaragoza, 50009 Zaragoza - Spain
[i] Dip. di Fisica e Matematica dell'Univ. dell'Insubria e Sez. INFN di Milano, Como I-22100 - Italy
[j] Dip. di Fisica dell'Università di Genova - Italy
[k] Sez. di Genova dell'INFN, Genova I-16146 - Italy
[l] Dept. of Physics, Univ. of California, Berkeley, CA 94720 - USA
[m] Dept. of Materials Sc. and Engin., Univ. of California at Berkeley, Berkeley, CA 94720 - USA
[n] Laboratori Nazionali di Legnaro, I-35020 Legnaro (Padova) - Italy
[o] Lawrence Livermore National Laboratory, Livermore, California, 94550 - USA
[p] Dip. di Fisica dell'Univ. di Roma La Sapienza e Sez. INFN di Roma, Roma I-00185 - Italy
[q] California Polytechnic State Univ., San Luis Obispo, CA 93407 - USA
[r] Univ. of Wisconsin, Madison, Wisconsin - USA
[s] Materials Sc. Division, Lawrence Berkeley National Lab., Berkeley, CA 94720 - USA

Abstract

CUORE R&D and Cuoricino results achieved in 2007 will be presented.

1   Introduction

If the neutrino is a Majorana particle, Neutrinoless double Beta Decay ($\beta\beta(0\nu)$) is one of the easiest way to get information concerning the absolute scale of neutrino mass. Consisting of an array of 988, 750 g, TeO_2 bolometers operating at $\sim$10 mK, the CUORE experiment is designed with a sensitivity capable of probing most of the range suggested by oscillation experiment results. The large natural abundance of ^{130}Te (33.87%) eliminates the requirement for the very expensive isotopic enrichment required in all of the other proposed next generation experiments [1]. The proposed array has a cylindrical structure consisting of 19 towers of 52 detectors each. One such tower has been successfully constructed and is being operated at Laboratori Nazionali del Gran Sasso (LNGS) as an independent experiment called CUORICINO since spring 2003. During current year (2007) CUORICINO has increased the statistic to $\sim$15 kg y of Te^{130} taking data with a duty cycle of about 60%. On the other hand, CUORE, already approved by the LNGS Scientific Committee in April 2004 and by the INFN Scientific Committee in September 2004, has completed its technical design and has entered the construction phase.

2   Cuoricino 2007

CUORICINO is a tower of 13 planes containing 62 crystals of TeO_2; 44 of them are cubes of 5 cm on a side, while the dimensions of the others are $3\times3\times6$ cm^3 (the two 9 crystal $3\times3\times6$ cm^3 planes are the only relevant difference between the CUORICINO and CUORE towers). The total mass of TeO_2 in CUORICINO is 40.7 kg, the largest by more than an order of magnitude than any other cryogenic detector. The statistics collected up to August 2007 for the $\beta\beta(0\nu)$ measurement corresponds to 15.6 kg(^{130}Te) y and it is fully analyzed. Other few months collected during 2007 will be added soon to the total statistic. No evidence of a 2530 keV peak is found in the analyzed data. A Maximum Likelihood procedure is used to establish the maximum number of $\beta\beta(0\nu)$ events compatible with the measured background. A lower bound for the ^{130}Te $\beta\beta(0\nu)$ half-life of 3×10^{24} years at 90% C.L. results, with a weak dependence on the used background function (linear or flat), and on the assumed $\beta\beta(0\nu)$ peak position (allowing it to span over the 1 sigma error quoted for the Q-value) and peak shape (symmetric or asymmetric gaussian).

CUORICINO not only is used to search for $\beta\beta(0\nu)$ but also it is a test bench for CUORE. As discussed in [3] CUORICINO has provided a lot of information concerning background sources. Also from the technical point of view of detector operation and optimization CUORICINO is capable of providing us important results. During year 2007 several test measurement were realized on the CUORICINO array to study the thermal stability problem (to optimize the techniques used for the thermal gain correction), the maximum acceptable rate (this in view of the choice of CUORE source calibration activity), the temperature range for the optimal working of the detectors (this to valuate exactly the temperature range in which the detectors have the best performances, in order

to know which is the maximum temperature at which they can work properly in CUORE). These tests reduced the live time of the experiment but gave relevant contribution to the CUORE experiment design.

At the end of year 2007 the installation of a muon detector covering part of the CUORICINO experiment has started. Based on large plastic scintiallators this detector will be used in the first 6 months of 2008 in order to disentangle the possible muon contribution to CUORICINO measured background. Once completed this measurements CUORICINO will be closed. CUORE-0 3.6 detector will replace the CUORICINO tower and will be the natural prosecution of the $\beta\beta(0\nu)$ measurement started with CUORICINO.

3 Cuore 2007

The CUORE Project [1] foresees the realization of a $\beta\beta(0\nu)$ experiment with an active mass of the order of 1 ton. CUORE will employ 988 natural TeO$_2$ bolometers each made of a cubic 5×5×5 cm^3 TeO$_2$ crystal with a mass of about 750 g. The goal of the CUORE collaboration is to reach, in the energy region of interest, a background level lower than 10^{-2} counts/keV/kg/y obtaining hence a sensitivity on the effective Majorana mass of neutrino of the order of 50 meV.

The CUORE array is designed in order to have the most compact structure reducing to a minimum the distance between the crystals and the amount of inert material interposed between them. The 988 bolometers of the array are arranged in a cylindrical matrix organized into 19 towers, each made of 13 planes. Every plane contains four crystals supported inside a copper frame. The entire array, surrounded by a 6 cm thick lead shield, will be operated at about 10 mK in a He^3/He^4 dilution refrigerator. A further thickness of 25 cm of low activity lead will be used to shield the array from the dilution unit of the refrigerator and from the environmental activity. A borated polyethylene shield and an air-tight cage will surround externally the cryostat. The experiment will be installed underground in the Laboratori Nazionali del Gran Sasso(LNGS) at a depth of 3400 m.w.e.

Despite operating a 1000 bolometer array at 10 mK could look rather challenging, the technical feasibility of CUORE has been extensively proved by the good performances of the CUORICINO experiment, while the possibility of cooling large masses in dilution refrigerators have been proved, for example, by the gravitational antenna experiments. The true challenge in CUORE - as in all the next generation $\beta\beta(0\nu)$ experiments - will be the background achievement. Up to now - thanks to the background knowledge acquired through CUORICINO and dedicated radioactive measurements of various type (NAA, ICMPS, HPGe ...) - the limiting factor appears to be the background coming from contamination of the detector surfaces (TeO$_2$ crystals and Cu mounting structure surfaces). With the present know-how the background in CUORE would be between 2 and 4 10^{-2} counts/keV/kg/y [3]. Background studies are however still in evolution.
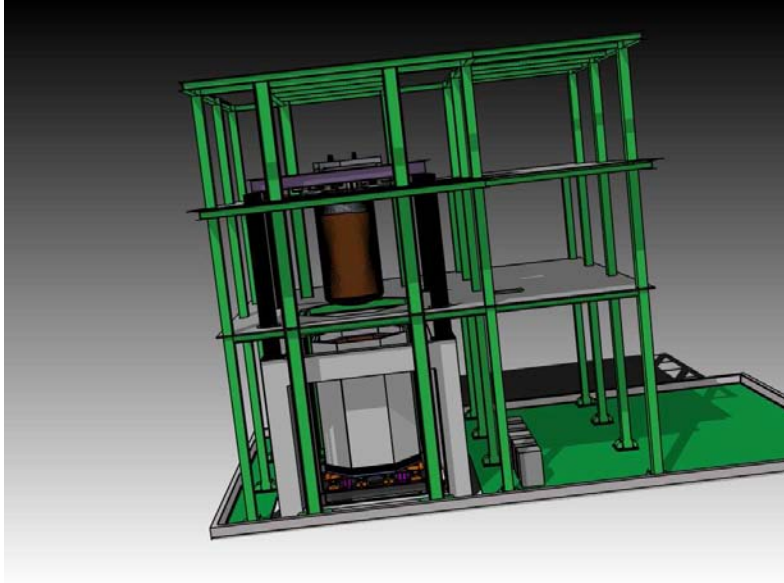
Figure 1: 3D view of the main CUORE building

3.1 Hut

During year 2007 the design of the building for the CUORE experimental apparatus was completed and its construction begun in the underground Hall A. The hut skeleton is visible in figure 1: in the low level the cryostat concrete supports and the shields structure (these lay on a lifting platform that will lift the shields in their final position), on the first level - closed inside a clean room - the mechanical structure holding the refrigerator (the Dilution Unit).

The hut will be completed by the end of 2008. By the same date also the external lead and polyetylene shields (figure 2) will be ready.

3.2 Cryostat

During 2007 the CUORE cryostat design has been completed. The design must satisfy a set of experimental requirements.

- the detector base temperature must be less than $10\,\text{mK}$ for optimal operation;

- the 988 detector array requires an experimental space at least $1000\,\text{mm}$ high and $940\,\text{mm}$ wide;

- the system must be instrumented with about 2600 wires;

- the level of the vibrations transmitted to the detectors has to be minimized.

The achievement of the CUORE target background in the energy range where the $\beta\beta$-0ν of ^{130}Te is expected ($Q_{\beta\beta}= 2530\,\text{MeV}$) requires a strong reduction of environmental radioactivity (especially ^{232}Th). This adds more requirements:
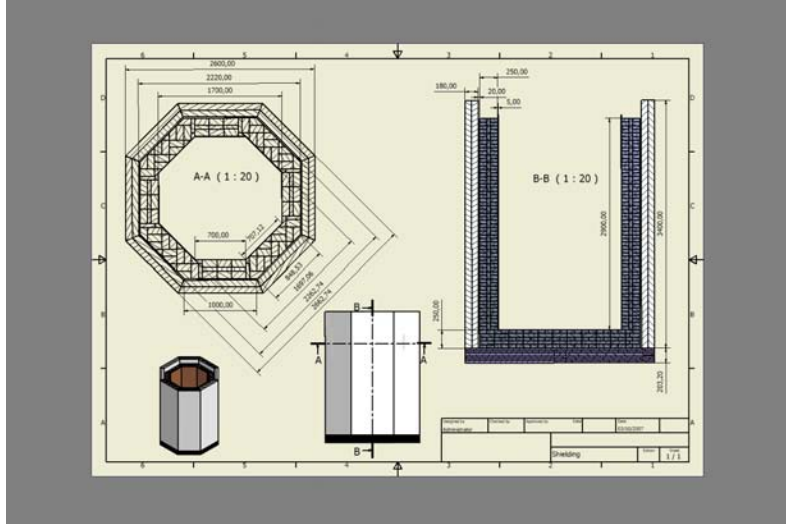
Figure 2: The external shields for CUORE

- the experiment must be shielded by at least 30 cm of lead in every direction;

- inside the lead shielding only selected radiopure materials can be used;

Since the CUORE measuring time may be as long as 10 years, further requirements are given by the need for a stable, service-free and high duty-cycle running:

- the cryogenic system must be cryogen-free;

- there must be at least one spare cryocooler;

The cryogenic apparatus is shown in figure 3. The cryostat is made of six nested vessels. There are two vacuum chambers: the Outer Vacuum Chamber (OVC) at room temperature and the Inner Vacuum Chamber (IVC) at a temperature of about 4 to 5 K. The OVC is about 3090 mm high and has an outer diameter of about 1620 mm. Between the OVC and the IVC there is a thermal radiation shield at a temperature between 40 and 50 K. The cooling of the IVC and of the 40 K radiation shield is provided by up to five Pulse Tubes (PT) mounted on the room temperature OVC top flange. The PTs chosen for this apparatus are the PT415 made by Cryomech, which have a cooling power as high as 1.5 W at 4 K. The base temperature without heat loads is expected to be less than 6 mK. Additional thermal radiation shielding is provided by 30 layers of Multilayer Insulation (MLI) covering the 40 K shield and by 10 layers on the IVC shield. The amount of MLI is limited by its radiopurity.

The cooling of the experiment is provided by a high-power cryogen-free ^{3}He/^{4}He dilution refrigerator heat sunk to the IVC flange. The DU is being especially made by Leiden Cryogenics for this system. It is a DRS-2000 unit modified to run without cryogens: a Joule-Thompson heat exchanger replaces the usual 1 K pot. The ^{3}He circulation is obtained by four V551 turbo pumps from Alcatel. The expected cooling powers outside the mixing chamber are > 1.5 mW, $30\,\mu$W and $5\,\mu$W at 120 mK, ≈ 20 mK and ≈ 12 mK

respectively. Inside the IVC there are two radiation shields connected respectively to the Still and to the Cold Plate of the dilution unit (DU). The temperature of the Still shield ranges from 0.6 to about 0.9 K, depending on the DU ^{3}He flow rate. The Cold Plate shield has a temperature between 50 and 100 mK. The innermost shield is connected to the DU Mixing Chamber (MC) to protect the experimental space. Its temperature is expected to be lower than 10 mK.

Inside the cryogenic apparatus there are three lead shields to protect the experiment from environmental radioactivity and from contaminations in the building materials. A 25 cm thick lead layer outside the OVC shields the detector from the bottom and from the sides. An equivalent shielding from the top has to be placed at cold inside the cryostat, just above the detector. This is a 300 mm thick lead disk with a diameter of about 900 mm: the weight of this shield is about 3300 kg. The lead disk is placed between the mixing chamber plate and the detector, but it is thermally linked to the Cold Plate. A lead ring-shaped shield placed on the Still flange closes the gap between the lead disk above the detector and the outer room temperature shield. The mass of this shield is about 1700 kg. An additional shielding of detector's sides and bottom is provided by a 60 mm lead layer just outside the Still shield. Its temperature maybe either the IVC or the Still one. The mass is about 5400 kg. This shield is required to protect the detector from contaminations in the MLI and on the outer vessels surfaces.

To accomplish the radiopurity requirements, the vessel mantles and bottoms are made of selected high purity copper that has been already bought and placed in the Gran Sasso Underground Laboratories to prevent cosmic ray activation. It will be brought to surface only for building the cryostat. The copper is produced by Norddeutsche Affinerie and the chosen alloy is the OFE (Oxygen Free Electrolytic) one except for the base temperature components which will be machined with the ETP1 alloy (Electronic Tough Pitch also called NOSV). The NOSV copper has been chosen for its low hydrogen content. The OVC and IVC top plates and flanges can be made of austenitic stainless steel (type 316LN for cryogenic applications) because of the thick lead shielding protecting the detector from the top. To withstand the vacuum the OVC copper wall thickness is about 12 mm. The top stainless steel plate is 60 mm thick to stand the atmospheric pressure ($\approx$ 20000 kg) and the weight of the inner structure ($\approx$ 16000 kg). The IVC vessel must also be able to stand a pressure difference of about 1 atm limited by passive safety valves. The IVC copper mantle is about 10 mm thick. The stainless steel IVC top plate is 60 mm thick. An additional copper layer on the top of the IVC plate may increase thermal conductance between the DU and the PTs. The copper Still plate - which is loaded by the lead ring-shaped shield - is 45 mm thick. The cold seal on the IVC flange will be made using a tubular metallic seal like the O-Flex seals from Helicoflex. Alternatively, the IVC top plate may be made out of copper to avoid any thermal gradient. In this case the tightness achievable with metallic seals must be checked.

To avoid radioactive contamination inclusions and to preserve the material mechanical properties, electron beam welding will be adopted for all structural components. Plasma arch welding maybe used for the radiation shields.

Three 316LN tie bars fixed to the OVC top plate support the 40 K radiation shield, the IVC, the Still and the two lead shields at the Still temperature. Each bar is split in two pieces: the upper one extends from the OVC to the IVC and has a diameter of

Table 1: Total masses in kg per material on each stage.

	OVC	40K	IVC	Still	Cold Plate	MC	detector
316LN	1122		768				
Copper	1943	990	1152	1137	1101	401	864
Lead				7126	2746		
TeO$_2$							751
total	3065	990	1920	8263	3847	401	1615

about 19 mm for a load of about 4000 kg. The lower segment extends from the IVC to the bottom of the Still shield and has a diameter of about 16 mm for a load of about 3000 kg. The Cold Plate is supported by three Ti-6Al-4V rods fixed to the Still plate. The MC plate is supported by three 316LN rods fixed to the Cold Plate.

The cold lead disk above the detector and the detector itself are supported by two independent struts. The lead is supported by three rods extending from the OVC top plate. Each rod is made of four pieces. Two 316LN bars are used from the OVC top to the IVC top plate and from the IVC to the Still plate. From the Still to just below the MC plate a Kevlar 49 rope with thimble eyes is used to minimize the heat load on the Cold Plate. From the MC to the bottom of the lead shield a copper bar is used. The detector suspension has been designed to minimize the transmission of mechanical vibrations both due to seismic noise and to the operation of cryocoolers and pumps. It is a two-stage low-frequency isolator in the vertical direction, while in the horizontal direction the structure is a pendulum with a natural frequency of about 0.4 Hz. The detector suspension is fixed to a "Y" shaped structure above the cryostat which is isolated from the top OVC flange by means of low-frequency isolators using a Negative Stiffness Mechanism made by Minus-K. The second isolation stage is provided by regular springs at the top end of the suspension bars. This configuration gives a low-pass filter with two poles at about 0.5 and 3.4 Hz. The detector suspension bars are made of four pieces as well as the lead suspension ones, but the lower end of the Kevlar 49 rope is thermally heat sunk to the MC.

Table 1 summarizes the amount of the different materials on the various stages of the apparatus.

A number of clear shot ports from the OVC to the IVC provide the access for the wires and the detector calibration sources. Additional ports are necessary to evacuate the IVC and as input for the cold helium gas forced flow during the initial phase of the cool-down. The wiring will be made by 0.1 mm thick manganine wires in woven ribbons, running through six access ports.

The cryostat and the DU will be both bought and delivered to LNGS by the end of this year. Their assembly and tests will take place during year 2009.

3.3 Assembly

During year 2007 important steps towards the definition of the final design of CUORE detector have been achieved:

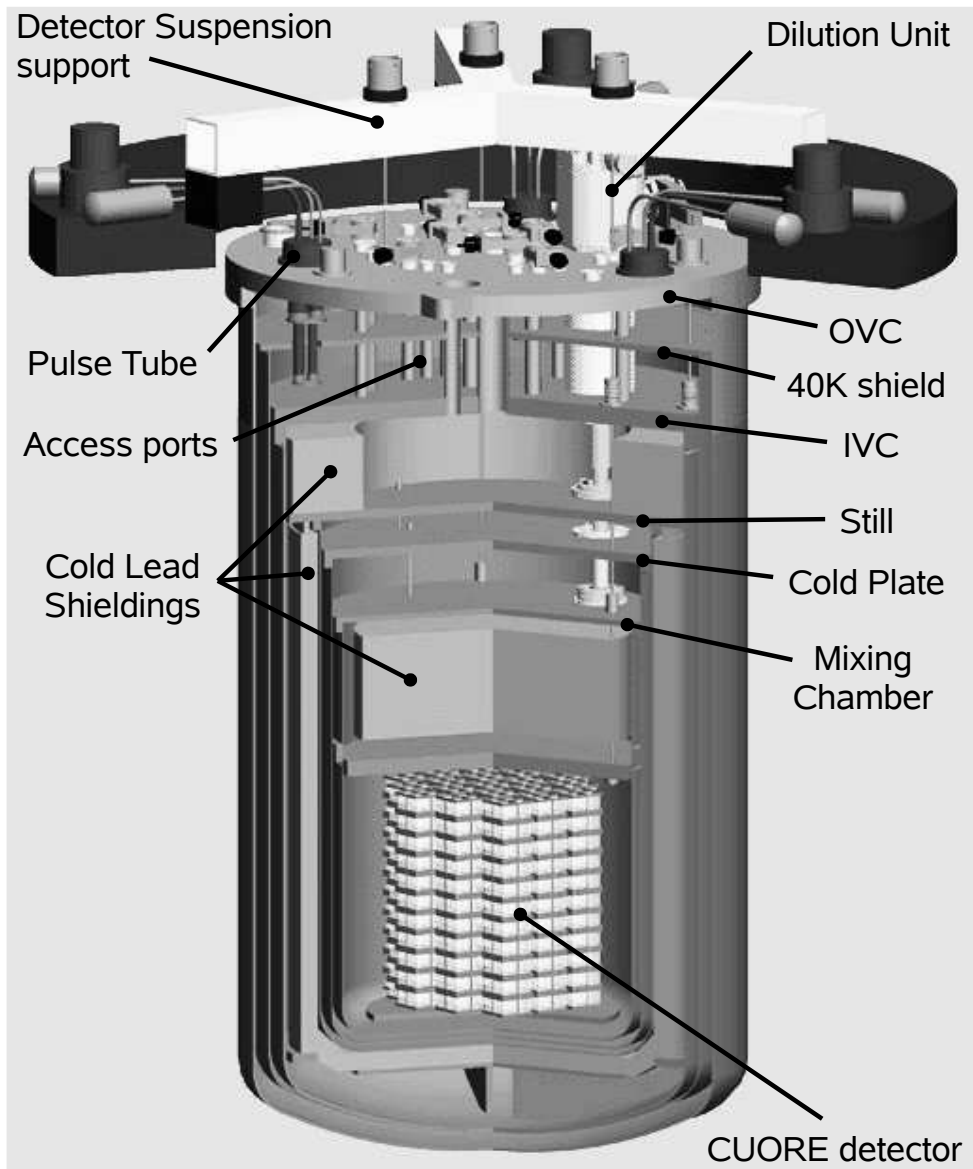1. There have been (standard and bolometric) tests on PTFE radioactivity and thermo-

Figure 3: 3D view of the cryogenic apparatus

mechanical characteristics (e.g. stress releases in PTFE at low temperature), definitively confirming the use of PTFE in CUORE to hold crystals.

2. The final decision on the material and technique to implement the bolometers readout was taken at the end of the year. It required many different tests and studies, as:

- the gamma and alpha radioactivity check on Cu-mylar ribbons and on all the connectors needed;

- the design and test of very special NTD thermistors, with gold contacts on top instead of lateral, to permit the gold wire ball bonding from thermistors to readout pads when the tower is already mounted;

- the confirmation of the possibility to wire bond, keeping the bonding machine in the vertical position. A "custom made" design of the machine was studied and tested for this scope, in collaboration with the factory, and is now being ordered;

- the validation of the strip design from the point of view of cross-talks and e.m. pickup noise;

- the Monte Carlo simulations to evaluate the loss in efficiency of anticoincidence within nearby crystals, due to the shadow of the read-out trays, thus fixing some limits in read-out ribbon width and therefore on the maximum number of channels per ribbon;

- the study of mechanical dumping and decoupling between readout ribbons and cryostat, so to not spoil the mechanical suspension of the CUORE Detector;

- the thermalization of the ribbons and the coupling to the cryostat wiring coming from room temperature down to the Mixing Chamber;

3. The final mechanical drawings, to be hold out to the factories for the real production, are still waiting for some very last inputs. We have been collecting, since the end of year 2007, information on the statistical distribution around the mean value of the more crucial parameters of the CUORE single tower achieved by different factories in the production of Cu frames and columns (see "Copper procurement and machining, surface treatment and test" subsection, hereafter), PTFE spacers and crystals. These data will be used to validate the CUORE parts production and to make the fine-tuning corrections to the mechanical drawing dimensions and tolerances, before going into the real CUORE structure production, to be started in the second half of 2008.

Meanwhile, since the best way to design a fruitful assembly line is to start from a very detailed "Assembly Project" document, we have spent some time in 2007 to write a kind of Project Execution Plan that takes into account all the needs and *caveat*s that must be fulfilled to reach the (very stringent) requirements on the detector. The document describes every single step needed for the assembly and at the end will contain all the protocols to be followed during construction, to reach the best results.

Some preliminary studies and drawings on the glove-boxes that will be used to mount every single tower of CUORE have been accomplished. They will all be custom made, and therefore will be optimized during 2008 using simulations of the real operations needed to assemble the tower, using a mock-up and fake glove-boxes. The final assembly line will be constructed only when these studies will end, making us confident in the possibility of building the detector in the best way.

Packaging, shipping and storage of all the detector parts, once cleaned to remove as much as possible surface radioactivity, are again very delicate steps to be accomplished before the detector construction to avoid as much as possible recontamination. The solutions studied are summarized in 2 sentences:

- "zero contact" philosophy. This means no exposure to air or contaminated gas and minimized (in space and time) exposure or contact with other materials;

- shortest time exposure to cosmic rays, which translates into very careful logistic plans to minimize the time elapsed above ground for any kind of preliminary (when the tower starts to be assembled this is no more an issue) treatment requested.

In year 2007 some preliminary studies for packaging and shipping of crystals from SICCAS (in Shanghai, China) have been accomplished. During the next year all these issues will need to be settled, since the first batch of CUORE crystals and structure parts will be delivered for the construction of CUORE-0.

3.4 Radioactivity

2007 was especially devoted to material selection, material procurement and optimization of cleaning and assembly procedures. The copper procurements and the storage of it underground was completed, a clean PTFE was selected and the tender for the material procurement was done at the end of the year, the analysis of the ancient roman lead for the internal shielding was started and will be completed soon, the tender of the external lead shield was started and will be completed before summer, selection of packaging and storage container was started; these are some examples of the activity on the selection materials that was completed or under development. Some of the previous mentioned items will be crucial for the realization of the detectors for radioactive test, practically we will be able to realize detectors for test purposes, using the same materials that will be used in e CUORE.

Cleaning procedures for many materials were also studied to optimize the background reduction due to surface radioactivity. In particular some measurements on special copper cleaning procedures studied and realized in Laboratori Nazionali di Legnaro (LNL) were realized in Padova with Laser Ablation MS and in Milano Bicocca using Silicon surface barrier detectors. All measurements indicates that the surface radioactivity obtained with the LNL protocol [1] are at the limits of sensitivity of all the applied measurement techniques. Moreover these limits are few times larger than the limits reported in the hall C measurements and a complete plan for a new bolometric test for the Legnaro copper cleaning was prepared for the middle of 2008.

The complete definition of the internal lead shield is related with the ^{238}U and ^{232}Th contamination of ancient roman lead. Especially for ^{232}Th the requested limits are in the range of 10^{-12} g/g, values difficult to reach using standard gamma rays spectrometry. To overcome this problem a series of NAA measurements were planned and partially completed during 2007. The preliminary results indicate limits of 7×10^{12} g/g for ^{232}Th that are very close to the CUORE request. The complete plan of measurements will be ready in few months during 2008.

The selection of PTFE on the basis of gamma and NAA measurements gives us the possibility to acquire the complete amount of needed material for CUORE and to store it underground. To analyze also the possible surface contribution produced by the new material measurements using surface barrier detectors were performed in 2007.

Packaging for crystals and copper was an important investigation of the 2007. The crystals production is approaching and it is mandatory a complete definition of the packaging procedure that must be organized in Shanghai. Packaging is also related to the assembly procedure in view of long storage time of samples in the underground laboratory. In order to minimize the contribution of packaging to the detector background, measurements were dedicated to materials selection and radon diffusion. The actual choice is to pack all the material under vacuum during transportation and later all parts will be reprocessed in the Gran Sasso underground Laboratory. Measurements on radioactive contamination of materials were done and also the impermeability to radon diffusion is under test.

A specific designed tight camera was built in order to study possible surface contamination induced on detector pieces when exposed to radon and radon progenies. Inside the camera we are able to reach a radon atmosphere of 300000 Bq/m^3, samples of copper, PTFE and crystals were exposed to such contaminated atmosphere and the deposited contaminations are measured using a surface barrier detectors. Preliminary results are encouraging and we plan to complete these tests during 2008.

3.4.1 Crystals procurement and surface treatement

The year 2007 was focused on preparing the large scale production of TeO$_2$ crystals needed for CUORE. Previous experience showed that Shanghai Institute of Ceramics of the Chinese Academy of Sciences (SICCAS) is the unique producer able to satisfy the very challenging demands of our experiment, especially for what concerns radio-purity specifications. Nevertheless, further actions were needed at SICCAS aimed at guaranteeing a high quality crystals production expanded on few years and performed in reliable and fully reproducible conditions. Special production conditions were defined and implemented at SICCAS allowing for the production of TeO$_2$ crystals compliant with CUORE requirements. These particular production conditions referred to:

- technological environment

- machineries and processing techniques

- procurement, handling, storage and shipment of raw materials, reactants, consumables, intermediary and final products
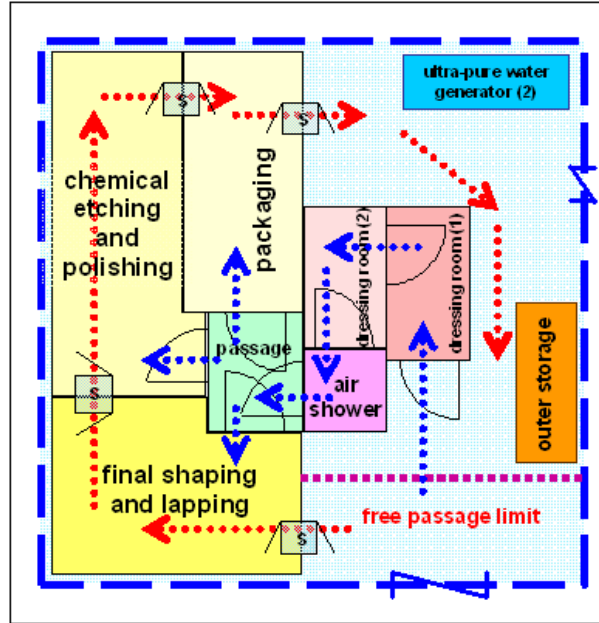
Figure 4: SICCAS/INFN Clean Room at Jiading production center near Shanghai. Arrows indicate circulation of materials (dashed red) and persons (dashed blue). Total surface of clean area: approx. 30m2; work capacity: 4-6 operators.

Substantial improvements were achieved in surface processing phase of crystal production. A dedicated clean room (figure 4) for CUORE crystals was mounted at Jiading production center near Shanghai and a radio-contamination safe surface processing protocol was implemented which includes chemical etching of crystal surface. Last but not least, special package and shipping procedures were implemented and will further be improved.

Efforts were also done in order to guarantee a further reduction of bulk radioactive contaminations. Dedicated areas for chemical synthesis and successive drying of TeO_2 powder to be used for CUORE crystals growth are guaranteed at Kunshan Jincheng Chemical facility. Concerning crystal growth and related operations (final drying of TeO_2 powder, Pt crucibles manufacturing, charging with TeO_2 powder and sealing before growth), a production area entirely dedicated to CUORE crystals is on the way to be organized and equipped at Jiading. The start of CUORE crystals production will be allowed only upon written conformity report made by INFN experts in radio-contamination prevention procedures. In order to check the effectiveness of different actions taken for TeO_2 crystal quality improvement, a total of 10 crystals were produced in 2007 in two batches and delivered in May (6 crystals) and November (4 crystals). The crystals have been tested for their performances in the Hall C cryostat obtaining the following results:

- the first 6 crystals showed a bulk contamination in ^{232}Th and ^{238}U largely compatible with the required standards for CUORE. These crystals have been treated in China with a new surface cleaning procedure: crystals were chemically etched to remove any residual of the crystal cut and of the optical polishing procedure necessary for crystallographic inspection. Later they were polished again with newly selected
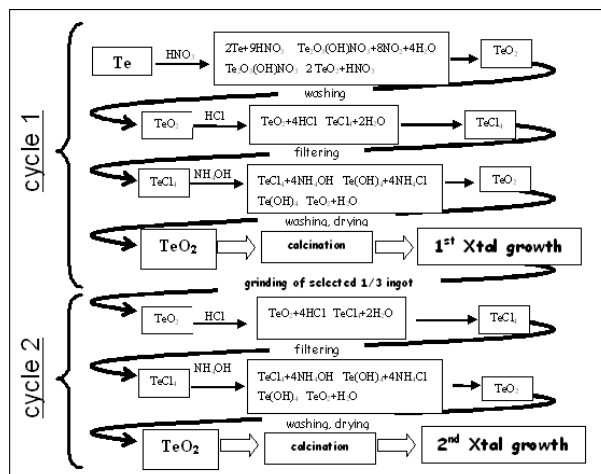
Figure 5: Production of ultra-pure TeO$_2$ crystals. Standard (wet) chemical purification is doubled by crystal growth which is by itself a purification process. The whole process (chemical synthesis + crystal growth) is repeated twice.

materials that should - in principle - guarantee both a good optical quality and a poor radioactive contamination. Transparency could be of help in detector mounting procedure, while radio-purity is a mandatory requirement. Unfortunately both the goals failed: the surface of the crystals resulted such rough to compromise the bolometric response of the detectors and the large amount of residuals from polishing material produced a dangerous surface contamination.

- the 4 crystals from the second batch were therefore treated in China with the procedure already succesfully tested in LNGS [3]. The results were quite satisfactory and now this last procedure - although not able to guarantee an optical quality of the crystals - is the baseline for CUORE crystal treatment.

The production of these 10 crystals offered also the opportunity of a detailed analysis of ultra-pure TeO$_2$ powder production and crystal growth process (figure 5). A detailed production protocol based on precautionary principle was defined in straight collaboration with SICCAS specialists in order to avoid any action which may lead to supplementary radio-contamination. The protocol includes several certification procedures for raw materials, reagents, intermediary products, tools and ancillaries, and immediate actions are foreseen in case of failure, including halt of crystals production till the problem is solved (figure 6). Following detailed discussion of contractual conditions the decision was taken to place the order for CUORE crystals: 500 pieces to be paid by INFN and other 60 pieces, by LBNL. The rest of 440 crystals needed for CUORE will be further paid by LBNL. Special clauses were included in the contracts aimed at avoiding the purchase of crystals not fully compliant with technical specifications requested by CUORE experiment. Contracts are expected to be signed at the beginning of 2008 and related series production of CUORE crystals is foreseen immediately after. Previous to effective large scale production of TeO$_2$ crystals at SICCAS-JiaDing the certification of different production step is foreseen, as follows:
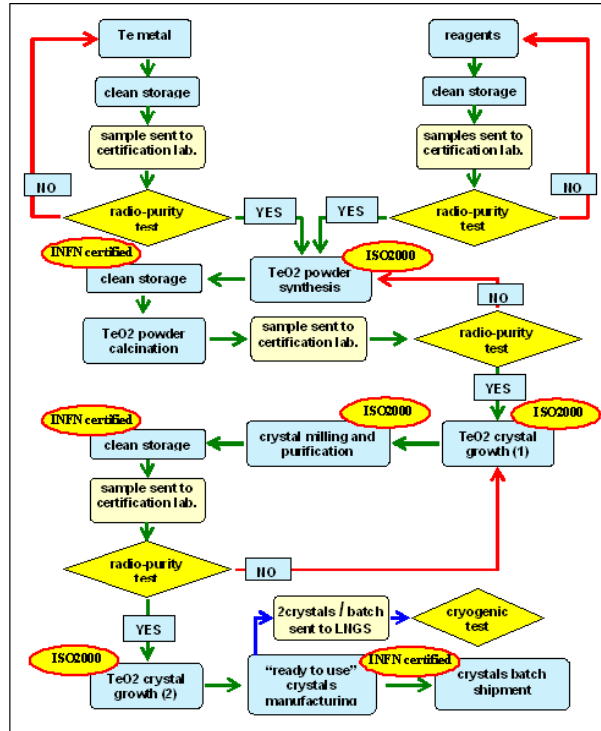
39

Figure 6: Qualification procedures during TeO$_2$ crystals production. Raw materials and intermediary products will be certified by ICPMS and/or HPGe gamma spectroscopy. Conformity to radio-contamination prevention rules will be certified by INFN experts.

- statement of conformity with radio-contamination safe production protocol released by CUORE Radioactivity Working Group (RWG) for the TeO$_2$ powder synthesis unit at Kushan Jincheng Chemical Reagent Co. Ltd. Certificate released by CUORE

- statement of conformity with radio-contamination safe production protocol released by RWG for a CUORE dedicated TeO$_2$ crystal growth unit at SICCAS JiaDing

- statement of conformity with radio-contamination safe production protocol released by RWG for a CUORE dedicated TeO$_2$ surface processing unit at SICCAS JiaDing

- procurement by CUORE Collaboration and certification by RWG as radio-contamination safe products of needed consumables and ancillaries for surface processing, packaging and shipping of TeO$_2$ crystals

The delivery at LNGS of the first batch of 60 TeO$_2$ crystals ready to use is foreseen for November 2008. The series crystals production will follow with a planned production rate of 30 crystals per month.

3.5 Copper procurement and machining, surface treatment and test

During 2007 the procurement of almost all the copper for the experimental setup was concluded. This includes the copper for the cryostat thermal shields (OF01 type, ~ 7 tons) and that for the CUORE detector (NOSV type, ~ 5 tons). The two types differ in the residual impurity content: OF01 is an oxygen-free copper suited for welding, while NOSV is a cryogenic copper with a low hydrogen content. Both types have been tested in past years for their radiopurity. They were cast by Norddeutsche Affinerie (NA) and then rolled in plates of different dimensions and mechanical properties by Carl Schreiber Neunkirchen (Germany). This work sequence was done keeping the total exposure to cosmic rays between 6 and 8 weeks. The copper is stored in the Gran Sasso underground laboratory until its use.

After the settlement of the CUORE detector structure in June 2007, the problem is now to produce all copper parts composing it. In particular, the frames holding the crystals have a special design that minimizes the amount of material facing the TeO$_2$ crystals and allows the correct vibrational stability of the detectors. In order to meet the stringent radiopurity and mechanical requirements and to have the correct surface roughness for the subsequent surface treatments, the frames must be produced by electrical discharge machining (EDM) under controlled conditions. Two options are presently under evaluation: the manufacturing of the ~ 300 CUORE frames by an external company or by the LNL workshop. At the end of 2007 a quality check of some external companies has been performed, while the first LNL prototypes are expected at the beginning of 2008. The final choice, around summer 2008, will weigh costs, production time, and obtained results. First prototypes of the other copper parts of the detector holding structure are presently being machined by the Milano-Bicocca INFN workshop.

After machining, all copper parts directly facing the TeO$_2$ crystals must undergo a special surface cleaning procedure optimized by the LNL group. Several tests on small copper samples, supported by LA-ICPMS measurements, have shown that this cleaning procedure can diminish the amount of ^{232}Th and ^{238}U traces in the copper. A final decisive cryogenic test on the actual detector mounting is expected within summer 2008. In this measurement a small 12 crystal tower will be assembled using the copper holding structure machined from CUORE copper by LNL and Milano-Bicocca workshops, and subsequently surface treated by the LNL group. The achieved radioactive background will then be compared with previous Hall C tests [3].

The following steps, all to be closed by the end of 2008, will include the organization of the logistics of copper machining and cleaning (to keep total exposure to cosmic rays within 4 months - in order to have negligible ^{60}Co activation), and the start of the production and cleaning of CUORE frames (expected rate: about 2 per week).

3.5.1 Electronics

Stringent requirements are asked to the electronic set-up, which is composed of many parts. Starting from the detector sides the amplifying chain consists of the preamplifier, the second stage and the anti-aliasing filter, connected to a commercial DAQ. The load

resistors and the detector biasing are also in charge to the set-up. In addition, the supply voltages are designed to show very low drift and noise. A calibrating pulse generator system that emulates the impinging particle on the detectors is also provided with stability close to 1ppm/C. All the listed parts have programmable many of their main features. In this way the central computing system can take care and monitoring of all the necessary parameters without human intervention in the detectors area. The Electronics for CUORE will be based on the set-up already designed, built and used for CUORICINO. Improvements are foreseen in space occupation, power dissipation and input noise. The design and prototyping of the newer set-up is in progress. A new JFET transistor pair to be used as the preamplifier input devices has been already designed, during the 2007, based on a semi-custom project. They feature a very small parallel input noise, the main source of noise be minimized. The JFET production for the whole CUORE array is already available in our laboratory. Within the current year, 2008, our goal will be the design and the prototype realization of the new preamplifier, the second stage, the initializing filter and the detector biasing system. Prototypes will be developed with local companies. The first samples will be characterized and tested in our INFN labs. Final production and finalized test should be made in the USA. In the first quart of the 2008 we are completing the design phase, while during the rest of the year the prototyping and characterization will occupy the rest of our effort. Starting in 2007 we have also taken care of the detector connecting link in its last part, from the mixing chamber down to the thermistors and heaters, supporting the activity of the Assembly group. The links have very stringent requirements in term of radioactive background of the material used and very compact packaging. We succeed in satisfy both characteristics using mylar as the substrate material. Some prototypes have been developed by a selected local company having this particular skillful capability. The electrical behavior of the prototypes has been found conformal to the requirements. Measurements are in progress of radioactivity contents of the selected material. Preliminary results seem to confirm the expectations. We foresee to start the production, with the same company, within the end of 2008 with the same selected company.

3.5.2 DAQ

The Data Acquisition and Slow control systems is basically completely designed in its main parts, and most of the software has been written. In order to test and validate the new system, the collaboration has decided to upgrade both the system in the Hall C setup and the one in use in Cuoricino using the very same hardware and software that will be used in Cuore.

During the summer of 2007 a brand new batch panel has been installed in Hall C that allows to split the signals and run the existing DAQ and a new one in parallel, for cross validation and check. The new DAQ has been installed as well. The architecture, although obviously somewhat reduced and simplified, is the same that will be adopted for Cuore. A National Instruments crate of Ni-PXI-6284 boards is used for the sampling of up to 48 channels. The software is identical to the one foreseen for Cuore and its design is such that all future upgrades will be installed in Hall C as well, for validation and tests, the only difference being the configuration defined by a set of data base records. The

new system also includes a brand new slow control system for front end, Bessel filters and pulser control. The new slow control system is completely integrated in the DAQ system, and it is designed to allow the complex functions like the automatic calculation of the load curves and the determination of the optimal working point for the bolometers. These features are already implemented and will be tested in the near future.

A similar activity is right now in progress in the Cuoricino setup. Also here a suitable designed patch panel allow the new and old DAQ system to work in parallel for cross checks and validation. Eventually, as soon as the test phase is completed, the old DAQ will be removed. The new DAQ system in Hall C has been up and running with no problem since September 2007 and the preliminary analysis of the data is encouraging. A complete analysis of the Hall C data acquired with the new DAQ will be done in the near future. The same will be done in Hall A (Cuoricino) as soon as the new run will resume, after a short break for system maintenance. The system in Hall A is also capable of reading out the data produced by a simple muon detection system, developed in collaboration with the Berkeley group and based on a set of plastic scintillators.

3.6 CUORE-0

3.6.1 Definition of CUORE-0

CUORE-0 is a single CUORE tower to be installed and operated in the existing dilution refrigerator placed in the hall A of the LNGS. This refrigerator is presently housing Cuoricino. CUORE-0 is foreseen to be taking data from April 2009.

3.6.2 Description of CUORE-0

CUORE-0 main features are listed below.

- 52 TeO_2 cubic crystals, 50.0 mm side, 750 g mass for a total of 5×10^{25} ^{130}Te nuclides, grown by SICCAS, Shanghai, China;

- crystal arrangement: 13 planes of 4 crystals each; each plane is made out of two copper frames; each copper frame is common to two adjacent planes;

- crystal holding method: 9 PTFE blocks per frame (4 single, 4 twofold, 1 fourfold);

- the resulting tower is covered with a copper cylinder acting as a thermal shield at base temperature (10 mK);

- each TeO_2 crystal will have a thermistor of the series B34C, with gold pads on two opposite faces and two small pads on the top face continuing "after the corner" the lateral pads, in order to allow frontal bonding; thermistors are developed at LBNL (California, USA), and heaters developed by IRST (TN, Italy).

3.6.3 Motivations

CUORE-0 motivations are manifold and listed below.

- Test of the CUORE assembly chain and procedure. CUORE-0 will be assembled according to the CUORE style, using semi-automatic procedures, and in a completely different way with respect to Cuoricino and CUORE-R&D detectors. It is therefore crucial to test the assembly procedure well in advance and its possible influence on background and detector performance.

- High statistics test of crucial components of the estimated CUORE background. The conservative target of the CUORE background is 0.01 c/(keV kg y). CUORE-0 will allow to measure this value in the 3-4 MeV window with 20 % precision in only one month. This result will give room to possible well-oriented changes to the CUORE structure. We would like to remark that the background in the region of neutrinoless Double Beta Decay cannot be better than 0.06 c/(keV kg y), since this is an unavoidable contribution from the ^{232}Th contamination in the superinsulation of the Cuoricino cryostat. However, this improvement make CUORE-0 a very competitive DBD experiment. After a few month of CUORE-0 data taking, the combined CUORE-0 / Cuoricino results will lead to a more stringent limit on ^{130}Te half life than that that would have been obtained with continuous Cuoricino operation. After that, the CUORE-0 half-life sensitivity will increase by a factor $\sqrt{3}$ faster than what obtainable with Cuoricino alone.

- Test of the bolometric behavior of the detectors. Some differences are introduced in the CUORE detector structure with respect to Cuoricino, such as the crystal holding method and the wire connection of the thermistors to the heat sink. CUORE-0 will allow the study of these technical detector changes on a large number of samples before final CUORE construction.

- Test of the CUORE Data Acquisition. The CUORE data acquisition is different in hardware and philosophy from the Cuoricino one. CUORE-0 will allow a full test of the new DAQ on a number-of-channel scale comparable to that CUORE and with detectors with exactly the CUORE features.

- Test of the CUORE analysis tools. The off-line signal processing and the data analysis of CUORE will be based on a radically new software system. CUORE-0 will offer a unique and crucial opportunity for a full debug of the renewed analysis tools based on a faithful anticipation of the final experiment.

- Educational role for undergraduate and PhD students. CUORE is an experiment that will remain for a long time in a purely engineering and assembly stage, without collection of real physics data. In this context, CUORE-0 offers an important educational occasion, allowing to teach students the bases of low temperature detection, the subtleties of a multichannel bolometric experiments and the extraction of relevant physical information from low-background high-energy resolution spectra.

- <u>Tasks and resources.</u> Additional resources for CUORE-0 with respect to CUORE are relatively limited. The main items are listed below and additional requirements are underlined when present.

  1. <u>Crystal procurement.</u> CUORE-0 will use the first 60 samples of the full CUORE production, without implying any modification of the growth and processing schedule with respect to CUORE. No additional resource is required for this item.

  2. <u>Heater and thermistor procurement.</u> The temperature-stabilization heaters to be used for CUORE-0 will belong to the first segment of the full CUORE production. No additional resource is required for this item.

  3. <u>Tower design and copper / PTFE procurement.</u> Given the total identity between the CUORE-0 and the CUORE towers, there is no additional designing work in this sense, apart from an anticipation for PTFE procurement.

  4. <u>Copper / PTFE machining and preparation.</u> Again, given the total identity between the CUORE-0 and the CUORE towers, there is no particular request for CUORE-0 in this sense. The copper and PTFE parts prepared for CUORE-0 will be the same as for CUORE and the production will start with the same features for both. The CUORE baseline foresees the use of unshielded copper, treated with plasma cleaning method. This special cleaning, appearing very promising in ICPMS measurements, will be tested in a dedicated hall C run in the first half of 2008.

  5. <u>Clean room and packaging / storage of separated parts.</u> CUORE-0 tower will be assembled in the Borexino clean room located in the hall C of the Gran Sasso Laboratories. A method (foreseen for 2008) for safe tower transportation from Borexino clean room to hall A refrigerator will be designed. Resources will be dedicated to design and realize packaging methods of small parts after cleaning.

  6. <u>Mechanical tower-cryostat interface.</u> It will be necessarily different from that of CUORE, due to the totally different refrigerator structure. It will be based mainly on the Cuoricino suspension method.

  7. <u>Cryogenics.</u> The hall A refrigerator presently housing Cuoricino needs a full maintenance, but it is essentially working and in a good shape.

  8. <u>Final operations.</u> Safe transportation of the CUORE-0 tower from Borexino clean room to hall A requires a careful analysis and a method that minimizes apparent forces that could damage the detectors. A special clean environment has to be prepared around the Cuoricino refrigerator for the final tower connection.

3.6.4 Schedule.

The CUORE-0 schedule is illustrated below. It is roughly divided in three parts:

1. 2007 - preparation;

2. 2008 - assembly;

3. 2009 - start up and data taking

The CUORE-0 crystals will arrive in two batches, in November 2008 (28 crystals) and December 2008 (28 crystals). The thermistors for CUORE-0 will be produced in Berkeley in September-October 2008 using existing raw materials. The production and the cleaning of the CUORE-0 copper parts (in particular the frames which hold the crystals) will be mainly made in LNL, from June 2008 until December 2008. Other less critical parts will be produced in external workshops and processed then in LNL. The gluing of the thermistors and heaters to the crystals (which will make use of a dedicated semi-automatic method, now under development, and easily transferable to CUORE) will occur in November-December 2008. The pre-cabling of the tower and the plane assembly will be done in January 2009. The positioning of the read-out wires and the ultrasonic bonding of the thermistors wires will occur in February 2009. The installation in the refurbished hall A refrigerator (Cuoricino will be stopped and removed in July 2008 to allow interventions on it) and the cool down are foreseen for March 2009. The measurement optimization and data taking will occur in April 2009.

References

[1] C. Arnaboldi et al., NIM A518 (2004) 775, R. Ardito et al, hep-ex/0501010.

[2] C. Arnaboldi et at., Phys. Lett. B 584 (2004) 260.

[3] CUORE Collaboration, LNGS Annual Report 2006.

DAMA. Dark Matter Search

P. Belli[a], R. Bernabei[a,@], A. Bussolotti[a,*], F. Montecchia[a], F. Nozzoli[a], A. d'Angelo[b], F. Cappella[b], A. Incicchitti[b], A. Mattei[b,*], D. Prosperi[b], M. Cini[c], R. Cerulli[c], C.J. Dai[d], H.L. He[d], H.H. Kuang[d], J.M. Ma[d], X.H. Ma[d], X.D. Sheng[d], Z.P. Ye[d,e], R.G. Wang[d], Y.J. Zhang[d]

in neutron measurements: M.Angelone[f], P.Batistoni[f], M.Pillon[f]

in some by-product results and small scale experiments: R.S. Boiko[g], F.A. Danevich[h], B.V. Grinyov[i], V.V. Kobychev[h], L.L. Nagornaya[i], S.S. Nagorny[h], D.V. Poda[h], A.V. Tolmachev[i], V.I. Tretyak[h], R.P. Yavetskiy[i], S.S. Yurchenko[h]

in some studies on $\beta^+\beta^+$, EC/β^+, EC/EC decay modes (under the joint Indo-Italian DST-MAE project): P.K. Raina[j], A.K. Singh[j], P.K. Rath[j], A. Shukla[j]

in precise measurements on isotopic abundances: N. Bukilic[k], J.R. de Laeter[k], M. Laubenstein[c], S. Nisi[c]

[a]Dip. di Fisica, Università di Roma "Tor Vergata" and INFN-Roma Tor Vergata, 00133 Roma, Italy.
[b]Dip. di Fisica, Università di Roma "La Sapienza" and INFN-Roma, 00185 Roma, Italy.
[c]Laboratorio Nazionale del Gran Sasso, INFN, 67010 Assergi (Aq), Italy.
[d]IHEP, Chinese Academy, P.O. Box 918/3, Beijing 100039, China.
[e]Physics Dept, Jing Gangshan University 343009, Jiangxi, China.
[f]ENEA - C. R. Frascati, P.O. Box 65, 00044 Frascati, Italy.
[g]Chemical Dept., Kiev National Taras Shevchenko University, MSP 01033 Kiev, Ukraine.
[h]Institute for Nuclear Research, 252650 Kiev, Ukraine.
[i]Institute for Scintillation Materials and Institute for Single Crystals, 61001 Kharkov, Ukraine.
[j]Indian Institute of Technology, Kharagpur, India.
[k]Dep. of Applied Physics, Curtin University, GPO, Box U1987 Perth, Western Australia.
@ Spokesperson
* technical staff

Abstract

DAMA is an observatory for rare processes and it is operative deep underground at the Gran Sasso National Laboratory of the I.N.F.N. (LNGS). The main experimental set-ups are: i) DAMA/NaI ($\simeq$ 100 kg of highly radiopure NaI(Tl)), which

completed its data taking on July 2002 and various data analyses are continuing; ii) DAMA/LXe ($\simeq 6.5$ kg liquid Kr-free Xenon enriched either in ^{129}Xe or in ^{136}Xe); iii) DAMA/R&D, devoted to tests on prototypes and to small scale experiments, mainly on the investigations of double beta decay modes in various isotopes; iv) the second generation DAMA/LIBRA set-up ($\simeq 250$ kg highly radiopure NaI(Tl)) in operation since March 2003; v) the low background DAMA/Ge detector mainly devoted to sample measurements; in some measurements on rare processes the low-background Germanium detectors of the LNGS facility are also used. Moreover, a third generation R&D is in progress towards a possible 1 ton set-up, DAMA proposed in 1996. In the following main arguments on the activity during 2007 are summarized.

1   DAMA/NaI

The highly radio-pure DAMA/NaI set-up [1, 2, 3, 4] has been a pioneer Dark Matter experiment of suitable exposed mass, sensitivity and stability of the running conditions, taking data at LNGS over seven annual cycles. The data taking has been completed in July 2002 and still results are produced by various kinds of studies.

The main aim of DAMA/NaI has been the investigation of the presence of Dark Matter (DM) particles in the galactic halo by exploiting the model independent annual modulation signature (see refs. [1, 2, 3, 4, 5, 6, 7, 8, 9, 10, 11, 12, 13] and in the 2007 publication list), originally suggested by [14, 15] in the middle of 80's. In addition, profiting by its low-background features and by the high collected exposure, several results have been achieved both on Dark Matter particle investigations with other approaches and on several other rare processes [16, 17, 18, 19, 20, 21, 22, 23, 24, 25].

The DAMA/NaI set-up has pointed out the presence of an annual modulation in the *single-hit* residual rate in the lowest energy interval $(2-6)$ keV (see Fig.1), which satisfies the many peculiarities of a DM particle induced effect. The presence of DM particles in our Galaxy is supported at 6.3 σ C.L. over seven annual cycles (total exposure: 107731 kg $\times$ day); see refs. [2, 3, 4, 5, 6, 7, 8, 9, 10, 11, 12, 13] and in the 2007 publication list. Systematic effects or side reactions able to account for the observed effect (that is able to account for the whole modulation amplitude and to contemporaneously satisfy all the many peculiarities of the signature) have been neither found nor suggested by anyone over more than one decade.

This result is model-independent; it represents the first experimental evidence of the presence of DM particles in the galactic halo. At present, apart from DAMA/LIBRA, no other experiment is sensitive, for mass, radiopurity and control of the stability, to such a model independent signature and use the same target material and procedures; thus, no other activity is available whose result can directly be compared with the one of DAMA/NaI.

On the basis of the obtained 6.3 σ C.L. model-independent result, corollary investigations can also be pursued on the nature of the DM particle candidate (see e.g. ref. [3, 4, 12, 13] and the 2007 publication list). This latter investigation is instead model-dependent and – considering the large uncertainties which exist on the astrophysical, nuclear and particle physics assumptions and on the parameters needed in the calcula-
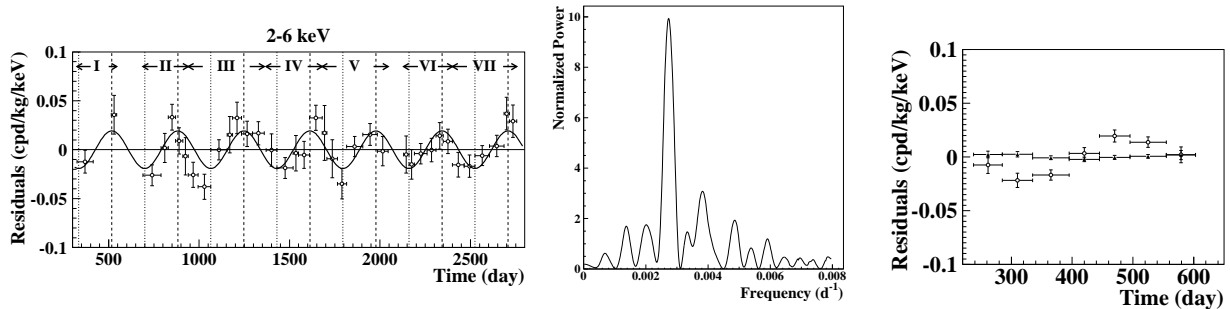
Figure 1: *Left:* experimental residual rate for *single-hit* events in the cumulative (2–6) keV energy interval as a function of the time over 7 annual cycles, end of data taking July 2002. The experimental points present the errors as vertical bars and the associated time bin width as horizontal bars. The superimposed curve represents the cosinusoidal function behaviour expected for a Dark Matter particle signal with a period equal to 1 year and phase exactly at 2nd June; the modulation amplitude has been obtained by best fit [3, 4]. *Center:* power spectrum of the measured *single-hit* residuals for the cumulative (2–6) keV energy interval calculated including also the treatment of the experimental errors and of the time binning. As it can be seen, the principal mode corresponds to a frequency of 2.737×10^{-3} d^{-1}, that is to a period of $\simeq 1$ year. *Right:* experimental residual rates over seven annual cycles for *single-hit* events (open circles) – class of events to which DM events belong – and over the last two annual cycles for *multiple-hits* events (filled triangles) – class of events to which DM events do not belong – in the (2–6) keV cumulative energy interval. They have been obtained by considering for each class of events the data as collected in a single annual cycle and using in both cases the same identical hardware and the same identical software procedures. The initial time is taken on August 7th.

tions – has no general meaning (as it is also the case of exclusion plots and of the DM particle parameters evaluated in indirect detection experiments).

For simplicity, the results of the corollary analyses are presented in terms of allowed volumes/regions obtained as superposition of the configurations at given C.L. for the considered model frameworks (see e.g. ref. [3, 4, 12, 13] and the 2007 publication list). They account for a large set of best fit values. The results briefly summarized here and the several other ones available in literature are not exhaustive of the many scenarios possible at present level of knowledge.

For the case of WIMP class candidates, it has been considered so far low (of order of few GeV) and high mass (up to many hundreds of GeV) candidates interacting with ordinary matter via: i) mixed SI&SD coupling; ii) dominant SI coupling; iii) dominant SD coupling; iv) preferred SI inelastic scattering. A detailed discussion on the volumes/regions allowed by the DAMA/NaI data for these candidates in some given model frameworks can be found in ref. [3, 4]. This analysis has also been extended in ref. [13] by including the possible effect of the presence of a non thermalized DM particle component in the dark halo due to the Sagittarius Dwarf Elliptical Galaxy, SagDEG. The effect of other possible non-thermalized substructures will be addressed in future.

Among the related theoretical works we just remind for the neutralino case ref. [26].

49

Moreover, other possibilities exist with a phenomenology similar, but not identical as for the WIMP cases: the mirror Dark Matter particles [27], the self-interacting dark matter particles [28], etc. and in principle even whatever particle with suitable characteristics, even not yet foreseen by theories, can be a good candidate as DM in the galactic halo.

In addition, the light ($\simeq$ keV mass) bosonic candidate, either with pseudoscalar or with scalar axion-like coupling, is also a good candidate to account for the observed effect [12]. For this latter candidate, the direct detection process is based on the total conversion in NaI(Tl) crystal of the mass of the absorbed bosonic particle into electromagnetic radiation. Thus, in these processes the target nuclei recoil is negligible and is not involved in the detection process; therefore, signals from these light bosonic DM candidates are detected in DAMA/NaI, but are lost in activities applying rejection procedures of the electromagnetic contribution to the counting rate (such as e.g. Cdms, Edelweiss, Cresst, Warp, Xenon10, etc.) [12]. Despite these particles are unstable, their lifetime can be of cosmological interest and offers valuable candidates for the DM signal, observed in DAMA/NaI [12].

During 2007 three main topics have been addressed:

- the ionization and the excitation of bound atomic electrons induced by the perturbation of the recoiling nucleus after a WIMP elastic scattering (this effect has so far usually been neglected in the field);

- the channeling effect of low energy ions along the crystallographic axes and planes of NaI(Tl) crystals. This existing effect implies a more complex evaluation of the luminosity yield for low energy recoiling Na and I ions;

- the DM candidate particles – foreseen by some extensions of the Standard Model – which can have a dominant coupling with the lepton sector of the ordinary matter. Thus, these candidates can be directly detected only through their interaction with electrons.

Other candidates and astrophysical scenarios will be addressed in near future studies; in particular, the corollary investigation in terms of Light Dark Matter candidates such as keV range sterile neutrino or MeV range Dark Matter is in progress.

1.1 On electromagnetic contributions in WIMP quests

In 2007 it has been investigated the role of the electromagnetic (e.m.) contribution produced in the interaction of the WIMP with target nuclei, named in the following Migdal effect [29, 30], not yet considered in WIMP-nucleus elastic scattering. In fact, a certain quantity of e.m. radiation (made of escaping electron and of X-rays and/or Auger electrons) arises from the rearrangement of the atomic shells by a recoiling atomic nucleus. This radiation is fully contained in a detector of suitable size and because of its e.m. nature, this part of the signal is lost in all those approaches based on rejection procedures of the e.m. component of the measured counting rate. Although quite small, the unquenched nature of this e.m. contribution can have appreciable impact in the DM direct searches

when interpreted in terms of low mass WIMP candidates. Note that in order to point out just the impact of the Migdal effect, the same scenarios as in ref. [3, 4] have been considered without any inclusion of the possible SagDEG contribution. Some examples of the results of the inclusion of the Migdal effect in the WIMP quests of ref. [3, 4] are reported in Fig. 2. An additional allowed region is present in the GeV range. We remind that GeV
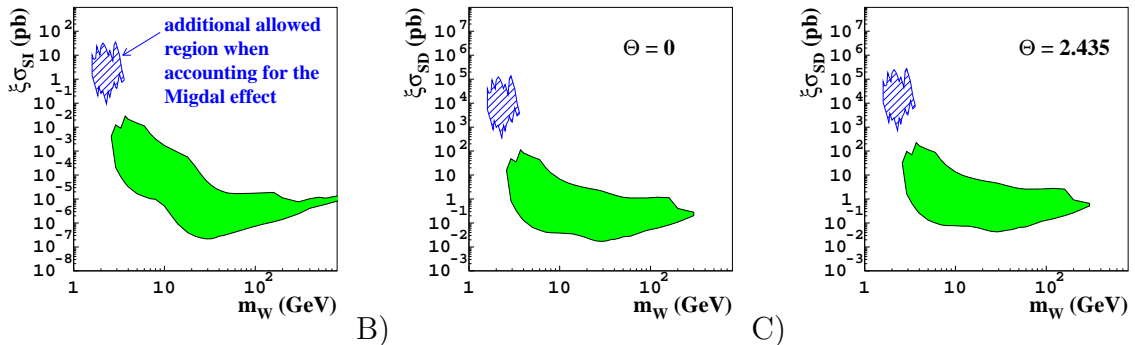

Figure 2: Examples of region/slices allowed in the considered model frameworks for: A) region allowed in the $(\xi\sigma_{SI}, m_W)$ plane in the considered model frameworks for pure SI coupling. B) and C) two slices of the 3-dimensional allowed volume $(\xi\sigma_{SD}, m_W, \theta)$ in the considered model frameworks for pure SD coupling. See text. The hatched regions appear when accounting for the Migdal effect. Inclusion of other contributions and/or of other uncertainties on parameters and models, such as e.g. the SagDEG contribution [13] or more favorable form factors, would further extend the region and increases the sets of the best fit values. For completeness and more see also [3, 4, 12, 13].

mass DM particles are theoretically well motivated and have been widely discussed in literature; they have been proposed in order to offer a mechanism able to account for the Baryon Asymmetry in the Universe and to naturally explain why $\Omega_{DM} \sim 5\Omega_b$. Moreover, it was shown that a GeV mass DM candidate would potentially solve the discrepancies between observations and ΛCDM model on the small scale structure of the Universe. Finally, among the GeV mass WIMP candidates we remind: i) the H dibaryon, already predicted within the Standard Model of particle Physics; ii) the *Darkon*, a real scalar field in an extended Standard Model; iii) the light photino early proposed in models of low-energy supersymmetry; iv) the very light neutralino in Next-to-MSSM; v) the scalar GeV mass DM candidates; vi) the mirror Deuterium in frameworks where mirror matter interactions with ordinary matter are dominated by very heavy particles. For details on the related theoretical and phenomenological arguments refer to the 2007 publication list.

1.2 On possible implications of the channeling effect in NaI(Tl) crystals

In 2007 we have also investigated the implication of the channeling effect in NaI(Tl) crystals. In fact, experimental results have shown that ions and recoiling nuclei move in a crystal in a different way than in amorphous materials. In particular, in the case of motion along crystallographic axes and planes, ions manifest an anomalous deep penetration into the lattice of the crystal and their range become much larger than the maximum they

would have in case of motion in other directions or in amorphous materials. This is due to the fact that a low-energy ion, entering in the lattice into a channel, transfers its energy mainly to electrons rather than to the nuclei and, thus, its quenching factor (namely the ratio between the detected energy in keV electron equivalent [keVee] and the kinetic energy of the recoiling nucleus in keV), q, approaches the unity.

It is worth to note that the results about quenching factor obtained for NaI(Tl) crystals (and in general also for other crystal detectors) using neutron source and published in literature can contain channeled events, but they cannot be singled out. In particular, Fig. 3 shows some examples of neutron calibrations of NaI(Tl) detectors at relatively low recoil energy. There the energy responses of the used NaI(Tl) detectors to Sodium recoils of 10 keV [31] and of 50 keV [32] are reported as solid histograms; the peaks corresponding to the quenched events are well clear. The superimposed continuous curves have been calculated including the channeling effect; the fully channeled events ($q \sim 1$), 6% and 0.15% of the total respectively, are smeared out by the energy resolution and only contribute to the higher energy tails in the energy spectra. Thus, Fig. 3 shows that – owing to the low-
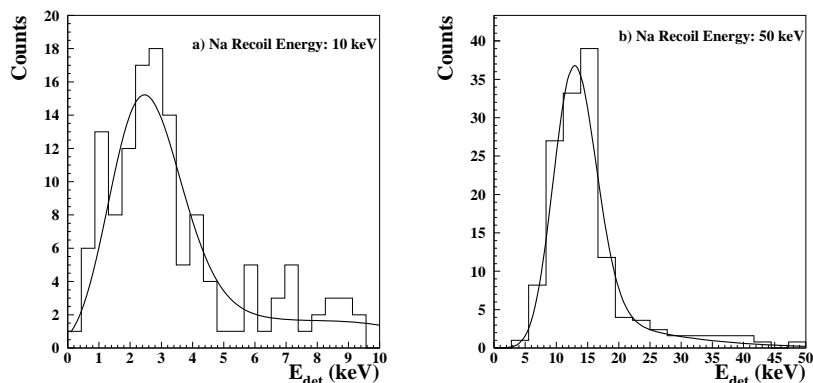

Figure 3: Examples of neutron calibrations of NaI(Tl) detectors at low recoil energy. In particular, the energy responses of NaI(Tl) detectors to Sodium recoils of 10 keV (left panel) [31] and of 50 keV (right panel) [32] are shown; the peaks corresponding to the quenched events are well clear. The superimposed continuous curves have been calculated including the channeling effect; the fully channeled events ($q \sim 1$), 6% and 0.15% of the total respectively, are smeared out by the energy resolution and can just contribute to the higher energy tails in the energy spectra.

statistics of these measurements, to the small effect looked for and to the energy resolution – the channeled events cannot easily be identified in the already-collected neutron data.

The inclusion of this existing effect gives an appreciable impact in corollary analyses in terms of WIMP (or WIMP-like) candidates since the quenching factor is a key quantity to derive the energy of the recoiling nucleus after an elastic scattering. In particular lower cross sections are explorable in given models for WIMP and WIMP-like candidates by crystal scintillators, such as NaI(Tl). Similar situation holds for purely ionization detectors, while a loss of sensitivity is expected when pulse shape discrimination is used in crystal scintillators (such e.g. in KIMS); obviously, no enhancement can be present either in liquid noble gas experiments (DAMA/LXe, WARP, Xenon, ...) or in bolometer experiments; moreover some loss of sensitivity can be expected in bolometer experiments
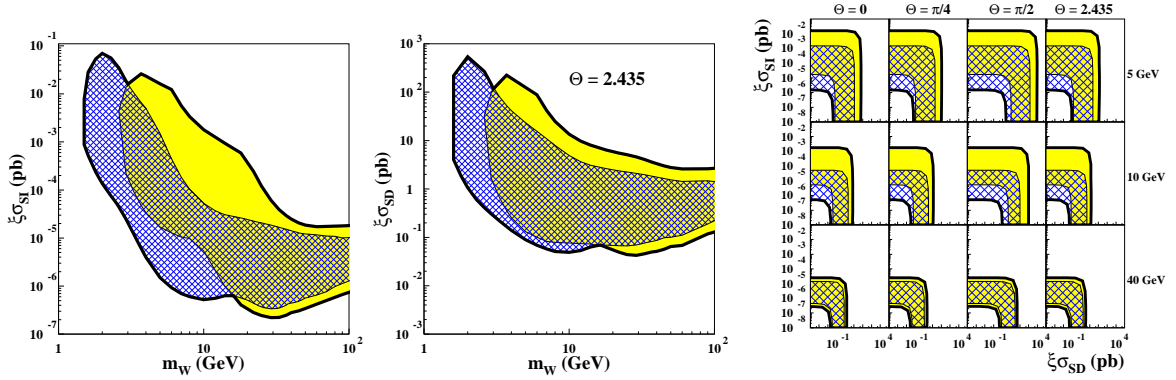
Figure 4: Examples of region/slices allowed in the considered model frameworks for: i) pure SI coupling (*left*); ii) pure SD coupling for the value $\theta = 2.435$ (note that θ can range from 0 to π) (*center*); iii) mixed SI&SD coupling for some mass and θ values (*right*). The dotted regions are obtained in absence of channeling effect, while the dashed ones are obtained when accounting for it. The dark line marks the overall external contours. It is worth to note that the inclusion of other contributions and/or of other uncertainties on parameters and models, such as e.g. possible stream contributions, the Migdal effect or more favorable form factors, different scaling laws, etc., would further extend the region and increases the sets of the best fit values. See the 2007 publication list for more and for details.

when applying discrimination procedures, based either on $q_{ion} << 1$ or on $q_{light} << 1$, since some events (those with $q_{ion} \simeq 1$ or $q_{light} \simeq 1$) are lost.

For details on the related theoretical and phenomenological arguments see the 2007 publication list.

Fig. 4 reports some examples of regions/ volumes allowed by the DAMA/NaI data when the channeling effect has been taken into account. It has been considered cases of a DM particle with pure SI, pure SD and SI&SD coupling in the same model frameworks of ref. [3, 4].

The results further show the role of the existing uncertainties and of correct/complete description and inclusion of all the involved processes (such as also those deriving by e.g. different form factors, different spin factors, different scaling laws, etc.) in the field of DM investigation.

1.3 On electron interacting dark matter

In 2007 it has also been investigated the case of a Dark Matter candidate interacting just on the electrons of the target detector. In fact, some extensions of the Standard Model provide DM candidates which can have a dominant coupling with the lepton sector of the ordinary matter. This is the case suggested for the U boson mediator and can also be the case of some extensions of the Standard Model providing a quark-lepton discrete symmetry $SU(3)_l \times SU(3)_q \times SU(2)_L \times U(1)$. In these latter models, leptons (as well as quarks) have "leptonic colours" and interact through the gauge group $SU(3)_l$, analogously as the QCD colour group $SU(3)_q$. Moreover, let us stress that there are domains in general SUSY parameter space where LSP-electron interaction can dominate LSP-quark one.

These DM candidates can also offer possible sources for the 511 keV positron annihilation gamma's observed from the galactic bulge.

The detection of electron interacting DM (χ^0) is based on the their interaction with electrons in detectors of a suitable experiment; thus, these candidates are lost by experiments based on the rejection of the e.m. component of the counting rate. Generally, the particle-electrons elastic scattering processes have not been taken into account in the DM field since the electron has been assumed at rest and for a particle with velocity $\simeq$ 300 km/s, the released energy would be of the order of few eV, well below the detectable energy in the detectors. However, also an electron bound in an atom at rest can have not negligible momentum and the interaction of DM particles with these high-momentum electrons can give rise to detectable signals. Few examples of the dependence of the maximum released energy in the scattering process, E_+, on the χ^0 mass are given in Fig. 5–*Left* as function of the electron's momentum, p, and of the χ^0 velocities for head-on collisions. The Fig. 5–*Left* also points out that χ^0 particles with m_{χ^0} larger than few GeV can provide sufficient energy to be detected. For details on the related theoretical and phenomenological arguments see the 2007 publication list.
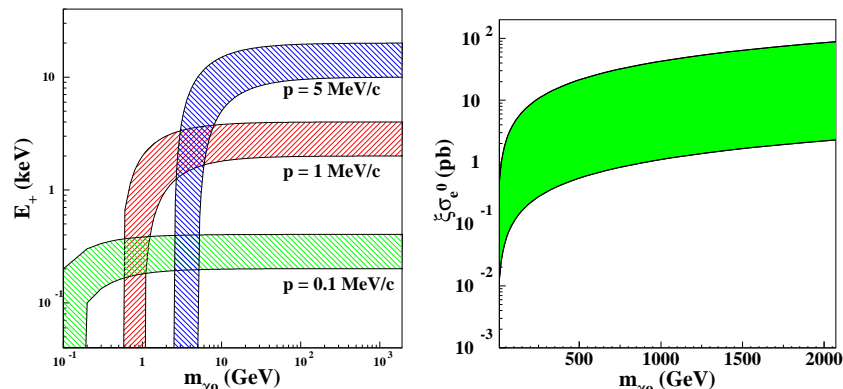

Figure 5: *Left:* Few examples of the dependence of the maximum released energy, E_+, on the χ^0 mass for electron's momenta of 0.1, 1 and 5 MeV/c, for v_{χ^0} ranging in the interval $1 \div 2 \times 10^{-3}c$ and for head-on collisions. *Right:* A case of electron interacting dark matter: DAMA/NaI region allowed in the plane particle mass versus its cross section on the electrons in the considered model frameworks (dashed). The regions enclose configurations corresponding to likelihood function values *distant* more than 4σ from the null hypothesis (absence of modulation). We note that, although the mass region in the plot is up to 2 TeV, χ^0 particles with larger masses are also allowed. For details see the 2007 publication list.

Finally, after the interaction, the final state can consist of a prompt electron and of an ionized or an excited atom providing possible X-rays/Auger electrons; the produced X-rays and electrons of relatively low energy are mostly contained in a detector of a suitable size.

In Fig. 5–*Right* the result of the analysis of the DAMA/NaI annual modulation data in terms of an electron interacting DM particle is reported. In particular, the region allowed in the plane particle mass versus its cross section on the electrons in some scenarios is shown. Note that, although the mass region in the plot is up to 2 TeV, particle candidates with larger masses are also allowed. This result holds for every kind of DM candidate

interacting with electrons and with cross section having a weak dependence on electron momentum and particle velocity.

The result can also give some information on the possible mediator of the DM particle interactions proposed in literature - the U boson - coupled only to the lepton sector of the ordinary matter. In particular, the obtained allowed interval for the mass of U, considering some reasonable hypothesis, is well in agreement with the typical requirements of the phenomenological analyses available in literature. Note that the U boson interpretation is not the unique one since, as mentioned, there are domains in general SUSY parameter space where LSP-electron interaction can dominate LSP-quark one.

1.4   Some comparisons in the field

No experiment is available so far – with the exception of presently running DAMA/LIBRA – whose results can be directly compared in a model independent way with that of DAMA/NaI. Thus, claims for contradictions have intrinsically no scientific meaning. Some discussions can be found e.g. in ref.[3, 4, 13].

In particular, as regards some claimed model-dependent comparisons presented so far we just mention – among the many existing arguments – that the other experiments available so far: i) are insensitive to the annual modulation signature; ii) use different exposed materials; iii) release just a marginal exposure (orders of magnitude lower than the one by DAMA/NaI) after several/many years underground; iv) exploit strong data selection and strong and often unsafe multiple rejection techniques of their huge counting rate, becoming at the same time insensitive to several DM candidates; v) have different sensitivities with respect to DAMA/NaI to many existing physical scenarios and are even blind to some of them; vi) consider a single model fixing all the astrophysical, nuclear and particle Physics assumptions as well as all the theoretical and experimental parameters at a single questionable choice; vii) generally quote in an incorrect/partial/not updated way the implications of the DAMA/NaI result.

Hereafter few considerations will be summarized. For the WIMP case they do not account for the existing uncertainties on the real coupling with ordinary matter, on the spin-dependent and spin-independent form factors and related parameters for each nucleus, on the spin factor used for each nucleus, on the real scaling laws for nuclear cross sections among different target materials, on the experimental and theoretical parameters, on the effect of different halo models and related parameters on the different target materials, etc. Moreover, large differences can be expected in the counting rate among nuclei fully sensitive to the SD interaction (as ^{23}Na and ^{127}I) with respect to nuclei largely insensitive to such a coupling (as e.g ^{nat}Ge, ^{nat}Si, ^{nat}Ar, ^{nat}Ca, ^{nat}W, ^{nat}O) and also when nuclei in principle all sensitive to this coupling but having different unpaired nucleon (e.g. neutron in case of the odd spin nuclei, such as ^{129}Xe, ^{131}Xe, ^{125}Te, ^{73}Ge, ^{29}Si, ^{183}W and proton in the ^{23}Na and ^{127}I). Obviously, when the detection of the DM particles involves electromagnetic signals (see, for example, the cases of the light bosons and of the electron interaction DM particles, but also the electromagnetic contribution in WIMP detection induced by recoiling nuclei, etc.), all the other experiments do lose the signal in their data selection and multiple "rejection" procedures of the electromagnetic contribution to the counting rate.

In addition, some critical points exist in their activities, e.g. regarding their assumed energy threshold, their energy scale determination in the energy range of interest for the investigation of DM candidate particles and their multiple selection procedures, on which their claimed "sensitivities" for a "single" set of assumptions and parameters' values (ignoring both experimental and theoretical uncertainties) are based. In addition, critical items in the used "rejection" procedures are the related stabilities with time and efficiencies, the systematics in the evaluations of the rejection factors (ranging from 10^{-4} to 10^{-8}), the stabilities and monitoring of the spill-out factors, etc.

For completeness, it is also worth to further note that no results obtained with different target material can intrinsically be directly compared even for the same kind of coupling, although apparently all the presentations generally refer to cross section on the nucleon. The situation is much worse than the one in the field of double beta decay experiments when different isotopes are used.

As regards the indirect searches, a comparison would always require the calculation and the consideration of all the possible DM particle configurations in the given particle model, since it does not exist a biunivocal correspondence between the observables in the two kinds of experiments. However, the present positive hints provided by indirect searches are not in conflict with the DAMA/NaI result.

Finally, it is worth to note that – among the many corollary aspects still open – there is f.i. the possibility that the particle dark halo can have more than one component; some example have already been considered in literature.

2 DAMA/LIBRA

In 1996 DAMA proposed to realize a ton set-up and a new R&D project for highly radiopure NaI(Tl) detectors was funded. As a consequence of the results of this second generation R&D, the new experimental set-up DAMA/LIBRA (Large sodium Iodide Bulk for RAre processes) was funded and realized. DAMA/LIBRA has made by $\simeq$250 kg highly radiopure NaI(Tl) crystal scintillators (matrix of twenty-five $\simeq$ 9.70 kg NaI(Tl) crystals). This set-up has replaced the previous DAMA/NaI; the experimental site as well as many components of the installation itself have also been implemented. For example, all the Copper parts have been chemically etched before their installation following a new devoted protocol and all the procedures performed during the dismounting of DAMA/NaI and the installation of DAMA/LIBRA detectors have been carried out in High-Purity Nitrogen atmosphere [33].

DAMA/LIBRA has started operations in March 2003. The main aim of the highly radiopure DAMA/LIBRA set-up is to further investigate the model independent evidence pointed out by DAMA/NaI with increased sensitivity. The larger sensitivity and a suitably larger exposure will also allow to better study some interesting physical and astrophysical aspects as mentioned in LNGS activity report 2006.

During 2007 the data taking has been continued and the analysis of an exposure of about 0.5 tons×year has been almost fully completed in all the aspects as regards the model independent annual modulation signature. The first release of results will occur not later than end of 2008.

The preparation for the DAMA/LIBRA upgrading foreseen in 2008 has been completed.

3   R&D-III towards DAMA/1ton

A third generation R&D effort towards a possible NaI(Tl) ton set-up has been funded by I.N.F.N. and related works are in progress. This new low background NaI(Tl) set-up will act as a "general purpose" experiment (as the previous ones) also allowing to investigate not only other approaches for Dark Matter, but also many other interesting topics in underground Physics having many competitive aspects; among them we remind: 1) well known technology; 2) high radiopurity reachable by material selections and protocols, by chemical/physical purifications, etc.; 3) large mass feasible; 4) high duty cycle; 5) routine calibrations feasible down to keV range in the same conditions as the production runs; 6) well controlled operational conditions and monitoring feasible; 7) absence of microphonic noise; 8) suitable signal/noise discrimination near the energy threshold profiting of the relatively high available number of photoelectrons/keV and of the well different timing structures of the PMT noise pulses (single fast photoelectrons with decay time of order of tens of ns) with respect to the NaI(Tl) scintillation pulses (time distribution with time decay of order of hundreds of ns); 9) high light response, that is keV threshold really reachable; 10) no necessity of re-purification or cooling down/warming up procedures (implying high reproducibility, high stability, etc.); 11) possibility to exploit the granularity of the set-up, an interesting feature for Dark Matter particle investigations and for background recognition; 12) sensitivity to both high (by Iodine target) and low (by Na target) mass WIMP candidates; 13) high sensitivity to the class of WIMP candidates with spin-independent (SI), spin-dependent (SD) and mixed (SI&SD) couplings; 14) high sensitivity to several other existing scenarios (see e.g. [3, 4, 12, 13], the 2007 publication list and in literature) and to many other possible candidates including those producing just electromagnetic radiation in the interaction; 15) possibility to effectively investigate the annual modulation signature in all the needed aspects; 16) "ecologically clean" set-up, thus no safety problems; 17) technique cheaper than every other considered in the field; 18) small underground space needed; 19) pulse shape discrimination feasible at reasonable level when of interest.

During 2007 the activities both on PMTs and crystals have been continued. In particular, two new prototypes are at hand and will be measured at end of 2008/beginning 2009 after the storage underground. The main design of the possible DAMA/1ton has also been defined.

4   DAMA/LXe

We pointed out many years ago (see e.g. ref. [34]) the possible interest in using the liquid Xenon as target-detector material for particle dark matter investigations. Since the end of 80's (former Xelidon experiment of the INFN) we have realized several liquid Xenon (LXe) prototype detectors and, then, we have preliminarily put in measurement the set-up used in the data taking of ref. [35, 36] at LNGS. This set-up (having a Cu

inner vessel filled by $\simeq$ 6.5 kg - i.e. $\simeq$ 2 l - of liquid Xenon) was firstly upgraded at fall 1995 [37, 38, 39, 40, 41]. At that time it used Kr-free Xenon enriched in ^{129}Xe at 99.5%. Then, in 2000 the set-up was deeply modified reaching the configuration of ref. [42] in order to handle also Kr-free Xenon enriched in ^{136}Xe at 68.8%. The main features of the set-up, details on the data acquisition, on the cryogenic and vacuum systems and on the running parameters control can be found in refs. [40, 41, 42, 43, 44]. Investigations on several rare processes have been carried out with time passing in the various configurations [35, 36, 37, 38, 39, 40, 41, 42, 45, 43, 46, 47, 48, 49]. In particular, first and/or competing results have been obtained on some approaches for Dark Matter investigations, on double beta decay modes in ^{136}Xe and ^{134}Xe, on possible charge non-conserving processes, on nucleon, di-nucleon and tri-nucleon decay into invisible channels both in ^{129}Xe and in ^{136}Xe.

On the contrary of the NaI(Tl) case, plans for enlarging the exposed mass have never been considered because of the technical reasons (specific of liquid noble gas detectors and, in particular, of liquid xenon detectors), we pointed out several times in the past (see e.g. [50]) and confirmed by the features of recent detectors; moreover, the extremely expensive cost of Kr-free and enriched Xenon is an additional constraint.

After the forbiddeness of using cryogenic liquids in the underground laboratories, the set-up has taken data just for several months until December 2004; then it has been put in standby waiting for the restart of LNGS cooling water plant and local water refrigeration system.

During 2007 a new chiller has been installed and some upgradings have been carried out. Thus, thanks to the new chiller system and the restoring of the use of water plans deep underground, the DAMA/LXe set-up has restarted the data taking in December 2007.

5   DAMA/R&D

The DAMA/R&D installation is a low-background set-up used for measurements on low background prototype scintillators and PMTs realized in various R&D efforts with industries. It is regularly used to perform small scale experiments also in collaboration with INR Kiev. This set-up has been upgraded several times. The small scale experiments mainly investigate double beta decay modes in various isotopes. Among the obtained results we remind the search for: i) $\beta\beta$ decay modes in ^{136}Ce and in ^{142}Ce [51]; ii) 2EC2ν decay mode in ^{40}Ca [52]; iii) $\beta\beta$ decay modes in ^{46}Ca and in ^{40}Ca [53]; iv) $\beta\beta$ decay modes in ^{106}Cd [54]; v) $\beta\beta$ and β decay modes in ^{48}Ca [55]; vi) 2EC2ν in ^{136}Ce and in ^{138}Ce and α decay in ^{142}Ce [56]; vii) 2β^{+}0ν and ECβ^{+}0ν decay in ^{130}Ba [57]; viii) cluster decay in ^{138}La and ^{139}La [58]; ix) possible CNC decay of ^{139}La into ^{139}Ce [59]. Both the active and the passive source techniques have been exploited as well as – sometimes – the coincidence technique. Fig. 6 summarizes the many results obtained by DAMA in the searches for double beta decay modes.

In 2007 the activity of DAMA/R&D was focused on:

1. Completion of data analysis of CaF$_2$(Eu) experiment, aiming to investigate the rare
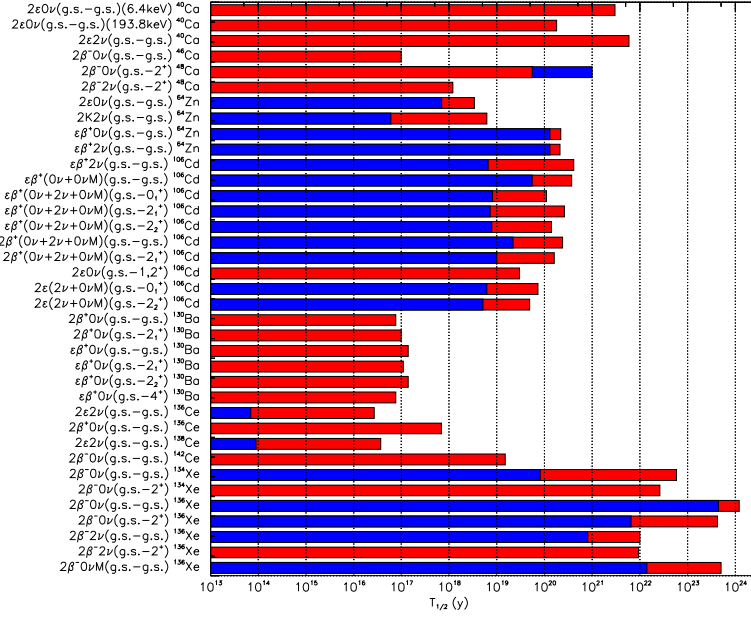
Figure 6: Summary of the $T_{1/2}$ limits obtained by DAMA (light shaded bars) and by previous experiments (dark bars) on various double beta decay processes All limits are at 90% C.L. except the $2\beta^{+}0\nu$ of ^{136}Ce and $2\beta^{+}0\nu$ of ^{142}Ce that are at 68% C.L..

α decay of ^{151}Eu;

2. Conclusion of the data taking of the CdWO$_4$ experiment;

3. New measurements with the ZnWO$_4$ detector with an increased energy scale.

4. New measurements with a larger ZnWO$_4$ crystal of 0.7 kg mass to improve the sensitivity of the experiment to $\varepsilon\beta^{+}$ decay of ^{64}Zn up to the level of 10^{21} yr; the data analysis is in progress.

5. New measurements with a ZnWO$_4$ crystal with much better light output to more carefully explore the low energy part of the ZnWO$_4$ energy spectrum, where the $2\nu 2K$ process in ^{64}Zn is expected. Other future improvements are under studies. In addition, the search for double beta decays of ^{70}Zn, ^{180}W and ^{186}W are planned to be realized as a by-product of the experiment.

6. A new larger BaF$_2$ scintillator is available for new measurements in future.

7. Preparation of a new experiment on double beta decay modes of ^{106}Cd by further purifying and depleting from the ^{113}Cd the $\simeq$ 150 g of enriched Cadmium, made available by the INR group.

5.1 Search for α decay of natural Europium

Both natural Europium isotopes, ^{151}Eu (natural abundance $\delta = 47.81(6)\%$ [60]) and ^{153}Eu ($\delta = 52.19(6)\%$) have a positive energy release to α decay and, thus, they are

potentially α radioactive. Corresponding Q_α values are: $Q_\alpha = 1.964(1)$ MeV for ^{151}Eu and $Q_\alpha = 0.273(4)$ MeV for ^{153}Eu [61]. While the low Q_α for ^{153}Eu gives no hope for experimental observation of its decay due to the very big expected half-life, the estimations of half-life for ^{151}Eu give values within the current experimental sensitivity.

A low background CaF$_2$(Eu) scintillator (BICRON), 3" in diameter by 1" in length (mass of 370 g), doped by Europium was used in the present work. The scintillator was optically coupled by Dow Corning Q2-3067 optical couplant through 10 cm long pure quartz light guide (TETRASIL-B) to low background PMT. The scintillation crystal and light guide were wrapped by PTFE reflection tape. The detector was installed in the DAMA/R&D set-up. An event-by-event data acquisition system records amplitude and arrival time of events. Moreover, the signals from the PMT were also recorded by a 160 MSa/s Transient Digitizer over a time window of 3125 ns.

The precise concentration of Eu in the CaF$_2$(Eu) crystal was determined with the help of the Inductively Coupled Plasma - Mass Spectrometry analysis (ICP-MS, Agilent Technologies model 7500a) to be: $(0.4 \pm 0.1)\%$; the uncertainty on the measurement is relative high because it also takes into account the uncertainty on the sample preparation procedure.

The energy scale and resolution of the CaF$_2$(Eu) detector for γ quanta was measured with ^{22}Na, ^{133}Ba, ^{137}Cs, ^{228}Th and ^{241}Am sources and the response to α particles was studied with a collimated ^{241}Am α source – by using different sets of absorbers – from 1 MeV to 5.25 MeV. The dependence of the α/β ratio (i.e. ratio of energy of α particle measured in γ scale by scintillator to its real energy) versus the energy of α particles has been derived. At the energy of ^{151}Eu α particles, $\alpha/\beta = 0.128(19)$, i.e. the expected energy of ^{151}Eu α peak in gamma scale is 245(36) keV. See details in the 2007 publication list.

The data of the low background measurements with the CaF$_2$(Eu) crystal were analyzed by using several approaches (time-amplitude analysis, pulse shape discrimination, double pulses, ...) and the presence of radioactive isotopes in the crystal has been studied (see Fig. 7–*left*).

To discriminate events from α decays inside the crystal from the $\gamma(\beta)$ background, the optimal filter method was applied and the energy dependence of the shape indicators (SI) was measured. Despite the rather low discrimination, this has allowed to check the nature of the events in the energy distribution (see Fig. 7–*left*).

The low energy part of the energy distribution measured by the CaF$_2$(Eu) crystal scintillator in the low background set-up during 7426 h is shown in Fig. 7–*right*. There is a peculiarity in the spectrum at the energy near 250 keV – in agreement with the expected energy of the ^{151}Eu alpha decay – which gives an indication on the existence of this process. Therefore, the half-life of ^{151}Eu relatively to the α decay to the ground state of ^{147}Pm has been evaluated to be: $T^\alpha_{1/2}(g.s. \rightarrow g.s.) = 5^{+11}_{-3} \times 10^{18}$ yr, or, in a more conservative approach: $T^\alpha_{1/2}(g.s. \rightarrow g.s.) \geq 1.7 \times 10^{18}$ yr at 68% C.L..

The pulse-shape discrimination analysis was used to clarify the nature of events in the $\approx$250 keV peak. As one can see on the bottom curve of Fig. 7–*right*, while this effect is present in the α component of the spectrum, there is no evidence for this peak in the $\gamma(\beta)$ component.

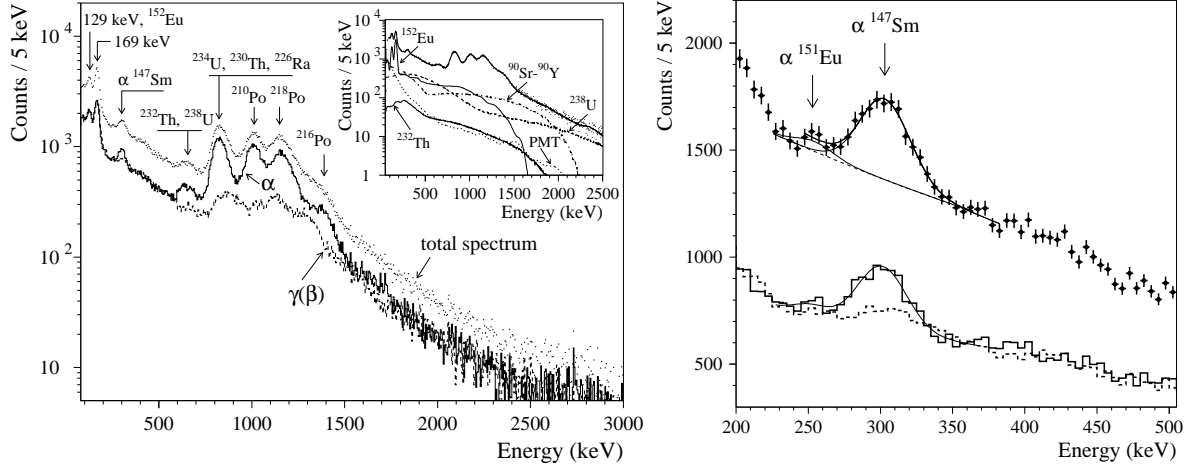In addition, for the decay of ^{151}Eu to the first excited (5/2$^+$,E_{exc}=91 keV) level of

60

Figure 7: *Left:* energy distribution measured by the CaF$_2$(Eu) scintillator during 7426 h in the low background DAMA/R&D set-up (points). The energy distributions, obtained by applying the pulse-shape discrimination technique, are shown by dashed line for $\gamma(\beta)$ component and solid line for α component (see also the 2007 publication list). (Inset) The fit of the total spectrum by simulated models in $90 - 2200$ keV energy interval is shown by solid line. The most important components of $\gamma(\beta)$ background are also shown. *Right top*: low energy part of the energy distribution. The peculiarity on the left of the ^{147}Sm peak can be attributed to the α decay of ^{151}Eu with the half-life $T_{1/2} = 5 \times 10^{18}$ yr. *Right bottom*: spectra obtained by applying the pulse-shape discrimination technique are shown by dashed ($\gamma(\beta)$ component) and solid (α component) lines. See the 2007 publication list for details.

^{147}Pm a limit has also been obtained: $T_{1/2}^{\alpha}(g.s. \to 5/2^+) \geq 6 \times 10^{17}$ yr at 68%C.L..

Theoretical half-lives for ^{151}Eu α decay calculated in different model frameworks are in the range of $(0.3–3.6) \times 10^{18}$ yr; in particular, the measured value of half-life of ^{151}Eu is well in agreement with the calculations of [62]. For details see the 2007 publication list.

5.2 Investigation of β decay of ^{113}Cd

The ^{113}Cd isotope is one of only three nuclei which enables the investigation of fourth-fold forbidden beta decays in a practical way, when rare transitions of this kind are not masked by much more rapid lower orders forbidden or allowed β decays (two other nuclides are ^{50}V and ^{115}In).

A low background CdWO$_4$ crystal scintillator was used to investigate the β decay of ^{113}Cd (half-life value and spectrum shape) with precision better than those of the previous experiments (4–12% uncertainty for $T_{1/2}$ in the recent ones).

The low background CdWO$_4$ crystal scintillator (40 mm in diameter by 43 mm in length; mass of 433.61 g) exploited in the experiment of ref. [63] was used in the present measurements. The crystal was stored in the Solotvina Underground Laboratory for 10 years at a depth of 1000 m w.e. In August 2005, the crystal was transported in a lead container (with walls $\approx$12 cm thick) by surface and immediately placed underground in the Gran Sasso National Laboratories to avoid cosmogenic activation. The crystal was

washed by ultra-pure nitric acid, and vacuum packed to prevent contact with radon from air.

The CdWO$_4$ crystal was fixed inside a cavity $\oslash47 \times 59$ mm in the central part of a polystyrene light-guide, 66 mm in diameter and 312 mm in length. The cavity was filled with high-purity silicon oil. The light-guide was optically connected on opposite sides by Dow Corning Q2-3067 optical couplant to two low radioactive 3" diameter PMTs. The light guide was wrapped by the PTFE reflection tape. The detector was installed deep underground in the low background DAMA/R&D set-up. An event-by-event data acquisition system records amplitude and arrival time of events. Moreover, the sum of the signals from the PMTs was also recorded by a 1 GS/s 8 bit DC270 Transient Digitizer by Acqiris over a time window of 100 μs. Taking into account the slow kinetics of the CdWO$_4$ scintillation decay ($\approx$13 μs), a sampling frequency of 20 MS/s was used during the experiment.

Precise mass spectrometric measurements of the isotopic abundance of the CdWO$_4$ crystal were performed in the Department of Applied Physics of the Curtin University (Perth, Australia) to determine the number of ^{113}Cd nuclei in the crystal. The abundance of ^{113}Cd in the CdWO$_4$ crystal was determined as 12.22(0.04)% (with the relative uncertainty at the 2 sigma level).

After a preliminary data taking for a period of 2554 h in the energy interval up to $\approx$1.7 MeV (Run 1), used to estimate the radioactive contaminations, the experiment was carried out for 2758 h with the upper energy threshold $\approx$0.6 MeV to investigate precisely the β spectrum of ^{113}Cd (Run 2).

The energy scale and resolution of the low background CdWO$_4$ detector for γ quanta were measured with ^{22}Na, ^{133}Ba, ^{137}Cs, ^{228}Th and ^{241}Am sources.

The energy spectrum accumulated in the low background set-up with the CdWO$_4$ detector during Run 2 is presented in Fig. 8–*left*. The counting rate in the spectrum below the energy of $\approx$380 keV is mainly provided by the β decay of ^{113}Cd.

The knowledge of the CdWO$_4$ crystal radioactive contamination is necessary to reconstruct the background in the energy interval of the β spectrum of ^{113}Cd. The time-amplitude analysis, the pulse-shape discrimination between $\beta(\gamma)$ and α particles, the simulation of the measured energy spectrum, and the data of the mass-spectrometry measurements by ICP-MS were used to estimate the radioactive contamination of the CdWO$_4$ detector (see the 2007 publication list).

To calculate the $T_{1/2}$ value, the behaviour of the spectrum at low energies has been determined and the model of the background in the energy interval of the β spectrum was built, as described in the 2007 publication list; the main components of the background are shown in Fig. 8–*left*. The background in the present experiment is only $\approx$1.8% of the β spectrum of ^{113}Cd. The effect to background ratio thus is 56/1, which is the best value among all the experiments where the β decay of ^{113}Cd was studied. The half-life of ^{113}Cd was determined as:

$$T_{1/2} = (8.04 \pm 0.05) \times 10^{15} \text{ yr},$$

with a better accuracy than in other measurements. The statistical error in the present experiment is much lower than systematic one (see the 2007 publication list).
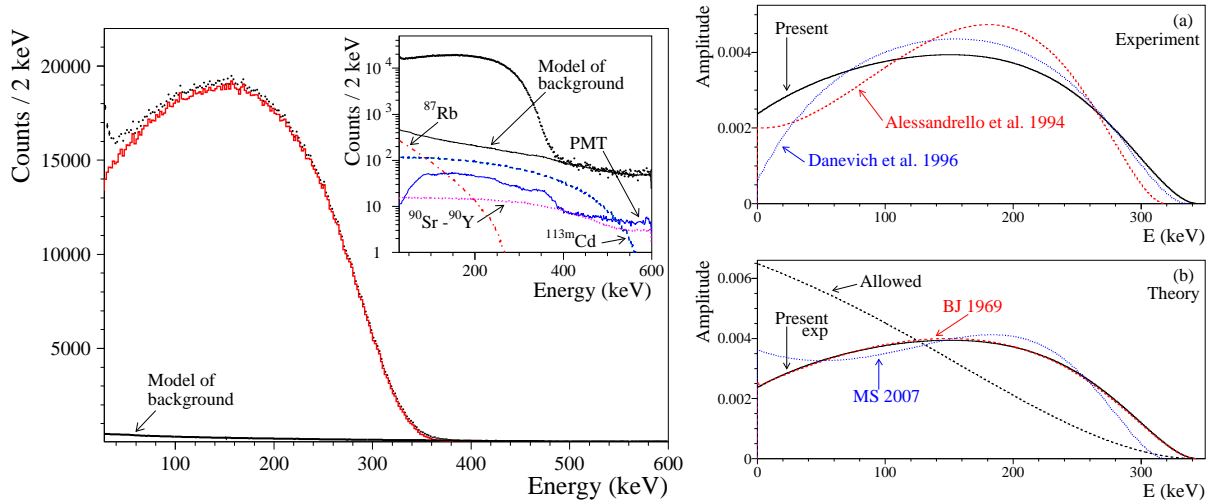
Figure 8: *Left:* energy distribution measured by the CdWO$_4$ scintillator over 2758 h in the low background DAMA/R&D set-up (dots). The energy spectrum is shown by histogram. (Inset) Energy distribution together with the model of the background and its main components. *Right:* energy distributions of electrons in the ^{113}Cd β decay: (a) experimental (without distortion due to finite energy resolution of the detector) and (b) theoretical. All spectra are normalized to area equal 1. Theoretical shape for the 3-fold forbidden unique β decay ($\Delta J^{\Delta\pi} = 4^-$) calculated in accordance with [64] (curve BJ 1969) practically coincides with the experimental spectrum obtained in this work for the ^{113}Cd 4-fold forbidden non-unique β decay ($\Delta J^{\Delta\pi} = 4^+$).

Moreover, the exploited improvements have also allowed the determination of the spectral shape of the ^{113}Cd β decay. A comparison with other experiments and theory (see Fig. 8–*right*) shows that some discrepancies exist; in particular, the theoretical shape for the 3-fold forbidden unique β decay ($\Delta J^{\Delta\pi} = 4^-$) calculated in accordance with [64] (curve BJ 1969) practically coincides with the experimental spectrum obtained in this work for the ^{113}Cd 4-fold forbidden non-unique β decay ($\Delta J^{\Delta\pi} = 4^+$). Further progress in the investigation of ^{113}Cd β decay and more precise measurements of its spectrum shape could be obtained , e.g., with CdWO$_4$ crystals of higher quality and with a further decrease of the background.

5.3 Search for 2β processes in ^{64}Zn with the help of ZnWO$_4$ crystal scintillator

Experimental investigations of the double beta decay are mostly concentrated on $2\beta^-$ decays, processes with emission of two electrons. Searches for $2\beta^+$ decays, processes with emission of two positrons (or $\varepsilon\beta^+$, electron capture with positron emission; or 2ε, capture of two electrons from atomic shells) are important because they could help to distinguish the mechanism of neutrinoless 2β decay (i.e., if it is due either to the non-zero neutrino mass or to the right-handed admixtures in weak interactions) [65].

The ^{64}Zn isotope is one of the few exceptions among $2\beta^+$ nuclei having big natu-

ral isotopic abundance (48.268%); the mass difference between ^{64}Zn and ^{64}Ni nuclei is 1095.7(0.7) keV and, therefore, double electron capture (2ε), and electron capture with emission of positron ($\varepsilon\beta^+$) are energetically allowed.
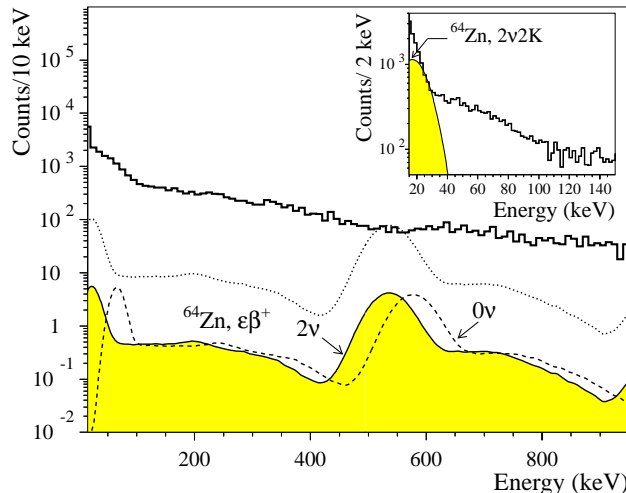

Figure 9: Energy distribution measured by the ZnWO$_4$ scintillation crystal (mass of 117 g, 1902 h of measurements) together with the distributions for $\varepsilon\beta^+$ processes in ^{64}Zn excluded at 90% C.L. Energy spectrum of $2\nu\varepsilon\beta^+$ decay with $T_{1/2} = 1.1 \times 10^{19}$ yr (central value of possible positive indication in Ref. [66]) is also shown by dotted line. *In the Inset:* Low energy part of the spectrum together with the $2\nu2K$ peak of ^{64}Zn with $T_{1/2} = 6.2 \times 10^{18}$ yr excluded at 90% C.L.

A clear, slightly colored ZnWO$_4$ crystal ($20 \times 19 \times 40$ mm, mass of 117 g), produced from monocrystal grown by the Czochralski method, was used for the investigation of double beta processes in ^{64}Zn with higher sensitivity. The ZnWO$_4$ crystal was fixed inside a cavity of $\varnothing 47 \times 59$ mm in central part of a polystyrene light-guide 66 mm in diameter and 312 mm in length. The cavity was filled up with high-purity silicon oil. The light-guide was optically connected on opposite sides by an optical couplant to two low radioactive 3" diameter PMTs. The light-guide was wrapped by the PTFE reflection tape. Such an assembling with use of oil allowed to increase the light transmission from the scintillator to PMTs and to improve the energy resolution of the detector [67].

The detector has been installed deep underground in the low background DAMA/R&D set-up. An event-by-event data acquisition system records the amplitude and the arrival time of events. Moreover, the sum of the signals from the PMTs was also recorded by a 1 GS/s 8 bit DC270 Transient Digitizer by Acqiris over a time window of 100 μs. To allow a good compromise to handle the data files and taking into account the slow scintillation decay of ZnWO$_4$, 20 MS/s sampling frequency was used during the data taking.

The energy scale and resolution of the ZnWO$_4$ detector for γ quanta were measured with ^{22}Na, ^{133}Ba, ^{137}Cs, ^{228}Th and ^{241}Am sources.

The energy spectrum measured with the ZnWO$_4$ crystal over 1902 h in the low background DAMA/R&D set-up, is presented in Fig. 9. Comparing the simulated response functions for different 2β decay processes in ^{64}Zn with the experimental energy distribution accumulated with the ZnWO$_4$ crystal, we did not find the peculiarities expected in

the spectra. Therefore, lower half-life limits can be set for the 2β processes in decay ^{64}Zn $\rightarrow$ ^{64}Ni at 90% C.L. (see Table 1) improving the previous results.

Table 1: Half-life limits on 2β processes in the decay ^{64}Zn $\rightarrow$ ^{64}Ni at 90% C.L.

Decay	Experimental $T_{1/2}$, yr		
channel	Present work	Previous results	
$0\nu\varepsilon\beta^+$	$> 2.2 \times 10^{20}$	$> 2.8 \times 10^{16}$ [68];	$> 2.4 \times 10^{18}$ [69]; $> 1.3 \times 10^{20}$ [70]
$2\nu\varepsilon\beta^+$	$> 2.1 \times 10^{20}$	$= (1.1 \pm 0.9) \times 10^{19}$ [66];	$> 4.3 \times 10^{18}$ [69]; $> 1.3 \times 10^{20}$ [70]
$0\nu2K$	$> 4.0 \times 10^{18}$	$> 1.2 \times 10^{17}$ [71]	
$2\nu2K$	$> 6.2 \times 10^{18}$	$> 6.0 \times 10^{16}$ [68]	
$0\nu2\varepsilon$	$> 3.4 \times 10^{18}$	$> 7.0 \times 10^{17}$ [69]	

The energy distributions expected for the $2\nu\varepsilon\beta^+$ and $0\nu\varepsilon\beta^+$ decay of ^{64}Zn, excluded at 90% C.L., are also shown in Fig. 9. There is also shown the $2\nu\varepsilon\beta^+$ spectrum, which should be expected in our experiment when $T_{1/2} = 1.1 \times 10^{19}$ yr (which is the central value of the possible positive indication by Ref. [66]) is assumed (dotted line). In this case all the events observed in our experiment in the region of the peak at $\simeq$550 keV have to be ascribed only to $2\nu\varepsilon\beta^+$ decay of ^{64}Zn, without contribution from the background; however, such an additional contribution exists, as can be derived considering the left and the right sides of the $\simeq$550 keV peak. Therefore, the positive indication with $T_{1/2} = 1.1 \times 10^{19}$ yr is excluded with high confidence by the present experimental data; this confirms and improves the result recently appeared in [70].

All obtained limits are summarized in Table 1 where results of the most sensitive previous experiments are listed too. The limits established in the present work are more stringent than those previously obtained in [69], and are better (up to four orders of magnitude) than limits from other experiments [66, 68, 70, 71].

New measurements with a larger ZnWO$_4$ crystal (mass of 0.7 kg) and with higher light output are in progress.

6 Measurements with DAMA/Ge and LNGS Ge facility

Various R&D developments to improve low background set-ups and scintillators as well as new developments for higher radiopure PMTs are regularly carried out. The related measurements on samples are usually performed by means of the DAMA low background Ge detector, specially realized with a low Z window. It is operative deep underground in the low background facility of the LNGS since many years. Some selected materials are in addition measured with high sensitivity ICP-MS and mass spectrometers.

During year 2007: i) measurements on samples have regularly been carried out; ii) a paper on the features of a Li$_6$Eu(BO$_3$)$_3$ crystal has been published [72] (see also LNGS report 2006); iii) new measurements with a Molybdenum sample (mass $\simeq$ 1 kg enriched in ^{100}Mo at 99.5%) installed in the 4π low-background HP Ge detectors facility (aiming to investigate the $2\beta2\nu$ decay of ^{100}Mo to the the first excited 0_1^+ level of ^{100}Ru) are continuing [73]; iv) measurements with LiF powders and LiF(W) crystal have been performed aiming mainly to investigate ^{7}Li solar axion; v) new measurements on various subjects for incoming years have been prepared.

7 Conclusions

In conclusion, the main activities during year 2007 can be summarized as in the following:

I. Further corollary investigations on the 6.3 σ C.L. model independent evidence for the presence of a particle Dark Matter component in the galactic halo, obtained by DAMA/NaI over seven annual cycles. Other ones are in progress. These works has also a general interest in the theoretical and phenomenological parts.

II. The new DAMA/LIBRA set-up is regularly in data taking. The analysis of an exposure of about 0.5 tons×year has been almost fully completed in all the aspects as regards the model independent annual modulation signature. DAQ modifications for the new Transient Digitizers, which will be installed during 2008, are at hand.

III. The RD-III towards the possible DAMA/1ton is progressing on the various aspects.

IV. The DAMA/LXe set-up has restarted the data taking.

V. The DAMA/R&D set-up has been used in various small scale experiments; several data analyses are in progress. The data taking is in progress with a new detector and various other relatively small scale experiments are in preparation.

VI. The DAMA/Ge is regularly selecting materials, while various small scale experiments are in progress and in preparation.

8 List of Publications during 2007

1. R. Bernabei, P. Belli, F. Montecchia, F. Nozzoli, F. Cappella, A. Incicchitti, D. Prosperi, R. Cerulli, C.J. Dai, H.L. He, H.H. Kuang, J.M. Ma, X.D. Sheng, Z.P. Ye, Dark Matter search: the status of art, in the volume "Frontier Objects in Astrophysics and Particle Physics", Società Italiana di Fisica (2007), 153.

2. R. Bernabei, P. Belli, F. Montecchia, F. Nozzoli, F. Cappella, A. d'Angelo, A. Incicchitti, D. Prosperi, R. Cerulli, C.J. Dai, H.L. He, H.H. Kuang, J.M. Ma, X.D. Sheng, Z.P. Ye, Future goals for the possible DAMA/1ton, now at R&D stage, in the volume "Frontier Objects in Astrophysics and Particle Physics", Società Italiana di Fisica (2007), 625.

3. R. Bernabei, P. Belli, F. Montecchia, F. Nozzoli, F. Cappella, A. Incicchitti, D. Prosperi, R. Cerulli, C.J. Dai, H.L. He, H.H. Kuang, J.M. Ma, X.D. Sheng, Z.P. Ye, DAMA at Gran Sasso: results and perspectives, in the volume "High energy Physics: ICHEP06", World Scie. (2007) 214.

4. R. Bernabei, P. Belli, F. Montecchia, F. Nozzoli, F. Cappella, A. Incicchitti, D. Prosperi, R. Cerulli, C.J. Dai, H.L. He, H.H. Kuang, J.M. Ma, Z.P. Ye, Dark Matter signals: from underground to space investigation, Nucl. Phys. B (Proc. Suppl.) 166 (2007) 87-95.

5. P. Belli, R. Cerulli, F.A. Danevich, B.V. Grinyov, A. Incicchitti, V.V. Kobychev, M. Laubenstein, S.S. Nagorny, A.V. Tolmachev, V.I. Tretyak, R.P. Yavetskiy, Intrinsic radioactivity of $Li_6Eu(BO_3)_3$ crystal and α decays of Eu, Nucl. Instr. & Meth. A 572 (2007) 734.

6. R. Bernabei, Results on Dark Matter and beta beta decay modes by DAMA at Gran Sasso, in the volume "Neutrinoless Double Beta Decay", Narosa pub. (2007), pagg. 121-134.

7. P. Belli, R. Bernabei, F. Cappella, R. Cerulli, C.J. Dai. F.A. Danevich, A. d'Angelo, A. Incicchitti, V.V. Kobychev, S.S. Nagorny, S. Nisi, F. Nozzoli, D. Prosperi, V.I. Tretyak, S.S. Yurchenko, Search for α decay of natural Europium, Nucl. Phys. A. 789 (2007) 15.

8. R. Bernabei, P. Belli, F. Montecchia, F. Nozzoli, F. Cappella, A. Incicchitti, D. Prosperi, R. Cerulli, C.J. Dai, H.L. He, H.H. Kuang, J.M. Ma, X. D. Sheng, Z.P. Ye, On electromagnetic contributions in WIMP quests, Int. J. Mod. Phys. A 22 (2007) 3155-3168.

9. R. Bernabei, P. Belli, F. Cappella, R. Cerulli, C. J. Dai, H. L. He, A. Incicchitti, H. H. Kuang, J. M. Ma, F. Montecchia, F. Nozzoli, D. Prosperi, X. D. Sheng, Z. P. Ye, On Direct Dark Matter search, in the volume "Science with new generation high energy gamma-ray experiments", INFN Frascati series ed. (2007), pagg. 121-128.

10. R. Bernabei, Windows beyond the Standard Model, to appear in the Proceed. of MEDEX07 Int. Workshop, June 2007, Prague, Czech Rep.

11. R. Bernabei, P. Belli, F. Montecchia, F. Nozzoli, F. Cappella, A. Incicchitti, D. Prosperi, R. Cerulli, C. J. Dai, H. L. He, H. H. Kuang, J. M. Ma, X. H. Ma, X. D. Sheng, Z. P. Ye, R.G. Wang, Y.J. Zhang, Recent DAMA activity on Dark Matter investigation at LNGS, to appear in the Proceed. of the Baksan 07 Int. School, Baksan Valley (Russia), April 2007.

12. R. Bernabei, Physics and Astrophysics with low background scintillators, to appear in Eur. Phys. J. Special Topics (ACFC 2007).

13. P. Belli, R. Bernabei, R.S. Boiko, F. Cappella, S. Castellano, R. Cerulli, C.J. Dai, F.A. Danevich, A. d'Angelo, S. d'Angelo, B.V. Grinyov, A. Incicchitti, V.V. Kobychev, B.N. Kropivyansky, M. Laubenstein, F.Montecchia, P.G. Nagornyi, S.S. Nagorny, S.Nisi, F.Nozzoli, D.V.Poda, D.Prosperi, A.V. Tolmachev, V.I. Tretyak, I.M. Vyshnevskyi, R.P. Yavetskiy, S.S. Yurchenko, Recent investigations on rare processes by DAMA at LNGS, to appear in the Proceed. of the Baksan 07 Int. School, Baksan Valley (Russia), April 2007.

14. R. Bernabei, P. Belli, F. Montecchia, F. Nozzoli, F. Cappella, A. Incicchitti, D.Prosperi, R. Cerulli, C.J. Dai, H.L. He, H.H. Kuang, J.M. Ma, X.D. Sheng, Z.P. Ye, Direct detection of Dark Matter particles in the galactic halo, in the volume "New trends in high energy Physics", ed. JINR-Dubna (2007), 71.

15. P. Belli, R. Bernabei, N. Bukilic, F. Cappella, R. Cerulli, C.J. Dai, F. A. Danevich, J. R. de Laeter, A. Incicchitti, V. V. Kobychev, S. S. Nagorny, S. Nisi, F. Nozzoli, D.V. Poda, D. Prosperi, V. I. Tretyak, S. S. Yurchenko, Investigation of beta decay of ^{113}Cd, Phys. Rev. C 76 (2007) 064603.

16. P. Belli, R. Bernabei, F. Montecchia, F. Nozzoli, F. Cappella, A. Incicchitti, D. Prosperi, R. Cerulli, C.J. Dai, H.L. He, H.H. Kuang, J.M. Ma, X.D. Sheng, Z.P. Ye, Results and developments with large mass highly radiopure NaI(Tl) at LNGS, in the Proceed. of DARK2007 Conf., Sydney (Australia).

17. F. Cappella, From DAMA/NaI to DAMA/LIBRA and beyond, to appear on Il Nuovo Cim. B.

18. P. Belli, R. Bernabei, F. Montecchia, F. Nozzoli, F. Cappella, A. Incicchitti, D. Prosperi, R. Cerulli, C.J. Dai, H.L. He, H.H. Kuang, J.M. Ma, X.D. Sheng, Z.P. Ye, From DAMA/NaI to DAMA/LIBRA and beyond, in the Proceed. of TAUP2007 Conf., Sendai (Japan).

19. P. Belli, Direct searches for Dark Matter particles (above LN$_2$ temperature), in the Proceed. of TAUP2007 Conf., Sendai (Japan).

20. P. Belli, R. Bernabei, F. Montecchia, F. Nozzoli, F. Cappella, A. Incicchitti, D. Prosperi, R. Cerulli, C.J. Dai, H.L. He, H.H. Kuang, J.M. Ma, X.D. Sheng, Z.P. Ye, Investigating the dark halo, in the Procced. of the 13° Lomonosov Conf. on Elementary Particle Physics, Moscow (Russia).

21. P. Belli, R. Bernabei, R.S. Boiko, F. Cappella, R. Cerulli, C.J. Dai, F.A. Danevich, A. d'Angelo, S. d'Angelo, B.V. Grinyov, A. Incicchitti, V.V. Kobychev, B.N. Kropivyansky, M. Laubenstein, P.G. Nagornyi, S.S. Nagorny, S.Nisi, F.Nozzoli, D.V.Poda, D.Prosperi, A.V. Tolmachev, V.I. Tretyak, I.M. Vyshnevskyi, R.P. Yavetskiy, S.S. Yurchenko, Search for rare processes at Gran Sasso, in the Procced. of the 13° Lomonosov Conf. on Elementary Particle Physics, Moscow (Russia).

22. R. Bernabei, P. Belli, F. Montecchia, F. Nozzoli, F. Cappella, A. Incicchitti, D. Prosperi, R. Cerulli, C.J. Dai, H. L. He, H. H. Kuang, J. M. Ma, X. H. Ma, X. D. Sheng, Z. P. Ye, R.G. Wang, Y.J. Zhang, Possible implications of the channeling effect in NaI(Tl) crystals, Eur. Phys. J. C. 53 (2008) 205 (arXiv:0710.0288).

23. P. Belli, R. Bernabei, F. Cappella, R. Cerulli, C.J. Dai, F.A. Danevich, B.V. Grinyov, A. Incicchitti, V.V. Kobychev, L.L. Nagornaya, S.S. Nagorny, F. Nozzoli, D.V. Poda, D. Prosperi, V.I. Tretyak, S.S. Yurchenko, Search for 2β processes in ^{64}Zn with the help of ZnWO$_4$ crystal scintillator, Phys. Lett. B 658 (2008) 193 (ROM2F/2007/13).

24. R. Bernabei, P. Belli, F. Montecchia, F. Nozzoli, F. Cappella, A. Incicchitti, D. Prosperi, R. Cerulli, C. J. Dai, H. L. He, H. H. Kuang, J. M. Ma, X. H. Ma, X. D. Sheng, Z. P. Ye, R.G. Wang, Y.J. Zhang, Investigating electron interacting dark matter, Phys. Rev. D 77 (2008) 023506 (arXiv:0712.0562).

References

[1] R. Bernabei et al., Il Nuovo Cim. A 112 (1999) 545.

[2] R. Bernabei et al., Eur. Phys. J. C18 (2000) 283.

[3] R. Bernabei el al., La Rivista del Nuovo Cimento 26 n.1 (2003) 1-73.

[4] R. Bernabei et al., Int. J. Mod. Phys. D 13 (2004) 2127.

[5] R. Bernabei et al., Phys. Lett. B 424 (1998) 195.

[6] R. Bernabei et al., Phys. Lett. B 450 (1999) 448.

[7] P. Belli et al., Phys. Rev. D 61 (2000) 023512.

[8] R. Bernabei et al., Eur. Phys. J. C 18 (2000) 283.

[9] R. Bernabei et al., Phys. Lett. B 509 (2001) 197.

[10] R. Bernabei et al., Eur. Phys. J. C 23 (2002) 61.

[11] P. Belli et al., Phys. Rev. D 66 (2002) 043503.

[12] R. Bernabei et al., Int. J. Mod. Phys. A 21 (2006) 1445.

[13] R. Bernabei et al., Eur. Phys. J. C. 47 (2006) 263.

[14] K.A. Drukier et al., Phys. Rev. D 33 (1986) 3495.

[15] K. Freese et al., Phys. Rev. D 37 (1988) 3388.

[16] R. Bernabei et al., Phys. Lett. B389 (1996) 757.

[17] R. Bernabei et al., Phys. Lett. B408 (1997) 439.

[18] P. Belli et al., Phys. Lett. B460 (1999) 236.

[19] R. Bernabei et al., Phys. Rev. Lett. 83 (1999) 4918.

[20] P. Belli et al., Phys. Rev. C60 (1999) 065501.

[21] R. Bernabei et al., Il Nuovo Cimento A112 (1999) 1541.

[22] R. Bernabei et al., Phys. Lett. B515 (2001) 6.

[23] F. Cappella et al., Eur. Phys. J.-direct C14 (2002) 1.

[24] R. Bernabei et al., Eur. Phys. J. A 23 (2005) 7.

[25] R. Bernabei et al., Eur. Phys. J. A 24 (2005) 51.

[26] A. Bottino et al., Phys. Rev. D69 (2004) 037302, Phys. Rev. D68 (2003) 043506.

[27] R. Foot, Phys. Rev. D 69 (2004) 036001.

[28] S. Mitra, Phys. Rev. D 71 (2005) 121302.

[29] A. B. Migdal, J. Phys. USSR 4 (1941) 449; G. Baur, F. Rösel and D. Trautmann, J. Phys. B: At. Mol. Phys. 16 (1983) L419.

[30] A. B. Migdal *Qualitative Methods in Quantum Mechanics* 1977 (Reading, Mass: Benjamin) p. 108; L. D. Landau and E. M. Lifshits *Quantum Mechanics, Non-Relativistic Theory* 1977 (Pergamon press), 3rd Ed., p. 149.

[31] H. Chagani et al., arXiv:physics/0611156.

[32] E. Simon et al., Nucl. Instr. & Meth A 507 (2003) 643.

[33] R. Bernabei et al., in the volume Frontier Objects in Astrophysics and Particle Physics, Vol. 90 (2005) 581.

[34] P. Belli et al., Il Nuovo Cim. 103A (1990) 767.

[35] P. Belli et al., Il Nuovo Cim. C 19 (1996) 537.

[36] P. Belli et al., Astrop. Phys. 5 (1996) 217.

[37] P. Belli et al., Phys. Lett. B 387 (1996) 222 and Phys. Lett. B 389 (1996) 783 (erratum).

[38] R. Bernabei et al., New J. Phys. 2 (2000) 15.1.

[39] R. Bernabei et al., Eur. Phys. J.-direct C11 (2001) 1.

[40] R. Bernabei et al., Phys. Lett. B 436 (1998) 379.

[41] R. Bernabei et al., in the volume "Beyond the Desert 2003", Springer (2003) 365.

[42] R. Bernabei et al., Nucl. Instr. & Meth. A482 (2002) 728.

[43] R. Bernabei et al., Phys. Lett. B 546 (2002) 23.

[44] F. Cappella, PhD Thesis, Università di Roma "Tor Vergata", 2005.

[45] R. Bernabei et al., Phys. Lett. B 527 (2002) 182.

[46] P. Belli et al., Phys. Rev. D 61 (2000) 117301.

[47] P. Belli et al., Phys. Lett. B 465 (1999) 315.

[48] R. Bernabei et al., Phys. Lett. B 493 (2000) 12.

[49] R. Bernabei et al., Eur. Phys. J. A 27 s01 (2006) 35.

[50] R. Bernabei et al., in the volume "Cosmology and particle Physics", AIP ed. (2001) 189.

[51] R. Bernabei et al., Il Nuovo Cimento A110 (1997) 189.

[52] R. Bernabei et al., Astrop. Phys. 7 (1997) 73.

[53] P. Belli et al., Nucl. Phys. B563 (1999) 97.

[54] P. Belli et al., Astrop. Phys. 10 (1999) 115.

[55] R. Bernabei et al., Nucl. Phys. A705 (2002) 29.

[56] P. Belli et al., Nucl. Instr. & Meth. A498 (2003) 352.

[57] R. Cerulli et al., Nucl. Instr. & Meth. A525 (2004) 535.

[58] R. Bernabei *et al.*, Nucl. Instr. and Meth. A 555 (2005) 270.

[59] R. Bernabei et al., Ukr. Journal of Physics 51 (2006) 1037.

[60] J.K. Bohlke et al., J. Phys. Chem. Ref. Data 34 (2005) 57.

[61] G. Audi, A.H. Wapstra, C. Thibault, Nucl. Phys. A 729 (2003) 337.

[62] D.N. Poenaru, M. Ivascu, J. Physique 44 (1983) 791; D.N. Poenaru et al., Phys. Rev. C 32 (1985) 2198.

[63] F.A. Danevich et al., Phys. Atom. Nucl. 59 (1996) 1.

[64] H. Behrens, J. Janecke, *Numerical tables for beta-decay and electron capture*, Berlin, Springer-Verlag, 1969.

[65] M. Hirsch et al., Z. Phys. A 347 (1994) 151.

[66] I. Bikit et al., Appl. Radiat. Isot. 46 (1995) 455.

[67] G. Bellini et al., Eur. Phys. J. C 19 (2001) 43.

[68] H. Kiel, D. Munstermann, K. Zuber, Nucl. Phys. A 723 (2003) 499.

[69] F.A. Danevich et al., Nucl. Instr. Meth. A 544 (2005) 553.

[70] H.J. Kim et al., Nucl. Phys. A 793 (2007) 171.

[71] T. Bloxham et al., Phys. Rev. C 76 (2007) 025501.

[72] P. Belli et al., Nucl. Instr. and Meth. A 572 (2007) 734.

[73] P. Belli et al., in the volume *"Current problems in Nuclear Physics and Atomic energy"*, ed. INR-Kiev (2006) 479.

The ICARUS T600 Experiment at Gran Sasso Laboratory

A. Ankowski[o], M. Antonello[c], P. Aprili[d], F. Arneodo[d], M. Armenante[b], B. Baiboussinov[a], M. Baldo Ceolin[a], G. Battistoni[f], P. Benetti[h], E. Calligarich[h], N. Canci[c], F. Carbonara[b], F. Cavanna[c], P. Cennini[j], S. Centro[a], A. Cesana[k,f], D.B. Cline[m], K. Cieślik[n], A.G. Cocco[b], A. Dąbrowska[n], R. Dolfini[h], C. Farnese[a], A. Fava[a], A. Ferrari[j,f], G. Fiorillo[b], S. Galli[c], V. Gallo[b], D. Gibin[a], K. Graczyk[o], A. Guglielmi[a], J. Holeczek[g], C. Juszczak[o], D. Kiełczewska[q], J. Kisiel[g], T. Kozłowski[p], M. Lantz[f], G. Mannocchi[t], M. Markiewicz[n], F. Mauri[h], A. Menegolli[h], G. Meng[a], P. Mijakowski[p], C. Montanari[h], S. Muraro[f], S. Otwinowski[m], O. Palamara[d], T.J. Palczewski[p], L. Periale[t], G. Piano Mortari[c], A. Piazzoli[h], P. Picchi[t], F. Pietropaolo[a], W. Półchłopek[v], M. Posiadala[q], M. Prata[h], P. Przewłocki[p], A. Rappoldi[h], G.L. Raselli[h], E. Rondio[p], M. Rossella[h], C. Rubbia[1][d], P. Sala[f], D. Scannicchio[h], A. Scaramelli[f], E. Segreto[c], F. Sergiampietri[m,w], J. Sobczyk[o], D. Stefan[n], J. Stepaniak[p], R. Sulej[x], M. Szeptycka[p], M. Szarska[n], M. Terrani[k,f], F. Varanini[a], S. Ventura[a], C. Vignoli[h], H. Wang[m], T. Wachala[n], A. Zalewska[n]

[a]*Università di Padova e INFN, Padova, Italy*
[b]*Università Federico II di Napoli e INFN, Napoli, Italy*
[c]*Università dell'Aquila e INFN, L'Aquila, Italy*
[d]*INFN - Laboratori Nazionali del Gran Sasso, Assergi, Italy*
[f]*Università di Milano e INFN, Milano, Italy*
[g]*Institute of Physics, University of Silesia, Katowice, Poland*
[h]*Università di Pavia e INFN, Pavia, Italy*
[j]*CERN, Geneva, Switzerland*
[k]*Politecnico di Milano (CESNEF), Milano, Italy*
[m]*Department of Physics, UCLA, Los Angeles, USA*
[n]*H.Niewodniczański Institute of Nuclear Physics, Kraków, Poland*
[o]*Institute of Theoretical Physics, Wrocław University, Wrocław, Poland*
[p]*A.Sołtan Institute for Nuclear Studies, Warszawa, Poland*
[q]*Institute of Experimental Physics, Warsaw University, Warszawa, Poland*
[r]*Institute of Mechanics and Machine Design, Cracow University of Technology, Kraków, Poland*
[t]*INFN Laboratori Nazionali di Frascati, Frascati, Italy*
[v]*University of Mining and Metallurgy, Kraków, Poland*
[w]*INFN, Pisa, Italy*
[x]*Warsaw University of Technology, Warszawa, Poland*

---

[1]Spokesman of the ICARUS Collaboration

Abstract

The ICARUS T600 detector is the largest liquid Argon TPC ever built, with a size of about 600 tons of fully imaging mass. The design and assembly of the detector relied on industrial support and represents the application of concepts matured in laboratory tests to the kton-scale.

The detector was developed to act as an observatory for astroparticle and neutrino physics at the Gran Sasso Underground Laboratory and a second generation nucleon decay experiment.

The ICARUS T600 was commissioned in 2001 for a technical run performed at surface in the Pavia INFN site. During this period all the detector features were extensively tested with an exposure to cosmic–rays. During 2004 the detector was moved from Pavia to the LNGS underground site. From 2005 to 2007 completion of the cryogenic system and remounting of the detector have been undertaken. The installation phase in the underground site at LNGS (HAll B) is nearly completed and final assembly of the cryogenic plant proceeding smoothly. The final commissioning is expected within 2008.

In this report a short overview of the main steps achieved during the installation phase in 2007 is given.

1   Introduction

The technology of the Liquid Argon Time Projection Chamber (LAr TPC), first proposed by C. Rubbia in 1977 [1], was conceived as a tool for a completely uniform imaging with high accuracy of massive volumes. The operational principle of the LAr TPC is based on the fact that in highly purified LAr ionization tracks can be transported practically undistorted by a uniform electric field over macroscopic distances. Imaging is provided by a suitable set of electrodes (wires) placed at the end of the drift path continuously sensing and recording the signals induced by the drifting electrons.

Non–destructive read–out of ionization electrons by charge induction allows to detect the signal of electrons crossing subsequent wire planes with different orientation. This provides several projective views of the same event, hence allowing space point reconstruction and precise calorimetric measurement.

The LAr TPC was developed in the context of the ICARUS programme and currently finds its application in studies concerning some of the major issues of particle and astroparticle physics:

- the study of neutrino oscillations with the CNGS beam;

- the detection of neutrinos following a Supernova explosion;

- the study of solar and atmospheric neutrino interactions;

- the study of nucleon decay for some channels predicted by GUTs;

After the original proposal, the feasibility of the technology has been first demonstrated by an extensive R&D programme, which included ten years of studies on small LAr volumes and five years of studies with several prototypes of increasing mass[2, 3, 4, 5, 6, 7, 8, 9, 10, 11, 12, 13, 14, 15, 16].

The second step was represented by the construction of the T600 module[17]: a detector employing about 600 tons of liquid Argon to be operated at LNGS. This step–wise strategy allowed to progressively develop the necessary know–how to build a multi–kton liquid Argon detector.

The realization of the T600 detector (from design to construction) lasted about four years and culminated with the full test of the experimental set–up, carried out at surface during 2001. This test demonstrated the maturity of the project. All technical aspects of the system, namely cryogenics, LAr purification, read–out chambers, detection of LAr scintillation light, electronics and DAQ had been tested and performed as expected. Statistically significant samples of cosmic–ray events (long muon tracks, spectacular high–multiplicity muon bundles, electromagnetic and hadronic showers, low energy events) were recorded. The subsequent analysis of these events, carried out in 2002-03, has allowed the development and fine tuning of the off–line tools for the event reconstruction and the extraction of physical quantities. It has also demonstrated the performance of the detector in a quantitative way, issuing in a number of papers published in 2003-04:

- Analysis of the liquid Argon purity in the T600 detector [18];

- Observation of very long ionizing tracks [19];

- Measurement of the muon decay spectrum [20];

- Study of ionization quenching in liquid Argon [21];

A detailed description of the T600 detector and of its technical performance as obtained from the acceptance tests has been reported in a dedicated milestone paper [22] published in 2004.
In 2005, a paper dedicated to the characterization tests at cryogenic temperature of the photomultipliers adopted in ICARUS for the detection of the LAr scintillation light has been published [23].

In 2006 other results, based on the T600 data from the test run, have been finalized from dedicated studies on (1) optimization of methods for particle identification and on (2) LAr scintillation light signal reconstruction and application for deposited energy reconstruction:

- Measurement of through-going particle momentum by means of multiple scattering with the ICARUS T600 TPC [24].

- Analysis of liquid Argon scintillation light signals with the ICARUS T600 Detector [26].

In parallel with data analysis from the T600 test run, another important data set from a 50 liters ICARUS-like chamber located between the CHORUS and NOMAD experiments at the CERN West Area Neutrino Facility (WANF) has been exploited for the study of the LAr-TPC capability to identify and reconstruct low multiplicity neutrino interactions. The results from this work have been also published in 2006:

- Performance of a liquid argon time projection chamber exposed to the CERN West Area Neutrino Facility neutrino beam [25].

In 2007 an accurate study dedicated to the π^0 detection and mass reconstruction, implying the development of electromagnetic shower reconstruction algorithms, has been finalized [27] and it is now being submitted for publication.

On hardware side, the activity has been fully concentrated on the reassembly of the detector and ancillary instrumentation in HAll B at LNGS: the insulation system of the LAr vessels (the two T300 units) has been positioned inside the existing sustaining structure, the two T300 modules have been moved from the temporary location to their final position inside the insulation walls, the cryogenics plant - a structured system composed by the N_2 cooling system and the auxiliary re-liquifaction system - has been progressively delivered and mounted in the underground site, the inner detector (LAr-TPC and auxiliary instrumentation) has been inspected and, finally, positioning and cabling of the electronics racks on top of the T600 Detector has started.
A brief description of the main issues of the remounting phase during 2007 is given below.

2 Installation and Mounting of the Cryogenic system (1)

2.1 *Vessels Insulation panels*

The insulation and cooling of the T300 vessels is provided by pre-assembled insulation panels (sides, front and rear ends) and by a cooling screens with two-phase N_2 circulation. The installation and mounting of these units took place during the first months of 2007, see Fig.1.

2.2 *Positioning of the T300 Vessels*

The two T300 vessels, temporary located downstream in Hall B, have been moved to their final position inside the insulation/cooling system. This operation represented the most crucial and delicate phase (June 2006). In Fig.2, Fig.3 and Fig.4 some picture taken during the translation from the temporary location to the final positioning of the two T300 modules are shown.

After the final position of the two T300 modules has been achieved, the installation of the CF200/CF250 chimneys (~ 100) that cross the insulation top has been performed and the man-holes to access the internal volume and the LAr-TPC detector have been opened, Fig.5.

Figure 1: *Picture of insulation panels [Left] and Cold Screens [Right] during the installation inside the mechanical sustaining structure.*

Figure 2: *Picture taken during the positioning of the first T300 module.*

Figure 3: *Picture taken during the positioning of the second T300 module..*

Figure 4: *Picture taken at positioning completed and after installation of the front insulation panel.*

Figure 5: *Picture taken on the top-side of the* T600 detector.

3 Inspection of the Inner Detector

3.1 *Wire chamber mechanics*

After the preliminary procedures of cleaning all equipments needed for the interventions inside the two half-modules, works began starting from the first of the two T300: the two manholes were opened, installing on the first one the ventilation system and on the second one (opposite side) a small clean room.

Firstly the movement locks applied to the internal mechanics for its safe transportation at LNGS were dismounted. Then the vertical race tracks were dismounted in order to enter inside the two chambers and the footbridges introduced in both chambers. At this point, the inspection of both chambers started by controlling wires integrity and wire position with respect to their spacers: no broken wire was found, whereas two wires of chamber 1, found to be outside their correct position, were brought back in position. The screws for the fastening of the cathode and the race track reference screws were controlled: none of them resulted untied. Finally, the tensioning of the wires in both chambers was controlled on selected samples of wires: 12 horizontal wires and 12 inclined wires per chamber. In the end, all equipments and the footbridges were removed from the first T300, the ventilation system moved to the second T300, and the manholes closed.

The preliminary procedures for the intervention inside the second half-module were the same as for the first one. The inspection also began by controlling wires integrity and wire position with respect to their spacers: no broken wire was found, whereas three horizontal wires of chamber 3, found to be outside their correct position, were brought back in position, as well as two wires of chamber 4. A spacer of two horizontal wires in chamber 3 was found to be broken but, being the spacers coupled, the second spacer bypasses this anomaly. Dust was not so much, less than the one found in the first half-

Figure 6: *Picture of Wire Chamber during the inspection.*

module. The screws for the fastening of the cathode and the race track reference screws were controlled: none of them resulted untied. Finally, the tensioning of the wires in both chambers was controlled on selected samples of wires: 12 horizontal wires and 12 inclined wires per chamber.

In the end, all equipments and the footbridges were removed from the first T300, the ventilation system moved out, and the manholes closed.

The inspection of both T300 half-modules showed that their internal mechanics is able to function again with the same mechanical performance obtained in 2001 Pavia test run.

3.2   HV system

In both T300 half-modules the Cathode and racetrack holding mechanics have been inspected. Field shape resistors 16+16 were mounted onto the race-tracks following the mapping drawn their dismounting. The HV feed-through mounting was the main issue of this phase, see Fig.7. The electrical continuity and the control of the resistive dividers in both half-modules has been then carried out during the mounting of the High Voltage feed-through. The HV system was found in perfect conditions and no effects due to transportation has been detected.

3.3   PMT system

The opening of the two T300 half-modules for the check of the status of the inner detector mechanical structure represented a unique opportunity to have a look of the PMT

Figure 7: *Picture of the HV feed-through during installation.*

detection system after the Pavia test run and the transportation to LNGS. Since it was not yet possible in this phase to feed the PMTs with any power supply, the inspection was focused on the following items: 1) a general survey of the PMT mechanical status; 2) a check of the TPB coatings on the PMT surfaces; 3)a search for waste TPB material inside the cryostats.

For what concerns the PMT mechanical status, the correct positioning of the devices on the mechanical supports behind the wire chambers and the correct positioning of the HV cables were checked. It was also looked for glass breaking on the PMT surfaces and possible disassembling of the supports occurred during the transportation at LNGS laboratory. No abnormal conditions in both cryostats were found, meaning that the Pavia test run and the transportation to LNGS did not affect the mechanical status of the PMTs.

In order to check the present status of the TPB coatings on the PMT surfaces an UV lamp operating at 254 nm was used. The TPB acts as a converter of the UV radiation emitting blue light. In this way it was visually verified the effectiveness of the TPB material after 7 years from the deposition and the uniformity of the coating on the PMT surfaces, particularly in the first T300 cryostat, which was operated with liquid Argon during the Pavia test run.
All the PMTs presented uniform TPB coatings on the surface, certifying the adopted deposition technique to make the coatings adherent and abiding. In Fig.8, as example, a PMT illuminated by the UV lamp is shown. Despite the immersion of the PMT surface in LAr during the Pavia test run, no evidence of deterioration of the TPB coating can be seen. The light interference due to the wires in front of the device is evident. The internal
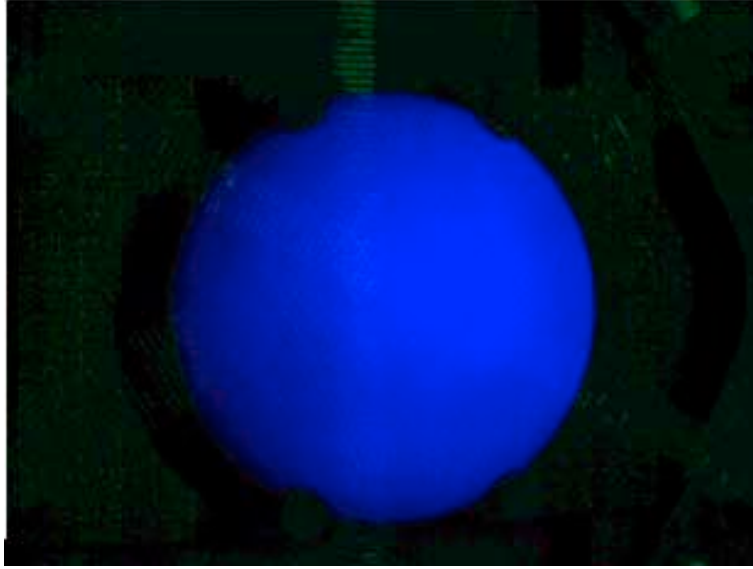
81

Figure 8: *Picture of a PMT illuminated by a UV (254 nm) lamp. Despite the washing of the PMT surface with LAr occurred during the Pavia test run, no evidence of deterioration of the TPB coating can be seen. The light interference due to the wires in front of the device is evident.*

surfaces of the two T300 half-modules were carefully inspected in order to search for possible dispersion of waste TPB material during the transportation at LNGS laboratory or during the LAr fillingempting of the Pavia test run. The inspection was carried out using the same UV lamp adopted for the coating check. No TPB dispersions were found inside the cryostats.

In conclusion, the inspection carried out inside the ICARUS T600 detector showed, though in a qualitative way, the present potential capability of the PMT system to detect the LAr scintillation light.

3.4   LAr Purity Monitors system

The Purity Monitor (PrM) numbering is performed according to Fig.9. In figure, entrance and beam now reads Hall B entrance.

3.4.1   Half-module 1

- PrM 1A & 2A. They are not accessible, being behind the wires. The electrical integrity of the resistive divider has been checked. Cables and fibers have been extracted from the chimney. PrM 1A has the fiber broken at the level of the external flange. Replacement is impossibile, an optical connector will be put on the fibers tip.
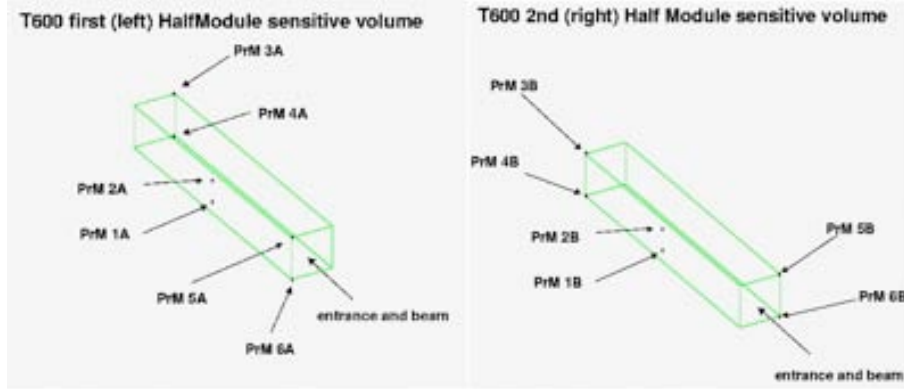
82

Figure 9: *ICARUS T600 PrMs numbering.*

- PrM 3A: a visual control after removal of the Faraday cage has been carried out. Grids and Resistors are fine. The photocathode (CdZnTe) has been replaced with sample GaAs3, tested beforehand (2.3V at 100V/cm). The Faraday cage cap has been re-made and replaced. Cables and fibers have been extracted.

- PrM 4A: visual check (w/o removing the cage) was fine. Resistors were also fine. Photocathode (CdZnTe) has been replaced with sample GaAs4. The cap of the Faraday cage hs been replaced. Cables and fiber have been extracted.

- PrM 5A: visual check was fine (removing cage). Grids, cables, electrodes, were also fine. The photocathode has been replaced with sample GaAs1. Cables and fiber have been extracted. The fiber is broken (that means shortened). We may consider to replace it if there is still time to enter the cryostat at the end of August, or else put a connector at its tip.

- PrM 6A: visual check of grids, electrodes, cables were fine. Some resistors were about to exit from their sockets, and one was actually broken. They have been fixed. Cables and fiber have been extracted.

One of the PrM has been shortened (20 cm to 4 cm drift) to provide sensitivity for low lifetimes (5-30microsec.), expected during LAr filling.

3.4.2 *Half-module 2*

- PrM 1B&2B: cables and fibers have been extracted.

- PrM 3B&4B Visual check: fine. Cables and fiber have been extracted.

- PrM 5B: Visual check, fine. Cables and fiber have been extracted.

- PrM 6B: Visual check fine. Photocathode has been replaced with sample GaAs5. Cables and fiber have been extracted.

3.5 *LAr point-like level meters (new installation)*

New, point-like resistive level meters were prepared and installed inside the two T300 half-modules in order to measure the level of the liquid Argon inside the detector at regime. The sensors are made of carbon resistors, whose resistivity changes significantly passing from cryogenic liquid to gas, electrically connected with RG 316 coaxial cables for the i/o signal. The measurement is carried out by applying a voltage to the resistor through the cable and reading back the current flowing inside it. A test with nitrogen showed that the current flowing inside the resistor placed in nitrogen vapours at 1.5 cm from the liquid nitrogen level is larger by the 20% at least than the current flowing in the situation with the resistor completely immersed in the liquid. 40 level meters were realized, to be placed at group of five at the four corners of each of the two T300 half-modules.
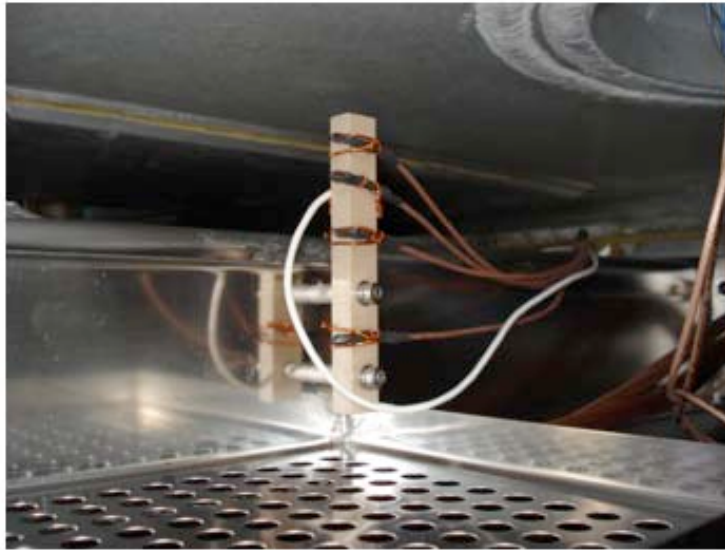
Figure 10: *Peek support with the five resistive level meters inside the first T300 half-module. Cables going to the way-out chimney are visible.*

Fig.10 shows one of the Peek supports with the five resistive sensors in their final position inside the first T300 half-module.

4 Installation and Mounting of the Cryogenic system (2)

After survey of the inner detector, the completion of the cryogenic system became the main issue of activity. The top side of the cryostat has been assembled with the insulation panels and the mechanical structure completed, Fig.11. The last (major) component of the cryogenic plant is represented by the Nitrogen re-liquefier system, Fig.12. This has been delivered at LNGS across the end of 2007. The assembly of this system and the connection to the cryostat through a dedicated piping system represents the last issue

Figure 11: *Top side of the* T600 *after positioning of the insulation panels..*

before commissioning. Completion of this last assembly phase is expected within the first months of 2008.

Figure 12: *Components of the Nitrogen re-liquefier system.*

5 Conclusions

The ICARUS T600 detector, a large–mass Liquid Argon TPC, is meant to be the basic unit for a multi-kton astroparticle observatory and neutrino detector to be installed in the underground Gran Sasso Laboratory.

An extended technical run with the T600 detector, performed at surface in the Pavia INFN site during 2001, has firmly demonstrated that it is feasible to master all technical issues related to the construction and operation of a large size LAr TPC, within and sometimes beyond the design specifications.

The design, the description of the basic components, assembly, start–up and test-run procedures of the detector have been published, as well as the demonstration of the off–line event reconstruction capabilities.

The detector space and energy resolution, particle identification and full events reconstruction have been also the subjects of several analyses published during the last three years.

The T600 detector has been transported from Pavia to the INFN Gran Sasso Underground Laboratory in 2004. The installation of the ancillary infrastructures in the LNGS Hall B represented the main hardware activity in 2005-06. The re-assembly of the detector components was the main goal of the activity during 2007 and it is here briefly summarized.

References

[1] C. Rubbia, *The Liquid-Argon Time Projection Chamber: A New Concept For Neutrino Detector*, CERN–EP/77–08, (1977).

[2] P. Benetti *et al.* [ICARUS Collaboration], *A 3 Ton Liquid Argon Time Projection Chamber*, Nucl. Instrum. Meth. A **332**, (1993) 395.

[3] P. Cennini *et al.* [ICARUS Collaboration], *Performance Of A 3 Ton Liquid Argon Time Projection Chamber*, Nucl. Instrum. Meth. A **345**, (1994) 230.

[4] F. Arneodo *et al.* [ICARUS Collaboration], *The ICARUS 50 l LAr TPC in the CERN neutrino beam*, arXiv:hep-ex/9812006.

[5] F. Arneodo *et al.* [ICARUS Collaboration], *First Observation Of 140-Cm Drift Ionizing Tracks In The Icarus Liquid-Argon Tpc*, Nucl. Instrum. Meth. A **449**, (2000) 36.

[6] F. Arneodo *et al.* [ICARUS Collaboration], *Determination Of Through-Going Tracks' Direction By Means Of Delta-Rays In The Icarus Liquid Argon Time Projection Chamber*, Nucl. Instrum. Meth. A **449**, (2000) 42.

[7] P. Cennini *et al.* [ICARUS Collaboration], *Detection Of Scintillation Light In Coincidence With Ionizing Tracks In A Liquid Argon Time Projection Chamber*, Nucl. Instrum. Meth. A **432**, (1999) 240.

[8] F. Arneodo *et al.* [ICARUS Collaboration], *Performance Evaluation Of A Hit Finding Algorithm For The Icarus Detector*, Nucl. Instrum. Meth. A **412**, (1998) 440.

[9] P. Cennini *et al.* [ICARUS Collaboration], *A Neural Network Approach For The Tpc Signal Processing*, Nucl. Instrum. Meth. A **356**, (1995) 507.

[10] P. Cennini *et al.* [ICARUS Collaboration], *Improving The Performance Of The Liquid Argon Tpc By Doping With Tetramethyl Germanium*, Nucl. Instrum. Meth. A **355**, (1995) 660.

[11] P. Benetti *et al.* [ICARUS Collaboration], *A 3D Image Chamber For The Lar Tpc On Multilayer Printed Circuit Board*, Nucl. Instrum. Meth. A **346**, (1994) 550.

[12] P. Benetti *et al.* [ICARUS Collaboration], *Argon Purification In The Liquid Phase*, Nucl. Instrum. Meth. A **333**, (1993) 567.

[13] A. Bettini *et al.* [ICARUS Collaboration], *A Study Of The Factors Affecting The Electron Lifetime In Ultrapure Liquid Argon*, Nucl. Instrum. Meth. A **305**, (1991) 177.

[14] S. Bonetti *et al.* [ICARUS Collaboration], *A Study Of The Electron Image Due To Ionizing Events In A Two-Dimensional Liquid Argon Tpc With A 24-Cm Drift Gap*, Nucl. Instrum. Meth. A **286**, (1990) 135.

[15] F. Arneodo *et al.* [ICARUS Collaboration], *Performance Of The 10 m^3 Icarus Liquid Argon Prototype*, Nucl. Instrum. Meth. A **498**, (2003) 293.

[16] F. Arneodo *et al.* [ICARUS Collaboration], *Detection Of Cerenkov Light Emission In Liquid Argon*, Nucl. Instrum. Meth. A **516** (2004), 348.

[17] ICARUS Collaboration, *A First 600 Ton ICARUS Detector Installed At The Gran Sasso Laboratory*, Addendum to Proposal by the ICARUS Collaboration, LNGS–95/10, (1995).

[18] S. Amoruso *et al.* [ICARUS Collaboration], *Analysis Of The Liquid Argon Purity In The ICARUS T600 TPC*, Nucl. Inst. Meth., A **516**, (2004) 68.

[19] F. Arneodo *et al.* [ICARUS Collaboration], *Observation Of Long Ionizing Tracks With The ICARUS T600 First Half–Module*, Nucl. Inst. Meth., A **508**, (2003) 287.

[20] S. Amoruso *et al.* [ICARUS Collaboration], *Measurement Of The Muon Decay Spectrum With The ICARUS T600 Liquid Argon TPC*, Eur. Phys. J., C 33 (2004) 233.

[21] S. Amoruso *et al.* [ICARUS Collaboration], *Study Of The Electron Recombination In Liquid Argon With The ICARUS TPC*, Nucl. Inst. Meth., A 523 (2004) 275.

[22] S. Amerio *et al.* [ICARUS Collaboration], *Design, construction and tests of the ICARUS T600 detector*, Nucl. Inst. Meth., A 527 (2004) 329.

[23] A. Ankowski *et al.*, [ICARUS Collaboration], *Characterization of ETL 9357 FLA Photomultiplier Tubes for cryogenic temperature applications*, Nucl. Inst. and Meth. A 556 (2005) 146.

[24] A. Ankowski *et al.*, [ICARUS Collaboration], *Measurement of through-going particle momentum by means of multiple scattering with the ICARUS T600 TPC*, Eur. Phys. J. C 48 (2006), 667.

[25] F. Arneodo *et al.*, [ICARUS-Milano Collaboration], *Performance of a liquid argon time projection chamber exposed to the CERN West Area Neutrino Facility neutrino beam*, Physical Review D (2006) (Vol. 74, No. 11).

[26] M. Antonello *et al.*, *Analysis of Liquid Argon Scintillation Light Signals with the ICARUS T600 Detector*, ICARUS-TM/06-03 (to be published on NIM A).

[27] R. Brunetti *et al.*, *Detection and reconstruction of π^0 mesons with the ICARUS T600 liquid argon TPC*, ICARUS-TM/07-01 (to be published).

[28] F.Arneodo *et al.*, [ICARUS Collaboration], *The ICARUS Experiment: a Second Generation Proton Decay and Neutrino Observatory at The Gran Sasso Laboratory*, LNGS-P28, 2001, LNGS-EXP13/89 add. 1/01.

LUNA. Laboratory for Underground Nuclear Astrophysics

D. Bemmerer[a], R. Bonetti[b], C. Broggini[c], F. Confortola[d], P. Corvisiero[d],
H. Costantini[d], Z. Elekes[e], A. Formicola[f], Zs. Fülöp[e], G. Gervino[g], A. Guglielmetti[b],
C. Gustavino[f], Gy. Gyürky[e], G. Imbriani[h], M. Junker[f], A. Lemut[d], B. Limata[h],
M. Marta[a], C. Mazzocchi[b], R. Menegazzo[c], P. Prati[d], V. Roca[h], C. Rolfs[i], C. Rossi
Alvarez[c], E. Somorjai[e], O. Straniero[j], F. Strieder[i], F. Terrasi[k], H.P. Trautvetter[i]

[a]Forschungszentrum Dresden-Rossendorf, Dresden, Germany
[b]Università di Milano and INFN, Milano, Italy
[c]INFN, Padova, Italy
[d]Università di Genova and INFN, Genova, Italy
[e]Institute of Nuclear Research (ATOMKI), Debrecen, Hungary
[f]INFN, Laboratori Nazionali del Gran Sasso (LNGS), Assergi (AQ), Italy
[g]Università di Torino and INFN, Torino, Italy
[h]Università di Napoli "Federico II", and INFN, Napoli, Italy
[i]Institut für Experimentalphysik III, Ruhr-Universität Bochum, Bochum, Germany
[j]Osservatorio Astronomico di Collurania, Teramo, and INFN Napoli, Italy
[k]Seconda Universitá di Napoli, Caserta and INFN, Napoli, Italy

Abstract

The principal goal of the LUNA Collaboration is the measurement of fusion cross sections relevant for stelar nuclear synthesis. In the course of the year 2007 measurements on several reations have been performed: ^{14}N(p,γ)^{15}O, ^{25}Mg(p,γ)^{26}Al and ^{15}N(p,γ)^{16}O.

1   Introduction

Accurate knowledge of thermonuclear reaction rates is important [1, 2] in understanding the generation of energy, the luminosity of neutrinos, and the synthesis of elements in stars. Due to the Coulomb barrier (height E_c) of the entrance channel, the reaction cross section $\sigma(E)$ drops nearly exponentially with decreasing energy E. Thus it becomes increasingly difficult to measure $\sigma(E)$ and to deduce the astrophysical $S(E)$ factor defined by the equation [2]

$$\sigma(E) = \frac{S(E)}{E} \, exp(-2\,\pi\,\eta), \qquad (1)$$

with the Sommerfeld parameter given by $2\,\pi\,\eta = 31.29\,Z_1\,Z_2(\mu/E)^{1/2}$. The quantities Z_1 and Z_2 are the nuclear charges of the interacting particles in the entrance channel, μ is the reduced mass (in units of amu), and E is the center-of-mass energy (in units of keV). The thermal energy region in stars is determined by the Gamow energy window $E_0 \pm \delta E_0$ (the Gamow peak) for a given stellar temperature and lies far below the height of the Coulomb barrier, approximately at $E_0/E_c = 0.01$. Consequently the observed $\sigma(E)$ data at higher energies often have to be extrapolated to thermal energies. The extrapolations are generally done using the R-matrix formalism and require high quality data over a wide energy range reaching as close as possible to the Gamow peak. But still such an extrapolation into the unknown can lead to considerable uncertainties and data measured inside the Gamow peak are preferred.

The low-energy studies of thermonuclear reactions in a laboratory at the earth's surface are hampered predominantly by the effects of cosmic rays in the detectors. Passive shielding around the detectors provides a reduction of gammas and neutrons from the environment, but it produces at the same time an increase of gammas and neutrons due to the cosmic-ray interactions in the shield itself. A 4π active shielding can only partially reduce the problem of cosmic-ray background. An excellent solution is to install an accelerator facility in a laboratory deep underground [3]. This approach has been persued by the LUNA–collaboration installing a 400 kV accelerator [4] in the underground laboratories of LNGS.

2 ^{14}N(p,γ)^{15}O ground state capture studied with a Clover detector

The rate of the hydrogen-burning carbon-nitrogen-oxygen (CNO) cycle is controlled by the slowest process, the ^{14}N(p,γ)^{15}O reaction. A recent LUNA study [5, 6] measured a cross section at low energy that was only half as large as previously [7] believed. This finding [5, 6] was later confirmed in an independent study [8]. These two recent studies [5, 6, 8] show good agreement in the experimental data. Their extrapolations in the R-matrix framework, however, disagree on the precise value of the partial cross section for capture to the ground state in ^{15}O. This discrepancy [5, 8] has 15% effect on the total cross section and dominates the uncertainty in the extrapolated rate of the CNO cycle in the sun.

Precise data on the solar CNO rate are now necessary in order to directly measure the metallicity at the center of the sun [9] using the expected CNO neutrino data from the BOREXINO detector.

Solid TiN targets have been irradiated at the LUNA 400 kV accelerator. The bombarding energies were chosen in the range $E_p = 360 - 400$ keV, an energy window that is sensitive to the low-energy extrapolation of the astrophysical S-factor [10]. In order to minimize the uncertainties in the experimental data, a Eurisys Clover-BGO γ-ray detection system [11] has been used (fig. 1). The true coincidence summing-in correction has
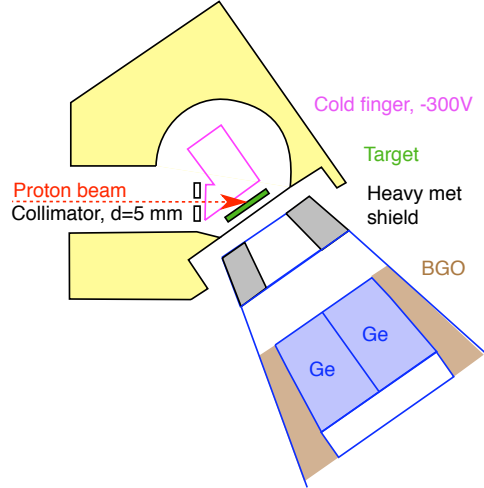
Figure 1: Schematic view of the experimental setup. Two of the four segments of the Eurisys Clover detector are shown.

been reduced from more than 200% [5, 8] to 43% (7% for the singles mode).

Data acquisition issues in the two Ortec 919E multiplexed ADC units have been studied extensively for *singles* (4 Ge crystals acquired independently and off-line gain matched and summed) and *add-back* mode (hardware sum of the 4 analog signals from the crystals, to give one spectrum), using radioactive sources and in-beam runs on resonance.

The γ-ray detection efficiency curve has been established for the low energy part with calibrated radioactive sources and extended to high energy considering the 1:1 ratio of the isotropically distributed γ-ray cascades from the resonance at E = 259 keV. ^{137}Cs and ^{60}Co sources were placed at the target position and the full energy peak efficiencies have been determined. Then the ratio between primary and secondary emission peaks of the cascades through 6792 and 6172 keV energy levels observed in on-resonance spectra have been used to obtain two more efficiencies at higher energy. The five points (sources and secondary γ-rays on resonance) have been fitted with a quadratic double logarithmic curve both for singles and add-back mode (fig. 2). As a check, also the ratio of the 5181 keV cascade γ-rays has been calculated and has been found to be in agreement with the obtained curves within 1%.

The effective energy has been determined directly from the γ-ray spectra considering the non resonant part of the 6792 keV primary emission and the ground state γ-ray. A straight-line background has been subtracted from the region of interest and an average has been calculated on the energies weighted for the counts in the corresponding channel. Recoil and Doppler effect have been considered and the position of the resonant peak has been checked to avoid any possible small shifts due to the energy calibration procedure. Slightly different values of effective energy for 6792 and ground state transitions have been obtained, as expected based on the different slope of the previous [5, 6, 8] R-matrix curves.

The first part of the data analysis concentrated on cross section ratios, with the cross section for capture to the ground state in ^{15}O measured relative to the cross section for capture to the 6792 keV level in ^{15}O. This analysis is now complete and a preliminary
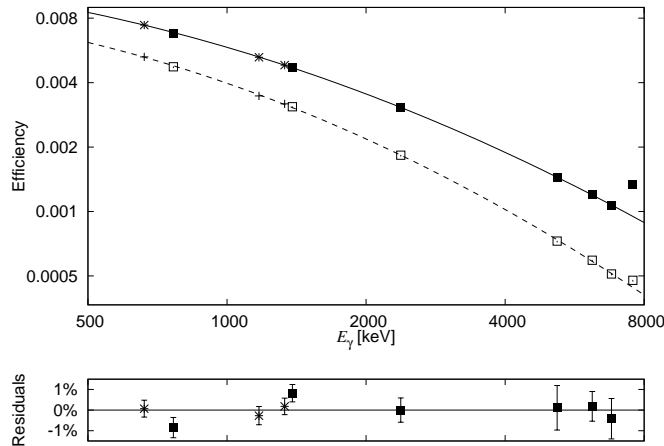
Figure 2: Top: γ-ray detection efficiency. Asterisks (crosses), data with radioactive sources for addback (singles) mode. Squares, in-beam data. Solid (dashed) curve, polynomial fit for addback (singles) mode. Bottom: Residual of the data relative to the fit for the addback mode. Error bars reflect the statistical uncertainty. The 43% (7%) summing effect on the ground state capture line in addback (singles) mode is visible.

summary has been presented [12]. An absolute cross section analysis and full R-matrix fit procedure is still underway.

3 ^{25}Mg(p,γ)^{26}Al

The reaction ^{25}Mg(p,γ)^{26}Al (Q = 6.3 MeV) is the slowest reaction of the Mg–Al cycle [2]. The β^+ decay of ^{26}Al$_{gs}$ to the exited state of ^{26}Mg gives rise to a 1.8 MeV γ–ray (Figure 3), one of the most important lines for γ–astronomy [13] as it can be observed directly with the COMPTEL [15] and INTEGRAL [16] instruments. In addition ^{26}Mg (extinct ^{26}Al) has been found in carbonaceous meteorites. [14]. The observation of this cosmic radioactivity with a lifetime considerably shorter than the age of the Galaxy shows clearly that the ^{26}Al nucleosynthesis is still active today even though the site for the ^{26}Al production has not been identified yet. Solving this puzzle requires more precise date for the ^{25}Mg(p,γ)^{26}Al reaction.

The aim of the experiment carried out by the LUNA Collaboration is to measure directly the strength of the resonances of particular relevance. It must be noted that in case of a strong resonance at low energies the Gamow peak is determined by the area of the resonance itsself. The resonances at 189 and at 89 keV in ^{25}Mg(p,γ)^{26}Al are examples of such a situations and also the resonance at 125 keV may be of interest, provided it is sufficiently strong. The existence of all resonances is confirmed by indirect studies. The excited states in ^{26}Al down to 6496 keV, corresponding to the resonance 189 keV in ^{25}Mg(p,γ)^{26}Al, have been studied directly and indirectly [17, 18, 19, 20] while the strength the resonances at 125 and 89 keV resonance have been determined only indirectly as, due to cosmic ray background, measurements of these important resonances have proven to be very difficult or even impossible in a laboratory above ground [13].
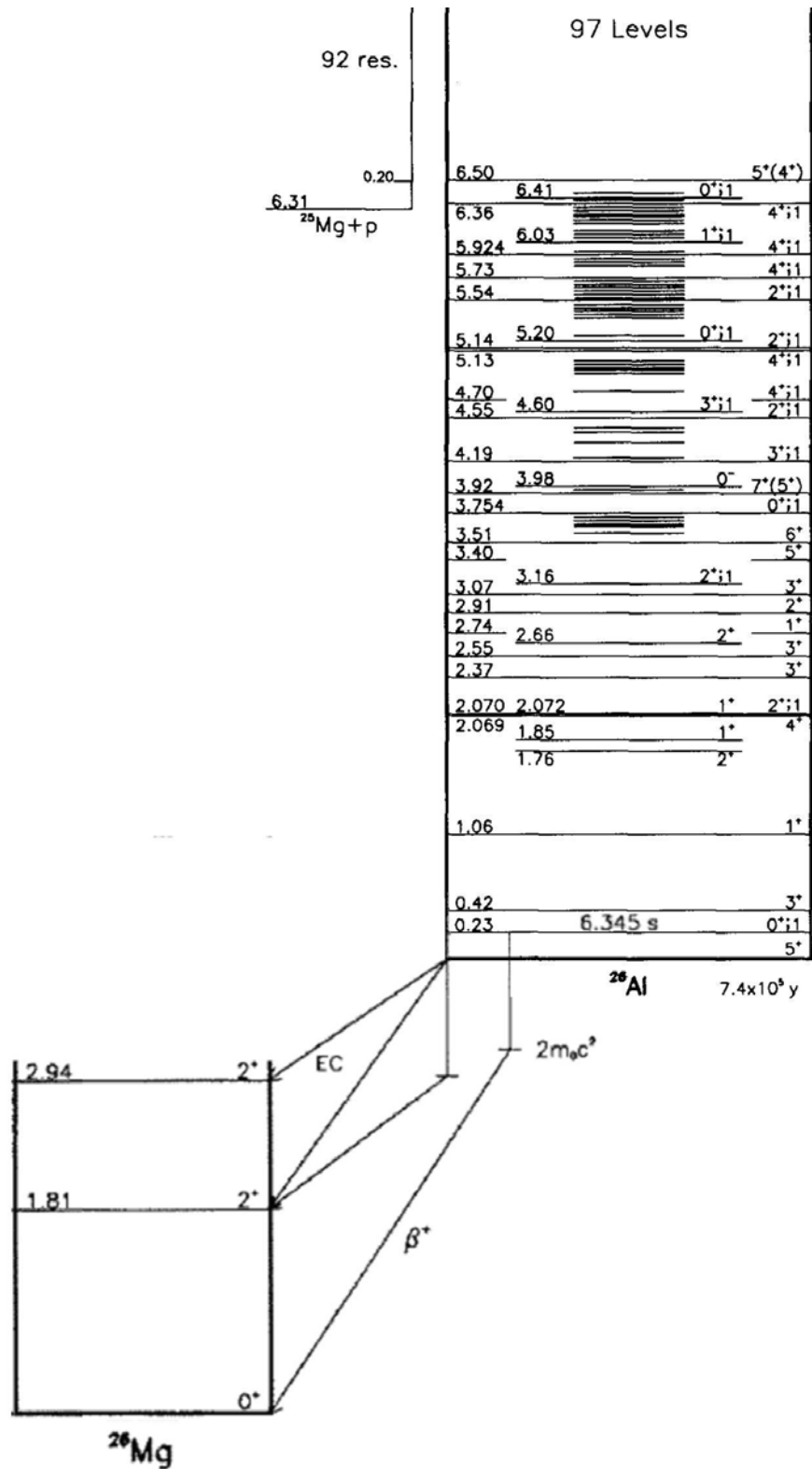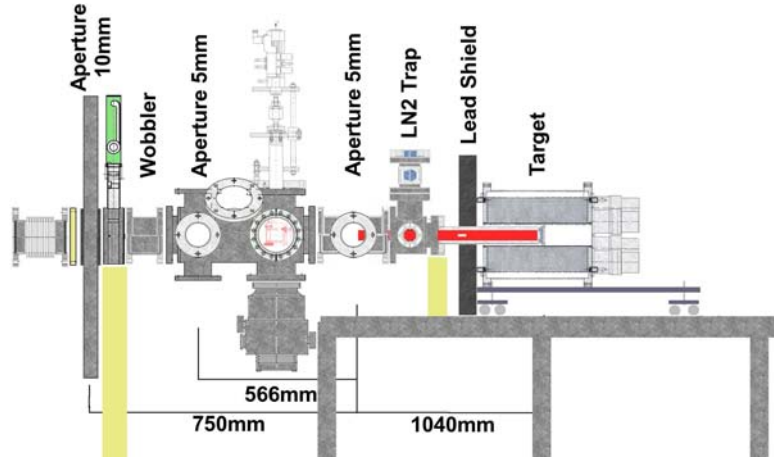
Figure 3: Level scheme of the ^{26}Al.

Figure 4: 2nd beamline installed at 400 kV LUNA accelerator for the 93 keV resonance measurement. The target is surrounded by the $\approx 4\pi$BGO detector.

Recently a measurement of the resonance strengths $\omega\gamma$ down to the resonance at 189 keV has been carried out by detecting the ^{26}Al produced in the reaction via Accelerator Mass Spectroscopy (AMS)[21]. The $\omega\gamma$ obtained in this experiment is a factor 5 smaller than the value previously published by [17, 18, 19, 20] [21].

Besides the discrepancy between the AMS and the prompt-γ measurements of the 189 keV resonance, the AMS technique provides a complementary information because it is sensitive only to the ground state transition while the transitions to the isomeric of ^{26}Al state cannot be detected via AMS due to short live time of this state. Thus an independent verification of [21] is highly demanded.

The aim of the LUNA ^{25}Mg(p,γ)^{26}Al experiment is to measure the strength of the most relevant astrophysical resonances at 189 and 93 keV directly via gamma spectroscopy. Moreover, some targets irradiated during the 189 keV prompt-γ measurement will be analyzed with the AMS technique, in order to investigate the discrepancy between [21] and [17, 18, 19, 20].

In a first step the branching ratios and the $\omega\gamma$ of the resonance at E$_p$ = 189 keV have been measured at LNGS using a 119% HPGe detector placed at 55° relative to the beam direction. The detector was put in close geometry in order to enhance the efficiency. The target quality has been monitored daily making use of the well known resonance in ^{25}Mg(p,γ)^{26}Al at E$_p$ = 317 keV. A first analysis yields a branching ratio for the ground state transition of 6% after corrrection for "summing in effect" and a $\omega\gamma$ between $6.8*10^{-7}$ and $7.7*10^{-7}$ eV [22] in agreement with direct measurements by [19]. A complete analysis based on a precise evaluation of the "summing out effect" is still in progress

Some of the irradiated targets produced during the HPGe phase of the experiment will be used for the AMS measurement. To ensures that ^{26}Al nuclei detected via AMS have been produced only on the 189 keV resonance, the stability of these targets has been monitored using the 223 keV resonance in ^{24}Mg(p,γ)^{25}Al reaction instead of the 317 keV resonance in ^{25}Mg(p,γ)^{26}Al. This has been possible as a small amount of ^{24}Mg is still present in the ^{25}Mg enriched targets and due to the low background at LNGS.
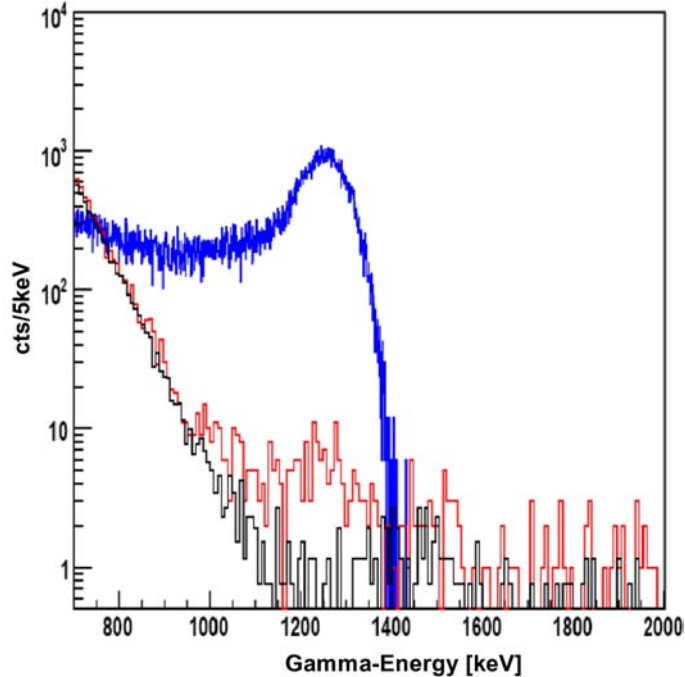
Figure 5: Red line: energy spectrum measured at the 93 keV resonance with the BGO summing crystal (5 keV/channel). Blue line: simulated spectrum Geant4 (not normalized to the measured spectrum). Black line: normalized background spectrum.

A new chemical procedure to extract the ^{26}Al out of the Mg bulk has been developed and tested in the LNGS chemistry laboratory. The new liquid–liquid extraction technique largely reduces the risk of material loss during the AMS sample preparation.

Several AMS tests have been done using LUNA targets irradiated at the 317 keV resonance at the VERA laboratory in Vienna [23] and at the CIRCE laboratory in Caserta [24]. The preliminary results obtained at CIRCE laboratory confirm the good quality of the experimental setup used for the first time for the ^{26}Al/^{27}Al isotopic ratio measurement. The LUNA irradiated targets will be shared with the VERA laboratory in order to minimize the systematic errors in the $\omega\gamma_{gs}$ measurement.

In order to determine the $\omega\gamma$ of the 93 keV resonance a solid state target system in combination with a high efficiency 4π detection system has been developed. The ^{25}Mg target is surrounded by the 4π BGO detector, in order to maximize the detection efficiency. The experimental setup is shown in Figure 4. Details of the setup have been given in [25]. The FAIR multiparameter acquisition system [26] allows to independently measure the energy signals of the six single BGO crystals. The total collected energy is reconstructed off line on an event by event base, improving thus the detector resolution by a proper energy calibration of the single crystals and allowing for a detailed analysis of the few expected good events. The target system and the detector are fully described in a GEANT4 simulation. To verify the simulation in addition to the 93 keV resonance also the resonances at 317 keV and 189 keV in ^{25}Mg(p,γ)^{26}Al have been measured with good statistics. Figure 5 shows a spectrum taken at LUNA on the 93 keV resonance

95

together with a background run with beam and a stimulated spectrum. The signature of the reaction is clearly visible above the background. The data taking has been concluded at the end of 2007 and the data analysis is still progress.

4 ^{15}N(p,γ)^{16}O

For stars with masses larger than the Sun, the CNO cycle is the most important process for energy production during the Hydrogen burning phase. The ratio between the reaction rate of the ^{15}N(p,γ)^{16}O and the ^{15}N(p,$\alpha\gamma$)^{12}C reactions determines directly the nucleosynthesis of the oxygen isotopes ^{16}O, ^{17}O and ^{18}O as well as the neutrino production coming from the β-decay of ^{17}F. ^{17}F neutrinos are expected to contribute to the low energy solar neutrino flux in Borexino [27]. The reaction rate at stellar energies has been obtained in the past by extrapolation based on the interference between two 1^- resonances at E$_p$ = 335 and 1028 keV [28]. The DC process is expected to contribute to the interference with the two resonances as well. Old measurements were performed from E$_p$ = 150 to 2500 keV [29, 30, 31] but at energies corresponding to the interference region between the two resonances around E$_p$= 500 keV and for energies E$_p$ < 300 keV the uncertainty of the data is rather large bringing to a big error on the extrapolated reaction rate. New precision experimental data at these energies are therefore extremely important.

The measurement of the reaction ^{15}N(p,γ)^{16}O [30, 31] is part of the LUNA proposal for the years 2008—2012, which has been accepted by the LNGS scientific committee in October 2007. The LUNA collaboration is preparing the experiment at LNGS making use of above ground accelerators and by reanalyzing data obtained in the past ^{14}N(p,γ)^{16}O experiments [32, 33]. These efforts are described in the following sections.

4.1 Measurement of the ^{15}N(p,γ)^{16}O reaction at the Nuclear Structure Laboratory of the Notre Dame University

During 2007 LUNA has started a collaboration with the Nuclear Structure Laboratory of the Notre Dame University with the goal to investigate this reaction in a wide energy range. At the Notre Dame University the reaction has been measured in the energy range E$_p$ = 290—1900 keV and at the beginning of 2008 the ^{15}N(p,γ)^{16}O will be measured at the LUNA 400kV accelerator with the same experimental setup in the energy range E$_p$ = 150—400 keV. In this way the combination of the two measurements will cover a very large energy region and in particular the two most important interference regions, allowing a much better extrapolation to astrophysical energies.

The measurement has been performed at Notre Dame using two different accelerators. For E$_p$ = 700—1900 keV the KN accelerator was used while for E$_p$ = 290—800 keV the JN accelerator was used. The experimental setup consisted in a TiN 99% ^{15}N enriched deposited target positioned at close geometry to a HpGe clover detector. The targets were 10 keV thick at 400 keV proton energy beam and were extremely stable lasting several days of beam bombardment. Typical currents were of the order of 10 μA. From previous measurements [31] the ^{15}N(p,γ)^{16}O reaction is expected to decay with a branching ratio
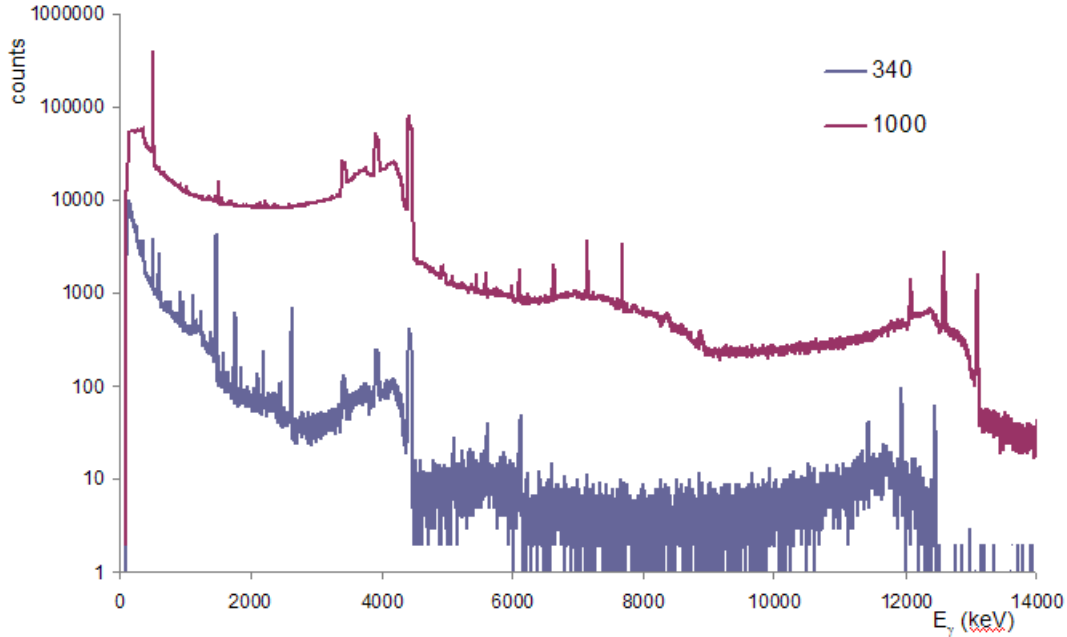
Figure 6: γ spectrum collected at $E_p = 1000$ and $E_p = 340$ keV with the clover detector: for obtaining these spectra the clover detector has been used in add-back mode for increasing the detection efficiency.

> 90% to the ground state. The γ spectra were collected with the detector positioned at an angle of 45° in respect to the beam direction in order to be almost independent to angular distribution effects. To avoid carbon deposition on the target a liquid nitrogen cold finger was put in front of the target. Experimental spectra collected at $E_p = 1000$ and 340 keV are shown in figure 6. The highest energy peaks around 12 MeV are coming from the ^{15}N(p,γ)^{16}O ground state transition, while the broad low energy peaks at 4.4 MeV are due to the γ of the ^{15}N(p,$\alpha\gamma$)^{12}C reaction. The detection efficiency has been obtained using the well known resonances at $E_p = 992$ and 1183 keV of the ^{27}Al(p,γ)^{28}Si reaction.

The data analysis is still in progress and will be coordinated with the analysis of the measurement of the low energy region that will be performed at LUNA at the beginning of 2008. The low energy data taken at LNGS will also provide important information concering the feasibility of an experiment with the LUNA BGO summing detector with a solid state target setup.

4.2   Feasibility study for a ^{15}N(p,γ)^{16}O experiment with the LUNA gas target – BGO setup

In order to study the feasibility of an experiment making use of the LUNA BGO detector and the gas gas target spectra acquired in the 2003-2004 experiments on the ^{14}N(p,γ)^{15}O cross section [32, 33] have been reanalyzed with a focus on the ^{15}N(p,γ)^{16}O reaction. These spectra were taken using a BGO summing detector and a windowless gas target cell [32, 33] filled with 1 mbar nitrogen gas of natural composition.
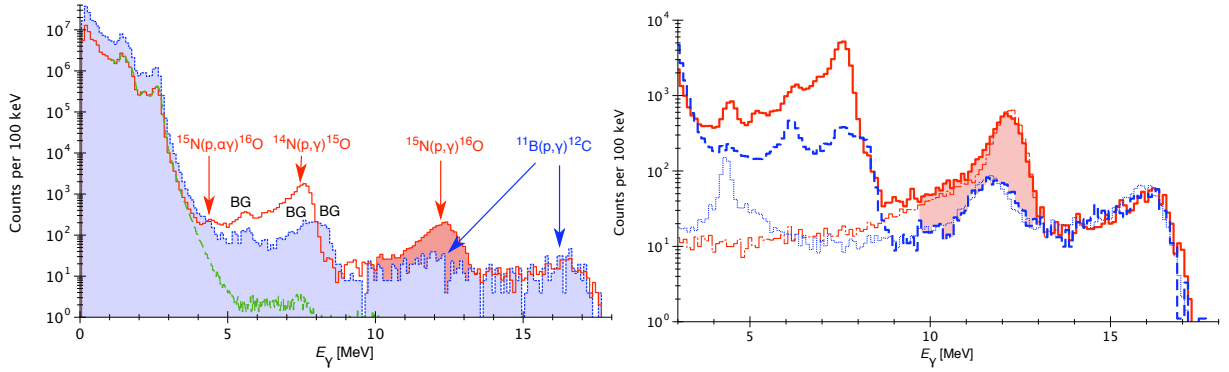
Figure 7: *Left panel:* γ-ray spectrum, $E_p = 150$ keV. Solid (dotted) line: Nitrogen gas in the target (helium gas, rescaled to match the nitrogen spectrum in the 14.4 – 18.0 MeV region). Dashed line, laboratory background. *Right panel:* γ-ray spectrum, $E_p = 220$ keV. Red solid (dot-dashed) line: Experimental, nitrogen gas (simulated, ^{15}N(p,γ)^{16}O). Blue dashed (dotted) line: Experimental, helium gas, rescaled as in the left panel (simulated, ^{11}B(p,γ)^{12}C).

In order to verify whether the gas has natural isotopic composition (0.3663% ^{15}N [34]), two gas samples (called sample A and B) have been taken from the 16-fold bottlepack containing N_2 of chemical purity 5.5 (99.9995%) underground at LUNA.

The samples were then analyzed using mass spectrometry, independently at three different laboratories. The resulting isotopic enrichment is expressed as

$$\delta^{15}\text{N} = \left(\frac{[A(^{15}\text{N})/A(^{14}\text{N})]_{\text{sample}}}{[A(^{15}\text{N})/A(^{14}\text{N})]_{\text{air}}} - 1 \right) \cdot 1000 \qquad (2)$$

with the standard being atmospheric air. The data show that the nitrogen gas used at LUNA has an isotopic composition within 3% of that of standard air (table 1). Consequently, in principle a ^{15}N(p,γ)^{16}O experiment can even be carried out using nitrogen gas of natural isotopic composition.

The Gran Sasso rock overburden essentially removes the laboratory background (0.1 counts/day [35]) at energies of importance for a ^{15}N(p,γ)^{16}O study. In order to evaluate the beam induced background, monitor runs with helium gas in the target chamber have been analyzed. In the present energy range ($E_p = 100 - 250$ keV), the ^{7}Li(p,γ)^{8}Be background was found to be negligible, and the ^{11}B(p,γ)^{12}C reaction (Q value = 15.957 MeV) has been found to be the only relevant source of beam induced background. This latter reaction produces a summing peak at $E_\gamma \approx 16$ MeV and primary ($E_\gamma \approx 12$ MeV) and

Sample	Measured at	δ^{15}N
A	CIRCE Caserta, Italy	-27.2
B	Max-Planck-Institute for Biogeochemistry Jena, Germany	-1.1
	ATOMKI Debrecen, Hungary	-0.4

Table 1: Enrichment δ^{15}N in nitrogen-15 of the Gran Sasso gas samples.

Level in ^{16}O [MeV]	Experiment	E_p [keV]	2σ upper limit
7.117	^{14}N(p,γ)^{15}O background study [35]	200	6%
	Clover ^{14}N(p,γ)^{15}O [38]	400	1.9%
6.049	Clover ^{14}N(p,γ)^{15}O [38]	400	1.8%

Table 2: Experimental upper limits relative to the literature [31] total ^{15}N(p,γ)^{16}O cross section for primary γ-rays from capture to exited states in ^{16}O.

secondary γ-rays from capture to the level at 4.439 MeV in ^{12}C. The primary γ-ray at $E_\gamma \approx 12$ MeV gives rise to a significant number of counts in the region of interest for the ^{15}N(p,γ)^{16}O analysis (fig. 7). These background counts can be subtracted using the experimental ratio of the 16 MeV and 12 MeV γ-rays in the helium monitor run at the same beam energy (fig. 7).

In order to properly describe these data, a detailed GEANT4 [36] simulation has been carried out, reproducing the efficiency data taken with radioactive sources and also the previous [33] GEANT3 simulation. The experimental ratio of the 16 MeV and 12 MeV γ-rays could be explained in the simulation by ^{11}B(p,γ)^{12}C γ-rays originating from the final collimator [35], taking into account the literature data on ^{11}B(p,γ)^{12}C branching ratios and angular correlations [37]. The ^{11}B(p,γ)^{12}C background arises from impurities independent from the gas pressure. Therefore, it will become negligible when using enriched ^{15}N targets.

In a summing detector like the LUNA BGO detector, the detection efficiency depends on the branching ratios for capture to excited states in the compound nucleus. The ^{15}N(p,γ)^{16}O reaction has previously been found to be dominated ($\geq$90%) by capture to the ground state in ^{16}O [31]. Only for two levels, non-zero capture branching ratios have been reported. For these levels, a reanalysis of previous ^{14}N(p,γ)^{15}O data [35, 38] has yielded experimental upper limits (table 2). Summarizing the feasibility study, a procedure to subtract the ^{11}B(p,γ)^{12}C beam induced background has been developed and validated with experimental data and simulations. The isotopic composition of bottled nitrogen gas has been measured and found to be close to the standard. Experimental upper limits were obtained for capture to two excited levels in ^{16}O. Concluding, there are excellent prospects for a dedicated ^{15}N(p,γ)^{16}O gas target experiment using enriched gas and the present BGO summing detector.

Acknowledgments

References

[1] W.A.Fowler, Rev.Mod.Phys. 56, 149 (1984)

[2] C.Rolfs and W.S.Rodney, Cauldrons in the Cosmos (University of Chicago Press, 1988)

[3] G. Fiorentini et al., Z.Phys. A350, 289 (1995)

[4] A. Formicola et al., NIM A 507, 609 (2003)

[5] A. Formicola et al., Phys. Lett. B 591, 61 (2004)

[6] G. Imbriani et al., Eur. Phys. J. A 25, 455 (2005)

[7] U. Schröder et al., Nucl. Phys. A 467, 240 (1987)

[8] R. C. Runkle et al., Phys. Rev. Lett. 94, 082503 (2005)

[9] W. Haxton, arXiV:0710.2295 (2007)

[10] C. Angulo and P. Descouvemont, Nucl. Phys. A 690, 755 (2001)

[11] Z. Elekes et al., Nucl. Inst. Meth. A 503, 580 (2003)

[12] H.-P. Trautvetter et al., J. Phys. G 35, 014019 (2008)

[13] LUNA Collaboration, Contrib. to LNGS Anual Report 2005, available at www.lngs.infn.it

[14] R.Diehl et al., A&A 298, 445 (1995)

[15] J.Knödlseder et al., A&A 345, 813 (1999)

[16] R.Diehl et al., A&A 411, L451L455 (2003)

[17] A. E. Champagne et al., Nucl.Phys.A 402, 179 (1983)

[18] P.M.Endt et al., Nucl.Phys.A 459, 61 (1986)

[19] Ch.Iliadis et al., Nucl.Phys.A 512, 509 (1990)

[20] D.C.Powell et al., Nucl.Phys.A 644, 263 (1998)

[21] A.Arazi et al., PRC 74, 025802 (2006)

[22] A Formicola et al, J. Phys.G 35, 014013 (2008)

[23] VERA - Vienna Environmental Research Accelerator, www.univie.ac.at/Kernphysik/VERA/welcome.htm

[24] F. Terrasi et al. NIMB 259, 14 (2007)

[25] LUNA Collaboration, Contrib. to LNGS Anual Report 2006, available at www.lngs.infn.it

[26] A.Ordine et al., IEEE Transaction in nuclear science 45 No.3, 873 (1998)

[27] L. Stonehill, J. Formaggio and R. Robertson, Phys. Rev. C 69, 015801(2004)

[28] C. Angulo et al., Nucl. Phys. A 656, 3 (1999)

[29] F.B. Hagedorn, Phys. Rev. 108, 735 (1957)

[30] D.F. Hebbard, Nucl. Phys. A 15, 289 (1960)

[31] C. Rolfs and W. Rodney, Nucl. Phys. A 235,450 (1974)

[32] A. Lemut et al., Phys. Lett. B 634, 483 (2006)

[33] D. Bemmerer et al., Nucl. Phys. A 779, 297 (2006)

[34] T. B. Coplen et al., Pure Appl. Chem. 74, 1987 (2002)

[35] D. Bemmerer et al., Eur. Phys. J. A 24, 313 (2005)

[36] S. Agostinelli et al., Nucl. Inst. Meth. A 506, 250 (2003)

[37] F. Cecil et al., Nucl. Phys. A 539, 75 (1992)

[38] H.-P. Trautvetter et al., J. Phys. G 35, 014019 (2008)

Pubblications

1. Gy. Gyurky, "^{3}He(α,γ)^{7}Be cross section at low energies", Phys. Rev. C 75 035805

2. F. Confortola, "Astrophysical S-factor of the ^{3}He(α,γ)^{7}Be reaction measured at low energy via prompt and delayed gamma detection", Phys. Rev. C 75, 065803

3. Gy. Gyurky et al., "Comparison of the LUNA ^{3}He(α,γ)^{7}Be activation results with earlier measurements and model calculations", J. Phys. G 014002

4. A. Formicola et al, "Measurement of the ^{25}Mg(p,γ)^{26}Al resonance strength via gamma spectroscopy", J. Phys.G 35 014013

5. H.P. Trautvetter, "Ground state capture in ^{14}N(p,γ)^{15}O studied above the 259 keV resonance at LUNA ", J. Phys. G 35 014019

6. M. Junker, "Underground Nuclear Astrophysics at LUNA", Proc. of the Carpatian Summer School of Physics 2007, Ed. L. Trache and Sabia Stoica, AIP Conference Proceedings 972, 249

List of Conferences

1. C. Broggini, "LUNA: New Results on ^{3}He+^{4}He", invited talk at the 12th international workshop on Neutrino Telescopes, March 6-9, 2007, Venice, Italy

2. M. Marta, "^{14}N(p,γ)^{15}O ground state capture studied above the 259 keV resonance at LUNA", talk on DPG Frühjahrstagung Hadronen und Kerne, March 12-16, 2007 Giessen, Germany

3. D. Bemmerer, "The ^{3}He(α,γ)^{7}Be reaction studied at LUNA", talk on DPG Frühjahrstagung Hadronen und Kerne, March 12-16 2007, Giessen, Germany

4. A. Formicola, "Measurement of the ^{25}Mg(p,γ)^{26}Al resonance strength via gamma spectroscopy", talk on the European Conference on Nuclear Physics in Astrophysics III, March 26-31 2007, Dresden, Germany

5. H.P. Trautvetter, "Ground state capture in ^{14}N(p,γ)^{15}O studied above the 259 keV resonance at LUNA ", poster on the European Conference on Nuclear Physics in Astrophysics III, Technische Universität Dresden, March 26-31 2007, Dresden, Germany

6. Gy. Gyurky, "Nuclear Physics and "Astrophysics III", Technische Universität Dresden, March, 26-31 2007, Dresden, Germany

7. H. Costantini, "Underground Nuclear Astrophysics experiments", invited talk at the 19th Rencontres de Blois "Matter and Energy in the Universe: from nucleosynthesis to cosmology", May 2007, Blois, France

8. P. Prati, "Astrophysical S-factor of the ^{3}He(α,γ)^{7}Be reaction measured at low energy via prompt and delayed γ emission", talk at INPC2007, International Nuclear Physics Conference, June 2-8, 2007, Tokyo, Japan

9. M. Junker, "Underground Nuclear Astrophysics at LUNA", Invited lecture at the Carpatian Summer School of Physics 2007, August, 20-31 2007, Sinaia, Romania

10. P. Prati, "Nuclear astrophysics at LUNA: Status and perspectives", Invited talk at FINUSTAR2: Frontiers In NUclear STructure, Astrophysics and Reactions FINUSTAR 2, September 10-14 2007, Aghios Nikolaos, Crete

11. C. Broggini "Laboratory for Underground Nuclear Astrophysics", invited lectures at Selected Topics in Nuclear and Atomic Physics, September 30 -October 4 2007, Fiera di Primiero, Italy

12. G. Imbriani, "^{15}N(p,γ) and ^{25}Mg(p,γ) at LUNA", invited talk at the IXth Torino Workshop on Evolution and Nucleosynthesis in AGB Stars, October 22-26 2007, Perugia, Italy

LVD. Large Volume Detector

N.Yu.Agafonova[9], M.Aglietta[14], E.D.Alyea[7], P.Antonioli[1], G.Badino[14], G.Bari[1], M.Basile[1], V.S.Berezinsky[9], M.Bertaina[14], R.Bertoni[14], A. Bonardi[14], G.Bruni[1], G.Bruno[14], G.Cara Romeo[1], A.Chiavassa[14], J.A.Chinellato[3], L.Cifarelli[1], F.Cindolo[1], A.Contin[1], V.L.Dadykin[9], E.A. Dobrynina[9], L.G.Dos Santos[3], R.I.Enikeev[9], W.Fulgione[14], P.Galeotti[14], M.Garbini[1,16], P.L.Ghia[5,14], G.Giuliani[5,14], P.Giusti[1], F.Gomez[14], F.Grianti[4], G.Iacobucci[1], E.Kemp[3], E.V.Korolkova[9], V.B.Korchaguin[9], V.V.Kuznetsov[9], M.Luvisetto[1], A.A.Machado[15], A.S.Malguin[9], H.Menghetti[1], N.Mengotti Silva[3], C.Morello[14], R.Nania[1], G.Navarra[14], K.Okei[10], L.Periale[14], R.Persiani[1], A.Pesci[1], P.Picchi[14], I.A.Pless[8], A.Porta[14], A.Romero[14], V.G.Ryasny[9], O.G.Ryazhskaya[9], O.Saavedra[14], K.Saitoh[13], G.Sartorelli[1], M.Selvi[1], N.Taborgna[5], N.Takahashi[12], V.P.Talochkin[9], G.C.Trinchero[14], S.Tsuji[11], A.Turtelli[3], P.Vallania[14], S.Vernetto[14], C.Vigorito[14], L.Votano[4], T.Wada[10], R.Weinstein[6], M.Widgoff[2], V.F.Yakushev[9], G.T.Zatsepin[9], A.Zichichi[1]

[1] *University of Bologna and INFN-Bologna, Italy*
[2] *Brown University, Providence, USA*
[3] *University of Campinas, Campinas, Brazil*
[4] *INFN-LNF, Frascati, Italy*
[5] *INFN-LNGS, Assergi, Italy*
[6] *University of Houston, Houston, USA*
[7] *Indiana University, Bloomington, USA*
[8] *Massachusetts Institute of Technology, Cambridge, USA*
[9] *Institute for Nuclear Research, Russian Academy of Sciences, Moscow, Russia*
[10] *Okayama University, Okayama, Japan*
[11] *Kawasaki Medical School, Kurashiki, Japan*
[12] *Hirosaki University, Hirosaki, Japan*
[13] *Ashikaga Institute of Technology, Ashikaga, Japan*
[14] *IFSI-INAF, Torino; University of Torino and INFN-Torino, Italy*
[15] *Centro Brasileiro de Pesquisas Fisicas, Rio de Janeiro, Brasil*
[16] *Museo Storico della Fisica, Centro Studi e Ricerche "E. Fermi", Rome, Italy*

Abstract

The Large Volume Detector (LVD) in the INFN Gran Sasso National Laboratory, Italy, is a ν observatory mainly designed to study low energy neutrinos from the gravitational collapse of galactic objects.

The experiment has been monitoring the Galaxy since June 1992, under increasing larger configurations: in January 2001 it has reached its final active mass $M = 1$ kt. LVD is one of the largest liquid scintillator apparatus for the detection of stellar collapses and, besides SNO, SuperKamiokande and Amanda, it is a charter member of the SNEWS network, that has become fully operational since July 1st, 2005.

During fall 2007 there was the second run of the CNGS project: LVD was fully operative; we report about the detected CNGS events.

1 The LVD experiment

1.1 Scientific ground

The Large Volume Detector (LVD), located in the hall A of the INFN Gran Sasso National Laboratory, Italy, is a multipurpose detector consisting of a large volume of liquid scintillator interleaved with limited streamer tubes in a compact geometry (a front view is shown in fig.1). The major purpose of the LVD experiment is the search for neutrinos from Gravitational Stellar Collapses (GSC) in our Galaxy [1].

Indeed, in spite of the lack of a "standard" model of the gravitational collapse of a massive star, the correlated neutrino emission appears to be well established. At the end of its burning phase a massive star $(M > 8M_{\odot})$ explodes into a supernova, originating a neutron star which cools emitting its binding energy $E_B \sim 3 \cdot 10^{53}$ erg mostly in neutrinos. The largest part of this energy, almost equipartitioned among neutrino and antineutrino species, is emitted in the cooling phase: $E_{\bar{\nu}_e} \sim E_{\nu_e} \sim E_{\nu_x} \sim E_B/6$ (where ν_x denotes generically $\nu_{\mu}, \bar{\nu}_{\mu}, \nu_{\tau}, \bar{\nu}_{\tau}$ flavors). The energy spectra are approximatively a Fermi-Dirac distribution, with different mean temperatures, since ν_e, $\bar{\nu}_e$ and ν_x have different couplings with the stellar matter: $T_{\nu_e} < T_{\bar{\nu}_e} < T_{\nu_x}$.
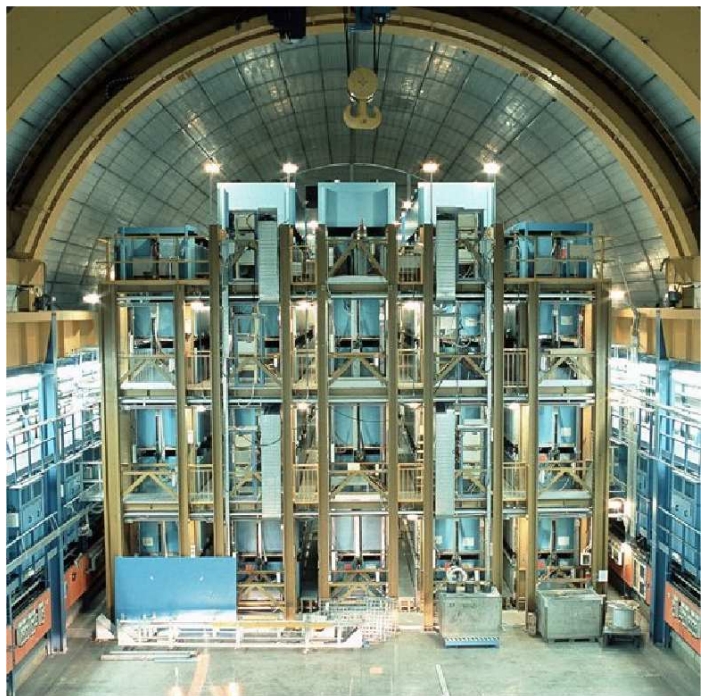

Figure 1: *Front view of the LVD detector in the hall A of the Gran Sasso National Laboratory, INFN.*

LVD is able to detect $\bar{\nu}_e$ interactions with protons in the scintillator, which give the main signal of supernova neutrinos, with a very good signature. Moreover, it can detect ν_e

through the elastic scattering reactions with electrons, $(\nu_e + \bar{\nu}_e)$ through charged current interactions with the carbon nuclei of the scintillator, and it is also sensitive to neutrinos of all flavors detectable through neutral currents reactions with the carbon nuclei. The iron support structure of the detector can also act as a target for electron neutrinos and antineutrinos. The products of the interaction can exit iron and be detected in the liquid scintillator. The amount of neutrino-iron interaction can be as high as about 20% of the total number of interactions. The signal observable in LVD, in different reactions and due to different kinds of neutrinos, besides providing astrophysical informations on the nature of the collapse, is sensitive to intrinsic ν properties, as oscillation of massive neutrinos and can give an important contribution to define some of the neutrino oscillation properties still missing.

1.2 The detector

The LVD experiment has been in operation since 1992, under different increasing configurations. During 2001 the final upgrade took place: LVD became fully operational, with an active scintillator mass $M = 1000$ t.

LVD consists of an array of 840 scintillator counters, 1.5 m^3 each, arranged in a compact and modular geometry; each of them is viewed on the top by three photomultipliers (visible in fig. 2). Up to 2004, before a re-calibration of the full detector, the counters were divided in two subsets: the external ones (43%), operated at energy threshold $\mathcal{E}_h \simeq 7$ MeV, and inner ones (57%), better shielded from rock radioactivity and operated at $\mathcal{E}_h \simeq 4$ MeV. After the re-calibration (which, started in 2004, ended during 2005) all the counters are operated at a common threshold, $\mathcal{E}_h \simeq 4$ MeV.

Figure 2: *Top view of the LVD detector in the hall A of the Gran Sasso National Laboratory, INFN.*

To tag the delayed γ pulse due to n-capture, all counters are equipped with an additional discrimination channel, set at a lower threshold, $\mathcal{E}_l \simeq 1$ MeV.

Other relevant features of the detector are:

(i) good event localization and muon tagging;

(ii) accurate absolute and relative timing: $\Delta t_{abs} = 1\,\mu$s, $\Delta t_{rel} = 12.5$ ns;

(iii) energy resolution: $\sigma_E/E = 0.07 + 0.23 \cdot (E/\text{MeV})^{-0.5}$;

(iv) very high duty cycle, i.e. $> 99.5\%$ in the last seven years;

(v) fast event recognition.

1.3 Supernova neutrino interactions in LVD

The observable neutrino reactions in the LVD scintillator are:

(1) $\bar{\nu}_e p, e^+ n$, (physical threshold $E_{\bar{\nu}_e} > 1.8\ MeV$) observed through a prompt signal from e^+ above threshold $\mathcal{E}_h$ (detectable energy $E_d \simeq E_{\bar{\nu}_e} - 1.8$ MeV $+2m_e c^2$), followed by the signal from the $np, d\gamma$ capture ($E_\gamma = 2.2$ MeV), above $\mathcal{E}_l$ and with a mean delay $\Delta t \simeq 185\ \mu$s.

(2) $\nu_e\ ^{12}C,^{12}N\ e^-$, (physical threshold $E_{\nu_e} > 17.3\ MeV$) observed through two signals: the prompt one due to the e^- above $\mathcal{E}_h$ ($E_d \simeq E_{\nu_e} - 17.3$ MeV) followed by the signal, above $\mathcal{E}_h$, from the β^+ decay of ^{12}N (mean life $\tau = 15.9$ ms).

(3) $\bar{\nu}_e\ ^{12}C,^{12}B\ e^+$, (physical threshold $E_{\bar{\nu}_e} > 14.4\ MeV$) observed through two signals: the prompt one due to the e^+ ($E_d \simeq E_{\bar{\nu}_e} - 14.4\,\mathrm{MeV} + 2m_e c^2$) followed by the signal from the β^- decay of ^{12}B (mean life $\tau = 29.4$ ms). As for reaction *(2)*, the second signal is detected above the threshold $\mathcal{E}_h$.

(4) $\overset{(-)}{\nu}_\ell\ ^{12}C, \overset{(-)}{\nu}_\ell\ ^{12}C^*$ ($\ell = e, \mu, \tau$), (physical threshold $E_\nu > 15.1\ MeV$), whose signature is the monochromatic photon from carbon de-excitation ($E_\gamma = 15.1$ MeV), above $\mathcal{E}_h$.

(5) $\overset{(-)}{\nu}_\ell\ e^-, \overset{(-)}{\nu}_\ell\ e^-$, which yields a single signal, above $\mathcal{E}_h$, due to the recoil electron.

Figure 3: *Cross section behavior for the different neutrino reactions observable in the LVD scintillator.*

The LVD detector is supported by an iron structure made basically by two components: the tank (mean thickness: 0.4 cm), containing the scintillator, and the "portatank" (mean thickness: 1.5 cm) hosting a cluster of 8 tanks. The higher energy part of the ν flux can thus be detected also with the $\nu(\bar{\nu})$Fe interaction, resulting in an electron (positron) that may exit the iron and release energy in the scintillator. The reactions of interest are the following:

(6) $\nu_e\ ^{56}Fe,^{56}Co\ e^-$. The mass difference between the nuclei is $\Delta_{m_n} = m_n^{Co} - m_n^{Fe} = 4.055$ MeV, the first Co allowed state being at 3.589 MeV. Other higher energy allowed states are present in ^{56}Co: considering $E_{e^-}^{kin} = E_{\nu_e} - \Delta_{m_n} - E_{level} - m_e$ MeV, where E_{level} is the energy difference between the excitation level and the ground state level, this can take values: $3.589, 4.589, 7.589, 10.589\ MeV$. The efficiency for electron and gammas (also produced in the interaction) to reach the scintillator with energy higher than $\mathcal{E}_h$ is greater than 20% for $E_\nu > 30$ MeV and grows up to 70% for $E_\nu > 100$ MeV. On average, the detectable electron energy is $E_d \simeq 0.45 \times E_\nu$.

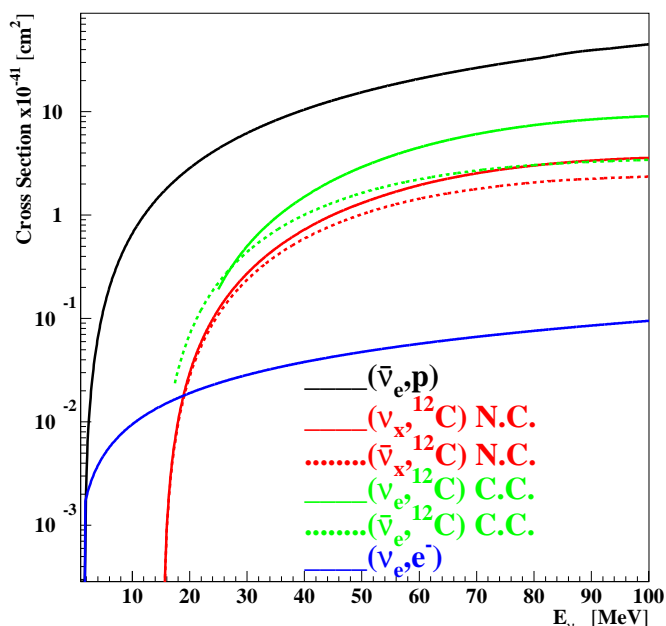*(7)* $\bar{\nu}_e\,{}^{56}\mathrm{Fe},{}^{56}\mathrm{Mn}\;e^+$, the energy threshold and the efficiency are very similar to those of reaction *(6)*.

The number of all the possible targets present in the LVD detector is listed in table 1.

Table 1: Number of targets in the LVD detector.

Target Type	Contained in	Mass	Number of targets
Free protons	Liquid Scintillator	$1000\,t$	$9.34\ 10^{31}$
Electrons	LS	$1000\,t$	$3.47\ 10^{32}$
C Nuclei	LS	$1000\,t$	$4.23\ 10^{31}$
Fe Nuclei	Support Structure	$900\,t$	$9.71\ 10^{30}$

1.4 Effects of neutrino oscillations in the SN signal

There are many experimental works suggesting neutrino conversion among flavors in the recent few years, through the study of atmospheric, solar, reactor and accelerator neutrinos. The interpretation of all these phenomena in terms of neutrino oscillations is rather robust, because it is able to include all the experimental data (except the LSND signal). In the standard three flavor scenario, six parameters must be determined by oscillation experiments: 3 mixing angles (θ_{sol}, θ_{13}, θ_{atm}), 2 squared mass differences ($\Delta m^2_{\mathrm{sol}}$ and $\Delta m^2_{\mathrm{atm}}$) and 1 CP-violation phase δ. A recent analysis of all the available experimental data constrains the "atmospheric" and "solar" parameters to be in the following 99% C.L. ranges:

$\Delta m^2_{\mathrm{sol}}\ (7.2 \div 8.9)\,10^{-5}\ \mathrm{eV}^2$
$|\Delta m^2_{\mathrm{atm}}|\ (1.7 \div 3.3)\,10^{-3}\ \mathrm{eV}^2$
$\theta_{\mathrm{sol}}\ 30° < \theta_{\mathrm{sol}} < 38°$
$\theta_{\mathrm{atm}}\ 36° < \theta_{\mathrm{atm}} < 54°$

However the other parameters are not completely determined: the θ_{13} mixing angle is only upper limited, mainly by the Chooz experiment data ($\sin^2\theta_{13} < 3.\,10^{-2}$ at the 99% C.L.), the sign of $\Delta m^2_{\mathrm{atm}}$ (that fixes the so–called mass hierarchy) is completely unknown, as well as the CP–violation phase δ.

Because of the wide range of matter density in the stellar envelope, a supernova explosion represents a unique scenario for further study of the neutrino oscillation mixing matrix. Indeed neutrinos can cross two resonance density layers and therefore the resulting possible mixing scenarios are different from the solar ones. The emerging neutrino spectra are sensitive to the sign of $\Delta m^2_{\mathrm{atm}}$ and to the value of θ_{13}.

We will show how neutrino oscillations affect the signal detected by LVD and also evaluate the impact on the signal of the astrophysical parameters of the supernova explosion mechanism, such as the total energy emitted in neutrinos, the star distance, the neutrino–sphere temperatures and the partition of the energy among the neutrino flavors. Preliminary results have been presented previously in [11] [12] [13] and are now published in [14].

For a normal mass hierarchy (NH) scheme, ν (not $\bar{\nu}$) cross two resonance layers: one at higher density (H), which corresponds to $\Delta m^2_{\mathrm{atm}}, U^2_{e3}$, and the other at lower density (L), corresponding to $\Delta m^2_{\mathrm{sol}}, U^2_{e2}$. For inverted mass hierarchy (IH), transitions at the higher

density layer occur in the $\bar{\nu}$ sector. Given the energy range of SN ν (up to ~ 100 MeV) and considering a star density profile $\rho \propto 1/r^3$, the adiabaticity condition is always satisfied at the L resonance for any LMA solution, while at the H resonance, this depends on the value of U_{e3}^2. When $U_{e3}^2 \geq 5 \cdot 10^{-4}$ the conversion is completely adiabatic, meaning that the flip probability between two adjacent mass eigenstates is null ($P_h = 0$). In the adiabatic case and NH, the $\bar{\nu}_e$ produced in the SN core arrive at Earth as ν_1, and they have a high ($U_{e1}^2 \simeq cos^2\theta_{12} \simeq 0.7$) probability to be detected as $\bar{\nu}_e$. On the other hand, the original $\bar{\nu}_x$ arrive at Earth as ν_2 and ν_3 and are detected as $\bar{\nu}_e$ with probability $U_{e2}^2 \simeq sin^2\theta_{12}$.

The oscillations scheme can be summarized as:

$F_e = P_h U_{e2}^2 F_e^0 + (1 - P_h U_{e2}^2)F_x^0$ and
$F_{\bar{e}} = U_{e1}^2 F_{\bar{e}}^0 + U_{e2}^2 F_{\bar{x}}^0$ for normal hierarchy;
$F_e = U_{e2}^2 F_e^0 + U_{e1}^2 F_x^0$ and
$F_{\bar{e}} = P_h U_{e1}^2 F_{\bar{e}}^0 + (1 - P_h U_{e1}^2)F_{\bar{x}}^0$ for inverted hierarchy,
where F_{any}^0 are the original neutrino fluxes in the star and F_{any} are the observed ν fluxes. One can notice that, in the antineutrino channel, the non adiabatic ($P_h = 1$), IH case, is equivalent to the NH case (which does not depend on adiabaticity).

With respect to the astrophysical parameters, we assumed a galactic supernova explosion at a typical distance of $D = 10$ kpc, parametrized with a pure Fermi–Dirac energy spectrum ($\eta = 0$) with a total energy $E_b = 3 \cdot 10^{53}$ erg and perfect energy equipartition $f_{\nu_e} = f_{\bar{\nu}_e} = f_{\nu_x} = 1/6$; we fixed $T_{\nu_x}/T_{\bar{\nu}_e} = 1.5$, $T_{\nu_e}/T_{\bar{\nu}_e} = 0.8$ and $T_{\bar{\nu}_e} = 5$ MeV.

For the chosen supernova parameters, it results that the expected number of events and their energy spectrum depend on the unknown oscillation parameters: the mass hierarchy and the value of θ_{13}.

In particular, the inverse beta decay interactions ($\bar{\nu}_e p, e^+ n$) are highly sensitive to the mass hierarchy: for adiabatic transition, the number of events increases of $\sim 25\%$ in the IH case, with respect to the NH one, since the detected $\bar{\nu}_e$ completely come from the higher energy ν_x. The mean energy of the detected positrons is correspondingly increased.

The total number of ($\nu_e + \bar{\nu}_e$) CC interaction with ^{12}C nuclei is highly increased taking into account neutrino oscillations, because of their high energy threshold. For adiabatic transition the expected number of events is higher than the non adiabatic one, because at least one specie (between ν_e or $\bar{\nu}_e$) comes significantly from the original and higher–energy ν_x in the star. However, if it is not possible to discriminate between ν_e and $\bar{\nu}_e$, the normal and inverted hierarchy cases present similar results. Indeed, in the NH (IH) case, the increase in ν_e ($\bar{\nu}_e$) is compensated by a decrease in $\bar{\nu}_e$ (ν_e).

The neutrino interactions with the iron of the support structure, which are studied in details in this work, are also increased by the oscillations. The efficiency for the detection of the produced charged leptons and gammas in the active part of the detector has been calculated with a full simulation of the apparatus. The contribution of ($\nu_e + \bar{\nu}_e$) Fe interactions can be as high as 15% of the total number of events (in the adiabatic NH case) and they contribute mostly to the high energy part of the spectrum.

With respect to the previous detection channels, the number of NC interactions with ^{12}C nuclei does not depend on oscillations. In principle they could be used as a reference to identify the ν_x–sphere temperature. However, this is partly limited by the unknowledge of the other astrophysical parameters.

In conclusion, for our choice of the astrophysical parameters, the expected signal of

neutrinos in the LVD detector from a supernova core collapse greatly benefits of the neutrino oscillation mechanism, practically in all the possible detection channels, especially if the transition is adiabatic and the hierarchy inverted (since in LVD the most relevand signal is given by $\bar{\nu}_e$).

The expected number of events in the various LVD detection channels and in the different oscillation scenarios are shown in table 2.

Table 2: Expected results in the various LVD detection channels and in the mean energy of the detected $\bar{\nu}_e\ p$ events.

	No Oscillation	Non Adiabatic	Adiabatic NH	Adiabatic IH
$\bar{\nu}_e\ p$	346.	391.		494.
$\langle E_{\bar{\nu}_e} \rangle$ in $\bar{\nu}_e\ p$	25. MeV	30. MeV		37. MeV
CC with ^{12}C	8.	22.	29.	27.
CC with ^{56}Fe	22.	72.	95.	92.
NC with ^{12}C	27			

However, being aware of the fact that the astrophysical parameters of the supernova mechanism are up to now not well defined, we performed the same calculations using different values of them. The resulting differences are in fact important; they are mainly due to the poor theoretical knowledge of the physics of the gravitational collapse. This will be hopefully improved after the occurence and detection of the next galactic supernova, to which the LVD experiment can give a significant contribution.

2 LVD and its experimental activity in 2007

2.1 Supernova physics

2.1.1 Monitoring the Galaxy

LVD has been continuously monitoring the Galaxy since 1992 in the search for neutrino bursts from GSC [1].

---

[1]The results of this search have been periodically updated and published in the ICRC Proceedings, since 1993 until 2007. [3, 4, 5, 6, 7, 8, 9, 10]

Its active mass has been progressively increased from about 330 t in 1992 to 1000 t in 2001, always guaranteeing a sensitivity to gravitational stellar collapses up to distances $d = 20$ kpc from the Earth, even in the case of the lowest ν-sphere temperature.

In fig. 4 we show the duty cycle of the experiment and the average active mass, during the last 7 years. Considering just the last year (2007) the average duty cycle was 99.94% and the average active mass in the same period 948 t.
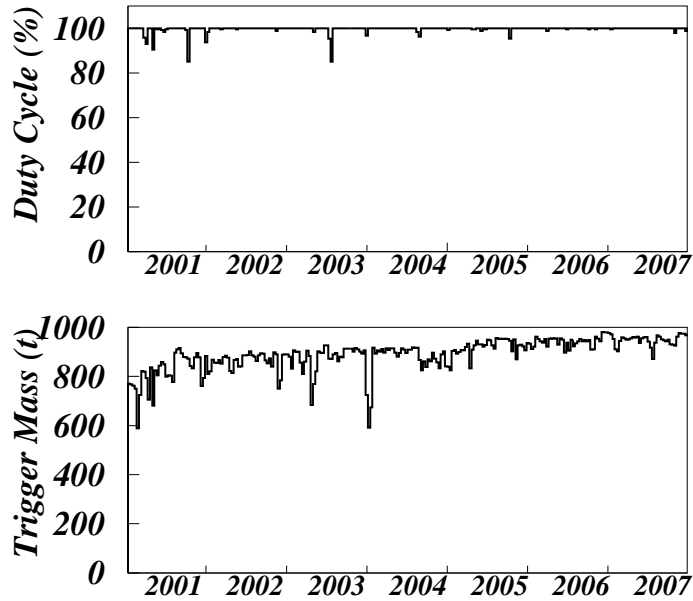

Figure 4: LVD duty cycle and trigger mass during the last seven years of data acquisition.

All events are processed on the base of their time sequence, searching for cluster not compatible with a poissonian fluctuation of the background. No significant signal has been registered by LVD during 15 years of data acquisition. Since the LVD sensitivity is higher than expected from GSC models (even if the source is at a distance of 20 kpc and for soft neutrino energy spectra) we can conclude that no gravitational stellar collapse has occurred in the Galaxy in the whole period of observation: the resulting upper limit to the rate of GSC, updated to 2007, at 90% C.L. is 0.16 events/yr.

2.1.2 On-line recognition of supernova neutrino bursts and SNEWS

Since the first, and unique, observation of ν's from gravitational stellar collapse was guided by the optical observation and since the optical observation of a stellar collapse in our Galaxy is not probable, the detector capabilities of identifying a ν burst in the absence of an "external trigger" must be carefully demonstrated. In the presence of an electromagnetic counterpart, on the other hand, the prompt identification of the neutrino signal could alert the worldwide network of observatories allowing study of all aspects of the rare event from its onset.

The SNEWS (SuperNova Early Warning System) [15, 16] project is an international collaboration including several experiments sensitive to a core-collapse supernova neutrino signal in the Galaxy and neighbour. Its goal is to provide the astronomical community with a prompt and confident alert of the occurrence of a Galactic supernova event, generated by the coincidence of two or more active detectors. In July 2005, after a few years

of tuning, the charter members of SNEWS (i.e., LVD, Super-K and SNO[2]) together with the newly joined Amanda/IceCube, started the effective operation of the network, which means that the alert is really sent to the list subscribers, in the case of an at least two-fold coincidence (see *http://snews.bnl.gov* to get your own SN alert !).

The LVD performances from the point of view of the on-line identification of a neutrino burst have been discussed in [17]. The core of the algorithm for the on-line selection of candidate neutrino bursts is the search for a cluster of H signals within a fixed-duration time window, Δt. The candidate burst is simply characterized by its multiplicity m, i.e., the number of pulses detected in Δt, and by Δt itself. All the other characteristics of the cluster, e.g., detailed time structure, energy spectra, ν flavor content and topological distribution of signals inside the detector are left to a subsequent independent analysis. Based on this principle, the LVD data are continuously analyzed by an on-line "supernova monitor". In detail, each data period, T, is scanned through a "sliding window" with duration $\Delta t = 20$ s, that is, it is divided into N = $2 \cdot \frac{T}{\Delta t} - 1$ intervals, each one starting in the middle of the previous one, so that the unbiased time window is 10 s. The frequency of clusters of duration 20 s and multiplicity $\geq$ m, due to background, is:

$$F_{im}(m, f_{\text{bk}}, 20\ s) = 8640 \cdot \sum_{\text{k} \geq \text{m}}^{\infty} P(k; 20 \cdot \frac{f_{\text{bk}}}{s^{-1}})\ event \cdot day^{-1} \qquad (1)$$

where f_{bk} is the background counting rate of the detector for $E_{\text{vis}} \geq E_{\text{cut}}$, $P(k; f_{\text{bk}}\Delta t)$ is the Poisson probability to have clusters of multiplicity k if $f_{\text{bk}}\Delta t$ is the average background multiplicity, and 8640 is the number of trials per day.[3] For example, a cluster with m=10 can be produced by background fluctuations once every 100 years if $f_{\text{bk}} = 0.03$ s^{-1}; to have the same significance with a higher background, e.g. $f_{\text{bk}} = 0.2$ s^{-1}, a cluster with much higher multiplicity, m=22, would be required (see figure 5 where m versus F_{im} is shown, for two different background conditions). For these background rates, $m = 10$ and $m = 22$ correspond to the minimum multiplicity, m_{min}, to have an imitation frequency $F_{\text{im}} < 1 \cdot 10^{-2}$ yr^{-1}.

In LVD the search for burst candidates is performed for both energy cuts: 7 and 10 MeV. The chosen F_{im}, below which the detected cluster will be an on-line candidate supernova event, is 1 per 100 year working stand-alone while it is relaxed to 1 per month working in coincidence with other detectors, as in the SNEWS project.

In figure 6 we show the distributions of the observed time intervals between selected clusters at the imitation frequency $F_{\text{im}} = 1$/day and $F_{\text{im}} = 1$/month during 688 days (between July 5th, 2005 and May 23rd, 2007) and $E_{\text{cut}} = 7$ MeV. The mean rates, derived from Poisson fits, are $F_{im}^{obs} = 1.24$ day^{-1} (with m_{min} varying between 13 and 15) and $F_{im}^{obs} = 1.28$ month^{-1} (m_{min} between 15 and 18), respectively, meaning that, within 25%, the time behavior of the background is consistent with expectations.

We can conclude that the background trend is predictable even during long periods of

---

[2]Actually the SNO experiment is stopped and under decommissioning

[3]Once a candidate cluster (m, 20s) has been identified, the algorithm will search for the most probable starting point of the signal within the time window. For all possible sub-clusters with multiplicity $2 \leq k \leq m$ and duration $0 \leq \Delta t \leq 20s$ the corresponding Poisson probability $P_{k \geq m}$ is calculated and the absolute minimum identified. The time of the first event of the least probable sub-cluster is assumed as the start time of the signal.

data acquisition and with variable detector conditions, allowing us to define the significance of a neutrino burst in terms of imitation frequency, F_{im}.
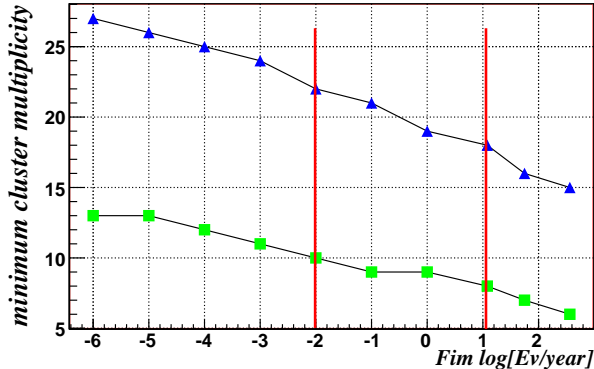

Figure 5: **Minimum cluster multiplicity m_{min} vs. the imitation frequency F_{im}. Triangles correspond to E_{cut}=7 MeV and f_{bk}=0.2 Hz, while squares to E_{cut}=10 MeV and f_{bk}=0.03 Hz. The two vertical lines represent the F_{im} thresholds of 1 candidate per 100 year (stand-alone) and of 1 per month (SNEWS).**
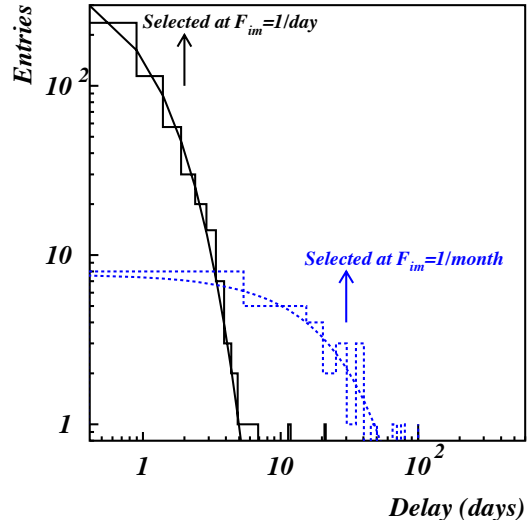

Figure 6: **Distribution of the time intervals between observed clusters (histograms) fitted by Poisson laws (lines) for $F_{\mathrm{im}} = 1/\mathrm{day}$ (solid) and $F_{\mathrm{im}} = 1/\mathrm{month}$ (dashed), during 688 days and $E_{\mathrm{cut}} = 7$ MeV.**

The selection method defines a candidate as any cluster of $m \geq m_{\mathrm{min}}$ signals within a window of $\Delta t = 20$ s. For a known background rate, m_{min} corresponds to a chosen F_{im} which is set as a threshold. This multiplicity represents the minimum number of neutrino interactions required to produce a supernova "alarm", and contains two terms, one due to the background, $f_{\mathrm{bk}}\Delta t$, and the other due to the neutrino signal. In particular, for LVD, considering only inverse beta decay (IBD) reactions, which are the dominant ones at least in the "standard" supernova model, and simply approximating the detector response to $E_{\mathrm{vis}} = E_{\bar{\nu}_{\mathrm{e}}} - 0.8$ MeV, one can write:

$$m_{\mathrm{min}} = f_{\mathrm{bk}}\Delta t + M_{\mathrm{act}}\ N_{\mathrm{p}}\ \epsilon(E_{\mathrm{cut}}) \int\limits_{0}^{10s} dt \int\limits_{E_{\mathrm{cut}}+0.8MeV}^{100MeV} \Phi(E_{\bar{\nu}_{\mathrm{e}}}, t) \cdot \sigma(E_{\bar{\nu}_{\mathrm{e}}}) dE_{\bar{\nu}_{\mathrm{e}}} \qquad (2)$$

where: M_{act} is the active mass, $N_{\mathrm{p}} = 9.34\ 10^{28}$ is the number of free protons in a scintillator ton, $\epsilon(E_{\mathrm{cut}})$ is the trigger efficiency approximated as constant ($\epsilon = 0.9$ for $E_{\mathrm{cut}} = 7$ MeV and $\epsilon = 0.95$ for $E_{\mathrm{cut}} = 10$ MeV), $\sigma(E_{\bar{\nu}_{\mathrm{e}}})$ is the IBD cross section and $\Phi(E_{\bar{\nu}_{\mathrm{e}}}, t)$ the differential $\bar{\nu}_{\mathrm{e}}$ intensity at the detector. The upper limit in the time integral (10 s) corresponds to the maximum unbiased cluster duration.

Hence the integral on the right side of (2) is the detector burst sensitivity, S, in terms of

minimum neutrino flux times cross section integrated over Δt and ΔE, and is expressed as number of neutrino interactions per target:

$S_{E_{cut}} = (m_{min} - f_{bk}\Delta t)/(M_{act} \cdot N_p \cdot \epsilon)$

The values of S are shown in table 3, for the two LVD thresholds of the imitation frequency, i.e., $F_{im} = 1$ per 100 years and $F_{im} = 1$ per month, two different masses, $M_{act} = 1000$ t and 330 t, and two values of E_{cut}. As it can be seen, an important improvement can be obtained by increasing the energy cut from 7 to 10 MeV. As was shown in figure 5, the minimum cluster multiplicity, for example at $F_{im} = 1$ per 100 years, goes from 22 to 10, allowing an improvement of almost a factor of two in the sensitivity $S_{E_{cut}}$.

It must be noted that in the on-line algorithm described so far we have neglected the capability of LVD to detect both products of the IBD reaction (see section 2.1). We can consider the signature of the reaction to build different burst selection algorithms. For example, we can require that all the H signals in the cluster are "signed", i.e., accompanied by a delayed L one (algorithm IBD-A). The sensitivity of the algorithm IBD-A is shown in Table 3: even if the minimum multiplicity is lower, and the background rate is reduced, because of the n-capture efficiency ($\epsilon_n = 0.5$) the IBD-A method has comparable effectiveness or even less then the on-line one.

We can also build several different algorithms, intermediate between the on-line and the IBD-A ones, requiring that only a fraction of the H signals in the cluster are accompanied by L ones (IBD-B)[4]. However, even if the IBD-B method efficiency results higher (as can be seen in Table 3, where an example is given), it does not exceed the on-line one enough to justify the loss of simplicity of the on-line algorithm and its independence from the model of supernova neutrino emission. Moreover, the on-line algorithm is sensitive to all possible neutrino interactions in LVD, both in the liquid scintillator and in the iron structure (that can represent up to 15% of the total number of interactions).

---

[4]We reject all the clusters which have a number of "signed" H signals $\leq k$, such that: $\sum_{r=0}^{r=k} P(r, m, p) \leq P_0$, where $P(r, m, p)$ is the binomial probability to have r signed pulses in a cluster of multiplicity m. We choose $P_0 = 0.1$ as an example, the case $P_0 = 0$ corresponding to the on-line algorithm.

Table 3: On-line burst sensitivity for different selection algorithms, for two energy thresholds E_{cut} and for two values of imitation frequency; M_{act} is expressed in ton; m_{min} represents the minimum cluster multiplicity (in parenthesis the minimum number of requested "signed" H signals for the IBD-B algorithm).

			$F_{im} = 1 \text{ month}^{-1}$		$F_{im} = 1 \cdot 10^{-2} \text{ year}^{-1}$	
E_{cut}=7 MeV	algorithm	M_{act}	m_{min}	$S_{E_{cut}}$	m_{min}	$S_{E_{cut}}$
	on-line	1000	18	$1.6 \cdot 10^{-31}$	22	$2.1 \cdot 10^{-31}$
		330	10	$3.0 \cdot 10^{-31}$	14	$4.5 \cdot 10^{-31}$
	IBD-A	1000	7	$1.5 \cdot 10^{-31}$	10	$2.2 \cdot 10^{-31}$
		330	5	$3.4 \cdot 10^{-31}$	7	$4.9 \cdot 10^{-31}$
	IBD-B	1000	15(5)	$1.3 \cdot 10^{-31}$	19(7)	$1.7 \cdot 10^{-31}$
		330	9(3)	$2.7 \cdot 10^{-31}$	12(5)	$3.8 \cdot 10^{-31}$
E_{cut}=10 MeV						
	on-line	1000	8	$8.3 \cdot 10^{-32}$	10	$1.1 \cdot 10^{-31}$
		330	5	$1.6 \cdot 10^{-31}$	8	$2.6 \cdot 10^{-31}$

2.2 CNGS beam monitor

The Cern Neutrinos to Gran Sasso (CNGS) project is a high energy, wide band ν_μ beam set up at Cern and sent towards the INFN Gran Sasso National Laboratory (LNGS). Its main goal is the observation of the ν_τ appearance, through neutrino flavour oscillation, by the Opera experiment.

As shown in [18], due to its large area and active mass, LVD can act as a very useful beam monitor, detecting the interaction of neutrinos inside the detector and the muons generated by the ν interaction in the rock upstream the detector. The monitor capabilities have been confirmed during the first CNGS run in August 2006 [19]. Here we report about the events detected by LVD during the CNGS run in fall 2007.

2.2.1 The CNGS beam

The information about the CNGS beam characteristics are taken by the LHCLOG_CNGS_OPERA database (hereafter DB) [20]. Two main quantities are relevant for each proton extraction:

- the UTC time of the spill (in ns),

- the number of extracted protons on target (p.o.t.)

The CNGS beam started its operation [5] on 24th September, 2007 (first spill at 08:46:12.270 UTC) and finished on 20th October (last spill at 02:55:32.670 UTC). In the following we will refer to this run as Run2007. The total number of protons delivered against the graphite target is $8.24 \ 10^{17}$. The beam intensity per each spill is shown in figure 7.
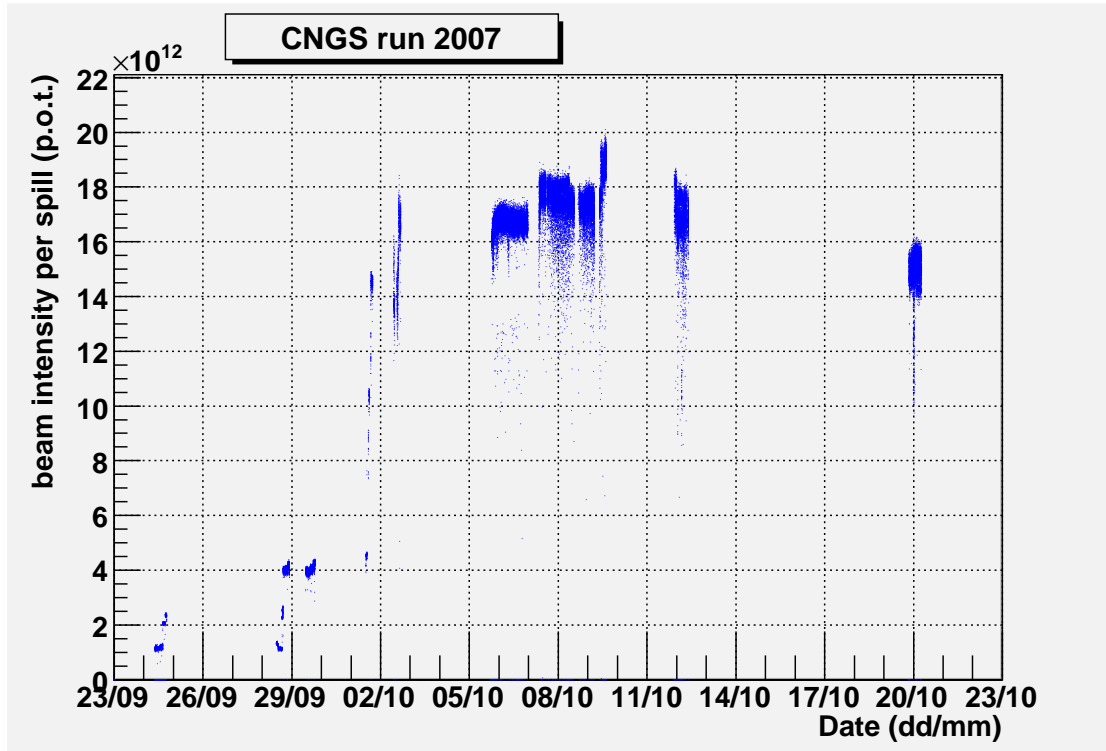

Figure 7: Beam intensity (in protons on target) per each spill.

2.2.2 MC simulation of the expected events

The CNGS events in LVD can be subdivided into two main categories:

- ν_μ charged current (CC) interactions in the rock upstream the LNGS; they produce a muon that can reach LVD and be detected,

- ν_μ CC and neutral current (NC) interactions in the material (liquid scintillator and iron of the support structure) of LVD.

We developed a full Montecarlo simulation that includes the generation of the neutrino interaction products, the propagation of the muon in the Gran Sasso rock and the response of the LVD detector. The details of the simulation were described in [18]; however, with respect to that paper, some modifications were done with up–to–date informations. In particular we now use the CNGS flux calculated in 2005 by the Fluka group [21]

---

[5]We consider only those extraction with both the UTC time and proton intensity informations present in the DB.

and the neutrino cross section NUX-FLUKA [22]. There are also some modifications in the detector: there are actually 7 active levels of scintillation counters instead of the 8 previously considered, and the energy threshold for the definition of a CNGS event is now 100 MeV instead of 200 MeV.

The resulting number of expected events, at the nominal intensity $4.5 \ 10^{19}$ p.o.t./y is 32160/y, equivalent to $7.147 \ 10^{-16}$ events per p.o.t. (considering 200 effective days per year it corresponds to ~ 160 CNGS events per day): 78% are muons from the rock, 17% are CC interactions in the detector and 5% are NC.

During Run2007 the total number of p.o.t. was $8.24 \ 10^{17}$, thus 588 events are expected in LVD.

2.2.3 CNGS detected events

The LVD events are filtered using a very loose selection cut: we require to have at least one scintillation counter with an energy release larger that 100 MeV. The resulting rate is quite stable, with an average value of about 0.1 Hz, see figure 8. As visible, during some short periods, one tower of the apparatus (about one third of the total active mass) was switched off for maintenance.
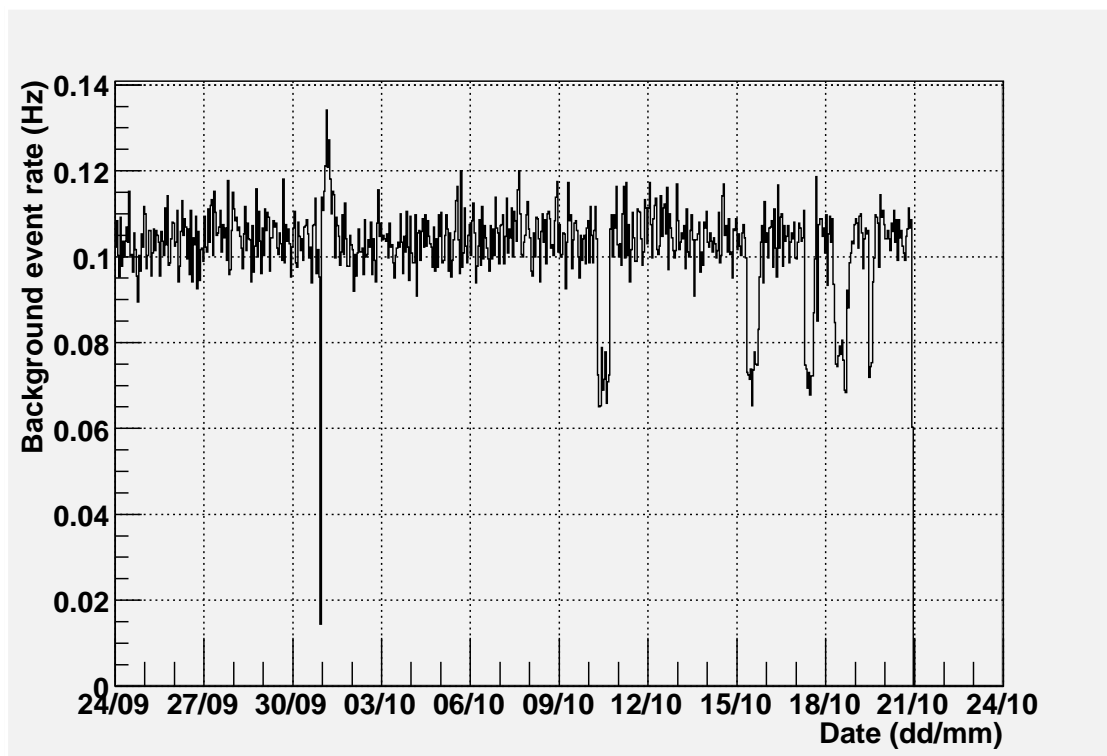

Figure 8: Background rate of events during Run2007. These events present at least one scintillation counter with an energy release larger than 100 MeV.

Among this sample the first selection criteria is based on the coincidence of the LVD event time with the beam spill time written in the DB. Two main corrections have been

done: the neutrino time of flight from Cern to the LNGS (2.440 ms) and the propagation of the GPS time signal from the outside laboratories to slave clocks in the underground hall (42116, 42064 and 42041 ns respectively for tower 1, 2 and 3), measured in July, 2006 together with the other experiments at LNGS [23].

After applying all these corrections, we search for the CNGS events in the interval $[-15, +25]$ μs around the start time of the beam spill. In this way 636 events are selected; their distribution in the time window is shown in figure 9.
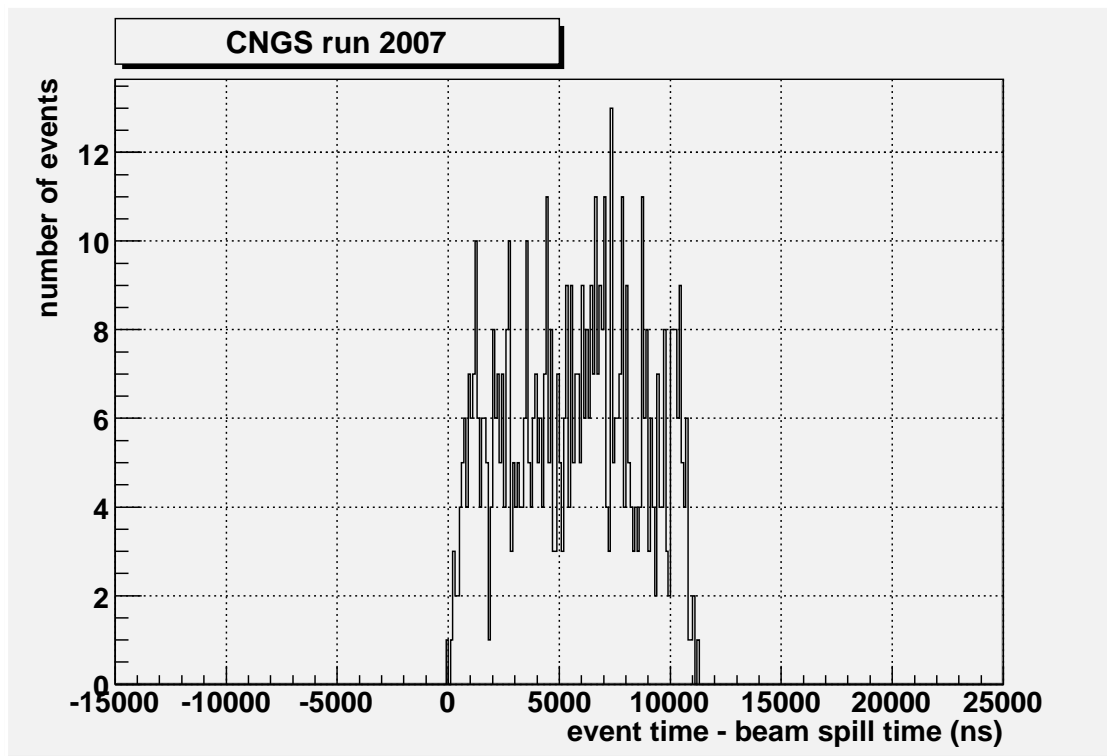

Figure 9: Distribution of the detection time of the CNGS events, with respect to the initial time of the beam spill.

In figure 10 we show the comparison between the expected and detected event rate per each day of data acquisition; in figure 11 the comparison of the integral number of events, hour by hour, is shown. Given the presently limited statistics, the agreement is good.
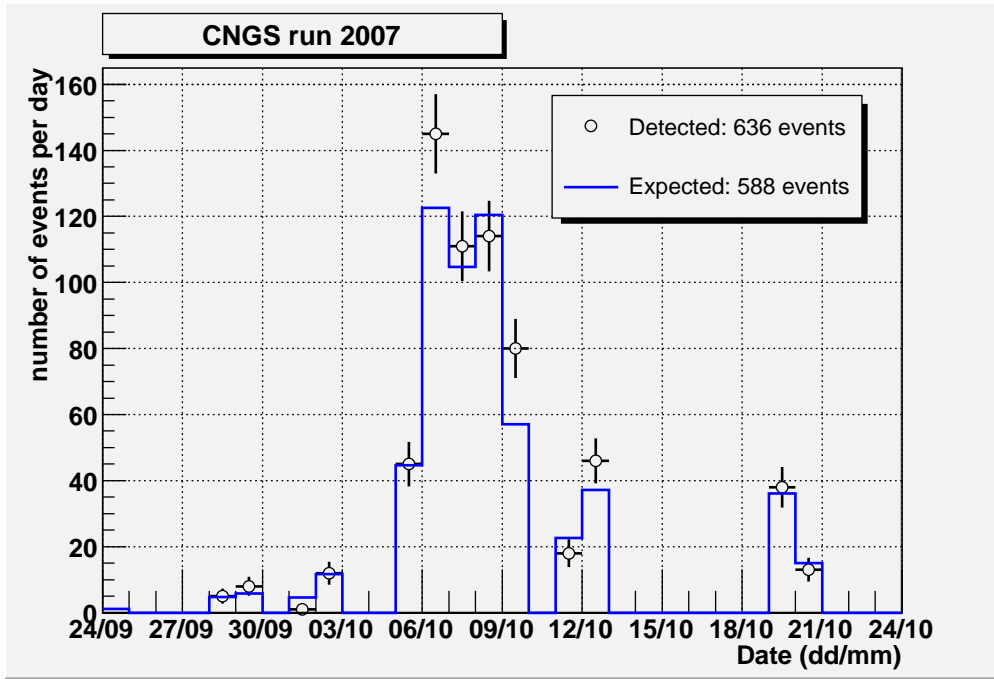
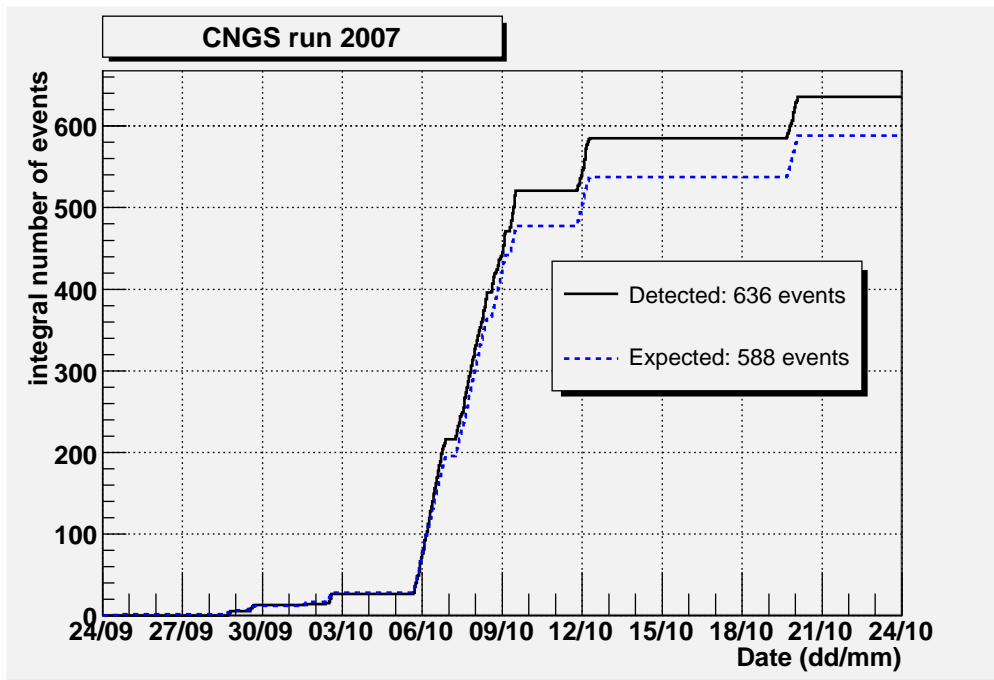Figure 10: Number of events per day: observed (black circles) and expected (blue line).

Figure 11: Integrated number of events: observed (black solid line) and expected (blue dashed line).

Two examples of typical CNGS events in LVD are shown in figure 12 (muon from the rock) and 13 (neutrino interaction inside the detector).
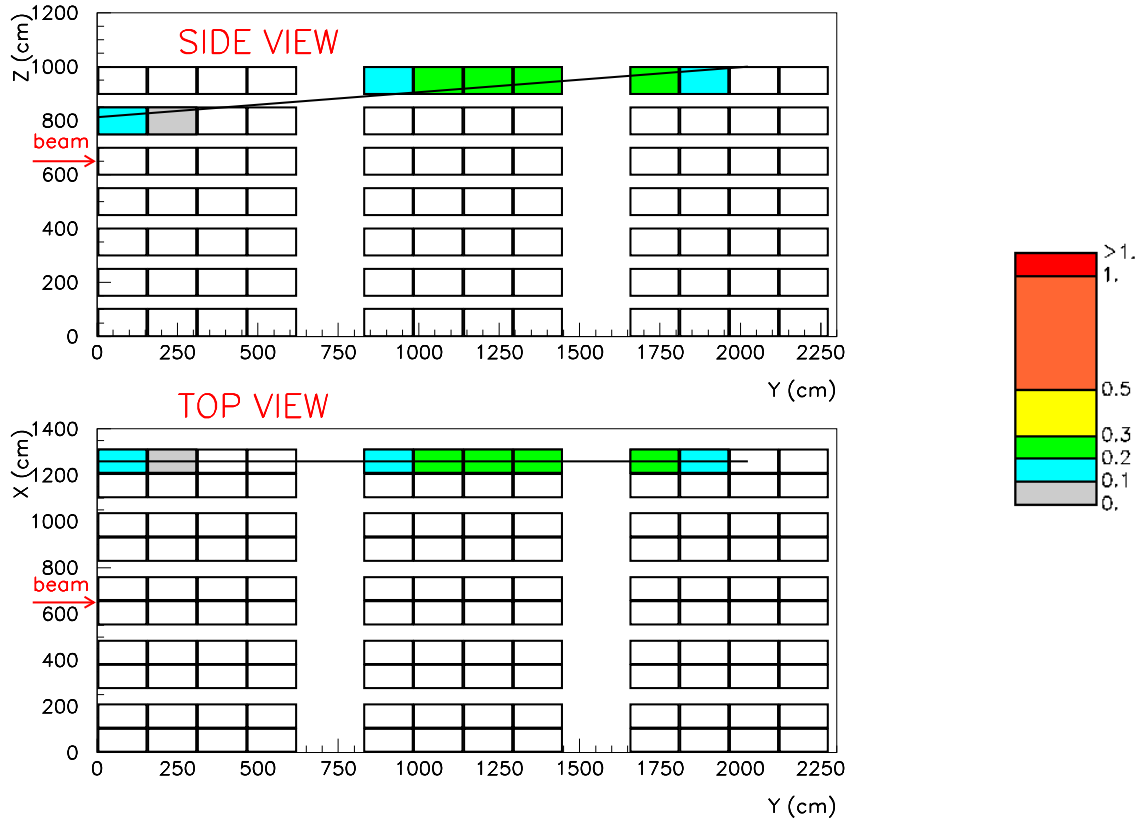
Figure 12: Display of a CNGS events: typical charged current interaction in the rock upstream LVD, producing a muons that go through the detector. The colours represent the amount of energy released in the scintillation counters; the legenda is expressed in GeV. The black straight line is the result of a linear fit to the hit counters.

Figure 13: Display of a CNGS events: neutrino interaction inside the LVD detector. The colours represent the amount of energy released in the scintillation counters; the legenda is expressed in GeV.

Background

The background is estimated considering the rate of events shown in figure 8 among which the CNGS events are searched for, with an average value of 0.10 Hz. The time window where we search for the events around the beam spill time is 40 μs wide, and the number of useful spills in the DB is 53984. Thus the number of events due to the background, during Run2007, is

$$N_{bkg} = 0.1 \ Hz \times 40 \ \mu s \times 53984 = 0.22$$

practically negligible.

2.2.4 Summary

We presented the results of the events detected in 2007 by the LVD detector in coincidence with the CNGS beam. The CNGS run was started in September 2007, with an overall number of 8.2 10^{17} protons delivered on the target. The LVD detector was fully operative during the whole run, with an average active mass of 950 t.

120

LVD can detect the CNGS neutrinos through the observation of penetrating muons originated by ν_μ CC interactions in the rock upstream the LNGS and through internal CC and NC neutrino interactions.

The expected number of events, as predicted by our Montecarlo simulation, is 588. We searched for the CNGS events by looking at the time coincidence with the beam spill time; the number of detected events is 636.

We estimate that the number of events due to the background is lower than one in the whole run time.

3   List of publications in 2007

- *On-line recognition of supernova neutrino bursts in the LVD detector*
  Astroparticle Physics 28 (2008) 516-522.
  e-Print Archive: 0710.0259 [astro-ph]

- *First CNGS events detected by LVD*
  Eur. Phys. J. C52 (2007) 849-855.
  e-Print Archive: 0710.1536 [hep-ex]

- *Study of the effect of neutrino oscillations on the supernova neutrino signal in the LVD detector*
  Astroparticle Physics 27 (2007) 254-270.
  e-Print Archive: hep-ph/0609305

- *Supernova neutrino detection with LVD.*
  Prepared for Workshop on Next Generation Nucleon Decay and Neutrino Detectors 2006 (NNN06 / Seattle), Seattle, Washington, 21-23 Sep 2006.
  Published in: AIP Conf. Proc. 944: 16-24, 2007.

- *First CNGS events detected by LVD.*
  Prepared for Workshop on Next Generation Nucleon Decay and Neutrino Detectors 2006 (NNN06 / Seattle), Seattle, Washington, 21-23 Sep 2006.
  Published in: AIP Conf. Proc. 944: 7-15, 2007.

- *First events of the CNGS beam detected by LVD*
  In: Proc. 30 ICRC, Merida, Mexico, 2007. Session: HE.1.5

- *Search for neutrino bursts from gravitational stellar collapses with LVD: update to 2007*
  In: Proc. 30 ICRC, Merida, Mexico, 2007. Session: HE.2.3

References

[1] LVD Collaboration, Il Nuovo Cimento **A105** (1992) 1793

[2] A. Strumia, F. Vissani, `astro-ph/0302055`.

[3] LVD Collaboration, 23th ICRC Conf. Proc., HE 5.1.1, Vol.4, 468, 1993

[4] LVD Collaboration, 24th ICRC Conf. Proc., HE 5.3.6, Vol.1, 1035, 1995

[5] LVD Collaboration, 25th ICRC Conf. Proc., HE 4.1.12, 1997

[6] LVD Collaboration, 26th ICRC Conf. Proc., HE 4.2.08, Vol.2, 223, 1999

[7] LVD Collaboration, 27th ICRC Conf. Proc., HE 230, 1093, 2001

[8] LVD Collaboration, 28th ICRC Conf. Proc., HE 2.3, 1333, 2003

[9] LVD Collaboration, 29th ICRC Conf. Proc., OG 2.5, 59, 2005

[10] LVD Collaboration, 30th ICRC Conf. Proc., HE 2.3, 2007

[11] LVD Collaboration, Nucl. Phys. B Proc. Sup. 110, (2002) 410-413, astro-ph/0112312

[12] A. Zichichi, *The most powerful scintillator supernova neutrino detector*, talk presented at the symposium *LVD: the First Ten Years*, LNGS, 28-29 October, 2002).

[13] LVD Collaboration, 28th ICRC Conf. Proc., HE 2.3, 1297, 2003

[14] N. Yu. Agafonova *et al.*, *Study of the effect of neutrino oscillations on the supernova neutrino signal in the LVD detector*, Astropart. Phys. **27**, 254-270 (2007) [arXiv: hep-ph/0609305].

[15] http://hep.bu.edu/∼snnet/

[16] P. Antonioli et al., New J. Phys., 6 (2004) 114

[17] N. Yu. Agafonova *et al.*, *On-line recognition of supernova neutrino bursts in the LVD detector*, Astropart. Phys. **28**, 516-522 (2008) [arXiv:0710.0259].

[18] M. Aglietta et al., *CNGS beam monitor with the LVD detector*, Nuclear Instruments and Methods in Physics Research **A 516**, 96 (2004).

[19] N. Yu. Agafonova et al., *First CNGS events detected by LVD*, Eur. Phys. J. **C 52**, 849-855 (2007) [arXiv:0710.1536 hep-ex].

[20] C. Roderick, LHC LOGGING - CNGS-OPERA gateway database user guide, https://edms.cern.ch/file/750206/1/LHCLOG_CNGS_OPERA_GW_DB_GUIDE.pdf.

[21] A. Ferrari et al., *An updated Monte Carlo calculation of the CNGS neutrino beam*, CERN-AB-Note-2006-038, EDMS No. 745389.
Fluxes available in http://www.mi.infn.it/∼psala/Icarus/cngs.html

[22] G. Battistoni et al., *The FLUKA nuclear cascade model applied to neutrino interactions*, Proceedings of NUINT'02, December 2002, University of California, Irvine, USA.
Available online at http://nuint.ps.uci.edu/proceedings/sala.pdf

[23] D. Autiero et al., *Measurement of the fibre delays for the GPS signal underground distribution*, internal note, (2006).

OPERA

R. Acquafredda[3], N. Agafonova[18], M. Ambrosio[24], A. Anokhina[21], S. Aoki[15], A. Ariga[23], L. Arrabito[17], D. Autiero[17], A. Badertscher[37], A. Bergnoli[28], F. Bersani Greggio[9], M. Besnier[2], M. Beyer[30], S. Bondil-Blin[27], K. Borer[5], J. Boucrot[27], V. Boyarkin[18], C. Bozza[31], R. Brugnera[28], S. Buontempo[24], Y. Caffari[17], J. E. Campagne[27], B. Carlus[17], E. Carrara[28], A. Cazes[9], L. Chaussard[17], M. Chernyavsky[20], V. Chiarella[9], N. Chon-Sen[33], A. Chukanov[8], R. Ciesielski[28], L. Consiglio[6], M. Cozzi[6], F. Dal Corso[28], N. D'Ambrosio[3], J. Damet[2], G. De Lellis[24], Y. Déclais[17], T. Descombes[17], M. De Serio[4], F. Di Capua[24], D. Di Ferdinando[6], A. Di Giovanni[16], N. Di Marco[16], C. Di Troia[9], S. Dmitrievski[8], M. Dracos[33], D. Duchesneau[2], B. Dulach[9], S. Dusini[28], J. Ebert[12], R. Enikeev[18], A. Ereditato[5], L. S. Esposito[3], C. Fanin[28], J. Favier[2], G. Felici[9], T. Ferber[12], L. Fournier[2], A. Franceschi[9], D. Frekers[22], T. Fukuda[23], C. Fukushima[10], V. I. Galkin[21], V. A. Galkin[26], R. Gallet[2], A. Garfagnini[28], G. Gaudiot[33], G. Giacomelli[6], O. Giarmana[17], M. Giorgini[6], L. Girard[17], C. Girerd[17], C. Goellnitz[12], J. Goldberg[11], Y. Gornoushkin[8], G. Grella[31], F. Grianti[9], C. Guerin[17], M. Guler[1], C. Gustavino[3], C. Hagner[12], T. Hamane[2], T. Hara[15], M. Hauger[25], M. Hess[5], K. Hoshino[23], M. Ieva[4], M. Incurvati[9], K. Jakovcic[36], J. Janicsko Csathy[25], B. Janutta[12], C. Jollet[33], F. Juget[25], M. Kazuyama[23], S. H. Kim[13], M. Kimura[10], J. Knuesel[5], K. Kodama[14], D. Kolev[32], M. Komatsu[23], U. Kose[1], A. Krasnoperov[8], I. Kreslo[5], Z. Krumstein[8], I. Laktineh[17], C. de La Taille[27], T. Le Flour[2], S. Lieunard[2], A. Ljubicic[36], A. Longhin[28], A. Malgin[18], K. Manai[34], G. Mandrioli[6], U. Mantello[28], A. Marotta[24], J. Marteau[17], G. Martin-Chassard[27], V. Matveev[18], M. Messina[5], L. Meyer[5], S. Micanovic[36], P. Migliozzi[24], S. Miyamoto[23], P. Monacelli[16], I. Monteiro[2], K. Morishima[23], U. Moser[5], M. T. Muciaccia[4], P. Mugnier[2], N. Naganawa[23], M. Nakamura[23], T. Nakano[23], T. Napolitano[9], M. Natsume[23], K. Niwa[23], Y. Nonoyama[23], A. Nozdrin[8], S. Ogawa[10], A. Olchevski[8], D. Orlandi[3], D. Ossetski[26], A. Paoloni[9], B. D Park[23], I. G. Park[13], A. Pastore[4], L. Patrizii[6], L. Pellegrino[9], H. Pessard[2], V. Pilipenko[22], C. Pistillo[5], N. Polukhina[20], M. Pozzato[6], K. Pretzl[5], P. Publichenko[21], L. Raux[27], J. P. Repellin[27], T. Roganova[21], G. Romano[31], G. Rosa[29], A. Rubbia[37], V. Ryasny[18], O. Ryazhskaya[18], D. Ryzhikov[26], A. Sadovski[8], C. Sanelli[9], O. Sato[23], Y. Sato[35], V. Saveliev[26], N. Savvinov[5], G. Sazhina[21], A. Schembri[29], W. Schmidt Parzefall[12], H. Schroeder[30], H. U. Schütz[5], L. Scotto Lavina[24], J. Sewing[12], H. Shibuya[10], S. Simone[4], M. Sioli[6], C. Sirignano[31], G. Sirri[6], J. S. Song[13], R. Spaeti[5], M. Spinetti[9], L. Stanco[28], N. Starkov[20], M. Stipcevic[36], P. Strolin[24], V. Sugonyaev[28], S. Takahashi[23], V. Tereschenko[8], F. Terranova[9], I. Tezuka[35], V. Tioukov[24], I. Tikhomirov[19], P. Tolun[1], T. Toshito[23], V. Tsarev[20], R. Tsenov[32], U. Ugolino[24], N. Ushida[14], G. Van Beek[7], V. Verguilov[32], P. Vilain[7], L. Votano[9], J. L. Vuilleumier[25], T. Waelchli[5], R. Waldi[30], M. Weber[5], G. Wilquet[7], B. Wonsak[12] R. Wurth[30], J. Wurtz[33], V. Yakushev[18], C. S. Yoon[13], Y. Zaitsev[19], I. Zamboni[36] and R. Zimmermann[12].

125

1. METU-Middle East Technical University, TR-06531 Ankara, Turkey
2. LAPP, Université de Savoie, CNRS/IN2P3, 74941 Annecy-le-Vieux, France
3. Laboratori Nazionali del Gran Sasso dell'INFN, 67010 Assergi (L'Aquila), Italy
4. Dipartimento di Fisica dell'Università di Bari and INFN, 70126 Bari, Italy
5. University of Bern, CH-3012 Bern, Switzerland
6. Dipartimento di Fisica dell'Università di Bologna and INFN, 40127 Bologna, Italy
7. IIHE-Inter-University Institute for High Energies, Université Libre de Bruxelles, B-1050 Brussels, Belgium
8. JINR-Joint Institute for Nuclear Research, 141980 Dubna, Russia
9. Laboratori Nazionali di Frascati dell'INFN, 00044 Frascati (Roma), Italy
10. Toho University, 274-8510 Funabashi, Japan
11. Department of Physics, Technion, 32000 Haifa, Israel
12. Hamburg University, 22043 Hamburg, Germany
13. Gyeongsang National University, 900 Gazwa-dong, Jinju 660-300, Korea
14. Aichi University of Education, 448 Kariya (Aichi-Ken), Japan
15. Kobe University, 657 Kobe, Japan
16. Dipartimento di Fisica dell'Università dell'Aquila and INFN, 67100 L'Aquila, Italy
17. IPNL, Université Claude Bernard Lyon 1, CNRS/IN2P3, 69622 Villeurbanne, France
18. INR-Institute for Nuclear Research of the Russian Academy of Sciences, 117312 Moscow, Russia
19. ITEP-Institute for Theoretical and Experimental Physics, 117259 Moscow, Russia
20. LPI-Lebedev Physical Institute of the Russian Academy of Sciences, 117924 Moscow, Russia
21. SINP MSU-Skobeltsyn Institute of Nuclear Physics of Moscow State University, 119992 Moscow, Russia
22. University of Münster, 48149 Münster, Germany
23. Nagoya University, 464-01 Nagoya, Japan
24. Dipartimento di Fisica dell'Università Federico II di Napoli and INFN, 80125 Napoli, Italy
25. Université de Neuchâtel, CH 2000 Neuchâtel, Switzerland
26. Obninsk State University, Institute of Nuclear Power Engineering, 249020 Obninsk, Russia
27. LAL, Université Paris-Sud 11, CNRS/IN2P3, 91898 Orsay, France
28. Dipartimento di Fisica dell'Università di Padova and INFN, 35131 Padova, Italy
29. Dipartimento di Fisica dell'Università di Roma "La Sapienza" and INFN, 00185 Roma, Italy
30. Fachbereich Physik der Universität Rostock, 18051 Rostock, Germany
31. Dipartimento di Fisica dell'Università di Salerno and INFN, 84084 Fisciano, Salerno, Italy
32. Faculty of Physics, Sofia University "St. Kliment Ohridski", 1000 Sofia, Bulgaria
33. IPHC, Université Louis Pasteur, CNRS/IN2P3, 67037 Strasbourg, France
34. UPNHE-Unité de de Physique Nucléaire et des Hautes Energies, 1060 Tunis, Tunisia
35. Utsunomiya University, 320 Tochigi-Ken, Utsunomiya, Japan
36. IRB-Rudjer Boskovic Institute, 10002 Zagreb, Croatia
37. ETH-Eidgenössische Technische Hochschulen Zürich, CH-8092 Zurich, Switzerland

Abstract

The OPERA neutrino detector at the underground Gran Sasso Laboratory (LNGS) is designed to perform the first detection of neutrino oscillations in appearance mode, through the study of $\nu_\mu \to \nu_\tau$ oscillations. The apparatus consists of a lead/emulsion-film target complemented by electronic detectors. It is placed in the high-energy, long-baseline CERN to LNGS beam (CNGS)in Hall C of Gran Sasso Underground Laboratory, 730 km away from the neutrino source. In August 2006 a first run with CNGS neutrinos was successfully conducted. A first sample of neutrino events was collected by the electronic detectors of OPERA; the sample was statistically consistent with the integrated beam intensity. In Summer 2007 a second run with CNGS neutrinos was conducted, and a sample of neutrino interactions in the lead/emulsion target of the experiment was collected. Unfortunately the beam delivery was stopped due to malfunctioning of some control equipment in the proton

beam target area; the beam will be resumed in Summer 2008. After a brief description of the beam and of the various sub-detectors, we report on the achievements obtained during 2007, presenting the first data, the status of the detector and of the needed infrastructures.

1   Introduction

The solution of the long-standing solar and atmospheric neutrino puzzles has come from the hypothesis of neutrino oscillations. This implies that neutrinos have non vanishing and not degenerate masses, and that their flavor eigenstates involved in weak interaction processes are a superposition of their mass eigenstates.

Several key experiments conducted in the last decades with solar neutrinos, and with atmospheric, reactor and accelerator neutrinos, have contributed to build-up our present understanding of neutrino mixing. Atmospheric neutrino oscillations, in particular, have been studied by the Super-Kamiokande, Kamiokande, MACRO and SOUDAN2 experiments. Long baseline experiments confirmed the oscillation hypothesis with accelerator neutrinos: K2K in Japan and MINOS in the USA. The CHOOZ and Palo Verde reactor experiments excluded the $\nu_\mu \rightarrow \nu_e$ channel as the dominant one in the atmospheric sector.

However, the direct appearance of a different neutrino flavor is still an important open issue. Long-baseline accelerator neutrino beams can be used to probe the atmospheric neutrino signal and confirm the preferred solution of $\nu_\mu \rightarrow \nu_\tau$ oscillations. In this case, the beam energy should be large enough to produce the heavy τ lepton. This is one of the main goals of the OPERA experiment that uses the long baseline (L=730 km) CNGS neutrino beam from CERN to LNGS. The challenge of the experiment is to measure the appearance of ν_τ from ν_μ oscillations. This requires the detection of the short-lived τ lepton (cτ = 87.11 μm) with high efficiency and low background. The τ is identified by the detection of its characteristic decay topologies, in one prong (electron, muon or hadron) or in three-prongs. The τ track is measured with a large-mass sampling-calorimeter made of 1 mm thick lead plates (absorber material) inter-spaced with thin emulsion films (high-accuracy tracking devices).

The OPERA detector is made of two identical Super Modules each consisting of a target section of about 900 ton made of lead/emulsion-film ECC modules (bricks), of a scintillator tracker detector, needed to pre-localize neutrino interactions within the target, and of a muon spectrometer.

The construction of the CNGS beam has been recently completed and a first run took place in August 2006 with good performance of the facility. First data were collected by the OPERA detector still without ECC bricks installed, yielding a preliminary measurement of the beam features along with the collection of a number of neutrino interactions (319) consistent with the integrated beam intensity of 7.6 $\times$ 10^{17} protons on target (p.o.t.). The OPERA experiment operated very satisfactorily during the run. In 2007 a second run was foreseen and some neutrino interactions¡ in the ECC bricks have been collected. Unfortunately the beam had to be stopped before schedule because of some malfunctioning of a temperature control system near the proton target. The beam will be resumed in Summer 2008

2 The CNGS beam and the OPERA experiment

The CNGS neutrino beam was designed and optimized for the study of $\nu_\mu \to \nu_\tau$ oscillations in appearance mode, by maximizing the number of charged current (CC) ν_τ interactions at the LNGS site. A 400 GeV proton beam is extracted from the CERN SPS in 10.5 μs short pulses with design intensity of 2.4×10^{13} p.o.t. per pulse. The proton beam is transported through the transfer line TT41 to the CNGS target T40. The target consists of a series of thin graphite rods helium-cooled. Secondary pions and kaons of positive charge produced in the target are focused into a parallel beam by a system of two magnetic lenses, called horn and reflector. A 1,000 m long decay-pipe allows the pions and kaons to decay into muon-neutrinos and muons. The remaining hadrons (protons, pions, kaons) are absorbed by an iron beam-dump. The muons are monitored by two sets of detectors downstream of the dump; they measure the muon intensity, the beam profile and its center. Further downstream the muons are absorbed in the rock while neutrinos continue their travel towards Gran Sasso.

The average neutrino energy at the LNGS location is ~ 17 GeV. The $\bar{\nu}_\mu$ contamination is $\sim 4\%$, the ν_e and $\bar{\nu}_e$ contaminations are lower than 1%, while the number of prompt ν_τ from D_s decay is negligible. The average L/E_ν ratio is 43 km/GeV. Due to the earth curvature neutrinos from CERN enter the LNGS halls with an angle of about 3° with respect to the horizontal plane.

Assuming a CNGS beam intensity of 4.5×10^{19} p.o.t. per year and a five year run about 31,000 CC plus neutral current (NC) neutrino events will be collected by OPERA from interactions in the lead-emulsion target. Out of them 95 (214) CC ν_τ interactions are expected for oscillation parameter values $\Delta m_{23}^2 = 2 \times 10^{-3}$ eV^2 (3×10^{-3} eV^2) and $\sin^2 2\theta_{23}=1$. Taking into account the overall τ detection efficiency the experiment should gather 10-15 signal events with a background of less than one event.

In the following, we give a brief description of the main components of the OPERA detector.

The target, subdivided in two Super Modules (SM1 and SM2) will consist of around 154000 lead/emulsion bricks arranged in 62 target planes (Fig. 1), each one followed by two scintillator planes with an effective granularity of 2.6×2.6 cm^2. These planes serve as trigger devices and allow selecting the brick containing a neutrino interaction. A muon spectrometer at the downstream end of each SM allows to measure the muon charge and momentum. A large size anti-coincidence detector placed in front of SM1 allows to veto (or tag) interactions occurring in the material and in the rock upstream of the target.

The construction of the experiment started in Spring 2003. The first instrumented magnet was completed in May 2004 together with the first half of the target support structure. The second magnet was completed in the beginning of 2005. In Spring 2006 all scintillator planes were installed. The production of the ECC bricks started in October 2006 with the aim of completing the full target for the high-intensity run of 2008. After some conditioning of BAM (Brick Assembling Machine) the high speed production started in 2007 and at the end of the year around 80000 bricks had been produced and inserted into the detector target by the BMS (Brick Manipulating System).

Fig. 2 shows a photograph of the detector in the underground Hall C of LNGS as it was during the neutrino run.
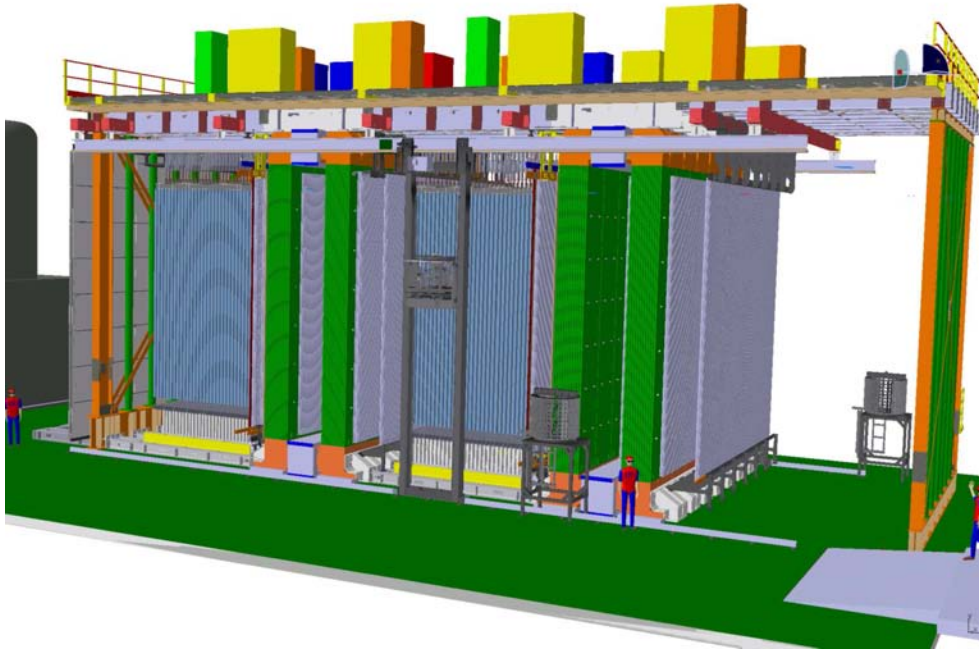
Figure 1: Schematic drawing of the OPERA detector at LNGS.

2.1 The electronic detectors

The construction in Strasbourg and the installation in the LNGS underground laboratory of the OPERA Target Tracker, responsible to indicate the right lead/emulsion brick to extract from the detector target, finished in May 2006. The Target Tracker is composed by 62 walls, each one associated with one brick wall. Each Target Tracker wall contains four horizontal and four vertical modules defining a sensitive area of about 7x7 m2. The Target Tracker modules enclose 64 scintillator strips readout by Wave Length Shifting fibres and multianode Hamamatsu photomultipliers. For the whole Target Tracker (496 modules), 992 photomultipliers, 31200 AMCRYS-H scintillator strips and about 300 km Kuraray WLS fibre have been used. Since summer 2006 the Target Tracker is fully operational. A big number of cosmic rays has been recorded since the end of the Target Tracker installation. These cosmic rays are used for alignment testing and m.i.p. detection efficiency evaluation. It has been verified that the Target Tracker detection efficiency is higher than 98%, as expected by the calibration tests done during the module construction

Muon identification and charge measurement are needed for the study of the muonic τ-decay channel and for the suppression of the background from the decay of charmed particles, featuring the same topology. Each muon spectrometer consists of a dipolar magnet made of two iron arms for a total weight of 990 ton. The measured magnetic field intensity is 1.52 T. The OPERA magnets have been commissioned in spring 2006 and were fully operative since the first CNGS run. In 2007 most of the activities have been devoted to the completion of the slow control. A set of hard-wired alarms have been installed to allow for automatic ramp-down of the magnet power supplies in the occurrence of failures at the cooling system. Moreover, an overall Alarm Manager has been developed and tested: it supervises the clients of all temperature probes both

Figure 2: Lateral view of OPERA in the LNGS Hall C.

in the magnets and in the cooling circuits, the status, currents and voltages of the power supplies and signal anomalies to on-call experts and on-site operators. This Manager is interfaced with the RPC/Magnet database (Postgres) and exchanges information with the OPERA DAQ through CORBA. Finally, two additional heat exchangers have been installed along the upper part of the bottom coil in both magnets.

During the 2007 physics runs the magnets were operated continuously. The livetime in the presence of neutrino beam has been 100% for both of them. Unwilled ramp-down have been reported only during power cuts (after the completion of the brick production, all services will be put under UPS). Since in 2007 the power supplies were permanently on without interruptions for several weeks, long term thermal tests have been carried out. It has been demonstrated that the coils reach thermal equilibrium in about 30 hours and the overall spectrometer, including the iron bulk, reaches equilibrium after ~ 5 days. The temperature increase of the OPERA Precision Trackers and the RPC never exceeded 1.5 degree.

In 2008, we plan to interface the standalone OPERA cooling system with the water circuits of LNGS through a dedicated heat exchanger; we will also setup an automatic refill system for demineralized water. Moreover, work is in progress to improve the accessibility of the Alarm Manager with emphasis on the development of web interfaces to the database and the alarms, and the commissioning of an automatic alerting system based on GPRS cards.

The two arms of magnets are interleaved with vertical, 8 m long drift-tube planes (PT) for the

precise measurement of the muon-track bending.

The Precision Tracker (PT) is built of thin walled aluminum tubes with 38 mm outer diameter and 8 m length. Each of the $\sim$ 10,000 tubes has a central sense wire of 45 μm diameter. They can provide a spatial resolution better than 300 μm. Each spectrometer is equipped with six fourfold layers of tubes.

For each SM three independent trigger stations are installed to identifiy muons from beam neutrinos but also to be sensitive to stopping muons from beam and cosmic rays.

Planes of Resistive Plates Chambers (RPCs) are inserted between the iron plates of the arms, providing a coarse tracking inside the magnet, range measurement of the stopping particles and a calorimetric analysis the hadronic shower.

RPCs identify penetrating muons and measure their charge and momentum in an independent way with respect to the PT. They consist of electrode plates made of 2 mm thick plastic laminate of high resistivity painted with graphite. Induced pulses are collected on two pickup strip planes made of copper strips glued on plastic foils placed on each side of the detector. The number of individual RPCs is 924 for a total detector area of 3,080 m^2. The total number of digital channels is about 25,000, one for each of the 2.6 cm (vertical) and 3.5 cm (horizontal) wide strips.

In order to solve ambiguities in the track, spatial-reconstruction each of the two drift-tube planes of the PT upstream of the dipole magnet is complemented by an RPC plane with two 42.6° crossed strip-layers called XPCs. RPCs and XPCs give a precise timing signal to the PTs.

Finally, a detector made of glass RPCs is placed in front of the first Super Module, acting as a veto system for interactions occurring in the upstream rock.

OPERA has a low data rate from events due to neutrino interactions well localized in time, in correlation with the CNGS beam spill. The synchronization with the spill is done offline via GPS. The detector remains sensitive during the inter-spill time and runs in a trigger-less mode. Events detected out of the beam spill (cosmic-ray muons, background from environmental radioactivity, dark counts) are used for monitoring. The global DAQ is built as a standard Ethernet network whose 1,147 nodes are the Ethernet Controller Mezzanines plugged on controller boards interfaced to each sub-detector specific front-end electronics. A general 10 ns clock synchronized with the local GPS is distributed to all mezzanines in order to insert a time stamp to each data block. The event building is performed by sorting individual subdetector data by their time stamps.

2.2   Emulsion films, bricks and related facilities

An R&D collaboration between the Fuji Company and the Nagoya group allowed the large scale production of the emulsion films needed for the experiment (more than 12 million individual films) fulfilling the requirements of uniformity of response and of production, time stability, sensitivity, schedule and cost. The main peculiarity of the emulsion films used in high energy physics compared to normal photographic films is the relatively large thickness of the sensitive layers ($\sim$ 44 μm) placed on both sides of a 205 μm thick plastic base.

A target brick consists of 56 lead plates of 1 mm thickness and 57 emulsion films. The plate material is a lead alloy with a small calcium content to improve its mechanical properties. The transverse dimensions of a brick are 12.7 $\times$ 10.2 cm^2 and the thickness along the beam direction is 7.5 cm (about 10 radiation lengths). The bricks are housed in support structures placed between consecutive TT walls.

In order to reduce the emulsion scanning load the use of Changeable Sheets, successfully applied in the CERN CHORUS experiment, was extended to OPERA. CS doublets are attached to the downstream face of each brick and can be removed without opening the brick. Charged particles from a neutrino interaction in the brick cross the CS and produce a trigger in the TT scintillators. Following this trigger the brick is extracted and the CS developed underground and analyzed in the scanning facility at LNGS.

The information of the CS is used for a precise prediction of the position of the tracks in the most downstream films of the brick, hence guiding the so-called scan-back vertex-finding procedure.

The hit brick finding is one of the most critical operations for the success of the experiment, since one aims at high efficiency and purity in detecting the brick containing the neutrino interaction vertex. This requires the combination of adequate precision of the TT, precise extrapolation and high track finding efficiency in the CS scanning procedure.

While running the experiment, after the analysis of their CS doublets, bricks with neutrino events are brought to the LNGS external laboratory, exposed for several hours to cosmic-ray muons for film alignment and then disassembled. The films are developed with an automatic system in parallel processing chains. In 2007 the large Laboratory for emulsion plate development, was arranged close to its final shape, and the first real-case bricks extracted after the CNGS pilot runs were successfully processed therein.

The Laboratory, designed to be hosted in the new building recently open to users at the surface LNGS site, is at close internal path from the Cosmic ray exposure pit (40 cm Fe shielding), in turn a branch of the same building. Apart from complementary equipment, it includes: a) A Chemical Plant with 1) large-scale equipment for filtering, thermal control and demineralization of large volumes of water, as a solvent of chemicals and for final plate washing; 2) large volume tanks for numerically controlled preparation of the chemicals needed for the emulsion development and fixation; 3) Intermediate tanks and pipelines to service the development lines; 4) differentiated collection and exhaustion of wasted solutions out to large external tanks. b) An Automated development system, hosted in large safelight darkrooms, with Six independent lines, running in parallel, and step-timed tanks, locally controlled by PLC's.

The expected number of bricks extracted per running-day with the full target installed and CNGS nominal intensity is about 30. The large emulsion surface to be scanned requires fast automatic microscopes continuously running at a speed of ~ 20 cm^2 film surface per hour. This requirement has been met after R&D studies conducted using two different approaches by some of the European groups of the Collaboration and by the Japanese groups.

3   The Brick Assembly Machine (BAM)

The construction of more than 150,000 bricks for the neutrino target is accomplished by an automatic machine, the Brick Assembly Machine (BAM) operating underground in order to minimize the number of background tracks from cosmic-rays and environmental radiation. The BAM has been mounted during 2006 in a specially constructed site in the underground laboratory and has started the brick production. After the pilot production of OPERA bricks in October 2006,

the list of items to be retuned in the BAM was clearly defined in order to comply with the new technical specs mostly on lead and emulsion sheets in terms of stickiness and the stability of CS boxes and skates. A plan of action was defined in order to refurbish the BAM line with additional options on the piling sections and to upgrade the software of the automatic quality control based on real time image processing. The main actions (concerning the piling speed and stability) were implemented in the first three months of 2007 and we had a successful start up of the brick mass production in middle of march 2007. A two shift running mode was activated with 16h total working time/day (6:00 to 22:00). At the same time the stability of the production was monitored in order to perform the natural fine tuning in the production process, profiting of the daily experience. A team of six BAM site managers was set, leading the BAM team of 14 shifters (2x7/day). After the initial training phase, the mass production in April 2007 had reached a rate of about 250 bricks/day which was gradually increased up to about 480 bricks/day by June 07. An upgrade of the software was needed in order to fulfill the new daily performance. Concerning the CS box gluing stability, a new CS glue deposit station was designed, installed and commissioned since July 2007. The original brick skating performances based on teflon skates were not stable as expected (loose gluing of skates on brick itself). The situation was improved with the use larger and thicker Tyvek skates, applied with a new automatic custom station.Unfortunately also this option later on turned out not to be perfect having a relevant amount of glue released in the long period during the brick insertion phase. A third option has been implemented (compatible with the same automatic station) using PE skates with better friction coefficient and no glue deposit during brick insertion operations. By the end of august a rate of about 700 bricks/day (3 drums/day) has been reached, reducing all the dead times in the production process. At this rate a hardware upgrading of the wrapping station was needed in order to have a contingency margin in wrapping station speed. This was clearly needed to minimise the amount of bricks to store on the floor in dark room and to let recover them in some forced pauses during the wrapping operations. Such a hardware upgrading was implemented by the end of 2007 and activated in beginning of 2008. The brick quality and uniformity was improved day by day profiting also af all the feedback received by the BMS team. During last part of the year, the production speed was reduced in order to let BMS team move their system from SM1 to SM2 on both side of the detector in Hall C. The year 2007 was closed with a global production of 82743 bricks.

4   The Brick Manipulating System (BMS)

The Brick Manipulator System (BMS) is an automated system conceived and developed by CNRS-LAPP Annecy to handle the 150 000 target bricks of OPERA. This system has two main functions. The first one is to install the bricks in the target supporting structure. This operation has to follow the rate of brick assembly by the BAM, the storage at the exit of the brick production line being limited to less than 1% of the total number of bricks (6 transport drums of 234 bricks). The second function of the Brick Manipulator System, when the detector records neutrino interactions from the CNGS beam, is to extract for analysis target bricks pointed by the electronic trackers as containing a neutrino vertex and to deliver them every day to brick processing. Two symmetric manipulators are moving along and operating separately on the sides of the OPERA

detector. Each system, or *portico*, allows a manipulation platform to be positioned in front of a given brick row. Porticoes move along the beam direction, and a manipulation platform moves vertically within each portico. The function of brick manipulation platforms is to slide bricks on their supporting target trays from a local storage carrousel, or back from trays to carrousel. Pushing jacks are used to load the bricks in the detector and a small vehicle equipped with a suction grip system can retrieve the bricks back to the carrousel. In addition, to load with bricks platform carrousels or unload them, special loading stations including three movements have also been developed. Revolving drums containing 9 levels of 26 bricks (the contents of 9 target trays) are filled in the BAM area and brought on top of these loading stations. Fig. 3 shows one of the BMS platforms, stationed between the orange vertical beams of its portico on the side of the OPERA detector. A loading station surmounted by a revolving drum is seen on the right side of the picture. Brick rows already inserted can be observed on the left.
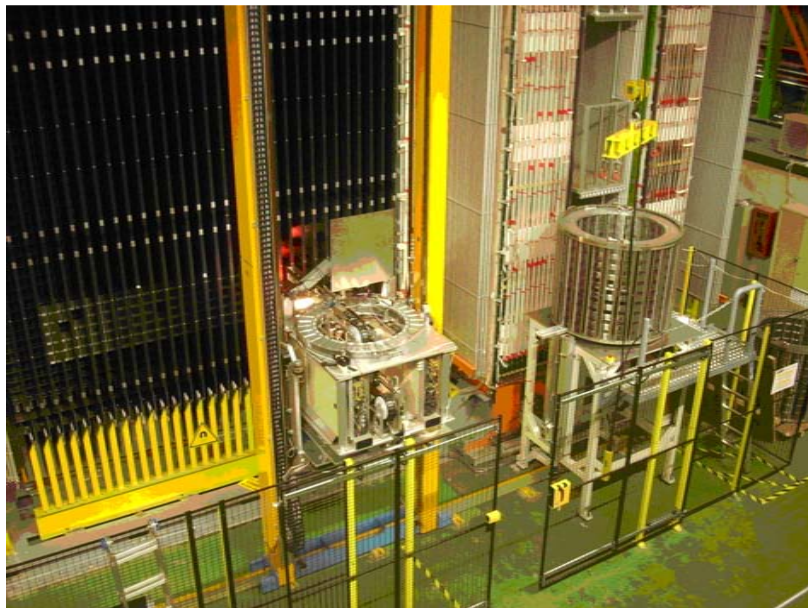

Figure 3: The BMS system inserting bricks in the second super-module of OPERA in December 2007.

4.1 BMS filling operations in 2007

By the end of 2006, the two BMS porticoes and their loading stations were already installed and commissioned in the LNGS underground laboratory. A pilot production of about 900 bricks was inserted by the BMS in the detector in October-November 2006. The brick final production started in February 2007 and its rate progressively ramped up from 1 transportation drum per day 234 bricks) to 2.5-3 drums per day towards the end of the year. In December, the first half of the detector, i.e. the first super-module target section, was filled. The BMS loading stations, first installed past the first target section to shorten the portico trips, were then moved to their final location at the rear of the experiment. This operation was done one side at a time to avoid stopping the brick production flux. At the end of 2007, the filling of the second target section was

started and more than 80000 bricks had been inserted in the OPERA detector. At the steadily sustained rate achieved presently for brick production and insertion, the completion of the detector filling is expected to be effective in June 2008.

4.2   BMS brick extractions in 2007

During the year 2007, brick extractions were first done with temporary procedures. This was the case for the first data taking with bricks in the OPERA targets, the Cosmic Run of April 07. Tests of final extraction procedures were completed by mid 2007. In September, extractions could be performed in final mode and candidate bricks from the Cosmic Run of September 07 were sent to analysis, together with more bricks from the April Cosmic Run, requested for complementary studies. A total of 25 bricks candidate for cosmic event analysis were retrieved that way in September. During the short October 2007 CNGS run, 38 neutrino interactions were collected in the OPERA bricks. At the time of the CNGS run, the first OPERA super-module was filled at about 80% with bricks. Since the prediction chain was tested for the first time, it was decided to extract more than one brick for each prediction according to the brick interaction probability map. To study the 38 neutrino events, a total of 88 bricks have been extracted from the detector by the BMS in 4 weekly operations through-out the October month and sent out for analysis. Following the operations performed at these different occasions, the extraction procedures by BMS can be considered as fully operational.

5   The 2007 run with CNGS neutrinos

In October 2007 a high intensity CNGS run was foreseen, aiming at intensity around 2.4 E13 POT/spill with SPS supercycles lasting 39.6 s and containing 3 fast spills for neutrino physics. The program did foresee a 3 weeks high intensity run with an expected integrated luminosity around 0.3 E19 protons on target. The physics run started smoothly on October 5th with an intensity around 1.7 E13 POT/spill essentially limited by beam losses at the PS. Beam delivery was subject to some major stops due to problems with the target station cooling system, until it stopped definitely on October 20th due to radiation damage on some electronics controlling the cooling system of the proton target station. The achieved integrated luminosity was 8.24 E17 POT, less than 30% of the value which was expected in case of good efficiency and intensity. The total number of neutrino interactions collected in the OPERA target was 38 events (CC+NC), to be compared with the expected number of 32 interactions in the bricks for the given integrated luminosity (around 10% additional events are due to interactions in the TT and in the supporting structure of the target). All the 38 events have been processed to reconstruct the location of the bricks where the neutrino interactions occurred, from the electronic detector data. As foreseen a sharing of 50% of CSd and bricks between Japan and Europe was applied in an unbiased way. Since the prediction/scanning chain was tested for the first time, it was decided to extract more then one brick for each prediction, according to the brick interaction probability map evaluated from the event reconstruction with electronic detector. All data collected during the scanning are stored in local ORACLE databases.

5.1 Status of the scanning in Europe

The scanning station at LNGS is equipped with 6 automatic microscopes devoted to the European CSd scanning allowing for a quick confirmation of the neutrino interaction and providing the prediction of the tracks for the brick scanning and event location. In 2008 two additional microscopes will be installed at LNGS, reaching a power adequate for the measurement of about 12 neutrino interactions per day. In the LNGS scanning station 35 CDs doublets related to 19 events were scanned. In 16 cases the events were confirmed with at least one track in the CDs and the related brick was sent to the scanning laboratories. For 2 events a special procedure has to be applied because the CDs had a high fog density due to the original vacuum tight packing of the emulsion doublets which has been afterwards abandoned. One event occurred probably just at the edge of the emulsions and has not jet been found. The scanning of the bricks for the interaction vertex location and analysis is performed in several scanning laboratories (Bari, Bologna, Bern, LNF, Lyon, Napoli, Padova, and Salerno) where 25 microscopes guarantee the requested scanning power. The bricks related to the confirmed events were scanned in EU laboratories and in 8 cases a clear multiprong vertex was found and reconstructed. In 2 cases the predicted tracks were found and scanned back to their starting point, and vertex confirmation is still in progress. The other events are still under investigations. Fig. 4 shows the display of first event located in the ECC brick.

5.2 Status of the scanning in Japan

19 events from the 2007 CNGS run have been scanned and analyzed at Nagoya University. The current status of the analysis is the following: 16 events with at least one confirmed track have been found in the CDs. 15 events have been sent to the brick scanning and for 9 events the scan back track stopping point was found, in 2 cases the found track is passing trough the brick (it means that the interaction occurred upstream of the measured brick, and in 4 cases the analysis is still going on in trying to connect the tracks from the CDs to the bricks. In 2008 a new physics run is foreseen for the CNGS beam; CERN will undertake all the actions needed to solve the problem of radiation damage on the control electronics set up of the target station cooling system which stopped the 2008 run.

References

[1] New Journal of Physics **8**, 303 (2006);
   R. Acquafredda *et al.*,

[2] M. Ambrosio *et al.*, IEEE Trans. Nucl. Sci. **51**, 975 (2004);
   A. Bergnoli *et al.*, Nucl Phys. Proc. Suppl. **158**, 35 (2006), A. Casas *et al.*, IOP Pub. Ltn and Sissa (2007).

[3] R. Zimmermann *et al.*, Nucl. Instrum. Meth. A **555**, 435 (2005) [Erratum-ibid. A **557**, 690 (2006)].

[4] T. Nakamura *et al.*, Nucl. Instrum. Meth. A **556**, 80 (2006).

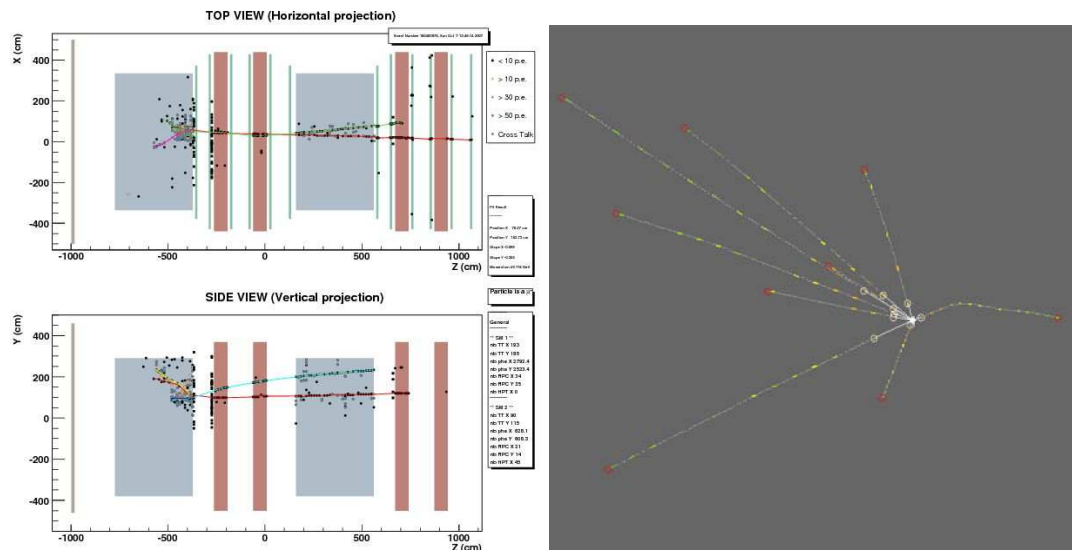[5] E. Barbuto *et al.*, Nucl. Instrum. Meth. A **525**, 485 (2004).

Figure 4: First located event of 2007 October run. Left: event display in the OPERA detector. Right: front view of the vertex reconstructed in the ECC brick.

[6] Nucl. Instrum. Meth. A **551**, 261 (2005);
    M. De Serio *et al.*, Nucl. Instrum. Meth. A **554**, 247 (2005);
    L. Arrabito *et al.*, Nucl. Instrum. Meth. A. **554**, 247 (2005);
    L. Arrabito *et al.*

[7] T. Adam *et al.*, Nucl. Instrum. Meth. A **577**, 578 (2007).

THEORY GROUP

The activity of research is organized in the five working groups: FA51, GS51, CT51, PI12, PI21, that are generically denoted as IS (from "Iniziative Specifiche"). It concerned as main areas: astroparticle physics (mainly FA51), phenomenology of Planck scale physics (GS51), supernova neutrinos (CT51), computer simulations of gauge theories (PI12), particle physics phenomenology (mainly PI21). There is a tradition of collaboration between the LNGS theory group and several experimental groups. In this report, we describe the activities of the theory group in 2007.

Members of the group: R. Aloisio, Z. Berezhiani, V. Berezinsky, D. Boncioli, P. Blasi, P. Ciarcelluti, M.L. Costantini, G. Di Carlo, A. Gazizov, A. Lepidi, E. Luzio, F. Nesti, G. Pagliaroli, P. Panci, L. Pilo, N. Rossi, F. Tortorici, F. Vissani.

Updated information and further info at: `http://theory.lngs.infn.it/index.html` .

—————— Astroparticle Physics (FA51) ——————

The Astroparticle group of LNGS in 2007 included R. Aloisio, E. Babichev, V. Berezinsky, F. Vissani and visitors V. Dokuchaev (Institute for Nuclear Research, Moscow), Yu. Eroshenko (Institute for Nuclear Research, Moscow), B. Hnatyk (Lviv University, Ukraine), S. Grigorieva (Institute for Nuclear Research, Moscow) and A. Gazizov (Stepanov Institute of Physics, Minsk, Belarus). The group worked in close collaboration with A. Vilenkin (Tufts University, USA), M. Kachelrieß (NUST, Trondheim, Norway), P. Blasi (Arcetri Observatory, Firenze), G. Senjanović (ICTP, Trieste), A. Strumia (Pisa University), F. Villante (Ferrara U., and, since late 2007, L'Aquila U.) and others.

Scientific work

The main field of the work is astroparticle physics, including ultra high energy cosmic rays, and high energy neutrino and gamma astrophysics. We work also in particle physics.

Conferences, seminars and other activities

R. Aloisio works as the scientific secretary of the LNGS scientific committee and as the organizer of LNGS seminar.

V. Berezinsky worked as an editor of Int. Journal *"Astroparticle Physics"* and as a mem-

ber of Int. Advisory board of JEM-EUSO.

R. Aloisio presented invited talks at *"Workshop on Cosmic Rays Physics"*, Aspen (Colorado,USA) April 2007, at *"TeV Particles Astrophysics"*, Venice, August 2007 and a talk at *"30th ICRC"* (Merida, Mexico) July 2007.

V. Berezinsky presented the invited talks at *"30th ICRC"* (Merida, Mexico) July 2007 and introductory talk at *"TAUP"* (Sendai, Japan), September 2007.

F. Vissani co-organized the Workshop *CRYODET2 "A large liquid Argon detector for future particle physics"* held on June at the LNGS giving there the introductory talk on theoretical physics scenarios, and co-organized the International Workshop on *"Grand Unification and Proton Decay"*, held on July 2007 at the ICTP, Trieste. He also presented an invited talk at the *"Rome International Conference on Astroparticle Physics"*, RICAP07.

The astroparticle group started in 2007 a collaboration with the group of P. Blasi of the Arcetri Observatory for theoretical studies in high energy astrophysics. This collaboration, coordinated by R. Aloisio, was funded by the Italian Space Agency with a three years contract.

Publications in journals, proceedings and preprints

[1] R. Aloisio, F. Tortorici.
Super Heavy Dark Matter and UHECR Anisotropy at Low Energy. e-Print: arXiv:0706.3196 [astro-ph]

[2] R. Aloisio, V. Berezinsky, P. Blasi, S. Ostapchenko.
Signatures of the transition from Galactic to extragalactic cosmic rays. Published in Phys.Rev.D77:025007,2008. e-Print: arXiv:0706.2834 [astro-ph]

[3] R. Aloisio, V. Berezinsky, A. Gazizov.
Ultrahigh Energy Cosmic Rays Diffusion in an Expanding Universe. To appear in the proceedings of 30th International Cosmic Ray Conference (ICRC 2007), Merida, Yucatan, Mexico, 3-11 Jul 2007. e-Print: arXiv:0706.2158 [astro-ph]

[4] Roberto Aloisio.
Propagation and Chemical Composition of Ultrahigh Energy Cosmic Rays. Invited talk at 6th Rencontres du Vietnam: Challenges in Particle Astrophysics, Hanoi, Vietnam, 6-12 Aug 2006. e-Print: astro-ph/0701623

[5] R. Aloisio, V. Berezinsky, Pasquale Blasi, A. Gazizov, S. Grigorieva, B. Hnatyk.
A dip in the UHECR spectrum and the transition from galactic to extragalactic cosmic rays. Published in Astropart.Phys.27:76-91,2007.

[6] Veniamin Berezinsky, Vyacheslav Dokuchaev, Yury Eroshenko.
Remnants of dark matter clumps. e-Print: arXiv:0712.3499 [astro-ph]

[7] V. Berezinsky.
Transition from galactic to extragalactic cosmic rays. To appear in the proceedings of 30th International Cosmic Ray Conference (ICRC 2007), Merida, Yucatan, Mexico, 3-11 Jul 2007. e-Print: arXiv:0710.2750 [astro-ph]

[8] Veniamin Berezinsky.
On origin of ultra high energy cosmic rays.
Published in Astrophys.Space Sci.309:453-463,2007.

[9] Veniamin Berezinsky, Mohan Narayan.
Phenomenological constraints on low-scale gravity.
Published in Phys.Rev.D75:105001,2007.

[10] Veniamin Berezinsky, A. Gazizov, S. Grigorieva.
On the status of the dip in UHECR spectrum. e-Print: astro-ph/0702488

[11] Veniamin Berezinsky, A.Z. Gazizov.
Diffusion of Cosmic Rays in the Expanding Universe. 2. Energy Spectra of Ultra-High Energy Cosmic Rays. e-Print: astro-ph/0702102

[12] Veniamin Berezinsky, Vyacheslav Dokuchaev, Yury Eroshenko.
Anisotropy of dark matter annihilation with respect to the Galactic plane. Published in JCAP 0707:011,2007.

[13] Francesco Vissani.
Neutrinos from Supernova Remnants After the First H.E.S.S. Observations. Proceedings of Vulcano06 Workshop, Frontier objects in astrophysics and particle physics, SIF Edizioni Scientifiche (2007) 117-135.

[14] F.L. Villante, F. Vissani.
Method to extract the primary cosmic ray spectrum from very high energy γ-ray data and its application to SNR RX J1713.7-3946, Published in Phys.Rev.D76:125019,2007. e-Print: arXiv:0707.0471 [astro-ph]

[15] Francesco Vissani and Francesco Lorenzo Villante.
Cosmic rays and neutrinos from supernova remnants (or: the time when H.E.S.S. met Ginzburg and Syrovatskii). Proceedings of RICAP 2007 Conference, NIM A (2008) doi:10.1016/j.nima.2008.01014.

Phenomenology of Planck Scale (GS51)

Members: A. Grillo, E. Luzio, R. Aloisio. Visitors: F. Girelli, S. Liberati, L. Maccione, F. Mendez, L. Sindoni. Collaboration with J.L. Cortes (University of Zaragoza).

Scientific work

The group has continued to investigate the possible emergence of deformed dispersion relations from (quantum gravity) fluctuations. On the other hand, we have started a program to study in detail phenomenological effects, also in view of the new results from Cosmic Ray experiments, that do not appear to leave much space for Lorentz Invariance Violations. This work has been mainly done in collaboration with the GS51 group in SISSA and with F. Mendez (Universidad de Santiago de Chile).

Conferences, seminars and other activities

A. Grillo gave talks in Trieste (Workshop on *"From Quantum to Emergent Gravity"*), in Santiago and in Sissa on the relevance for Planck Scale Phenomenology of the recent results from the Pierre Auger Observatory.

—————— Supernova Neutrinos (CT51) ——————

Members: M.L. Costantini, G. Pagliaroli, F. Vissani. They worked in collaboration with A. Ianni of Borexino; W. Fulgione (Turin U.), M. Selvi (Bologna U.) and other members of the LVD team; E. Coccia, G.M. Guidi (Urbino U.) and A. Viceré (Urbino U.) of VIRGO; and with the theorists A. Drago (Ferrara U.) and F.L. Villante (Ferrara U., and, since late 2007, L'Aquila U.), who visited LNGS in 2007. CT51 is a new IS at LNGS.

Scientific work

Preparatory work for this activity is documented in the Master and PhD theses of M.L. Costantini [1] and in past publications of the members of the group (e.g., ref. [2] concludes a work with members of LVD team begun with astro-ph/0112312).

The first project (part of the PhD thesis of G. Pagliaroli) is a very detailed analysis of the events from SN1987A. Preliminary results have been reported at conferences and in [3, 4]; the final results are being elaborated at the moment of writing.

As a natural continuation, a second project was begun, in collaboration with the members of the VIRGO team and with W. Fulgione, aiming to assess the importance of a detailed analysis of the neutrino signals for gravitational wave detectors.

Finally, an investigation of signals from the transition to quark matter was started under the lead of A. Drago.

Conferences, seminars and other activities

G. Pagliaroli gave a talk at the National Conference IFAE 2007, Naples. F. Vissani presented invited talks at the Conference on *"20th Anniversary of SN1987A"*, INR Lebedev Ph. Inst., Moscow and at the *"XXVIII ENFACP"*, Aguas de Lindoya, MG, Brasil; he pre-

pared an essay for *"Ulisse"* (http://ulisse.sissa.it/biblioteca/saggio/2007/Ubib070330s001) and lectured on neutrino oscillations at LNS, Catania.

Publications in journals, proceedings and preprints

[1] Maria Laura Costantini,
Expected neutrino signals from supernovas and supernova remnants,
L'Aquila University Doctorate Thesis, defended on Feb. 23, 2007.
Advisors: F. Cavanna and F. Vissani.

[2] N.Yu. Agafonova et al. (with F. Vissani).
Study of the effect of neutrino oscillations on the supernova neutrino signal in the LVD detector. Published in Astropart.Phys.27:254-270,2007.

[3] G. Pagliaroli, M.L. Costantini, A. Ianni, F. Vissani.
The first second of SN1987A neutrino emission. e-Print: arXiv:0705.4032 [astro-ph]

[4] Maria Laura Costantini, Aldo Ianni, Giulia Pagliaroli, Francesco Vissani.
Is there a problem with low energy SN1987A neutrinos?
Published in JCAP 0705:014,2007.

— Computer Simulations of Gauge Theories (PI12) —

Member: G. Di Carlo. We have a longstanding collaboration based on the INFN-MEC agreement with the University of Zaragoza (Spain) and in particular with V. Azcoiti.

Scientific work

Our scientific activity during 2007 mainly regarded the study of models with θ term in the action: using the methods we have introduced in the last years we continue this study with the simulation of other models with topological terms, in particular CP^N and $SU(2)$ gauge. Our recent interest has been focused on the CP^1 model; our analysis shows the existence of a line of second order phase transition points at $\theta = \pi$ for intermediate coupling constant beta, with critical exponents varying continuously along the line. We completed the analysis of the phase structure of the CP^1 model and described the results in ref. [1].

We also continue the interest in non-zero baryon density QCD. It is clear that radically new methods are needed for a significant step forward in the comprehension of this problem. Hence our main interest, now, is in the development of new possible approaches to sign problem.

Publications in journals, proceedings and preprints

[1] V. Azcoiti, G. Di Carlo, A. Galante.
Critical behaviour of CP^1 at $\theta = \pi$, Haldane's Conjecture and the relevant universality class, Phys. Rev. Lett. 98, 257203 (2007)

——— Particle Physics Phenomenology (PI21) ———

Members: Z. Berezhiani, P. Ciarcelluti, A. Lepidi, F. Nesti, P. Panci, L. Pilo, N. Rossi. Visitors: D. Comelli (INFN Ferrara), O. Kancheli (ITEP Moscow), A.S. Sakharov (CERN & MEPHI, Moscow), A.P. Serebrov (PNPI St.-Petersburg), C. Savoy (CEA, Saclay), M. Gogberashvili (IP, Tbilisi), J. Ulbricht (ETHZ, Zurich)

Scientific work

One research line was focused on the Massive Phase of Gravity following from the breaking of Lorentz Symmetry. This was realized by coupling general relativity to additional spin-two fields (so called bigravity or multi-gravity) predicting massive gravitational waves and infrared modification of the Newton law [1]. The modified exact solutions *á la* Schwarzschild have also been found and will be reported soon. This part of the activity is carried on in collaboration with D. Comelli.

In collaboration with R. Percacci (SISSA) we studied also the unification of gravity with the weak interactions, through the enlargement of the gauge group of gravity [2], and its possible experimental tests. A related approach related to a geometric definition of spinors also leads to such scenario, predicting the unification of gravity and a Pati-Salam unified group [3]. Ongoing work is concentrated on the fully symmetric phase.

Conferences, seminars and other activities

International Workshop *"Key Problems in Cosmology"*, Cargese, France, Apr. 2007 (invited talk of Z. Berezhiani); International Workshop PLANCK'07, Warsaw, June 2007 (talks of F. Nesti and L. Pilo at parallel sessions); International Conf. ACFC'07 *"Astrophysics, Clocks and Fundamental Constants"*, Bad Honeff, Germany, June 2007 (invited talk of Z. Berezhiani and a poster presentation of N. Rossi); International Conf. GUT'07 *"Grand Unification and Proton decay"*, Trieste, Italy, July 2007 (invited talks of Z. Berezhiani and F. Nesti); 12th Gran Sasso Institute *"Particles and Gravity"*, LNGS, Oct. 2007 (seminars of F. Nesti and L. Pilo).

Z. Berezhiani gave invited seminars at the CEA, Saclay and at the ILL, Grenoble; F. Nesti gave invited seminars at the ICTP, Trieste, SISSA, Trieste, INFN Ferrara and University of Ljubljana.

Publications in journals, proceedings and preprints

[1] Z. Berezhiani, D. Comelli, F. Nesti, L. Pilo.
Spontaneous Lorentz Breaking and Massive Gravity. Phys. Rev. Lett. 99, 131101
(2007); e-Print: hep-th/0703264

[2] F. Nesti, R. Percacci.
Graviweak Unification. e-Print: arXiv:0706.3307 [hep-th]; Journ. Phys. A - in press

[3] Fabrizio Nesti.
Standard Model and Gravity from Spinors. e-Print: arXiv:0706.3304 [hep-th]; Phys.
Lett. B - in press

[4] Possible Types of Dark Matter Particle Interactions, P. Panci, 2007, Thesis of Laurea
(supervisor Z. Berezhiani)

[5] Phenomenology and Cosmology of Millicharged Particles and Experimental Prospects
for Their Search, A. Lepidi, 2007, Thesis of Laurea (supervisor Z. Berezhiani)

[6] The Dark Sector: Particle Mixing Phenomenology and Gravitational Effects, Nicola
Rossi, 2007, Thesis of Doctorate (supervisor Z. Berezhiani)

The WArP Programme

R.Acciarri[a], M.Antonello[b], B. Baibussinov[c], M.Baldo-Ceolin[d], P.Benetti[e], F.Calaprice[f], E.Calligarich[g], M.Cambiaghi[e], N.Canci[a], F.Carbonara[h], F.Cavanna[a], S. Centro[d], A.G.Cocco[i], F.Di Pompeo[a], G.Fiorillo[h], C.Galbiati[f], V. Gallo[h], L.Grandi[b], G. Meng[c], C.Montanari[g], O.Palamara[b], L.Pandola[b], F. Pietropaolo[c], G.L.Raselli[g], M.Roncadelli[g], M.Rossella[g], C.Rubbia[1][b], E.Segreto[b], A.M.Szelc[j], F.Tortorici[b], S. Ventura[c], C.Vignoli[g]

[a] *Università dell'Aquila e INFN, L'Aquila, Italy*
[b] *INFN - Laboratori Nazionali del Gran Sasso, Assergi, Italy*
[c] *INFN - Sezione di Padova, Padova, Italy*
[d] *Università di Padova e INFN, Padova, Italy*
[e] *Università di Pavia e INFN, Pavia, Italy*
[f] *Princeton University - Princeton, New Jersey, USA*
[g] *INFN - Sezione di Pavia, Pavia, Italy*
[h] *Università di Napoli e INFN, Napoli, Italy*
[i] *INFN - Sezione di Napoli, Napoli, Italy*
[j] *IFJ PAN, Krakow, Poland*

Abstract

The WArP programme is a graded programme intended to search for cold Dark Matter in the form of WIMPs. These particles may produce via weak interactions nuclear recoils in the energy range 10 - 100 keV.

A cryogenic noble liquid like Argon permits the simultaneous detection of both ionisation and scintillation induced by an interaction, suggesting the possibility of discriminating between nuclear recoils and electrons mediated events.

A 2.3 litres two-phase Argon detector prototype has been used to optimize many technological aspects and establish a first physics result with an extended WIMP search run at LNGS.

A new version of the 2.3 lt chamber, made with selected low radio-active materials, has been built and will be used in a forthcoming extended run with a first batch of Argon depleted in the content of ^{39}Ar, a radioactive isotopic contaminant produced by cosmic rays.

Argon from natural gas wells is of interest because ^{39}Ar production induced by cosmic rays is strongly suppressed underground. Extraction of ^{39}Ar-depleted Ar in large quantities from US underground natural gas reservoirs is under investigation within the WArP R&D program.

---

[1]Spokesman of the WArP Collaboration

Parallel studies and tests are also under way, to further optimize various aspects of the experimental technology, like investigations about the effects on the scintillation light collection capability due to different residual contaminants (N_2, O_2, H_2O, ...) and about the light collection efficiency with different choices of the optical system in use.

Finally, the status of realization of the WArP 100 lt detector is summarized. The 100 litres sensitive volume device, with largely extended potential sensitivity for WIMP search, is going to be installed in the underground HallB. Delivery at LNSG of the main parts of the layout took place during 2007 and the assembly phase is being started.

1 General considerations

There is very strong evidence that a large fraction of the matter in the Universe is dark and that galaxies are immersed in a dark halo, which outweights the visible component. The nature of Dark Matter is one of the fundamental puzzles in astrophysics today. From astrophysical considerations we know that the density of matter is $\Omega_m = 0.238 \pm 0.080$. Nonbaryonic Dark Matter (NBDM) must be present, since the gravitational density is apparently much larger than the contribution from the Big Bang Nucleo-Synthesis, $\Omega_b = 0.05 \pm 0.011$. The existence of Dark matter can be considered as a confirmed result because of its gravitational effects. The open question is about the presence of an electroweak coupling to ordinary matter, which would permit the direct observation on Earth of such a missing component of cosmic matter.

A direct detection of the existence of relic WIMP in an underground laboratory may rely on the observation of the tiny recoils produced in ordinary matter by the elastic scattering reaction on target nuclei with the subsequent recoiling nucleus, mediated by weak interactions (neutrino-like). Evidently the specific signature of these events as recorded by the detector must be such as to isolate nuclear recoil events from the much more abundant background due to natural radioactivity. Since Ω_{DM} is known, the number of particles can be roughly estimated once the mass of the elementary particle is given. For instance, for a mass of 100 GeV/c^2, the flux on earth is about 10^6 ptcl/cm^2/s, about six orders of magnitude smaller than the one of solar neutrinos.

To reach a sufficient experimental sensitivity, both active mass and background discrimination should be incremented as much as possible. This is the reason of the conceptual advances and technological developments we have been concentrating over the last decades and the creation of a new line of dark matter detectors based on noble cryogenic liquids.

2 The WArP experimental programme

The searches for massive WIMP have been traditionally performed with the help of cryogenic detectors in the milli-K range (EDELWEISS, CDMS, etc.). An alternative technol-

ogy based on noble liquids (Xe and Ar) at much more conventional temperatures has been developed originally by us as a spin-off of the ICARUS programmes. Both technologies are capable of an apriori comparable WIMP counting rate for a given active mass and recoil threshold. The interest in using pure noble liquids at standard temperature (87 K for liquid Argon) is that larger active masses, ultimately of many tons, can be easily instrumented.

Our pioneering work in the nineties developed both at CERN and in Pavia was based on the concept of liquid Xenon, with the simultaneous detection of scintillation and ionization signals from the heavy ionizing elastic recoils from WIMP at an appropriate threshold of about 20-30 keV. Later on, we have replaced Xenon with Argon for many reasons, the most relevant being the very high discrimination power between e/γ signals and elastic recoils generated both by hypothetical WIMP and/or by neutron recoils (acting as strongly interacting WIMP). Presently the remarkable e/γ rejection limit of one part in 10^{-8} has been attained, and we are confident that it might be even further improved. These developments have evolved into the WArP programme (Wimp Argon Programme), intended to actually search for Cold Dark Matter in the form WIMP's at the LNGS.

The cryogenic noble liquid detector, such as Argon, unlike an ordinary scintillator, permits the simultaneous detection of both ionisation and scintillation. These particles may produce via weak interactions nuclear recoils in the energy range 20-150 keV, taking advantage from the favorable Ar form factor. When a particle interacts in the liquid region excitation and ionization occur: the ratio of primary scintillation over secondary ionization signal and the shape of the primary scintillation depend on the kind of particle producing excitation and ionization. The detector consists on a two-phase (liquid with above gas) cryogenic container in which both the primary scintillation light and the drifted electron signal, also converted into light by a multiplying grid, are recorded. Three simultaneous criteria are used to discriminate potential WIMP recoils from e/γ backgrounds:

- Simultaneous detection of prompt scintillation and drift time-delayed ionisation in Liquid Argon: pulse height ratio strongly dependent from columnar recombination of ionizing track

- Pulse shape discrimination of primary scintillation: wide separation in rise times between fast (~ 5 ns) and slow ($\sim 1.4\ \mu$s) components of the emitted UV light.

- 3D reconstruction of the event position: additional rejection of multiple neutron recoils and gamma background.

The programme at the LNGS consists of 4 phases which are fully approved and funded and a 5th phase under consideration:

Phase 1 A small (2.3 l) two-phase chamber tested first in Pavia and later at LNGS, firstly without and later with passive neutron shield. In this phase, ordinary Argon has been deliberately used with a high background rate, which has permitted to explore the very high rejection rates in a relatively short time. A paper with the details of the method has been published on Astroparticle Physics. An early limit on WIMP has been given, comparable to the one of EDELWEISS.

149

Phase 2 A main background, due to the ^{39}Ar natural contamination will be strongly reduced ($\sim 1/100$) by using ^{39}Ar depleted Argon. A new 2.3 lt chamber made with selected low-radioactive materials is going to be filled with a depleted Ar sample produced by isotopic separation by a commercial manufacturer. Data taking with the new 2.3 l chamber is expected to start in March-April 2008. This should improve the sensitivity by about an order of magnitude compared to the previous WIMP run.

Phase 3 A new, larger detector with a 100 lt two-phase chamber is under assembly and it will be operational at LNGS by summer 2008. The main new features are: (a) localization of the centroid of the ionization signal, permitting the three dimensional location of the event to better than 1 cm; (b) a large, 4π active, hermetic anticoincidence ($\sim$ 8 ton of L Ar) to further reduce the presence of neutrons and γ.
The possibility to fill the inner detector with ^{39}Ar depleted Argon obtained from ug reservoirs is presently under consideration.

Phase 4 The sensitive volume of the detector may be later extended to 1 ton with minor modifications which will keep the main setup unchanged, including the outer active anticoincidence, depending on the background level attained during phase 3.

Phase 5 An even greater sensitive volume, of the order of $\geq$ 10 tons is presently under consideration. However such a large extrapolation from the present detectors at this stage is still strongly dependent on the progress associated to phases 3 and 4.

In this report some issues related to *Phases* 1 to 3, result of activity performed during 2007, are briefly summarized.

3   Result from the WArP -2.3 lt WIMP run

The (first) WArP 2.3 lt prototype has been operated underground at the Gran Sasso INFN Laboratory (LNGS), in the tunnel connecting HallA to HallB.
The detector is a two-phase drift chamber, with a lower liquid Argon volume and an upper region with Argon in the gaseous phase, both viewed by the same set of photo-multipliers (PMTs) [2]. Free electrons generated by ionization in the liquid are drifted by means of an electric field to the liquid-gas interface, where they are extracted through the boundary and detected by the proportional scintillation light generated by the electrons accelerated in a high electric field.
The drift volume, 7.5 cm long, is delimited by a 20 cm diameter stainless steel cathode and by a system of field-shaping electrodes that generate very uniform electric drift fields in the 1.87 lt sensitive volume ($\simeq$ 2.3 lt total volume). A grid (g1) placed just below the liquid level closes the uniform drift field region, while two additional grids (g2 and g3 from bottom to top) are placed in the gas phase. In normal data taking conditions, the chamber is operated with a drift field of EF = 1 kV/cm.
Four 12-stage 3" photo-multipliers (PMTs), manufactured in order to operate at LAr temperature and placed at about 4 cm above the last grid, detect both the primary scintillation

in the liquid (the S1 signal) and the proportional scintillation light in gas phase (S2 signal). Sensitivity to VUV photons emitted by the scintillating Argon is achieved by coating the photo-multiplier window with an appropriate compound, i.e. Tetra-PhenylButadiene (TPB), which acts as a fluorescent wavelength shifter of the VUV scintillation light to the photo-multiplier sensitive spectrum. In order to improve the light collection efficiency from the drift volume, a high performance diffusive reflector layer with TPB deposit surrounds the inner drift volume and the gas volume between the top grid and the PMTs. The system is contained in a stainless steel, vacuum-tight cylindrical vessel. The whole container is cooled down to about 86.5 K by an external liquid Argon bath. This set-up ensures in the inner container a constant absolute pressure few mbar above the external atmospheric pressure ($P \simeq 900$ mbar).

At filling, GAr is flushed through a standard Oxysorb/Hydrosorb cartridge for removal
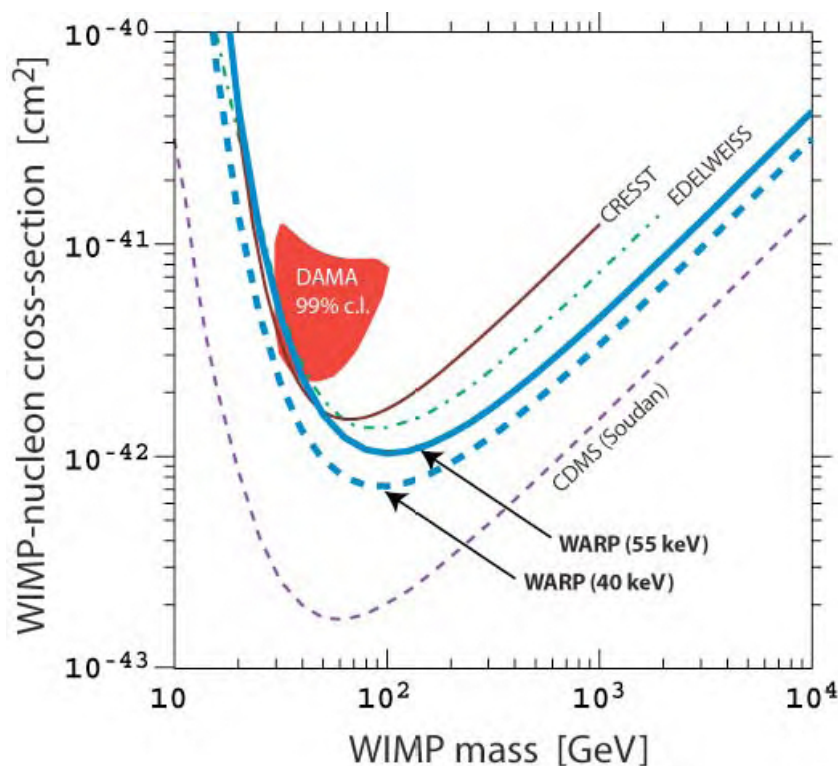
Figure 1: *90 % C.L. spin independent limits (solid blue curve) obtained by WARP-2.3l for a total fiducial exposure of 96.5 kgd and a threshold of 55 keV. An analogous curve for $E_{rec} \geq 40$ keV under the assumption that the observed 5 events are due to background is also plotted (dashed blue curve). More stringent limits (not shown in the figure) from Zeplin II and Xenon appeared in pre-print during 2007 and a new one from CDMS is expected by early 2008.*

of O_2 and H_2O. An Argon recirculation system is implemented working in closed loop and providing a further continuous re-purification of the Argon contained in the chamber.
The anode signal from of each PMT is integrated (shaping time 120 μs), digitized and

sent to a 10 bit flash ADC. At each trigger the memory buffer is then recorded to disk.

During the long data acquisition period (2005-06) the resulting trigger rate is of the order of 6 counts/s, due to several radio-nuclides that are present either in the liquid Argon or in the surrounding walls of the detector, for which no specific attention to material radio-purity has been exercised. In this preliminary phase of technological development, the presence of such impurities has been indeed beneficial, since it permitted to quickly develop efficient rejection criteria against spurious events due to backgrounds.

These methods acquire a strong statistical significance provided the number of primary photoelectrons is sufficiently high (typically > 50 phe for kinetic Argon recoil energies > 40 keV). In particular the simultaneous introduction in actual underground conditions of the two independent discrimination methods, namely the pulse shape discrimination parameter F and the ratio (S2)/(S1) between the delayed electrons signal extracted from the liquid to the gas (S2) and the initial luminescence photoelectron yield (S1), appear to be absolutely necessary in order to ensure a sufficient robustness to the identification of a possible WIMP signal.

Notwithstanding the small size, the 2.3 litre table-top test chamber has already permitted to reach a sensitivity limit against WIMP which is quite comparable with the one of traditional cryogenic detectors at mK temperatures. In the WIMP search run, started just after optimization of a stable layout configuration, a large data sample has been collected (2.8×10^7 triggers), in a total live time of 52.76 days, corresponding to a total exposure of 96.5 kg $\times$ day. The analysis of the data allowed to establish an exclusion limit in the parameter space relevant for WIMP search, as reported in Fig.1

4 Discovery of underground Argon with low level of radioactive ^{39}Ar

The sensitivity of WArP (or any Argon-based detector) to WIMP Dark Matter is limited by background from the decay of ^{39}Ar (E_{max}=565 keV, $t_{1/2}$=260 yr), a radioactive contaminant of Argon in the atmosphere produced by cosmic rays. Its specific activity is 1.01 Bq/kg of Argon, equivalent to a ^{39}Ar/Ar ratio of 8.1×10^{-16} and to an activity of 16.7 mBq/m^3 of air [4]. The use of ^{39}Ar-depleted Argon would eventually allow the construction of multi-ton argon-based WIMP Dark Matter detectors and the reduction of the main background source intrinsic to the target. Isotopic separation by centrifugation or differential thermal diffusion are established techniques for separation of ^{39}Ar from ^{40}Ar, but on a multi-ton scale could become extremely expensive and require a long production time. Argon from natural gas wells is of potential interest because ^{39}Ar production induced by cosmic rays is strongly suppressed underground. Also, the large quantity of Argon stored in underground natural gas reservoirs would be sufficient to provide material for the construction of a multi-ton WIMP detector.

A first measurement of ^{39}Ar in Argon from underground natural gas reservoirs has

been performed during 2007, within the WArP R&D program [5].

The gas stored in the US National Helium Reserve was found to contain a low level of ^{39}Ar. The ratio of ^{39}Ar to stable Argon was found to be $\leq$ 4 $\times 10^{-17}$, i.e. less than 5% the value in atmospheric Argon (^{39}Ar/Ar=8×10^{-16}). The total quantity of Argon currently stored in the National Helium Reserve is estimated at 1000 tons. The findings reported demonstrate the possibility of constructing large multi-ton argon detectors with low radioactivity suitable for WIMP Dark Matter searches.

Extraction of ^{39}Ar-depleted Ar from US underground natural gas reservoirs is under way, and possibly the extracted amount will be used within *Phase 3* with the WArP-100 lt detector (second stage).

5 Effects of Nitrogen contamination in liquid Argon

The WArP technology is based on the simultaneous collection of scintillation light and free electron charge from ionization events.

In the case of the ionization charge, the main limitation to its full collection comes from electron attachment process due to contaminations of electro-negative impurities like Oxygen present at residual level in (commercial) Argon. Detailed studies have been performed and led to the development of adequate purification systems (Oxygen reactants and molecular sieves, down to ≤ 0.1 ppb of Oxygen equivalent concentration), normally employed in experimental applications.

On the other hand, the effects of impurities on the scintillation light yield are rather less precisely explored. Quenching (i.e. non-radiative) process in two-body collision of impurity-molecules with Ar_2^* excimer states, otherwise decaying with VUV light emission, may take place depending on the type of impurity and the concentration level. This led to include within the WArP R&D program investigations on Oxygen and Nitrogen contamination effects on LAr scintillation light. Two experimental tests have been thus performed [6], [7].

Contamination at ppm level of N_2 leads to a substantial reduction of the scintillation light intensity while no appreciable effects from N_2 contamination on the free electron charge can be expected, due to the low electron affinity of the N_2 molecule.

During 2007, a dedicated test has been performed by means of a controlled N_2 contamination procedure [6]. Measurements have been done by *mip* particle excitation (Compton electrons from γ-sources in the MeV range).

The effect on the scintillation light collection has been measured over a wide range of N_2 concentration, spanning from $\sim 10^{-1}$ ppm up to $\sim 10^3$ ppm, though a *saturation* effect of the solute (Nitrogen) in the LAr solvent has been presumably found at the highest contaminations.

The rate constant of the light quenching process induced by Nitrogen in LAr has been found to be $k(N_2)$=0.11 $\mu s^{-1}ppm^{-1}$ (in agreement with some early measurements reported in literature). This implies that, for example, at $\sim$ 1 ppm level a $\sim$ 20% reduction of

the scintillation light is experienced due to the N_2 quenching process. The quenching factor affecting the light yield has been determined over the whole explored range of N_2 concentrations.

The experimental test also allowed to extract the main characteristics of the scintillation light emission in pure LAr, thanks to the direct PMT signal acquisition by fast waveform recording.

The light signal shape is well represented by the superposition of three components with exponential decay. The fast and the slow components, with decay time constants τ_S=4.9 ns and τ_T=1260 ns, are recognized to be associated to the decay of the singlet $^1\Sigma_u$ and the triplet $^3\Sigma_u$ excimer states of Ar_2^*. An intermediate component is also found to be present (as sometime reported in literature), whose origin could presumably be ascribed to PMT instrumental effects.
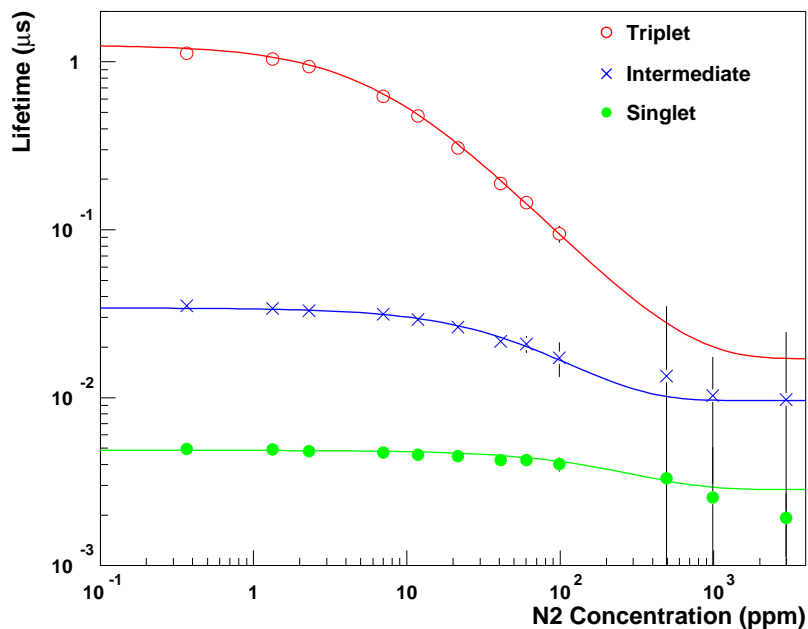
Figure 2: *Effective decay times of the individual components (τ_j', $j = S, T, I$ in corresponding color an symbol) as function of N_2 concentration. For [N_2]$\geq$500 ppm, $\tau_T' \to 0$ (not shown). Lines in corresponding color are from the fit with the rate constant $k(N_2)$ of the light quenching process induced by Nitrogen in LAr as free parameter.*

The main effect of residual N_2 in LAr is of reducing the slow component lifetime at increasing concentration (Fig.2), and consequently of varying the ratio of the relative amplitudes to higher values. This makes the slow signals from γ/e background less distinguishable in Pulse Shape vs the fast Ar-recoils signals possibly induced by WIMP interactions, in Dark Matter search experiments.

Therefore, the implementation of dedicated methods for removal of the residual N_2 content results to be recommended with LAr based detectors, or at least the use of best grade commercial Argon with reduced Nitrogen contamination (below $\sim$0.5 ppm) appears as definitively necessary.

6   Installation of the WArP 100-lt detector

The WArP 100-lt detector layout is composed by an external passive shield (a polytene 70 cm thick layer as n-shield and a lead 10 cm thick shield for γ's) sustained by a stainless steel anti-seismic structure, inside the external shield a large 15 ton LAr cryostat (a double wall cryogenic vessel insulated with vacuum and super-insulation and made of stainless steel selected for low radioactive contamination) contains (1) the inner detector (100 lt of active LAr target), (2) the active Veto formed by about 8 ton of LAr around the inner detector and (3) externally to the active veto, also immersed in LAr, a 10 cm thick shield of polyethylene. The layout is schematically shown in Fig.3.
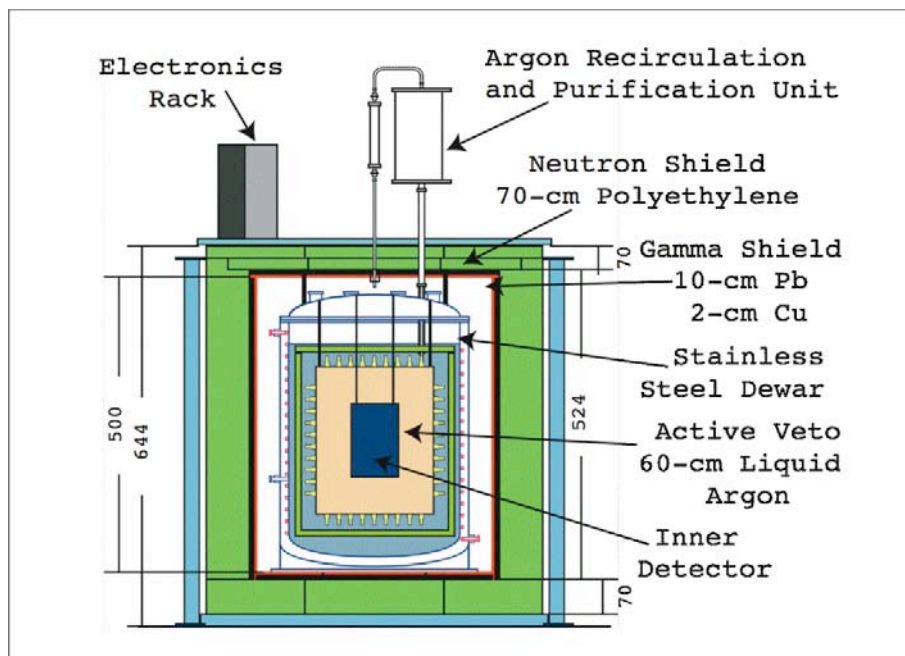
Figure 3: *Schematic layout of the* WArP *100-lt installation.*

The inner detector, equipped with field-shaping electrodes for the drift field, grids for extraction of ionization electrons from liquid to the gas phase and proportional light production, and PMTs for the readout of the primary and secondary light signals, is suspended at the center of a LAr volume.
This volume works as active shield (veto) against gamma and neutron backgrounds. Minimum thickness of the active LAr shield is 60 cm. It consists of a set of 3 photomultipliers

that are held in place by PEEK supports that are connected to a thin copper structure that delimits the external surface of the active shield volume. On the Cu structure are also mounted the basic elements of the waveshifting/reflecting layer (TetraPhenylButadiene waveshifter, deposited on a highly reflective plastic substrate). A total of 436 3" phototubes are installed on the active shield for 10% photocathode coverage of the inner surface and a nominal threshold of 10 keV for argon recoils (10 photoelectrons). The inner detector and the active shield are optically separated (to avoid vetoing of events occurring in the central volume).

Both the inner detector and the active shield are designed in such a way to reduce as much possible the amount of material request for their assembly and that all materials (mainly copper, PEEK, Kapton and PMTs glass) are selected for a low radioactive contamination. The presence of a wide anticoincidence shield is of primary importance in order to reduce the general background produced externally and internally the detector.

Figure 4: *View of the* WArP *-100 active Veto structure during the assembly test.*

The drift field region of the inner detector is delimited by the cathode (a copper disk, 2 mm thick), a set of field shaping rings (copper strips printed on a Kapton foil) and a grid (stainless steel wires stretched on an annular stainless steel frame) placed just below the liquid argon surface. Additional grids, placed in the gas phase, provide the field shaping for extraction from the liquid, acceleration for secondary light production and final collection of ionization electrons. A set of 37 PMTs, placed in the gas phase just above the upper grid, readout the primary and secondary light signals. The gas pocket is enclosed into a copper, vacuum isolated, cup placed upside down. A set of small heating resistances placed just below the liquid surface, together with the heat produced by the PMTs dividers, provide a continuous evaporation of the liquid. The excess gas is evacu-

ated through small holes (1 mm diameter) in the copper cup placed in correspondence of the required level of the liquid to gas interface. This technique ensures both the correct positioning of the liquid level and a continuous recirculation of the LAr in the drift volume. The internal surfaces of the inner detector are also covered with the high reflectivity waveshifting layer to enhance at maximum the scintillation light collection efficiency at the PMT sensitive photo-cathodic area. A foil of copper deposited on Kapton support surrounds the body of the internal detector. This external layer is put to ground and ensures that no residual field is present in the active veto region.

Figure 5: *Picture of the* WArP *100-lt cryostat during transportation to LNGS (Mar.,'07).*

The main top flange of the cryostat (Fig.5) hosts all the ports with the electrical feed-throughs for PMTs HV supply and readout (about 2500 ceramic feed-throughs on 8 CF250 flanges produced at INFN-Padova), for HV supply of the drift field and of the extraction/multiplication grids, for supply and readout of the auxiliary instrumentation (LAr purity monitor, temperature probes, etc.). The cryogenic installation is completed by the vacuum system, the argon gas recirculation unit and the liquid argon recirculation unit. These units are installed outside the external shield.

The WArP 100-lt experimental layout is under assembly at LNGS. The main cryostat has been positioned inside the external shield sustaining structure (Hall B) in March, '07, Fig.6. All components of the inner detector and active veto are being delivered. PMT's have been individually tested and characterized at the INFN-Naples facility and are being

157

Figure 6: *Picture of the* WArP *-100 experimental site in HAll-B (underground LNGS). Visible the cryostat in its final position, inside the external shield sustaining structure.*

shipped to LNGS.

At the beginning of 2008 the assembly procedures will start. Completion of this phase is expected in few months and immediately after the commissioning of the detector will take place. Experimental operation is expected by summer 2008.

7   Conclusions

Liquid Argon at 87 K has been proven to be an unique target for WIMP searches, because of its high sensitivity to signals and its superior background rejection capabilities.

Many years of effort have firmly established the new two-phase technology, now being implemented underground in the WArP -100 detector. This technology is characterized by identification capability of e/γ signals and of elastic atomic recoils at unprecedented levels, established with the WArP -2.3 prototype programme, intentionally designed as high background detector.

The WArP -100 detector ready by summer 2008 will bring a further upgrade on light yield. Background will be further minimized. We expect a big step in sensitivity for WIMP Dark Matter Searches.

The mass upgrade to 1 ton as soon as possible is an implicit next step. LAr is a mature technology, ultimately capable of very massive detectors with a relatively low cost. A very large ultimate detector with$\geq$ 10 tons could be readily constructed at the LNGS. It is already at the level of a conceptual design, the main open question to be perfected in phases 2-4 being a background rejection sufficient to separate out the potential signal.

Such a large sensitive mass is necessary in order to cover the entire set of options predicted by SUSY/WIMP.

We believe that at the present state of the art, cryogenic detectors are the most suited for such very large masses.

The WArP experiment is funded, by INFN (LNGS, L'Aquila, Napoli, Padova and Pavia), by NSF (Princeton) and by the Polish Academy of Sciences (Krakow).

References

[1] C. Rubbia *et al.*, A programme to search for WIMP particles in Liquid Argon at the LNGS, Letter of intent, Univ. of Pavia, July 1999.

[2] WArP Collaboration, Status Report of the current progress of the WArP Experiment, **LNGS-EXP 32/05** (2005);

[3] WArP Collaboration, First results from a dark matter search with liquid argon at 87 K in the Gran Sasso underground laboratory, Astropart. Phys. **28** (2008), 495.

[4] WArP Collaboration, Measurement of the specific activity of ^{39}Ar in natural argon, Nuclear Instruments and Methods in Physics Research A 574, 83 (2007).

[5] D. Acosta-Kane *et al.* (WArP Collaboration), Discovery of underground argon with low level of radioactive 39Ar and possible applications to WIMP Dark Matter detectors, arXiv:0712.0381v1 [astro-ph] (3 Dec 2007)

[6] WArP Collaboration, Effects of Nitrogen contamination in Liquid Argon, to be submitted to Nucl. Inst. and Meth. A

[7] WArP Collaboration, Oxygen contamination in liquid Argon: combined effects on ionization electron charge and scintillation light, to be submitted to Nucl.Inst. and Meth.A

The XENON10 Dark Matter Experiment

J. Angle[a], E. Aprile[b,*], F. Arneodo[c], L. Baudis[d], A. Bernstein[e],
A. Bolozdynya[f], P. Brusov[f], L. Coelho[g], C.E. Dahl[h], L. DeViveiros[i],
S. Fattori[c,l], A. Ferella[d],L. Fernandes[g], S. Fiorucci[i],
R.J. Gaitskell[i], K.L. Giboni[b], R. Gomez[j],
R. Hasty[k], L. Kastens[k], J. Kwong[h], J.A.M. Lopes[g], N. Madden[e],
A. Manalaysay[a], A. Manzur[k], D. McKinsey[k], M.E. Monzani[b], K. Ni[k],
U. Oberlack[j], J. Orboeck[d], G. Plante[b], R. Santorelli[b], J. M. F. dos Santos[g],
P. Shagin[j], T. Shutt[f], P. Sorensen[i], S. Schulte[d], C. Winant[e]
and M. Yamashita[b]

[a] Department of Physics, University of Florida, Gainesville, FL 32611, USA
[b] Department of Physics, Columbia University, New York, NY 10027, USA
[c] INFN, Laboratori Nazionali del Gran Sasso, Assergi, 67100, Italy
[d] Department of Physics, RWTH Aachen University, Aachen, 52074, Germany
[e] Lawrence Livermore National Laboratory, 7000 East Ave., Livermore, CA 94550, USA
[f] Department of Physics, Case Western Reserve University, Cleveland, OH 44106, USA
[g] Department of Physics, University of Coimbra, R. Larga, 3004-516, Coimbra, Portugal
[h] Department of Physics, Princeton University, Princeton, NJ 08544, USA
[i] Department of Physics, Brown University, Providence, RI 02912, USA
[j] Department of Physics, Rice University, Houston, TX 77251, USA
[k] Department of Physics, Yale University, New Haven, CT 06511, USA
[l] Dipartimento di Fisica, Università de L'Aquila, Italy

[*] Spokesperson

Abstract

XENON10 is a direct dark matter detection experiment using liquid Xenon as target for weakly interacting, massive particles (WIMPs). A dual-phase (liquid/gas) time projection chamber with 15 kg mass has been installed in the Gran Sasso Underground Laboratory in March 2006 [2]. The detector has taken data in a stable

configuration for several months, until April 2007. A blind analysis of 58.6 live days of data, acquired between October 6, 2006 and February 14, 2007, and using a fiducial mass of 5.4 kg, excludes previously unexplored parameter space, setting a new 90 C.L. upper limit for the WIMP-nucleon spin-independent cross-section. A paper reporting this important result has been published [1].

1 Introduction

The goal of XENON [3] is to search for interactions of massive, cold dark matter particles in liquid xenon. The motivation of this search comes from our current understanding of the universe. Over the last ten years, a variety of cosmological observations, from the primordial abundance of light elements, to the study of large scale structure, to the observations of high redshift supernovae, to the detailed mapping of anisotropy of the cosmic microwave background, have led to the construction of a so-called concordance model of cosmology. In this model, the universe is made of $\sim 4\%$ baryons which constitute the ordinary matter, $\sim 23\%$ nonbaryonic dark matter and $\sim 73\%$ dark energy [4]. Understanding the nature of dark matter poses a significant challenge to astrophysics. The solution may involve new particles with masses and cross sections characteristic of the electroweak scale. Such Weakly Interactive Massive Particles (WIMPs), which would have been in thermal equilibrium with quarks and leptons in the hot early universe and decoupled when they were non-relativistic, represent a generic class of dark matter candidates [5, 6]. If WIMPs do exist their density in the Milky Way halo may allow them to be detected in laboratory experiments by looking for the nuclear recoils produced in elastic WIMPnuclei collisions [7]. A WIMP with a typical mass between 10 GeV and 10 TeV will deposit a nuclear recoil energy below 100 keV in a terrestrial detector. The expected rates are determined by the WIMP-nucleus cross section and by their density and velocity distribution in the vicinity of the solar system [6]. Direct-detection experiments, in particular CDMS II [8, 9], CRESST [10], EDELWEISS [11], ZEPLIN II [12] and WARP [13], are beginning to significantly constrain the WIMP-nucleon scattering cross section and, for the first time, start to probe the parameter space which is predicted by supersymmetric extensions to the Standard Model (reviews can be found in [14, 15, 16]). Detectors based on liquid noble elements (Ar, Xe) are rapidly evolving and constantly improving their sensitivity. Liquid xenon (LXe) has excellent properties as dark matter target. It is an intrinsic scintillator, with high scintillation ($\lambda = 175$ nm) and ionization yields. It is available in large quantities (although at a significant cost) and can be purified to 1 ppt (part per trillion)-levels. Scintillation in LXe is produced by the formation of excimer states, which are bound states of ion-atom systems. If a high electric field (~ 1 kV/cm) is applied, ionization electrons can also be detected, either directly or through the secondary process of proportional scintillation. Measuring both the primary scintillation signal (S1) and a secondary process (S2) yields a method of discriminating between electron and nuclear recoils. An advantage of LXe versus other noble liquids (e.g. Argon) is its high density (3 g/cm^3), which provides self-shielding and allows for compact detectors, and the high atomic number (Z=54, A=131.3), which is favorable for scalar WIMP-nucleus interactions. Moreover, since natural Xe has two isotopes with spin (^{129}Xe,^{131}Xe, at the combined level of almost 50% abundance), a liquid Xenon detector is susceptible for both

coherent and axial-vector WIMP-nucleus couplings.

2 The XENON10 TPC

Fig. 1 shows a schematic of detector and cryostat, along with a picture of the cryostat while being inserted the gamma/neutron shield. The sensitive volume of the XENON10 TPC is defined by a Teflon cylinder with an inner diameter of 20 cm and a height of 15 cm for a total active mass of 15 kg of LXe. Teflon is used as effective UV light reflector [19] and as electrically insulating support. The TPC structure is defined by four meshes, two in the liquid and two in the gas, labeled from 1 to 4 from bottom to top. Mesh 1 and 2 are the ones in the liquid. Mesh 1, serving as cathode, is located at the bottom of the Teflon cylinder and mesh 2 is located at its top. They define a uniform field in the drift region, together with a series of field shaping rings surrounding the Teflon cylinder and spaced 0.76 cm apart. The liquid/gas interface is located near the middle of the gap between meshes 2 and 3. Mesh 3, serving as anode, is at the most positive potential of about +3.5 kV. Mesh 2 and 3 set up a high field of 5 kV/cm for efficient electron extraction from the liquid to the gas phase, and for proportional scintillation in the gas. Mesh 4 closes the field lines of this region. The meshes are chemically etched from a 0.008 inch thick plate of 304 stainless steel and electropolished (no sharp edges were observed under microscope examination). They feature a bar width of 0.182 mm and 2.0 mm x 2.0 mm square holes, yielding an optical transparency of 84% for normal incidence. Custom-made capacitors are used to monitor the liquid level: one cylindrical capacitor is used to measure the liquid level and four parallel-plate capacitors are used to measure the inclination of the detector, in order to ensure that the liquid/vapor interface is parallel to the wire meshes. One of the parallel-plate capacitors is filled with Teflon and is used as a reference capacitor: the capacitances of other parallel-plate capacitors are compared with the reference value to control the inclination of the detector. The working principle of this double phase detector is to detect both the primary scintillation light (S1) produced by any interactions in the liquid phase, and the secondary, proportional light (S2) produced by the resulting ionization electrons. Those electrons are drifted towards the liquid surface by the applied electric field and then extracted into the gas phase where they emit proportional scintillation light while reaching Mesh 3. The ratio S2/S1 is a powerful discriminating parameter between 'normal' ionization events (such as produced by electrons, or muons) and nuclear recoils, since the latter class of events will produce very few, if any, ionization electrons and hence a very small, or absent, S2 signal. The active volume is viewed by 89 PMTs: the bottom array of 41 PMTs is located 1.5 cm below the cathode, fully immersed in LXe, to detect S1. The 48 PMTs of the top array, in the gas, are used to detect S2. The HV to the cathode is supplied via a custom-made feedthrough. The XENON10 TPC was designed to operate with a maximum field of 1 kV/cm across the 15 cm drift gap. The nominal operating field is 700 V/cm. A resistive voltage divider made of 19 individual 1 GigaOhm resistors directly mounted on the shaping rings provides the appropriate field levels. The total power dissipation by the divider chain is 0.20 mW.

The detector is contained in a low-background shield, a parallelepiped whose walls are 40

cm thick (20 cm of lead and 20 cm of polyethylene). The structure wieights roughly 35.6 tons (1.6 tons of polyethilene and 34 tons of lead). The detector is fixed to inner side of the shield door, which can slide on rails, so that the detector can be easily accessed at any time.
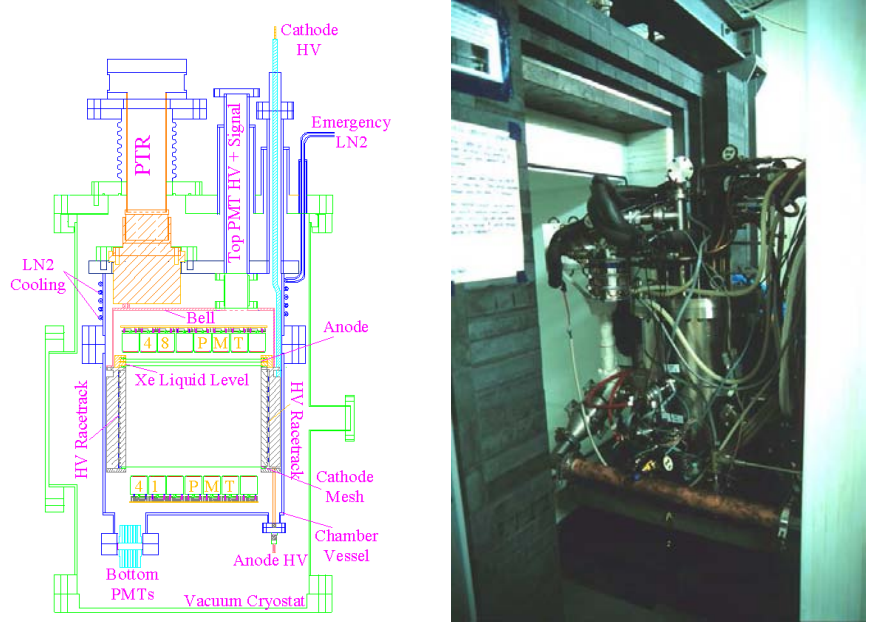

Figure 1: (left) Schematics of he XENON10 TPC and (right) picture of the cryostat during insertion in the gamma-neutron shield.

3   The Xe Purification and Recirculation

The 15 cm depth of the XENON10 detector imposes high purity requirements on the LXe, in order for electrons to drift freely from the event site to the liquid surface. Electronegative impurities must be well below 1 part per billion (ppb), otherwise the S2 signal cannot been detected because of excessive attenuation of the ionization charge. Moreover, stable operation of the detector demands that this high purity be maintained over long periods of time. For the detector and gas system ultra high vacuum materials and procedures are used, and for cleaning the Xe gas a single high temperature getter is used. The PMTs limit the bake-out temperature of the detector to 70°C. In addition, LXe is a good solvent due to Van der Waals interactions with impurity molecules. Thus, once pure Xe is liquefied in the detector, the purity level could change. Therefore a close circulation system is implemented to continuously clean the gas through the getter, after initial liquefaction. The heat of evaporation is used to cool the re-purified xenon in a heat exchange, before re-introducing it in the vessel. The electron lifetime inferred from calibration data is in excess of (1.8±0.4) ms which corresponds to 1 ppb (part per billion O_2 equivalent) purity.
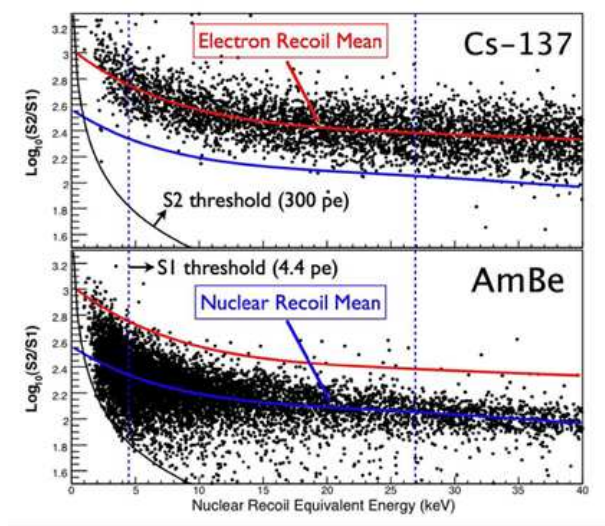
Figure 2: Log10(S2/S1) as a function of energy for electron recoils (top) and nuclear recoils (bottom) from calibration data. The colored lines are the mean Log10(S2/S1) values of the electron recoil (upper, red) and nuclear recoil (lower, blue) bands. The region between the two vertical dashed lines is the energy window (4.5 - 26.9 keV nuclear recoil equivalent energy) chosen for the WIMP search. An S2 software threshold of 300 pe is also imposed (black lines).

4   Calibrations

To achieve a reliable and accurate detector calibration, with minimum impact on WIMP search exposure time, the XENON10 shield was designed to allow introduction of external calibration sources without exposing the detector cavity to outside air. The gamma calibration sources are ^{57}Co (122 keV) and ^{137}Cs (662 keV). On December 1, 2006, the XENON10 detector was calibrated with an encapsulated AmBe neutron source with an activity of 200 neutrons/s. Such a calibration allows to determine the predicted WIMP signal region as well as the detectors ability to distinguish between nuclear and electron recoils down to its energy threshold. The energy threshold was determined to be at $\sim$10 keV nuclear recoil energy (keVr) with a light yield of 0.7 photo-electrons/keVr.

Moreover in March, 2007 a small amount of neutron activated xenon gas was added to the XENON10 detector. Two xenon meta-stable states, ^{131m}Xe and ^{129m}Xe decay emitting 164 keV and 236 keV gamma rays with half-lives of 11.8 days and 8.9 days, respectively. These photons allow for a more uniform energy and position calibration across the LXe active volume.

5   Data Anaysis

The S1 signal associated with each triggered event is searched for in the off-line analysis. By requiring a coincident signal in at least two PMTs, the efficiency of the S1 signal search algorithm is larger than 99%, above a threshold of 4.4 photoelectrons (pe), or 4.5 keV nu-
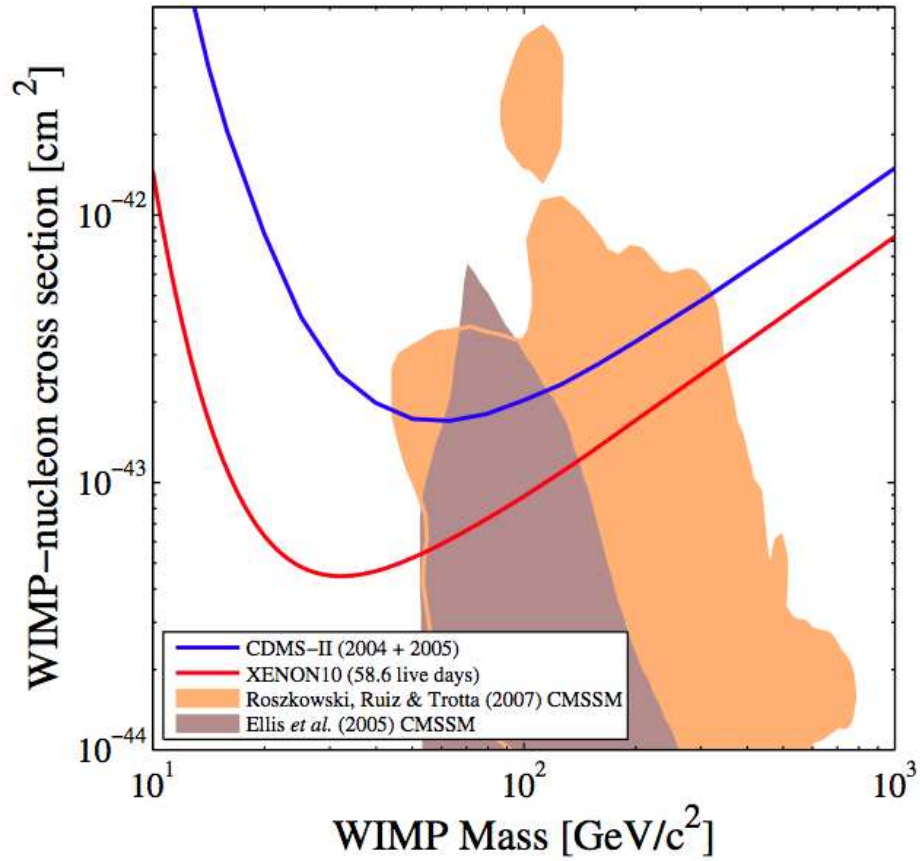
Figure 3: Spin-independent WIMP-nucleon cross-section upper limits (90% C.L.) versus WIMP mass. Shown curves are for the previous best published limit (upper, blue) and the current work (lower, red). The shaded area is for parameters in the constrained minimal supersymmetric models .

166

clear recoil equivalent energy. The S2 hardware trigger threshold is 100 pe, corresponding to about 4 electrons extracted from the liquid, which is the expected charge from an event with less than 1 keV nuclear recoil equivalent energy [21]. The S2 trigger efficiency, with a software threshold of 300 pe, is more than 99% for 4.5 keV nuclear recoils. Basic-quality cuts are used to remove uninteresting events (e.g. multiple scatter and missing S2 events), with a cut acceptance for single-scatter events better than 99%. Background rejection is based on the ionization/scintillation (S2/S1) ratio, which is different for nuclear and electron recoils in LXe. Figure 2 shows the energy dependence of the logarithm of this ratio for electron recoils from ^{137}Cs gamma ray and for nuclear recoils from AmBe fast neutron calibrations. The separation of the mean Log10(S2/S1) values between electron and nuclear recoils increases at lower energy. In addition, the width of the electron recoil band is also smaller at lower energy. The combination of these two effects gives a better electron recoil rejection efficiency at the lower energy, reaching down to 99.9%.

After all the cuts were finalized for the energy window of interest, 58.6 live-days of WIMP-search data have been analyzed. The analysis was performed blind; i.e., the events in and near the signal region were not analyzed until the final signal acceptance window and event cuts were tested and defined, using low energy electron and nuclear recoils from calibration data, as well as 40 live days of unmasked WIMP-search data. From a total of about 1800 events, ten events were observed in the WIMP search window after cuts. About seven statistical leakage events were expected. To set conservative limits on WIMP-nucleon cross sections, all ten observed events were considered, with no background subtraction. Figure 3 shows the 90% C.L. upper limits on WIMP-nucleon cross sections as a function of WIMP mass calculated using the maximum gap method in [22] and using the standard assumptions for the galactic halo [23]. The current work gives a WIMP-nucleon cross section 90% C.L. upper limit of 8.8 x $10^{-44} cm^2$ at a WIMP mass of 100 GeV/c^2, a factor of 2.3 lower than the previously best published limit [22]. For a WIMP mass of 30 GeV/c^2, the limit is 4.5x10$^{-44} cm^2$. A constant 19% nuclear recoil scintillation efficiency has been used to derive the limit. The result varies by $\pm$ 20% ($\pm$35%) for mass 100 (30) GeV/c^2 WIMPs when varying the nuclear recoil scintillation efficiency Leff over a range of 12% to 29% , corresponding to the lowest energy data points measured in [24] and in [25]. The measured single scatter nuclear recoil spectrum from the AmBe calibration data is consistent at the 20% level with the Monte Carlo predicted spectrum, both in absolute event rate and spectral shape, when Leff is taken as 19% over the energy range of interest. In April, 2007, a paper was submitted to Physical Review Letters [1], reporting the above descripted analysis.

6   List of Publications during 2007

- J. Angle *et al.* [XENON Collaboration], "First Results from the XENON10 Dark Matter Experiment at the Gran Sasso National Laboratory," arXiv:0706.0039 [astro-ph] E. Aprile, L. Baudis and B. Cabrera, "Search for weakly interacting massive particles with CDMS and XENON," J. Phys. Conf. Ser. **60** (2007) 58.

- E. Aprile, K. L. Giboni, P. Majewski, K. Ni and M. Yamashita, "Observation of Anti-correlation between Scintillation and Ionization for MeV Gamma-Rays in Liq-

uid Xenon," arXiv:0704.1118 [astro-ph].

- C. M. B. Monteiro *et al.*, "Secondary Scintillation Yield in Pure Xenon," JINST **2** (2007) P05001 [arXiv:physics/0702142].

References

[1] J. Angle, E. Aprile et al. (XENON Colaboration), PRL 100, 021303 and arXiv:0706.0039 [astro-ph]

[2] LNGS Annual Report, 2006

[3] E. Aprile *et al.* (XENON Collaboration), New Astr. Rev. **49** (2005) 289.

[4] D.N. Spergel *et al.*, Astrophys. J. Suppl. **148** (2003) 175.

[5] B.W. Lee and S. Weinberg, Phys. Rev. Lett. **39** (1977) 165.

[6] G. Jungman, M. Kamionkowski and K. Griest, Phys. Rep. **267** (1996) 195.

[7] M. W. Goodman and E. Witten, Phys. Rev. **D 31** (1985) 3059.

[8] D. S. Akerib *et al.* (CDMS Collaboration), Phys. Rev. Lett. **96** (2006) 011302.

[9] D. S. Akerib *et al.* (CDMS Collaboration), Phys. Rev. **D 73** (2006) 011102.

[10] G. Angloher *et al.* (CRESST Collaboration), Astropart. Phys. **23** (2005) 325.

[11] A. Benoit *et al.* (EDELWEISS Collaboration), Phys. Lett. **B 545** (2002) 43.

[12] G. J. Alner *et al.* (ZEPLIN-II Collaboration), astro-ph/0701858.

[13] P. Benetti *et al.* (WARP Collaboration), astro-ph/0701286.

[14] G. Chardin in "Cryogenic Particle Detection", editor C. Enss, Springer, Heidelberg, (2005).

[15] R.J. Gaitskell, Ann. Rev. Nucl. Part. Sci. **54** (2004) 315.

[16] L. Baudis, Int. J. Mod. Phys. **A 21** (2006) 1925.

[17] E. Aprile *et al.*, Phys. Rev. **D 72** (2005) 072006.

[18] E. Aprile *et al.*, Phys. Rev. Lett. **97** (2006) 081303.

[19] T. Shutt, C.E. Dahl, J. Kwong, A. Bolozdynya and P. Brusov, astro-ph/0608137.

[20] M. Yamashita *et al.*, Nucl. Instrum. Meth. **A 535** (2004) 692.

[21] M. Yamashita et al., Astropart. Phys. 20, 79 (2003).

[22] S. Yellin, Phys. Rev. D 66, 032005 (2002). The one-sided interval at the 90% C.L. from this method is about as constraining as a two-sided interval at the % 85

[23] J. D. Lewin and P. F. Smith, Astropart. Phys. 6, 87 (1996).

[24] J. Angle et al. (XENON Collaboration), Sensitivity of the XENON10 WIMP Search to Spin-Dependent Interactions (to be published).

[25] E. Aprile et al., Phys. Rev. D 72, 072006 (2005).

ERMES. Monitoring of radon in geogas at the Gran Sasso National Laboratory

G. De Luca[a] and W. Plastino[b]

[a] Istituto Nazionale di Geofisica e Vulcanologia (INGV)
Centro Nazionale Terremoti (CNT),
Via di Vigna Murata, 605 - Rome, Italy
[b] Department of Physics, University of Roma Tre,
Via della Vasca Navale, 84 - Rome, Italy

Abstract

In the middle part of 2005, in the framework of the ERMES (Environmental Radioactivity Monitoring for Earth Sciences) research project, started the realization of a regional seismic network. The acquisition system and analysis data is located in the external building of the Gran Sasso National Laboratory (LNGS). A summary of this research activity is presented.

1 Introduction

The ERMES research project includes a regional seismological monitoring. In the past few years, the Italian seismic monitoring system was greatly improved by the *Istituto Nazionale di Geofisica e Vulcanologia (INGV)* thanks to the financial support of the *Dipartimento di Protezione Civile nazionale (DPC)* and, for southern Italy, of the *Project "ProSIS"* funded by the *Italian Ministery for University and Research (MUR)* [1].

The development of the National Network (*Rete Sismica Nazionale, RSN - www.ingv.it*) led actually about 260 seismic stations connected in real time to the acquisition centre in Rome, most of which equipped with broad band (40, 120, a few 240 s) or extended band (5 to 20 s) seismometers. Many stations are also equipped with a strong motion sensor. Transmission of the data is mostly based on satellite links or telephone lines.

In addition, in Central Italy (Marche, Umbria, Tuscany and Abruzzi regions), *INGV*

171

incremented the number of real time and dial-up stations, in cooperation with the Service of *Civil Protection of Marche Region, Osservatorio Bina (Perugia, Umbria), Fondazione Prato Ricerche (Prato, Tuscany)* and *INFN - Laboratori Nazionali del Gran Sasso (LNGS) - (L'Aquila, Abruzzi)*, respectively.

The dial-up stations operating today in the four regions are 52, in particular for Abruzzi region (Abruzzi regional network) we have 18 digital 3-components seismic stations with short period sensor (MARK L4C-3D - 1 Hz of natural frequency).

The first station of this regional network was installed at the end of 2005 and the last in the April 2007, so about one seismic station per month. A detailed description of the network is reported on two web sites [2, 3] where both waveforms and bulletin data are published routinely. Moreover, it is necessary remember that in the past (1991-2002) was running a regional seismic network [4, 5].

2   Results

The regional seismic network and the more important change of positions (arrow) of 3 stations that will happen in the 2008 are reported in Figure 1. The red triangles represent the RSN whereas the blue ones are the 18 regional seismic stations.

As an example of the quality of the recorded data, we show only the vertical component waveforms of a magnitude 1.9 earthquake recorded by both the RSN and regional networks (Figure 2); in this figure it is possible to note also for such a small event a good signal to noise ratio up to more than 100 km distance and 27 triggered stations of both *RSN* and *Regional Seismic Networks*. In the figure 2 we show only the 17 stations; the nearest one at the earthquake is at the top of figure.

The Figure 3 represents the seismicity of the area monitored from the regional network in the period January 2006 - December 2007.

The regional seismic network recorded 582 events in the period January 2006 - December 2007. The magnitude range is from 0.7 ± 0.2 to 4.5 ± 0.1. The Figure 4 shows the efficiency of the network during the installation.

In the Figure 5 we represent the two sections, latitude and longitude vs. depths of earthquakes. The seismicity is located in the 5-20 km layer. The depth seismicity (up to 30 km) is not real but are the events out of region. The residuals (in seconds) vs depth are represented in Figure 6.

In the last two figures (Figs 7 and 8) we shown the selected events using cut offs in gaps, rms, depth errors, and minimum number of phase read.

3   Conclusions

The Abruzzi regional seismic network has been completed on 2007 following the scheduled deadline. It recorded 582 events in the period January 2006 - December 2007 with magnitude ranging from 0.7 ± 0.2 to 4.5 ± 0.1, and located in the 5-20 km layer.

4 Acknowledgments

References

[1] Amato A., L. Badiali, M. Cattaneo, A. Delladio, F. Doumaz and F. Mele, 2006. The real-time earthquake monitoring system in Italy. Gosciences, BRGM, 4, 70-75.

[2] Monachesi G and G. De Luca (eds.), 2007a. Le rilevazioni delle Reti Dial Up in Italia centrale. Istituto Nazionale di Geofisica e Vulcanologia, Dipartimento della Protezione Civile, Sistema Regionale di Protezione Civile e Sicurezza Locale della Regione Marche, Laboratori del Gran Sasso dell'Istituto Nazionale di Fisica Nucleare, Osservatorio Sismico "A. Bina", Istituto Geofisico Toscano. Roma. http://cnt.rm.ingv.it/ dun/index1home.htm

[3] Monachesi G and G. De Luca (eds.), 2007b. Data base on line della Rete Sismometrica Abruzzese Istituto Nazionale di Geofisica e Vulcanologia, Dipartimento della Protezione Civile, Laboratori Nazionali del Gran Sasso dell'Istituto Nazionale di Fisica Nucleare. L'Aquila, http://www.lngs.infn.it/dbrsa/index.htm

[4] De Luca G., Scarpa R., Filippi L., Gorini A., Marcucci S., Marsan P., Milana G. and Zambonelli E. (2000). A detailed analysis of two seismic sequences in Abruzzo, Central Apennines, Italy. Journal of Seismology 4, 1-21.

[5] De Luca G., Del Pezzo E., Di Luccio F., Margheriti L., Milana G. and Scarpa R. (1998). Site response study in Abruzzo (Central Italy): underground array versus surface stations. Journal of Seismology 2, 223-236.

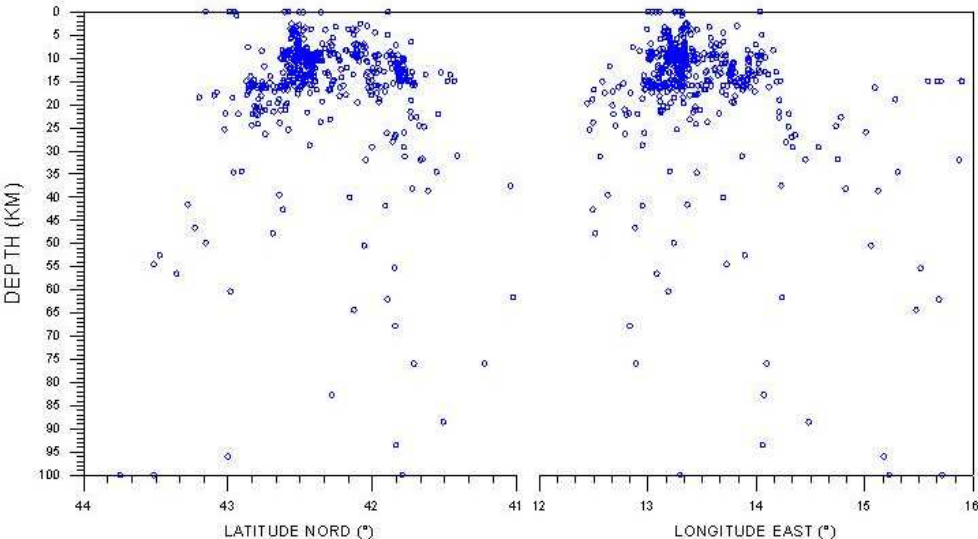Fig. 1
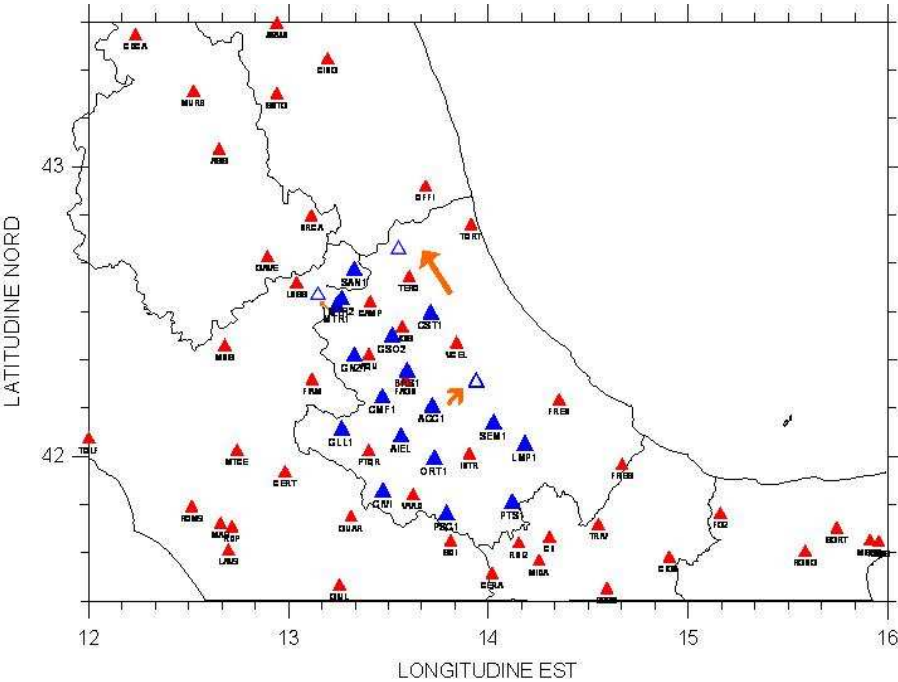
Fig. 2
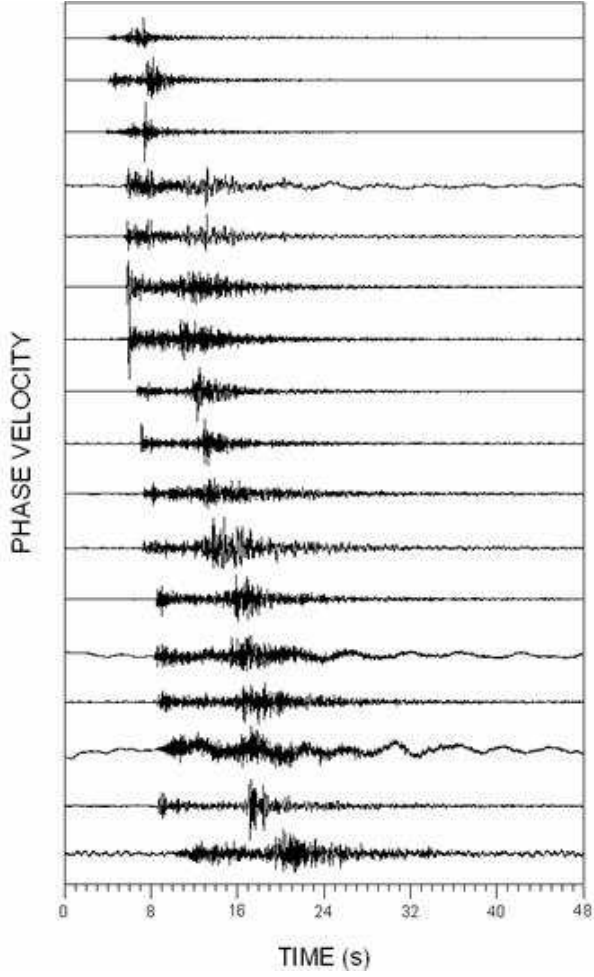
Fig. 3

Fig. 4
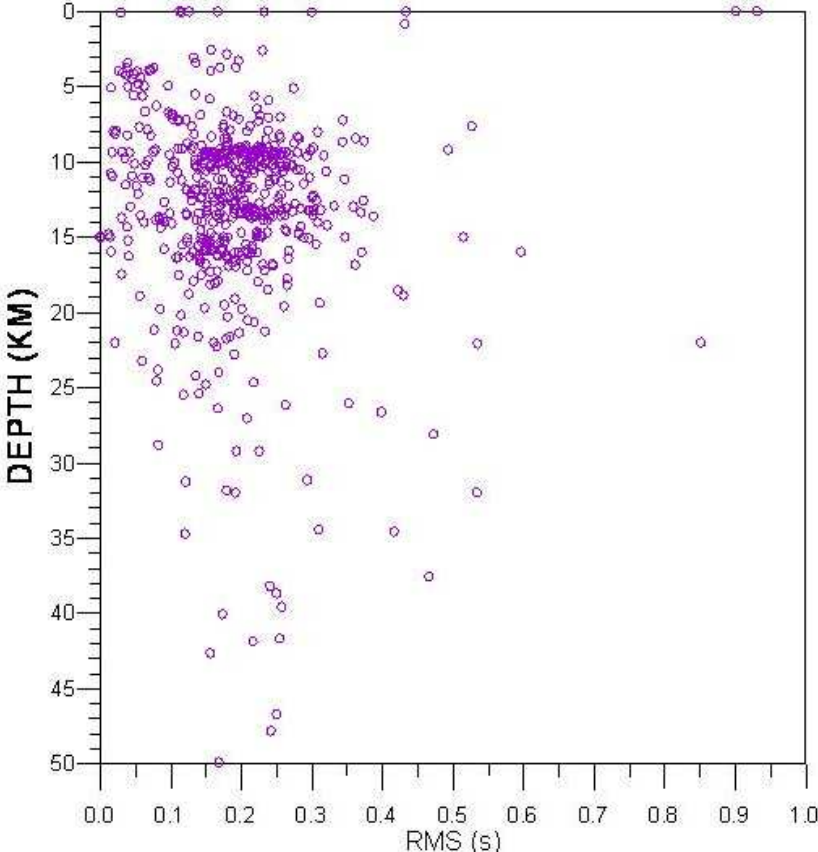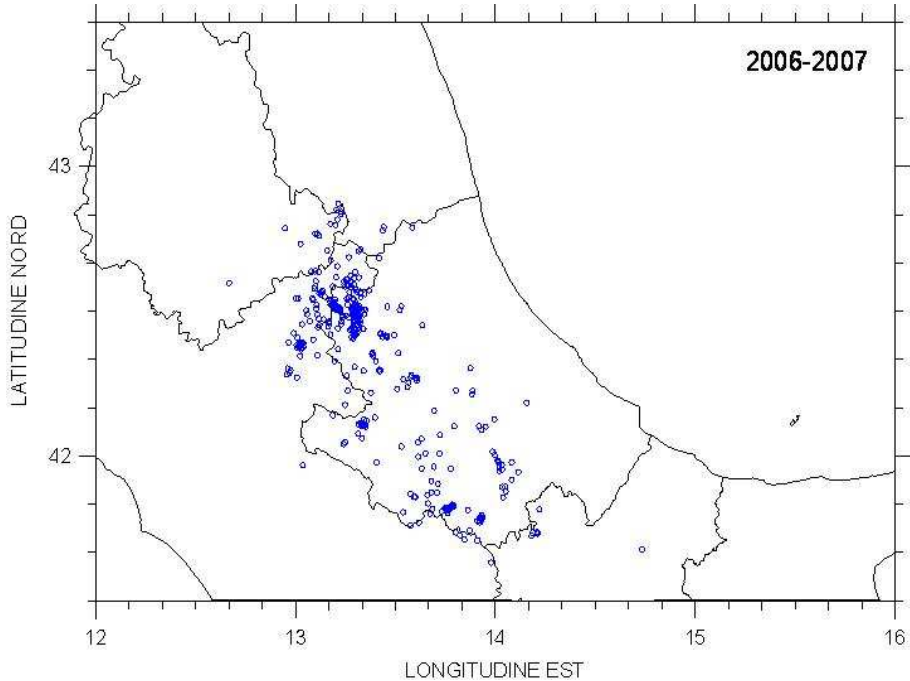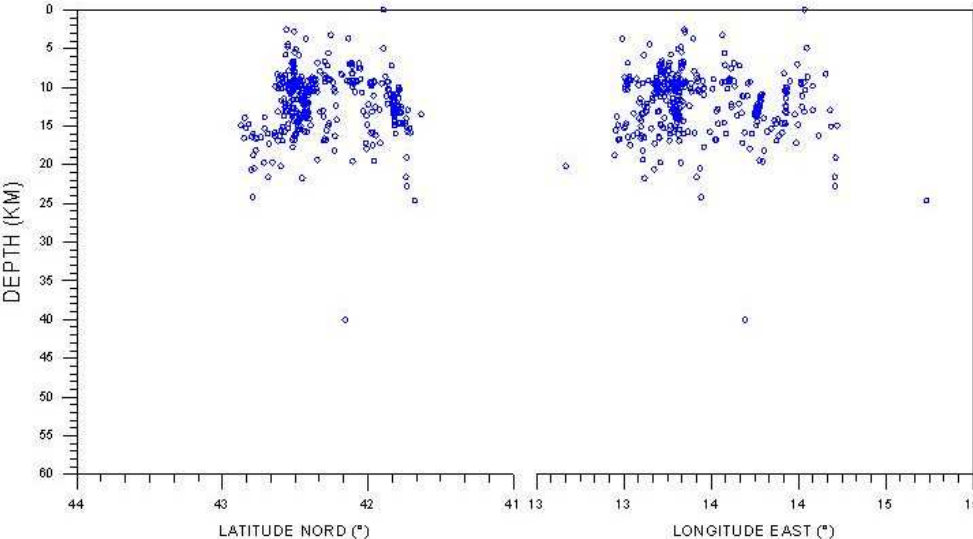

Fig. 5

Fig. 6

178

Fig. 7

Fig. 8

179
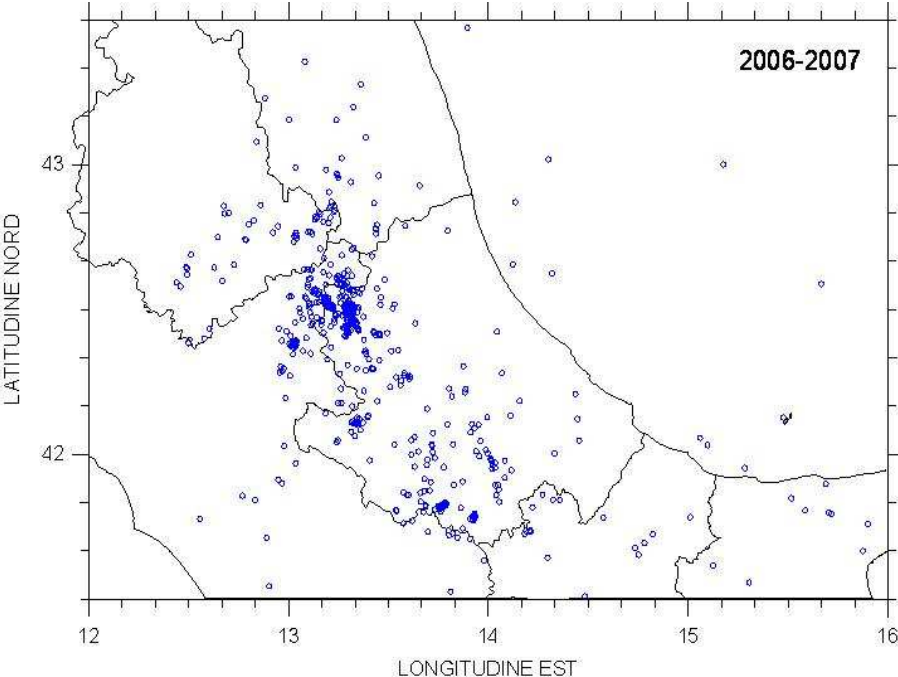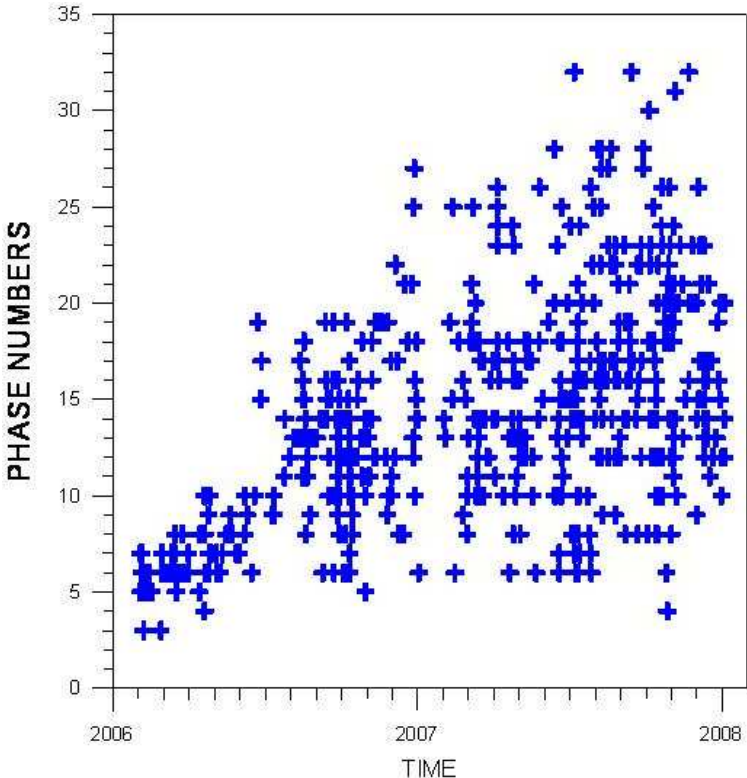
GIGS. The Interferometric Station at LNGS

Antonella Amoruso[a,b], Luca Crescentini[a,b,c]

[a] Dip.to di Fisica Univ. di Salerno, Salerno - Italy
[b] INFN - Gruppo collegato di Salerno, Salerno - Italy
[c] Spokeperson

1 Introduction

Since several years two Michelson-type laser interferometers, operating as geodetic extensometers, are working at LNGS. Until 1999 one interferometer measured difference in extension between the two baselines in an equal-arm configuration, since then two independent unequal-arm interferometers are monitoring extension along the two orthogonal directions, striking N66E and N24W. Both instruments are unequal-arm Michelson interferometers, using a 90-m long measurement arm and a <40-cm long reference arm, and sharing the same stabilized HeNe laser source.

Pre-2005 configuration required expensive electro-optical components, a very accurate optical alignment and electronic adjustment, and an occasionally careful data pre-analysis to correct for wrong reset counting. Thus we decided to test a simpler electro-optical configuration where the reference arm only included what required to get two quadrature signals at one output for each interferometer (the other output is no more used) i. e. a polarizer and a quarter-wave retarder plate, and external optics do not include Faraday rotators any more. Also electronics is now much more simple, consisting only in what necessary to measure light intensity at the photodiodes. As a drawback, phase is no more linearly related to the ADC output, which can not be simply low-passed and decimated before storage. Real time conversion from light intensity to phase (i. e., strain) is not possible, because instabilities of DC level and amplitude of the interference signal, and phase lag fluctuations between the quadrature signals ask for nonlinear fitting of the Lissajou figure given by few hours of quadrature data. Quadrature signals are sampled and stored at 600 Hz, to avoid artificial mixing of frequencies due to nonlinearity. Intensity-to-phase conversion is accomplished on stored signals when needed. The Gran Sasso geodetic interferometers have been equipped with the new electro-optical system in June 2006. Data acquisition is in progress since November 2006. Unfortunately, the instruments suffered technical (laser source and vacuum system malfunction) logistic (heavy water infiltration inside the control room, recently resolved) administrative (long delays in funds availability) problems (in part still holding). Nevertheless, management of the instruments and data appears much simpler than in the past, without degradation of retrieved strain.

A couple of years ago, preliminary tidal analysis of about 4-year of strain data had been performed using different codes in order to evidence the fluid core resonance (FCR)

effect in the diurnal tidal band and study the resonance function. The Free Core Nutation (FCN) is a rotational eigenmode which appears in addition to the well-known Chandler period ($\approx$ 435 days). This mode is due to the pressure coupling between the liquid core and the solid mantle which acts as a restoring force. The FCN causes a resonance on the Earth response to tidal forcing whose period T_{FCR} (situated in the diurnal tidal band) and quality factor Q depend on the core-mantle boundary (CMB) ellipticity, the Earth's inelasticity, and the viscomagnetic coupling of the CMB.

The FCN has been observed using tidal gravimetry, because the amplitude and phase of some diurnal tides of lunisolar origin are perturbed by the resonance process, and Very Long Baseline Interferometry (VLBI), which allows to measure changes in the Earth orientation: from these Earth orientation parameters, the nutations can be determined, and from the nutation coefficients it is possible to investigate the FCN. Strain data are more affected by local effects (e.g. topographic distortion of the strain field) than gravimetric data, but changes of the Love and Shida numbers (which give the Earth response to tidal forcing and whose computed values depend on the Earth model) at frequencies near to resonance induce relative disturbances in strain that are about ten times larger than in gravity tide. In this latter case, resonance effects are often comparable with uncertainties on ocean loading.

The unusual depth of the Gran Sasso station largely reduces contamination caused by atmospheric effects in the diurnal band of recorded tides. Predicted ocean loading effects are small, mainly for one of the two monitored directions. In this condition an uncomplete removal of oceanic tidal loading and atmospheric effects is expected to affect results less severely than in other stations, but the effects of ocean loading is .

Preliminary analyses had been performed using ETERNA 3.40 ([7]), VAV ([6]), ACS ([4]) and GOTIC2 ([5]) with Earth models 1066A and GB and global ocean models NAO.99b and CSR4.0, but neglecting any environmental effect. We have show that values of the FCR period, T_{FCN}, are consistent with but slightly lower than those previously published and values of the quality factor Q are more realistic than those obtained from gravity data. Ocean loading corrections suggested supplement by local tidal models ([1], [2]).

2   Progress in ocean loading modelling

Ocean loading effects in the diurnal tidal band of measurements performed at Gran Sasso are small but still comparable with the effects of FCR, which amount to about 25% in amplitude and 7° in phase for the K_1 tidal component (one of the most easily investigable). Ocean loading has been predicted using SPLOTL ([3]), which include CSR3.0, FES95.2, GOT00.2, and TPX06.2 global ocean models (see Table 1). Discrepancies among models are as high as 50% in amplitude and 70° in phase (Figure 1); however, since the effect of ocean loading on total tide is small, discrepances among total tides predicted using different models lowers to about 2% in amplitude and 1° in phase (Figure 2).

The Mediterranean Sea, even if is characterized by liquid tides of small amplitude with respect to open oceans, gives the largest contribution to ocean loading at Gran Sasso. The shallow bathymetry of the Mediterranean Sea makes it difficult to model its liquid tides,

Table 1:

Model	Cell Size	Latitude Limits	Constituents
CSR 3.0	0.5°	78°90°	O1, P1, K1, Q1, N2, M2, S2, K2
FES 95.2	0.5°	86°90°	O1, K1, Q1, N2, M2, S2, K2
GOT00.2	0.5°	90°90°	O1, P1, K1, Q1, N2, M2, S2, K2
TPXO6.2	0.25°	90°90°	M f , Mm, O1, P1, K1, Q1, N2, M2, S2, K2

and this results in the observed large differences among ocean loading predictions using different sea models. Figures 3-6 enlighten the low resolution (if any) of the Adriatic Sea, that obviously strongly affects strain measurements at Gran Sasso, and the general poor coverage of the Mediterranean Sea.

We have included the local Mediterranean model developed at the Oregon State University (where the global model TPX06.2 has also been developed, ftp://ftp.oce.orst.edu/-dist/tides/regional/med.tar.Z) into SPOTL. Unfortunately, even if the local Mediterranean model is characterized by higher spatial coverage and resolution ($1/12°$, see Figure 7) with respect to global models, it includes only four tidal components, i. e. two diurnal (O_1 and K_1) and two semidiurnal (M_2 and S_2) ones. So we could perform computations referring to O_1 and K_1 only.

Comparing O_1 and K_1 predictions by global models with the one by the local Mediterranean model, it seems that FES95.2 gives the best agreement, suggesting the use of the FES95.2 global model combined with the O_1 and K_1 components of the local model. It is noticable that discrepancies in total (i. e., solid and ocean loading) O_1 and K_1 tides among global models, when the local Mediterranean model is added, reduces to 0.2% in amplitude and 0.1° in phase.

We have recently obtained an improved Mediterranean model from the Oregon State University. This is completely new solution at 1/30 degree resolution. Bathymetry source is GEBCO 1min bathymetry. The model assimilates 531 cycles of Topex + Jason and 114 cycles of Topex2 (interlaced between old Topex tracks). It includes eight constituents (M_2, S_2, N_2, K_2, K_1, O_1, P_1, and Q_1). We will also check for the new FES04 global model at 1/8 degree resolution.
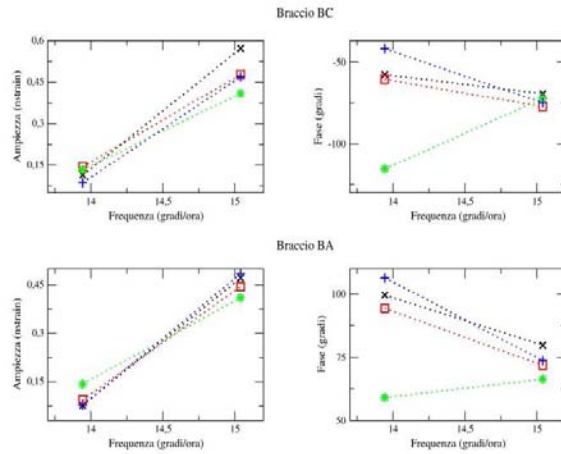
Figure 1. Ocean loading prediction: black crosses, CSR3.0; red squares, FES95.2; green stars, GOT00.2; blu pluses, TPX06.2
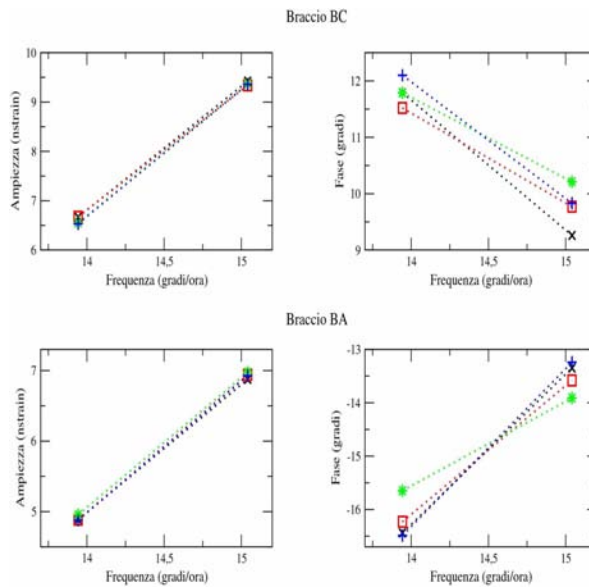

Figure 2. Total tides prediction: black crosses, CSR3.0; red squares, FES95.2; green stars, GOT00.2; blu pluses, TPX06.2
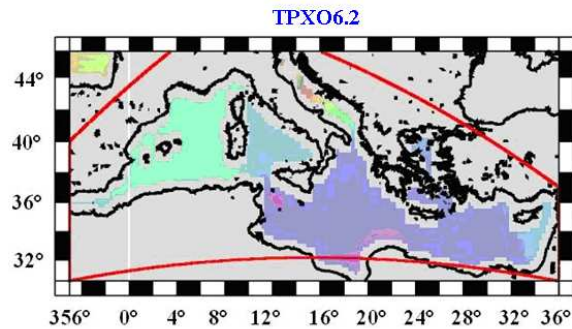
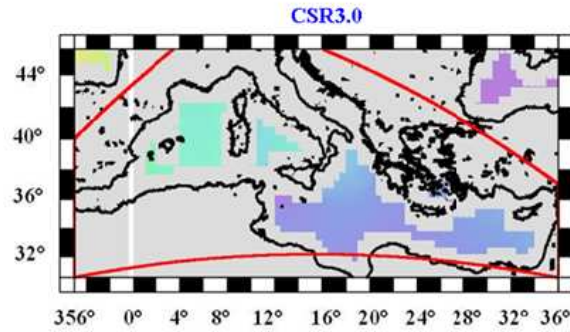Figure 3. Amplitude of the K1 tidal component in the Mediterranean region using TPX06.2

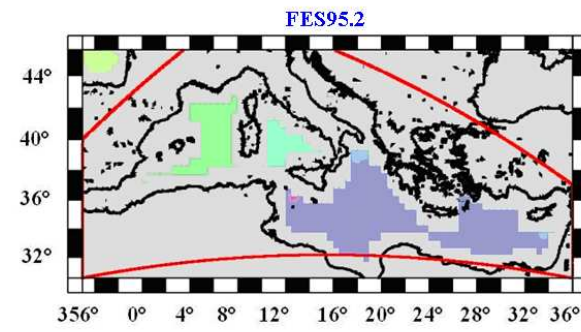Figure 4. Amplitude of the K1 tidal component in the Mediterranean region using CRS3.0

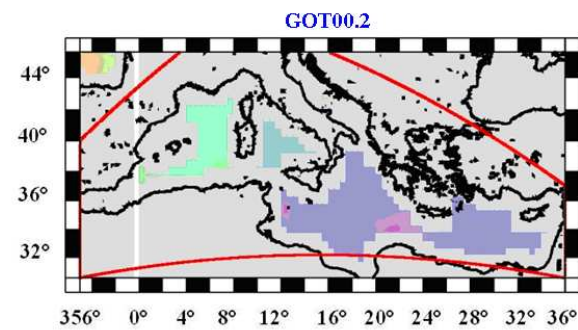Figure 5. Amplitude of the K1 tidal component in the Mediterranean region using FES95.2

Figure 6. Amplitude of the K1 tidal component in the Mediterranean region using GOT00.2
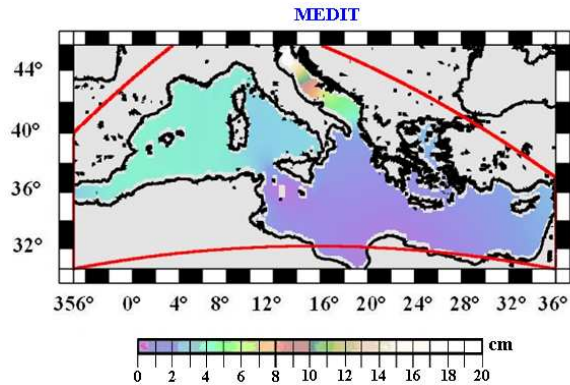
Figure 7. Amplitude of the K1 tidal component in the Mediterranean region using the local model

3   Acknowledgments

References

[1] Crescentini L., A. Amoruso, and L. Ruggiero, Observation of the Fluid Core Resonance With two Laser Extensometers at Gran Sasso, Italy, AGU Fall Meeting, S. Francisco, 2004.

[2] Amoruso A., L. Crescentini, and L. Ruggiero, Free Core Resonance parameters from the analysis of strain data recorded by the Gran Sasso geodetic interferometers, EGU 2nd General Assembly, Wien, 2005.

[3] Agnew D.C., SPOTL: Some programs for ocean-tide loading, SIO Ref. Ser. 96-8, 35 pp., Scripps Institution of Oceanography, La Jolla, CA, 1996.

[4] Amoruso A., L. Crescentini, and R. Scarpa, Removing tidal and atmospheric effects from Earth deformation measurements, *Geophys. J. Int.*, **140**, 493-499, 2000.

[5] Matsumoto K., T. Sato, T. Takanezawa, and M. Ooe, GOTIC2: A program for computation of oceanic tidal loading effect, *J. Geod. Soc. Japan*, **47**, 243-248, 2001.

[6] Venedikov A. P., J. Arnoso, and R. Vieira, VAV: a program for tidal data processing, *Computers and Geosciences*, **29**, 487-502, 2003.

[7] Wenzel H.-G., Tha nanogal software: Earth tide data processing package ETERNA 3.30, *Bull. Inf. Marees Terrestres*, **124**, 9425-9439, 1996.

TELLUS. Ground deformations and their effects in the near-Earth Space

A. Buzzi[a], L. Conti[b], V. Sgrigna[a], L. Stagni[c], D. Zilpimiani[d]

[a] Dipartimento di Fisica e Sezione INFN, Università Roma Tre, Rome, Italy.
[b] Sezione INFN di Perugia e Dipartimento di Fisica, Univ. Roma Tre, Rome, Italy.
[c] Dipartimento di Ingegneria Meccanica e Industriale, Univ. Roma Tre, Rome, Italy.
[d] Institute of Geophysics, Georgian Academy of Sciences, Tbilisi, Georgia.

Abstract

During 2007 a three-axial search-coil magnetometer and a 1-D electric device have been made to detect electric and magnetic fields in the ULF-HF frequency band. The equipment is constituted by three magnetic sensors, one pre-amplified electric probe, three signal conditioning and analog-to-digital conversion boards, and one data processing unit (FPGA and DSP boards). The equipment has been assembled and calibrated in the ESPERIA Laboratory of the Department of Physics of the Roma Tre University. It can store, process and transfer data to a mass memory unit.

1 The Tellus experiment

The activity carried out during 2007 by the TELLUS team was to built a three-axial magnetometer (fig. 1) and a broad band pre-amplified electric probe (fig. 2) for detecting ULF-HF electric and magnetic signals in the near-Earth space.

The equipment aims at monitoring electromagnetic perturbations in the topside ionosphere possibly reconciled with electromagnetic emissions generated by Earth's seismic and/or anthropogenic sources. In particular, the TELLUS team has designed a signal conditioning and data acquisition system (fig. 3) for the three-axial magnetometer and the electric probes (laboratory models) built during the year 2006 [1]. At end 2007 the construction and calibration of the system was concluded. The signal conditioning board of the system allows the analog signals to flow in 8 channels and to be filtered from about 1 mHz to about 10MHz. Data acquisition is performed by a 16-bit ADC at a sampling rate of 250kHz and 40MHz for magnetic and electric signals, respectively. Data processing is performed by an ACTEL FPGA and a TI DSP board. Amplification of signals is adjustable in the different channels and an on-line calibration is performed by a dedicated FPGA on the basis of the spectral content of each channel. Data acquisition is obtained by a floating point TI DSP @ 200MHz, which performs a signal processing on the FPGA

(a)
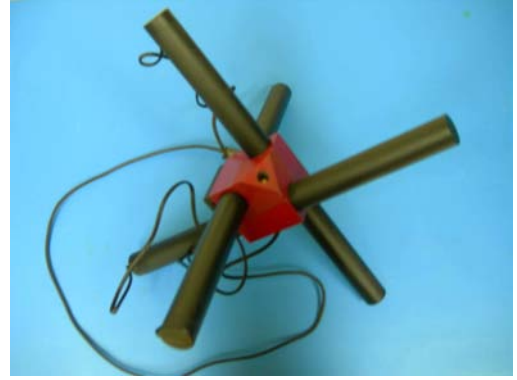
(b)

Frequency band of receiver signals	$0.5 \div 50000$ Hz
Shape of transfer function	linear – flat
Type of output	Symmetrical
Transformation factor at both output terminals:	
• at linear part (0.5 – 5 Hz)	$f*4$ mV/(nT*Hz)
• at flat part (5 – 50000 Hz)	20 mV/nT
Transformation factor error:	
▪ at flat part of band pass without edges	$\leq \pm 0.25$ dB
▪ at flat part band pass edges	≤ 3 dB
Magnetic noise level, pT*Hz$^{-1/2}$:	
▪ at 5 Hz	≤ 0.4
▪ at 100 Hz	≤ 0.02
▪ at 5 kHz	≤ 0.004
▪ at 50 kHz	≤ 0.02
Nominal output load	≤ 200 pF ≥ 50 kΩ
Power supply voltage	$\pm (15 \pm 0.2)$ V
Power consumption	300 mW
Temperature range of operation	$-30\,^{\circ}$C $\div +50\,^{\circ}$C
Outer dimensions (without prominent parts)	$l = 400$ mm $d = 32$ mm
Length of the output cable	0.7 m
Weight	≤ 320 g

(c)

Figure 1: Three-axial search-coil magnetometric probes (a) and layout of the 3D assembly of the same components (b). Magnetometric probe specifications are also reported (c).

output, produces related spectrograms, and performs a pattern recognition of the "significant" signals for the study. The signal recognition is obtained by applying a devoted Neural Network specifically developed for the project. After data compression, necessary to data flow reduction, signals can be stored in a MMC/SD memory card or sent out by a RS232, or USB, or Ethernet output interface. Each signal conditioning board is designed to process only one signal each time (i.e. one magnetic component of the three-axial magnetometer, or the differential output from a couple of electric probes). On the contrary, the FPGA+DSP acquisition system can be connected simultaneously to three pre-processing boards, so to alternatively mange the three magnetic sensors of the three-axial magnetometer or the four electric probes. Electronic hardware has been designed in collaboration with the National Institute of Geophysics of the Georgian Academy of Sciences. The signal conditioning and data acquisition system has been designed for space applications, then only radiation tolerant and low power consumption electronic components and microcircuits have been adopted. To reduce costs, the assembly of laboratory prototypes has been made using "commercial" versions of space qualified components.

The system is wholly modular and re-adjustable. It can work either in autoranging mode

Frequency band of received signals	DC - 200 kHz
Shape of transfer function	flat
Gain factor error in full frequency band	< 1 dB
Input capacitance	7 pF
Input resistance	27 MOhm*
Temperature average drift	±3 µV/ °C
Noise level	
at 0.1 Hz,	≤ 100 nV/√Hz
at 10 Hz,	≤ 20 nV/√Hz
at 1 kHz,	≤ 20 nV/√Hz
at 100 kHz	≤ 20 nV/√Hz
Power supply voltage	± (5±0.2) V
Current consumption	± 3.5 mA
Temperature range of operation	minus 80 ...+ 75°C
Outer dimensions	l = 183 mm
	D = 76 mm
Weight	0.180 kg

Figure 2: Laboratory prototype electric probe (left). The red cilinder is the probe enclosure. Electric probe specifications (right).

(by self-choosing and optimizing the measurement scales) or in manual mode (by setting manually the basic parameters, which in the perspective of a space-based experiment, should be changed and optimized by remote controls). For future satellite applications it will be possible to change and update the DSP software by reliable up-link procedures, and an antifuse FPGA with a standard core FFT program (which guarantees excellent performances and high-reliability) has been adopted for safety's sake and radiation tolerance.
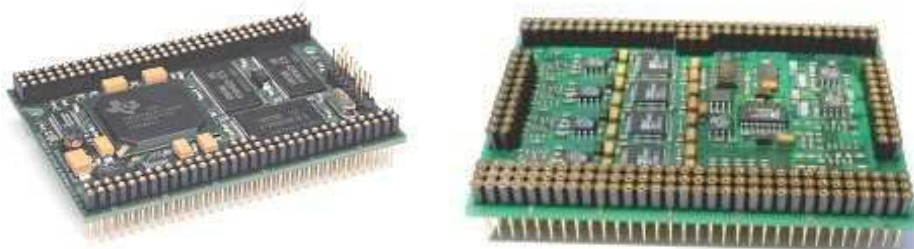

Figure 3: DSP and ADC boards of the TELLUS electromagnetic data acquisition system.

2 Training of personnel

Within the project a collaboration has also been developed with the Actel Italia Company, which provided us with FPGA radiation tolerant components. In particular, two training courses for people involved in the project have been carried out in May and December 2007

at Dipartimento di Fisica "E.Amaldi" , Università di Roma Tre and seminars and lessons about ACTEL's $LIBERO^{TM}$ developing software and VHDL programming language were given by Actel's specialists.

List of Publications during the year 2007

1. Sgrigna, V., Buzzi, A., Conti, L., M. Parrot, J.L. Pincon, Stagni,C, Zilpimiani, D., 2007. *TELLUS. Ground deformations and their effects in the near-Earth space*, Laboratori Nazionali del Gran Sasso, INFN, Annual Report 2006, LNGS/EXP-02/07, July 2007, pp. 217-228.

2. Eftaxias, K., Sgrigna, V., Chelidre, T., 2007. *Mechanical and electromagnetic phenomena accompanying pre-seismic deformation: From laboratory to geophysical scale*, Tectonophysics, 431, 1-5.

3. Sgrigna, V., Altamura, F., Ascani, S., Battiston, R., Bencardino, R., Blasko, S., Buzzi, A., Casolino, M., Conti, L., Lucidi, S., Minori, M., Papi, A., Picozza, P., Rossi, S., Stagni, C., Zilpimiani, 2007. *First data from the EGLE space experiment onboard the ISS*, Microgravity and Sci. Technology, XIX-2, 45-49.

4. Sgrigna, V., Buzzi, A., Conti, L., Picozza, P., Stagni, C., Zilpimiani, D., 2007. *Seismo-induced Effects in the Near-Earth Space: Combined Ground and Space Investigations as a contribution to Earthquake Prediction*, Tectonophysics, 431, 153-171.

5. Sgrigna, V., A. Buzzi, L. Conti, P. Picozza, C. Stagni, D. Zilpimiani, 2008. *The ESPERIA satellite project for detecting seismic-associated effects in the topside ionosphere. First instrumental tests in space*, Earth Planets and Space, 60, 1-13.

6. Buzzi, A., Conti, L., Parrot, M., Pinçon, J.L., Sgrigna, V., Zilpimiani, Z., 2007. *Statistical study of anomalous fluctuations of whistler data recorded by DEMETER*, 2007 IUGG XXIV General Assembly, IAGA-IASPEI-IAVCEI Joint Section "JSS010: Progress in electromagnetic studies on earthquakes and volcanoes - Seismo-electromagnetic studies using space technology", Abstr. 10032, Perugia, Italy, July 2-13, 2007 (Poster presentation n.2090).

7. Conti, L., Buzzi, A., Parrot, M., Pinçon, J.L., Sgrigna, V., Zilpimiani, Z., *Possible influence of seismic activity on the propagation of anomalous whistlers recorded in space*, 2007 IUGG XXIV General Assembly, IAGA-IASPEI-IAVCEI Joint Section "JSS010: Progress in electromagnetic studies on earthquakes and volcanoes - Seismo-electromagnetic studies using space technology", Abstr. 10093, Perugia, Italy, July 2-13, 2007 (Oral Presentation n.2072).

8. Sgrigna, V., and L. Conti, 2007. *Experience on the Magnetic and Electric detectors of the EGLE-LAZIO technology demonstrator*, International Workshop on Early Warning and Monitoring Earthquake by Using Electromagnetism Detecting Satellite, 25 - 27 July 2007 Jakarta, Indonesia.

UNDERSEIS - Underground Seismic Array

C. Fischione[a,*], D. Galluzzo[a], M. La Rocca[a], G. Saccorotti[c],
R. Scarpa[a,b], F. Tronca[a,*]

[a] Osservatorio Vesuviano, I.N.G.V. - Napoli, Italy
[b] Dipartimento di Matematica e informatica, Università di Salerno - Fisciano (SA), Italy
[c] I.N.G.V. - Sez. Pisa, Italy
[*] Spokesperson

Abstract

This report describes a geophysical instrument installed in the underground
physics laboratories of Gran Sasso (LNGS-INFN), located in the seismic zone of
central Apennines, Italy. This instrument is aimed to monitor seismic radiation
with very high sensitivity; it is a small aperture seismic array composed by 20
three-components short period seismometers (Mark L4C-3D).

1   Introduction

The physics of earthquakes is based on the measurements of radiated seismic waves and
ground displacement associated with this phenomena. The inertial pendulum is the olde-
st and most diffused instrument used to measure the main features of seismic waves. The
advantages of this instrument are the simplicity of the theory, the high sensitivity, the
robust design and the simple calibration methods, in spite of the quite reduced frequency
band and linearity (Wielandt, 1983). Other instruments based on different physical princi-
ples, such as strainmeters and gyroscopes, are only partially used by seismologists (Benioff,
1935; Farrell, 1969; Aki and Richards, 1980). Networks of short period seismometers are
as far the most diffused system to monitor local and regional seismicity (Lee and Stew-
art, 1981). Broad-band instruments make up a powerful system to study the details of
seismic sources and also to study large earthquakes at global scale (Lee and Wallace,
1995). Strainmeters and tiltmeters (Agnew, 1986) are used to study the lower frequencies
radiated from seismic sources and allow to detect slow earthquakes and strain steps (i.e.
anelastic deformations around seismic sources). Moreover arrays of seismometers and
accelerometers are used to study the Earth structure at global, regional and local scale
(Green, 1965; Kedrov and Ovtchinnikov, 1990; Mikkeltveit, 1985), earthquake source
process (Spudich and Oppenheimer, 1986; Goldstein and Archuleta, 1991), nuclear un-
derground explosions (Bolt, 1976; Chouet, 1996) and, more recently, for the analysis of
complex signals associated to the volcanic activity (see f.i. Goldstein and Chouet, 1994;

Chouet et al., 1997; Almendros et al., 1991). The main advantage of the seismic arrays consists in their ability to detect small signals through multichannel waveform stacking (Capon, 1969). The area is interested by relevant seismicity associated with the mainly distensive tectonics affecting the Apennines since the late Pliocene (D'Agostino et al., 2001; Galadini et al., 2003). The last large historical event is the 1915, $M_S = 6.8$ Fucino earthquake, which caused about 32000 casualties, recently modelled by a normal fault striking along the Apennines (Amoruso et al., 1998). In addition, swarms of low-to moderate-size earthquakes occur quite frequently, the most recent on 1992, 1994 and 1996 (De Luca et al., 2000). This massif is intersecting a main seismogenetic fault where the occurrence of slow earthquakes has been recently detected through two wide-band geodetic laser interferometers (Crescentini et al., 1999; Amoruso et al., 2002). This quite relevant rate of seismicity, joint to the low-noise conditions and site response associated to the underground setting, make the Gran Sasso underground laboratories an ideal site for high-resolution seismic observations (De Luca et al., 1998).

2   The Underground Seismic Array

A seismic array is a set of seismographs distributed over an area of the Earth's surface at spacing narrow enough so that the signal waveform may be correlated between adjacent seismometers (Aki and Richards, 1980).
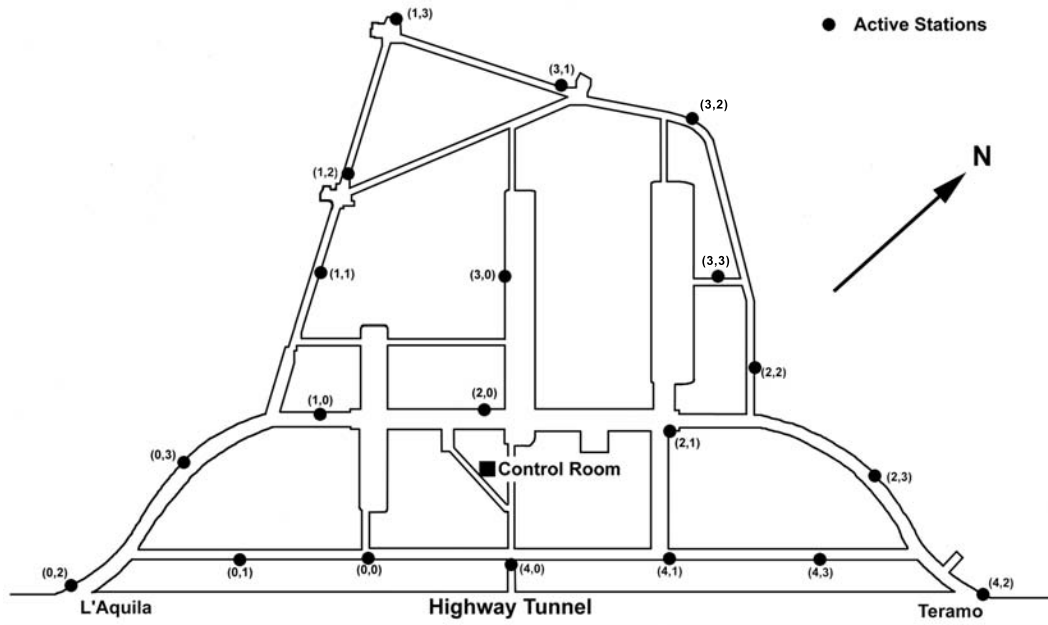

Figure 1: Map of the Underground Seismic Array. The notation (n,m) shows the line number (n) and the station number (m).

The design of the UNDERSEIS hardware and software components began on the late 90's; over the following years, major upgrades were developed under a technological effort

192

jointly carried out by engineers from the University of Granada (Spain), University of L'Aquila (now the team moved to the University of Salerno), and INGV - Osservatorio Vesuviano. The array become fully operative since May, 2002. In its present configuration, it consists of 20 elements, each equipped with a MARK Product L4C-3D, 1 Hz, 3-component seismometer. The average sensor spacing is on the order of 90 m, and the largest distance among sensors is about $400m$. Seismic signals are digitized locally at each individual seismometer with a dynamic range of 24 bits and sampling frequency of 100 Hz. Data synchronization is achieved via a Master Oscillator which transmit the UTC synchronized pulses from an atomic clock to the different ADC boards. The synchronized data packets are then sent via serial cable connection to a set of five nodal PCs, which are in turn connected via an Ethernet network to a central data server and an on-line processor (Scarpa et al., 2004).

3 Analysis of rumble events occours inside underground galleries

This section describes the analysis of two events recorded by the Gran Sasso Underground Seismic Array (UnderSeis). These two events occurred July 21, 2006 (jday 202) at 05:02:10 Gmt and November 24, 2006 (jday 328) at 10:43:12. Both events were felt like a rumble by users which were then present in the underground laboratories.
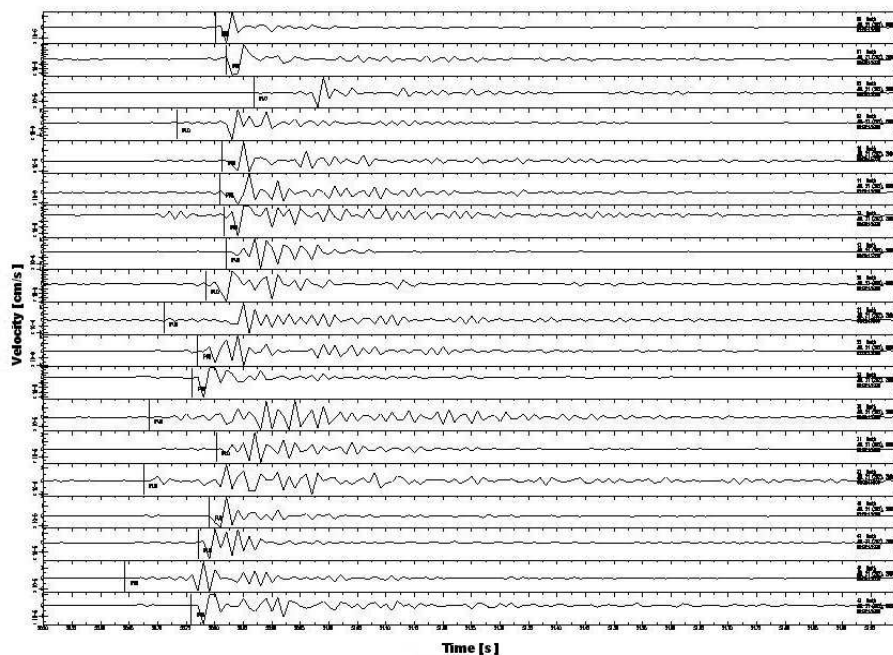

Figure 2: Event 202, as recorded by 19 array stations, North component

Figures 2 and 3 depict the original array recordings of the two events, while figure 4 depicts a magnitude 3.2 earthquake recorded September 1, 2006 and located in the Monti

della Laga area, as far as $20Km$ NW from the laboratories (this was the strongest event recorded during the last 9 months). The two events were plotted and analysed in a $1.5s$ long window and they have a duration of about $1s$. Comparing the two rumble events with a typical earthquake (figure 4 and 5) we note some waveform differences: signals plotted in figures 2 and 3 show a more impulsive waveform an a stronger amplitude compared to those plotted in figures 4 and 5: the earthquake event shows strong signal coherency among the various array stations (see figure 5); this is not true for the "rumble" events (figure 2 and 3). This fact can be related too:

1. time under sampling: the typical frequencies of the rumble events are greater than the sampling frequency, so the original waveform is not correctly sampled;

2. high signal complexity: the rumble waveform is due to acoustic and seismic wave superposition and to trapping and diffraction phenomena at the tunnel walls.

3.1   Event location: algorhythm and results

First step in data analysis was phase picking: this was done manually, directly on the waveform recordings. The phase arrival times were then fitted according to a plane wave model (PWF - Del Pezzo and Giudicedipietro, *Computer and Geosciences*, 28, 2002, 59-64). Apparent velocities of the two rumble events were then computed using the following formula:

$$V_{app} = \frac{1}{\sqrt{S_x^2 + S_y^2}}$$

where S_x and S_y are the components of the slowness vector. Computed apparent velocity values are $V_{app} = 5.36\frac{Km}{s}$ for the 328 event and $V_{app} = 3.28\frac{Km}{s}$ for the 202 event.

In order to verify the goodness of the plane wave approximation, we proceeded to the wave front reconstruction by plotting the arrival times at every station vs the spatial coordinates of the stations themselves, choosing one as axis origin (station 4.0, figure 6). The results for the 328 event are shown in figure 6: the picture shows clearly a spherical wave front. This fact convinced us to change to the spherical wave front approximation using the following formula:

$$T_p = T_0 + \frac{r}{v}$$

where T_p is the arrival time at every single station, v is the apparent velocity and $r = \sqrt{dx^2 + dy^2 + dz^2}$, where $dx = x - x_0$, $dy = y - y_0$, $dz = z - z_0$, with x, y, z the station coordinates and x_0, y_0, z_0 the source coordinates, to be computed. A grid search is then performed for the x_0, y_0, z_0 values which best reproduces the observed arrival times: that is, for every grid point, theoretical and observed travel times are computed, the mean value is removed and the residuals are computed.

The x_0, y_0, z_0 values which best represent the event source are those corresponding to the minimum residual value. At first we chose a three dimensional grid ranging from -5 to 5 km with a step of $100m$; then, after a model refining, we chose a grid with dimensions ranging from -1 to 1 km and step of $25m$ for the horizontal and step of $50m$ for the vertical. The results are resumed as follows: the 328 event was located with $x_0 = -150m$, $y_0 = -25m$ and $z_0 = 950m$, while the 202 event was located with $x_0 = 550m$, $y_0 = 675m$
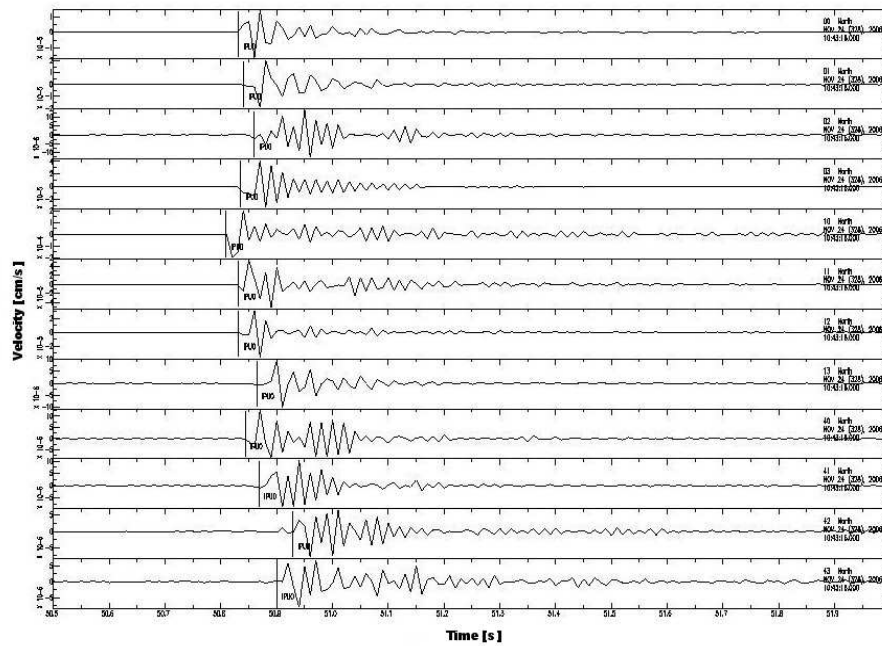
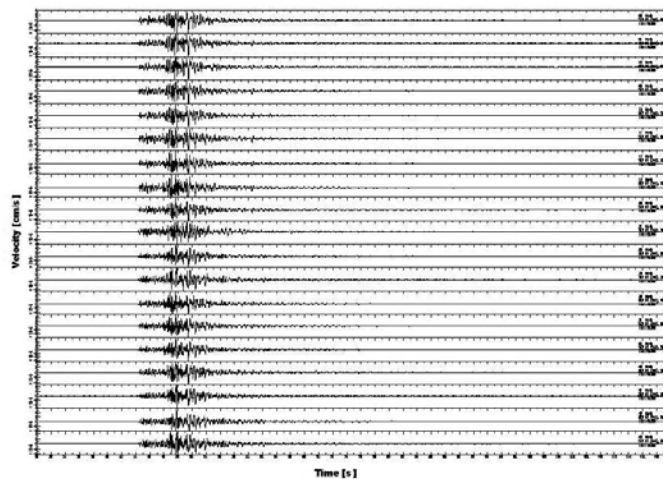Figure 3: Event 328, as recorded by 12 array stations, North component

Figure 4: Monti della Laga 3.2 event (Sept. 1, 2006), as recorded by 19 array stations, North components in a 90 s long window
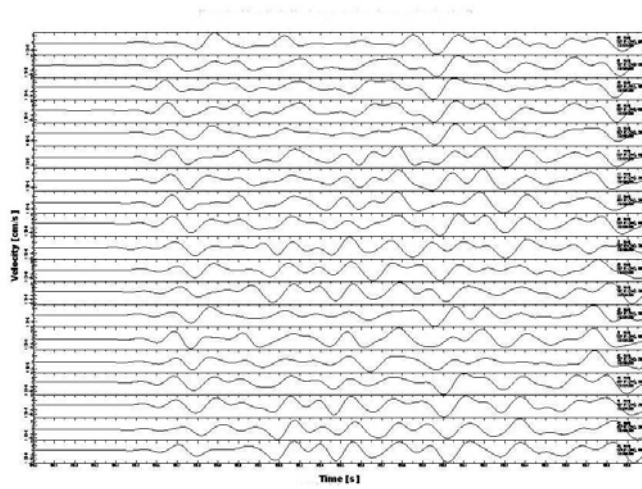
195

Figure 5: Monti della Laga 3.2 event (Sept. 1, 2006): zoom on the P-wave arrival. The window is 4.5 s long and shows the signal coherency among the various stations.
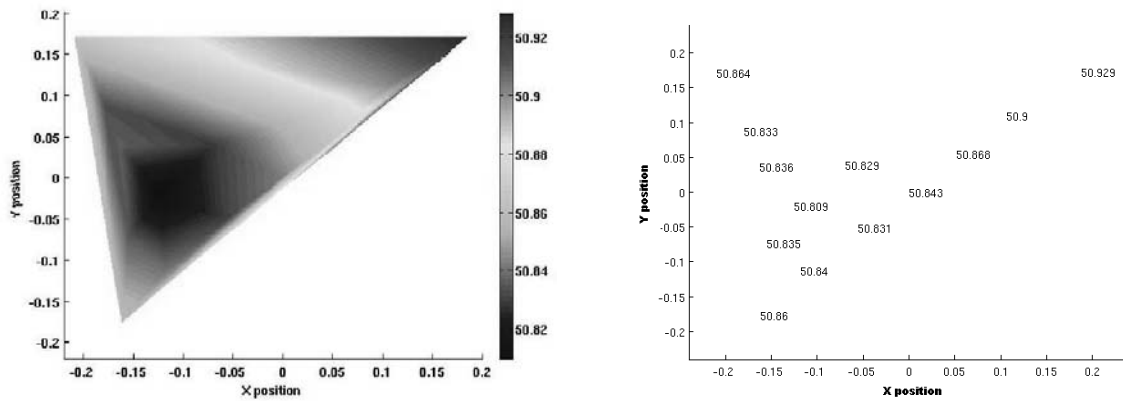

Figure 6: Left picture shows the waveform contour plot; right picture shows the stations location in the underground laboratories and the wave arrival times.

196

and $z_0 = 965m$. Figure 7 shows event 328 plotted on the laboratories map, while 202 events is located about $550m$ far from the laboratories in the NE direction. All codes were written in MatLab language.

3.2   Discussion

The analysis of the two "rumble" events shows how their sources were located extremely near to the underground laboratories. The noise felt by people was due to a seismic/acoustic conversion of the wave front on the tunnel walls. From a geophysical point of view, a good hypothesis is that these events were due to rock micro faulting. An accurate monitoring of these events it's really interesting, but their amplitude is really small and they can't be captured by an external seismic network. So, the UnderSeis activity is of crucial importance in order to guarantee an accurate seismic survey of the underground laboratories.
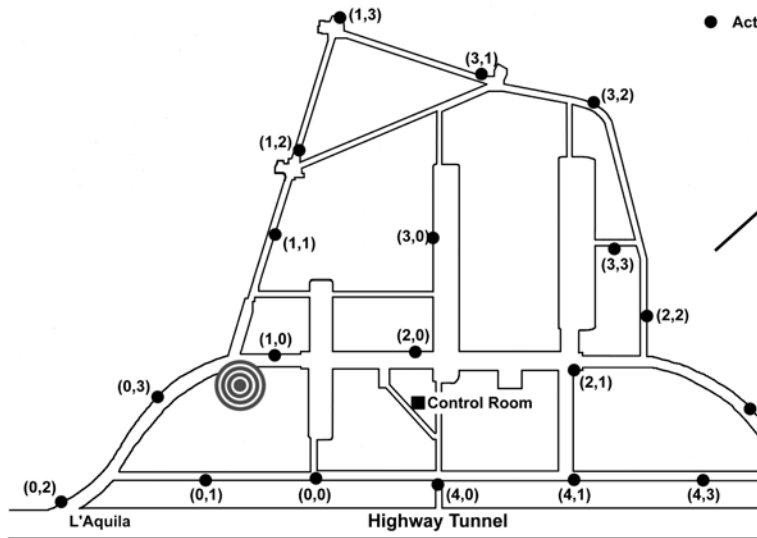

Figure 7: Location of the 328 event (November 24, 2006)

4   The Fontary Array (FonArray) in Campo Imperatore

Since the beginning of June 2007, a new temporary surface array, consisting of 6 stations, was installed in the Fontari Plain, near Campo Imperatore ($1950m$ above sea level). It was placed with good approximation vertically above the underground array (UnderSeis). Figure 7 (on the right) shows the geometric configuration of FonArray, and the technical details are:

- channels: 18

- sensors: 6 short period 3D seismometers Lennartz LE 3D Lite (frequency $1Hz$)

- data storage: magneto-optical disk ($512Mb$) or memory cards ($1Gb, 2Gb$ or $5Gb$);

- time synchronization: GPS;

- power supply: $12V$ by solar panels and batteries;

- acquisition: continuous, $125Hz$ of sampling frequency;

Four stations were installed indoor (garages, old buildings), but two had to be installed outdoor. Figure 8 (on the left) shows the configuration of the station known as FON6. Array acquisition lasted about 6 months, from June to November 2007. Maintenance operations were carried out weekly: they consisted in data recovering (disks and memory card substitution), GPS time synchronization check, solar panels and batteries charge check, in addition to occasional operations.
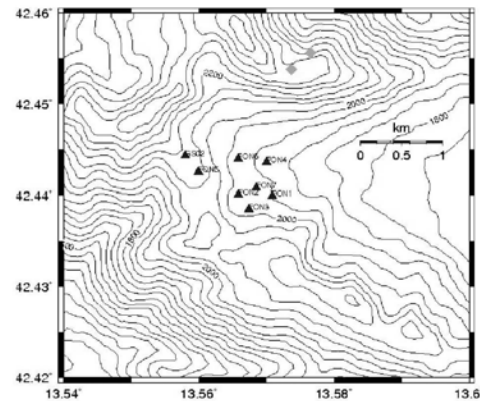

Figure 8: Left: FON6 station, as all the other FonArray ones, consisted in a Lennartz 3D-lite sensor, a solar panels and batteries power supply and a Lennartz MarsLite station with a GPS timing system. Right: FonArray geometric configuration. Stations GS02 and FON5 are also shown in the picture: after a short period of acquisition, they were dismantled

FonArray data can be used for several data analysis, especially if analysed together with UnderSeis ones. Arguments for next research activities are resumed as follows:

- seismic noise analysis with array techniques, in order to evaluate a surface velocity model;

- comparison between seismic noise recorded at FonArray and seismic noise recorded at UnderSeis;

- earthquakes analysis with various techniques, giving particular attention to events recorded together by FonArray and UnderSeis.

- polarization studies of primary and secondary waves for local and regional earthquakes

- polarization analysis of seismic noise.

5   Acknowledgements

6   List of Publications

1. F. Tronca, C. Fischione, G. Saccorotti, R. Scarpa, 2007. *Recent seismicity in central Italy as observed by the Gran Sasso underground seismic array.* Submitted to Bull. Seism. Soc. Am.

References

[1] Agnew D. C., 1986. *Strainmeters and tiltmeters.* Rev. Geophys. 24, 579-624.

[2] Aki K. and Richards P., 1980. *Quantitative seismology: Theory and methods.* Freeman, San Francisco, California, 932 pp.

[3] Aki K., Christoffersson A. and Husebye E. S., 1977. *Determination of the three dimensional seismic structure of the lithosphere.* J. Geophys. Res. 82, 277-296.

[4] Benioff H., 1935. *A linear strain seismographs.* Bull. Seism. Soc. Am. 25, 283-309.

[5] Bolt B. A., 1976. *Nuclear explosions and earthquakes. The parted veil.* Freeman, San Francisco.

[6] Capon J., 1969. *High resolution frequency-wavenumber spectrum analysis.* Proc. IEEE 57, 1408-1418.

[7] Chouet B., 1996. *New methods and future trends in seismological volcano monitoring.* In "Monitoring and mitigation of volcano hazards", R. Scarpa and R. Tilling (Eds.), Springer-Verlag, New York.

[8] Chouet B., G. Saccorotti, M. Martini, P. Dawson, G. De Luca, G. Milana and R. Scarpa (1997). *Source and path effects in the wavefields of tremar and explosions at Stromboli Volcano, Italy.* J. Geophys. Res., 102, 15,129-15,150.

[9] De Luca G., Scarpa R., Del Pezzo E. and Simini M., 1997. *Shallow structure of Mt. Vesuvius volcano, Italy, from seismic array analysis.* Geophys. Res. Lett. 24,481-484.

[10] De Luca G., Del Pezzo E., Di Luccio F., Margheriti L., Milana G. and Scarpa R., 1998. *Site response study in Abruzzo (centraI Italy): underground array versus surface stations.* J. Seismol., 2, 223-226.

[11] Farrell W. E., 1969. *A gyroscopic seismometer: measurements during the Borrego earthquake.* Bull. Seism. Soc. Am. 59, 1239-1245.

[12] Green Jr., Frosh B. A. and Romney C. F., 1965. *Principles of an experimental large aperture seismic array.* Proc. IEEE 53, 1821-1833.

[13] Kedrov O. K. and V. M. Ovtchinnikov, 1990. *An on-line analysis system for three component seismic data: method and preliminary results.* Bull. Seism. Soc. Am. 80, 2053-2071.

[14] Lee W. H. K. and Stewart S. W., 1981. *Principles and applications of microearthquake networks.* Academic Press, New York, 293 pp.

[15] Lay T. and Wallace T. C., 1995. *Modern Global Seismology.* Academic Press, New York, 517 pp.

[16] Mikkeltveit S., 1985. *A new regional array in Norway: design, work and results from analysis of data from a provisional installation, in The Vela Program.* A twenty- Five Review of Basic Research, edited by U. A. Kerr (Defence Advanced Research Project Agency), 546-553.

[17] Milana G., Barba S., Del Pezzo E. and Zambonelli E., 1996. *Site response from ambient noise measurements: new perspectives from an array study in CentraI Italy.* Bull. Seism. Soc. Am. 86, 1-9.

[18] Schmidt R. O., 1986. *Multiple emitter location and signal parameter estimation.* IEEE Trans Antennas Propagation 34, 276-280.

[19] Wielandt E., 1983. *Design principles of electronic inertial seismometers.* In H. Kanamori and E. Boschi (Eds.) "Earthquakes: Observation, Theory and Interpretation". Proc. Int. School of Phys. "E. Fermi", North Holland, Amsterdam.

[20] R. Scarpa, R. Muscente, F. Tronca, C. Fischione, P. Rotella, M. Abril, G. Alguacil, W. De Cesare, M. Martini, 2004. *UNDERSEIS - Underground Seismic Array.* Seis. Res. Lett. Vol. 75, number 4, July/August 2004.

[21] Fischione C., Martini M., Tronca F., Saccorotti G., Scarpa R., 2003, 2004, 2005, 2006. *UNDERSEIS - Underground Seismic Array.* Annual Reports, I.N.F.N., Laboratori Nazionali del Gran Sasso, Italy.

[22] G. Saccorotti, B. Di Lieto, F. Tronca , C. Fischione, R. Scarpa, R. Muscente, 2006. *Performances of the UNDERground SEISmic array for the analysis of seismicity in central Italy.* Annals of Geophysics, Vol. 49, number 4/5, August/October 2006.

THE PIERRE AUGER COSMIC RAY OBSERVATORY

F. Arneodo[a], D. Boncioli[c], P.L. Ghia[a,b], A.F. Grillo[a], M.Iarlori[c],
C. Macolino[c], S. Parlati[a], S. Petrera[c], V. Rizi[c], F. Salamida[c]
for the Auger Collaboration

[a] LNGS-INFN - Italy
[b] INAF - Italy
[c] Universitá dell'Aquila - Italy

Abstract

The Pierre Auger Project is an international Collaboration involving over 300 scientists from 17 countries, with the objective of studying the highest energy cosmic rays. The commissioning of southern site of the Pierre Auger Observatory, located in Malargue (Argentina), is almost complete and it has been collecting data from more than 3 years, so that the size of the data set now exceeds that form earlier experiments.
The group from Gran Sasso/L'Aquila University is part of the Collaboration and it is involved in the experiment set-up and monitoring as well as in the analysis. The status of the experiment and the activities of the group during 2007 are here reported.

1 Introduction

Ultra-high energy cosmic rays are of intrinsic interest as their origin and nature are unknown. It is quite unclear where and how particles as energetic as $\simeq 10^{20}$ eV are accelerated. Over 40 years ago it was pointed out that if the highest energy particles are protons then a fall in the flux above an energy of about $\times 10^{19}$ eV is expected because of energy losses by the protons as they propagate from distant sources through the CMB radiation. At the highest energies the key process is photo-pion production in which the proton loses part of its energy in each creation of a Δ^+ resonance. This is the Greisen-Zatsepin-Kuzmin (GZK) effect. It follows that at 10^{20} eV any proton observed must have come from within about 50 Mpc and on this distance scale the deflections by intervening magnetic fields in the galaxy and intergalactic space are expected to be so small that point sources should be observed. Despite immense efforts in the period since the prediction, the experimental situation remains unclear. The main problem in examining whether or not the spectrum steepens is the low rate of events which, above 10^{20} eV, is less than 1 per km^2 per century

so that the particles are only detectable through the giant air showers that they create. These showers have particle footprints on the ground of $\simeq 20$ km^2 and suitably distributed detectors can be used to observe them. Also the showers excite molecules of atmospheric nitrogen and the resulting faint fluorescence radiation, which is emitted isotropically, can be detected from distances of several tens of kilometers.

The Pierre Auger Observatory has been developed by a team of over 300 scientists and $\simeq 100$ technicians and students from $\simeq 70$ institutions in 17 countries. When completed the Observatory will comprise 1600 10 m$^2 \times$ 1.2 m water- Cherenkov detectors deployed over 3000 km^2 on a 1500 m hexagonal grid. This part of the Observatory (the surface detector, SD) is over-looked by 24 fluorescence telescopes in 4 clusters located on four hills around the SD area which is extremely flat. The surface detectors contain 12 tonnes of clear water viewed by 3×9" hemispherical photomultipliers. The fluorescence detectors (FD) are designed to record the faint ultra-violet light emitted as the shower traverses the atmosphere. Each telescope images a portion of the sky of 30° in azimuth and 1°-30° in elevation using a spherical mirror of 3 m^2 effective area to focus light on to a camera of 440×18 cm^2 hexagonal pixels, made of photomultipliers complemented with light collectors, each with a field of view of 1.5° diameter.

For ICRC 2007 data recorded from January 2004 to the end of February 2007 have been analysed. Over this period the number of fluorescence telescopes was increased from 6 to 24 and the number of water tanks from 125 to 1198. Here results from an exposure about 3 times greater than AGASA, and comparable to that of the monocular HiRes detectors at the highest energies, are reported. Above 10^{18} eV, more events have been recorded at the Auger Observatory than have come from the sum of all previous efforts. As at 9 July 2007, 1438 water-tanks had been deployed, with 1364 currently taking data. All 24 telescopes are working and thus over 85% of the instrument is operational. Except for an area near the centre of the SD array, all landowner issues have been resolved and completion is scheduled for early 2008. Undoubtedly one of the highlights of the Observatory is that such a large and multi-national collaboration has succeeded in developing this complex instrument in a rather remote place (Malarge, Mendoza Province, Argentina) and has used it to produce the results described below in a relatively short time.

An important feature of the design of the Observatory was the introduction of the hybrid technique as a new tool to study airshowers. It is used here for the first time. The hybrid technique is the term chosen to describe the method of recording fluorescence data coincident with the timing information from at least one surface detector. Employing these two complementary observation methods provides the Auger Observatory with high quality information about angular reconstruction, determination of the core position of the shower and of the types of particles in the primary cosmic rays. Comparing results from the different types of detectors also helps scientists reconcile the two sets of data and produce the most accurate results about the energy of primary cosmic rays.
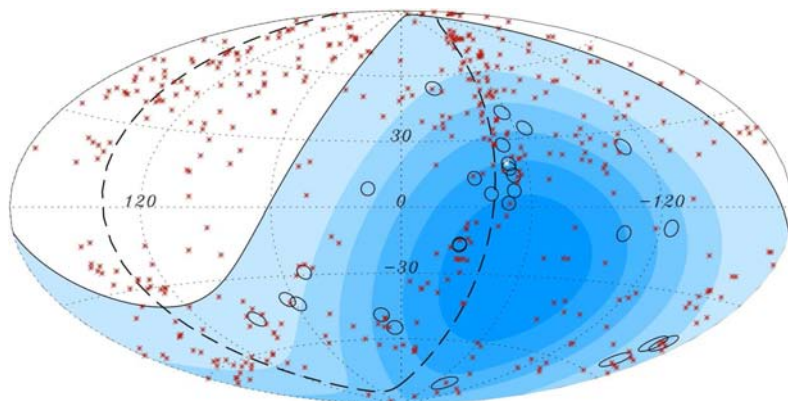
2 The status of the Pierre Auger Cosmic Ray Observatory

In this section recents measurements relating to correlation with nearby extragalactic objects, mass composition and energy spectrum above 10^{18} eV are presented[1].

2.1 Correlation with Nearby Extragalactic Objects

The Pierre Auger experiment has observed a correlation between the arrival directions of the cosmic rays with highest energies measured and the positions of nearby AGN from the 12th edition of the catalog of quasars and active nuclei by Véron-Cetty and Véron (V-C catalog)[2]. The data set analyzed consists of the cosmic-ray events recorded by the surface array of the Observatory from 1 January 2004 to 31 August 2007. It contains 81 events with reconstructed energies above 40 EeV and zenith angles smaller than 60°. The integrated exposure is 9.0×103 km2 sr year.

The amount of correlation between the arrival directions and the positions of known AGN has been explored, by tuning several factors: a cutoff for the maximum distance of an AGN, a cutoff for the minimum energy of cosmic rays, and the angular separation of an event from some AGN. A key element of this study is the probability P for a set of N events from an isotropic flux to contain k or more events at a maximum angular distance Ψ from any member of a collection of candidate point sources. In May 2006 a strong

Figure 1: Aitoff projection of the celestial sphere in galactic coordinates with circles of radius 3.1° centered at the arrival directions of the 27 cosmic rays with highest energy detected by the Pierre Auger Observatory. The positions of the 472 AGN (318 in the field of view of the Observatory) with redshift z < 0.018 (D < 75 Mpc) from the 12th edition of the catalog of quasars and active nuclei [2] are indicated by red asterisks. The solid line represents the border of the field of view (zenith angles smaller than 60°). Darker color indicates larger relative exposure. Each colored band has equal integrated exposure. The dashed line is the supergalactic plane. Centaurus A, one of our closest AGN, is marked in white.

association between the cosmic-ray directions and nearby AGN has been found[3]. Of 15 events with energies greater than about 60 EeV, 12 were located within 3.1° of AGN

closer than 75 Mpc from Earth (about 250 million light-years). The likelihood of a random isotropic set of arrival directions conspiring to fool people this much was small. Once fixed these values of the correlation parameters and applied them to new data collected after June 2006 until August 2007, the correlation has been confirmed.

In figure 1 it is presented a sky map in Galactic coordinates of our 27 highest-energy events ($E > 57$ EeV), as determined by our most recent version of the reconstruction code. The anisotropy is clearly visible. We note the proximity of several events close to the supergalactic plane, and also that two events arrive within $3°$ of Centaurus A, one of the closest AGN, marked in white on the figure. confirmed the correlation.

Interpretation of these results merits some caution. The catalog of AGN used is known to be incomplete, especially in directions in which we peer through the dusty plane of our Galaxy and beyond 300 million light-years away from Earth. (It is notable that most of the few events that do not appear to be near AGN are indeed somewhat near the Galactic plane.) This is not an obstacle to demonstrating the existence of anisotropies but may affect the ability to identify the cosmic-ray sources unambiguously. The AGN themselves tend to be distributed among the nearby galaxies, and so based on the statistics of the present data it is possible only to declare that the cosmic-ray sources are correlated with the distribution of nearby matter, including AGN. However, because of the energetic processes within them, AGN have long been considered as likely sources of cosmic rays. The data suggest that they remain the prime candidates.

2.2 The Mass Composition of the Primary Particles

The mass composition can be inferred only indirectly by making assumptions about the hadronic interactions at the highest energies. Models of the interactions, such as the SIBYLL or QGSJET families, fit accelerator data up to the energy of the Tevatron with extrapolations being made to the energies of interest. The centre-of-mass energy in the collision of a 10^{20} eV proton with a fixed target is $\simeq 30$ times that available at the LHC. Extrapolations of cross-sections, multiplicities, inelasticities etc are necessary. The systematic uncertainties in mass or in energy estimates derived using hadronic interactions are inherently unknowable but will become better constrained with LHC data.

A promising approach is to compare measurements of the depths of shower maxima with the predictions from Monte Carlo calculations using different models of interaction.

The maxima can be found with an accuracy of < 20 g cm^{-2} using the FD if suitable cuts are adopted. Each event in this Auger data set is a hybrid event in which at least one surface detector has been used to constrain the geometry. In figure 2 measurements of X_{max} based on 4105 events across two decades of energy are shown together with predictions for proton and iron primaries made using three models of hadronic interactions. It is clear that a single slope does not fit the data and that the rate of increase of X_{max} with energy is smaller above 2×10^{18} eV than in the region below. A preliminary conclusion from figure 2 is that the mass spectrum is not proton-dominated at the highest energies. This unexpected result assumes that the shower models are broadly correct. The position of each data point with respect to the model lines can be used to extract an estimate of $\langle \ln A \rangle$, where A is the atomic mass.

The resolution of the question as to whether each data point is associated with a single
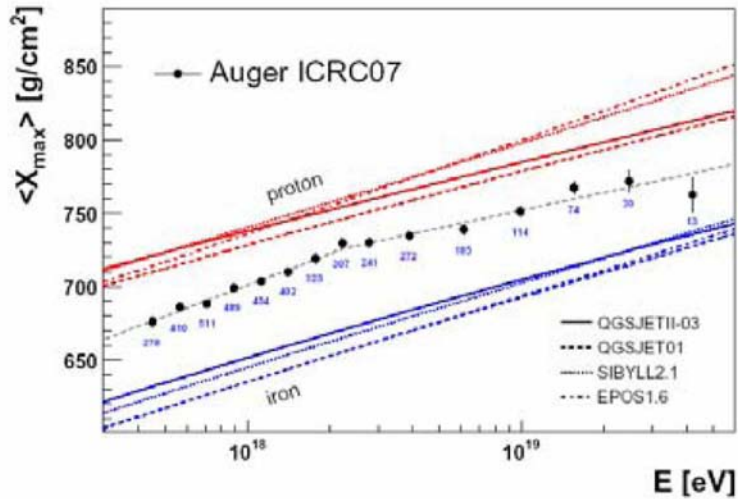
Figure 2: The depth of maximum as a function of energy. The upper sets of lines are predictions for protons for a range of models: the lower set are under the assumption of Fe nuclei.

mass species or with a mixture of masses will be assessed by studying the fluctuations in X_{max} at a given energy.

The data of figure 2 are in broad agreement with those from previous experiments but the uncertainties in the earlier works are larger. For example, in the HiRes report [6], where stereo events were used, there are only 419 events above 10^{18} eV and the final energy bin is centered at 2.5×10^{19} eV. Mass interpretation is an area where cosmic ray physicists look to the LHC for help. Although the present models agree well with data at Tevatron energies there are big differences in the predictions for the LHC. For example at LHCf the flux of gamma rays at 4000 GeV predicted using QGSJET-II is twice that from SIBYLL. The predicted spectrum is much harder than in the case of QGSJET-II.

These two models differ in the assumptions that are made about the distribution of partons in protons and pions. The cross-sections predicted for p-air and π-air collisions with air nuclei differ by $\simeq 20\%$ at 10^{20} eV with the SIBYLL value the higher while the multiplicity predictions differ by nearly a factor of 2 at the same energy with the QGSJET multiplicity being the larger. The EPOS model includes baryon-anti-baryon production. To reconcile the Xmax data with protons would require even larger cross-sections and/or multiplicities. A description of the differences between the SIBYLL and QGSJET models has been given in [7].

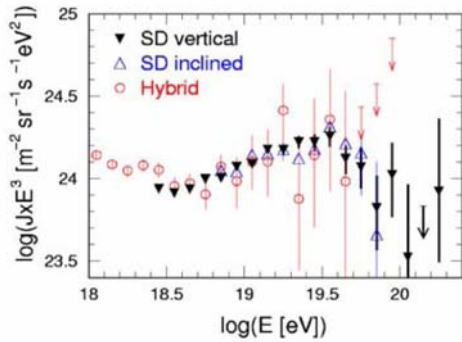## 2.3 The Energy Spectrum

The hybrid nature of the Auger Observatory enables the energy spectrum of primary cosmic rays to be found without strong dependence on assumptions about the mass and hadronic interactions. This contrasts with what is necessary with an all-surface detector system such as used at AGASA. The Auger approach is to use a highly-selected sample
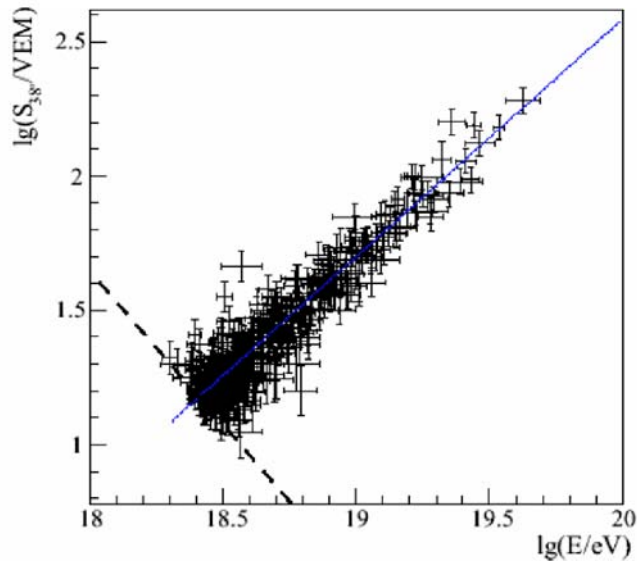
Figure 3: The 387 events which have simultaneous measurements of S(1000) and of an energy derived from the fluorescence detectors.

of hybrid events in which the energy can be estimated accurately using the fluorescence detectors. Thus far there are 357 events that satisfy strict criteria with the most energetic being at 4×10^{19} eV. Each measurement with a fluorescence detector gives the electromagnetic energy deposited in the atmosphere in a manner similar to what is done with calorimeters at accelerators. The estimate of the electromagnetic energy must be augmented by what is carried by high energy muons and neutrinos which travel into the ground below the atmosphere to give the energy of the primary cosmic ray. This "missing energy" is assessed using assumptions about the primary mass and the hadronic interaction model. The correction decreases as the energy increases (largely because of the reduced probability of decay of high-energy pions) and increases as the mass increases. Typical values of the correction, assuming a mean mass of 50% protons and 50% iron nuclei, are 19 and 11% at 10^{17} and 10^{20} eV respectively. At 10^{19} eV the average correction is $\simeq 12\%$, with a systematic uncertainty of $\pm$ 5%, taking as limits the upper value from EPOS and Fe and the lower value from QGSJET and protons. The derived energy estimates are uncertain by this amount. The calibration curve which is subsequently used to find the energies of the bulk of the events in which there are only surface detector measurements is shown in figure 3. The parameter chosen to characterise the size of each SD event is the signal at 1000 m from the shower axes, S(1000), normalised to the mean zenith angle of events of 38°. The reasons for the choice of S(1000) as the "ground parameter" are described in [8] while justifications for the normalisation to 38° is set out in [9]. The energy spectrum derived from over 12000 SD events above 3×10^{18} eV is also shown in [9]. The spectra from three independent methods of measurement are shown in figure 4. The bulk of the data [9] are from events with $\theta < 60°$ and the energies are found using the calibration method just described. The area over which such SD events fall and are recorded with 100% efficiency becomes independent of energy above 3×10^{18} eV.

Figure 4: A comparison of the spectra measured with inclined events (60° < θ < 80°) and with hybrid events. As the energy scales are identical only the statistical uncertainty is shown.
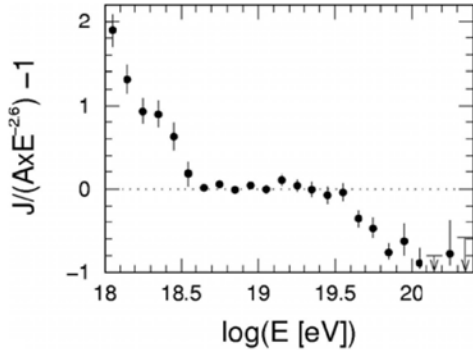
Figure 5: The Auger spectrum, derived by combining the data of figure 4. Each point is shown as a residual from $AE^{-2.6}$.

The exposure up to 28 February 2007 is 5165 km^2 sr yr, about three times that achieved at AGASA and very similar to the monocular HiRes at the highest energies. The slope between 4.5×10^{18} and 3.6×10^{19} eV is (-2.62 ± 0.03) based on 5224 events. If this slope is extrapolated to higher energies the numbers expected above 4×10^{19} and 10^{20} eV are (132 ± 9) and (30 ± 2.5), whereas the observed numbers are 51 and 2 respectively. It is thus clear that the slope of the spectrum increases above $\simeq 4 \times 10^{19}$ eV, with the significance of the steepening being $\simeq 6\,\sigma$. The slope in the highest energy range is (-4.1 ± 0.4) based on 51 events, 2 of which have energies above 10^{20} eV. The limited number of events available for the calibration curve (figure 3) leads to a random uncertainty in the energy scale of 18%. Additionally there is a systematic uncertainty in the fluorescence measurement which is presently 22% and is dominated by the uncertainty in the fluorescence yield. Measurements are underway at Frascati and Argonne to improve understanding of the fluorescence yield. An additional exposure of 1510 km^2 sr yr is readily available by using events at larger zenith angles (60° < θ <80°). The size parameter adopted to characterise the horizontal showers is obtained by comparing maps of the observed signal distributions with those from predictions of what is expected at 10^{19} eV. The pattern of the maps does not depend on the mass or hadronic model and gives the muon number in each event. The events are calibrated in the same manner as above but using the muon number as the ground parameter. Presently only 38 inclined hybrid events are available for calibration. The spectrum from inclined showers above 6.3×10^{18} eV contains 734 events and the slope above this energy is (-2.7 ± 0.1). The data are shown in figure 4. The spectrum has been extended to lower energies using hybrid data in which at least one tank has registered a signal. Details of this analysis, which takes the spectrum down to 10^{18} eV can be found in [10]: again there is a common calibration for the energy and the measurements are shown in figure 4. The three spectra are consistent where they overlap. A presentation summarising the situation is shown in figure 5 where the differential intensity J at each energy E is compared with the expectation from a standard spectrum. This technique of comparing spectrum data through residuals has been advocated previously [11]. The

Figure 6: SDE shift: intervention on a SD detector.

standard spectrum chosen here has a slope of -2.6 and passes through the point at 4.5×10^{18} eV which is based on 1631 events. It is clearly desirable to collect more events and this will occur rapidly as the exposure is expected to double within the next 12 months following completion of the Observatory by early 2008. An advantage of this style of presentation is that the y-axis is linear so that the forgiving nature of a log-log plot is avoided, as are the many limitations in J E^3 vs. E plots which arise when the energy scales differ between different measurements. In addition to the steepening of the spectrum at $\simeq 4 \times 10^{19}$ eV, an ankle is seen at 4.5×10^{18} eV with a change in the slope from (-3.30 $\pm$ 0.06) to (-2.62 $\pm$ 0.02), while above 3.6×10^{19} eV the spectrum steepens to a slope of (-4.115 $\pm$ 0.4). Because of the composition result, caution needs to be exercised over interpretation of the steepening as the long-sought Greisen-Zatsepin-Kuzmin effect.

3 Activities of the Group during 2007

## 3.1 Shifts and maintenance of SD electronics

Our local group is also involved in the deployment and maintenance shifts of the SD Electronics. The deployment of electronics "kits" is going on quite steadily and the local staff is now performing it in a very efficient way. At the end of 2007, more than 1400 tanks had the electronics on and were taking data. The shifts on the site have seen us concerned with occasional, anomalous behaviors of the detectors which are individually diagnosed and cured (figure 6). We are maintaining a web accessible database which keeps track of all the failures or problems of the detectors in the field and of their behavior after the intervention. This instrument is precious for the shifter(s) and allows a quick overview of the current problems and an easy planning of the interventions.

3.2 Atmospheric Monitoring: the Raman Lidar

Our group is also responsible for the hardware set-up and analysis of a Raman Lidar for the determination of the fluorescence light transmission in the atmosphere. The Raman Lidar system of the Pierre Auger Observatory was operating in its standard configuration since November 2005, although an intervention to obtain better mechanical stability was done in August 2006, and a change in the DAQ electronics in April 2007. In July 2007, probably due to the extremely low temperatures attained in Malargue, the laser broke and is now in its way to the manufacturer for reparation. Anyway, since August 2006 the system is in a (relatively) stable configuration. It is therefore possible to compare the Raman data with CLF measurements until January 2007 (official CLF reconstruction) or to Napoli group CLF reconstruction (until May 2007). It appears that there is both a large dispersion of the data, and a relative shift of the values. In particular Raman Vertical Aerosol Optical Depth (VAOD) values tend to be larger than CLF ones. On the other end, if we normalize the VAOD measurements in each month to a different reference (clear or Rayleigh) night, a better agreement is obtained. The aerosol backscatter measurements of the Raman lidar are less affected by optical or mechanical instabilities of the system setup, and good aerosol density profiles can be obtained, which, in most cases, clearly show the behaviour of the aerosol into the planetray boundary layer. The values of the integrated backscatter profiles are proportional to VAOD in the case of single aerosol composition, and other strategies to compare with CLF data are possible (to obtain VAOD values from integrated backscatter ratios would require knowledge of the Lidar Ratio).

As said before at present the laser head is broken and awaiting repair. In the meantime there are projects to improve the stability of the system and the signal/background ratio. As for the stability, some improvement will follow from the planned change in cover movement and of the lidar roof in LL. Concerning the signal/noise ratio we need to optimize the optical coupling between the telescope and the optical fiber (to the receiver box). This optimization will be tested in laboratory in L' Aquila and duplicated in LL. Also work on the DAQ electronics is needed, and this work can be done in L'Aquila too where a (partially) duplicated system exists. A possibly very useful change might be the substitution of the Oxygen raman lidar channel with a Water Vapour one. This only amounts to change some filters in the receiver. Presently the Oxygen channel is of little use, while the Water Vapour channel can give twice a day an estimate of humidity up to 5-7 km which is relevant for the fluorescence yield. Finally, it is important to notice that the Raman Lidar can easily take measurements in periods outside the FD shifts. These measurements are of little relevance for Auger, but may be of interest for the larger atmospheric community. We are presently starting a collaboration with the Rosario group, both on the analysis of the data for Auger and their possible wider atmospheric physics interest. In this context a possible contribution from atmospheric physics groups might be looked for.

The database of aerosol backscatter and extinction profiles, measured with the Raman lidar from August 2006 to July 2007 at the Pierre Auger Observatory (PAO), provides also the opportunity of an extented climatological analysis of the atmospheric aerosol content over PAO. The figure 7 shows the temporal behaviour of the monthly mean Vertical Aerosol Optical Depth (VAOD) and of the monthly mean Integrated aerosol
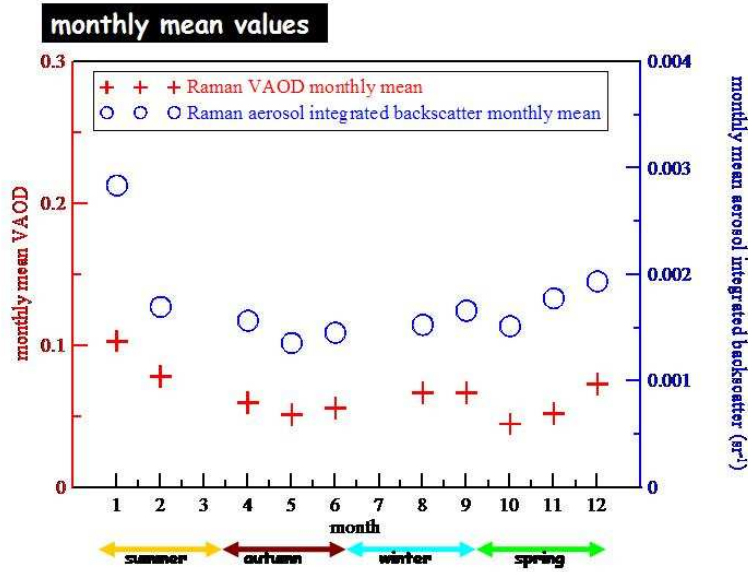
Figure 7: Seasonal variation of the monthly mean of the Vertical Aerosol Optical Depth (VAOD) and of the Integrated aerosol backscatter (INTAbeta).

backscatter (INTAbeta). The seasonal cycle is quite evident: high aerosol content in spring/summer months and low aerosol levels during late autumn and winter. In addition, the observed aerosol backscatter profiles reveal the peculiar structure of the Planetary Boundary Layer (PBL) over this region (dry pampa plateau): the PBL heights (the width of the atmospheric region, close to the ground, that contains most of the aerosols) clearly indicate a seasonally variability. The last results suggest a more realistic seasonal model (or a new parameterization) for the vertical profile of the aerosol optical properties (namely the VAOD), that may improve the simulation of the atmospheric scattering processes, needed for the off-line reconstruction of the PAO FD (fluorescence detectors) observations.

3.3 Search for clustering of ultra high energy cosmic rays

Another approach in the search of the origin of high-energy cosmic rays is the search of clustering signals by the means of the autocorrelation analysis. The autocorrelation analysis does not depend on *a priori* knowledge of the possible sources and, therefore, gives complementary information with respect to other sources.

The autocorrelation signal of the highest-energy events, with the contribution of the L'Aquila group, is therefore being investigated[4].

The two-point angular correlation function is given by the number of pairs separated by less than an angle α among the N events with energy larger than a given threshold E:

$$n_p(\alpha) = \sum_{i=2}^{N} \sum_{j=1}^{i-1} \Theta(\alpha - \alpha_{ij})$$

212

where α_{ij} is the angular separation between events i and j and Θ is the step function. The expected number of pairs is obtained by generating a large number of Monte Carlo simulations with the same number of events with an isotropic distribution modulated by the exposure of the detector, from which the mean number of pairs and the 95% CL band is extracted for each angular scale. The chance probability for any excess of pairs at a fixed angle α and energy threshold is found with the method proposed by Finley and Westerhoff[5], in which a scan over the minimum energy and the angle is performed. For each value of E and a chance probability is estimated by generating a large number of isotropic Monte Carlo simulations of the same number of events, and computing the fraction of simulations having an equal or larger number of pairs than the data for those values of E and . The most relevant clustering signal corresponds to the values of α and E that have the smaller value of the chance probability, P_{min}.

Finally, the probability that such clustering arises by chance from an isotropic distribution is estimated by performing a similar scan on a large number of isotropic data sets simulated by the Monte Carlo technique and finding the fraction of the simulations having a smaller P_{min} than the data. We show in 8 the result of the scan above a minimum energy of 20 EeV and up to a maximum angle of $30^{\cdot}$. A broad region with an excess of corre-
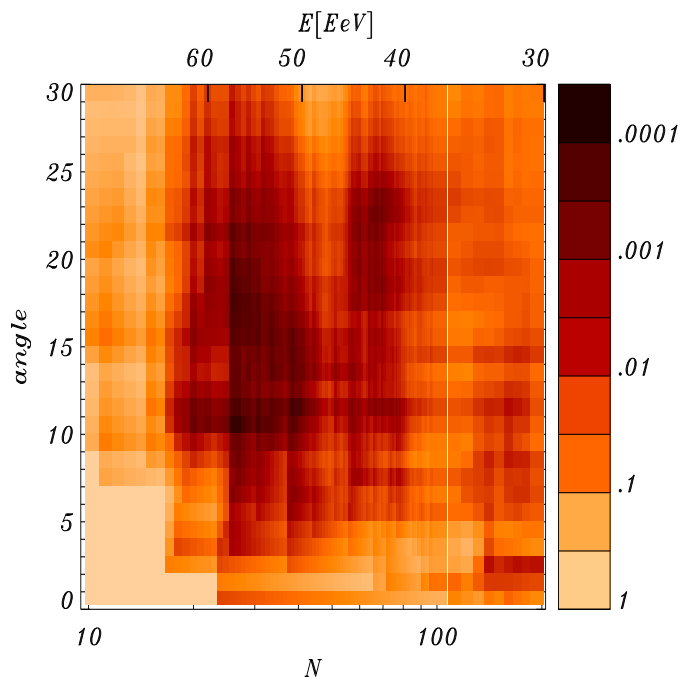
Figure 8: Autocorrelation scan for events with energy above 20 EeV and angles up to $30°$.

lation appears at intermediate angular scales and large energies. The minimum appears at $7°$ for the 19 highest energy events (E $>$ 57.5 EeV), where 8 pairs are observed, while 1 was expected. The fraction of isotropic simulations with larger number of pairs at that angular scale and for that number of events is $P_{min} = 10^{-4}$, obtained by comparing the observed number of pairs with that arising in 10^6 isotropic simulations. An extended scan for the 1672 events with E $>$ 10 EeV shows no new minimum. The chance probability of

213

a $P_{min} < 10^{-4}$ to arise from an isotropic distribution, obtained by performing the same scan to 10^5 simulations, is $P \simeq 2 \times 10^{-2}$.

The result of the autocorrelation function analysis depends of course on the values of α and E considered. However, the fact that the deflections expected from galactic and extragalactic magnetic fields and the distribution of the sources are largely unknown makes it difficult to fix these values a priori. The significance of an autocorrelation signal at a given angle and energy when these values have not been fixed a priori is a delicate issue, that has made the AGASA small scale clustering claim very controversial.

In conclusion, an extensive scan in angle and energy threshold shows some hints of clustering at larger energies (E > 50 EeV) and intermediate angular scales, that could be a signal of the large scale distribution of nearby sources. However, taking into account the scan performed, the probability that this kind of signals appear by chance from an isotropic flux is P = 2%. Thus it is only marginally significant with our present statistics. Auger future data will be used to check if this correlation is real.

3.4 Detection of Gamma Ray Bursts signals with the Fluorescence Detector

We have done a study on the capabilities of the fluorescence detectors (and in particular the FD of the Auger Observatory) to detect GRB signals. Individual photons hitting the atmosphere with energies in the range from MeV to TeV are absorbed through two concurring processes: Compton scattering and pair production (with a subsequent cascade development). In both processes the excitation of nitrogen molecules by electrons and positrons gives rise to a fluorescence emission in the visible-UV frequency band. This emission does not produce signals observable in fluorescence detectors, whose trigger threshold for hadron showers is of the order of 10^{17} eV. On the other hand these detectors monitor routinely the background flux [12] to control the detector response and prevent possible damages to the apparatus. This flux is sampled with time periods usually long (few to tens of seconds) with respect to the development of the showers, but roughly of the same size as the duration of the GRB. Therefore we can expect that the GRB induced fluorescence emission produces an increase of the measured background. The aim of the present paper is to estimate if such an increase is detectable under reasonable assumptions on the GRB fluxes. The calculation of the fluorescence emissivity in the atmosphere has been developed, based upon the following assumptions:

- Curved Earth

- Grammage vs height dependence as for the U.S. standard atmosphere [13].

- The absolute fluorescence yield of the 337 nm band in air was taken to be 5.05 photons/MeV of energy deposit at 293 K and 1013 hPa, derived from [14]. The wavelength and pressure dependence of the fluorescence spectrum was obtained from the AIRFLY experiment [15].

- The high energy GRB flux on Earth is assumed as

$$F(E) = F_0 \left(\frac{E}{\text{MeV}} \right)^{-\alpha} \tag{1}$$
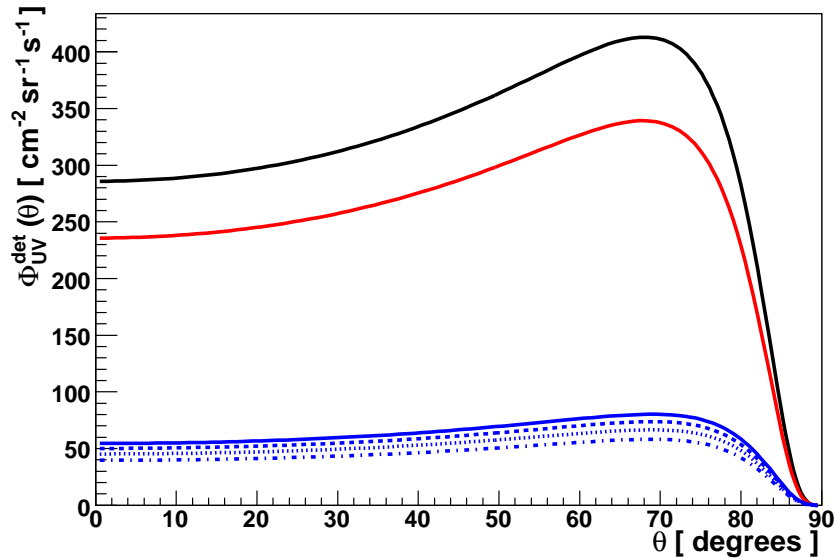
Figure 9: Fluorescence photon flux at ground as a function of the zenith angle. The red line refers to low energy. The solid, dashed, dotted and dot-dashed blue lines refer to the high energy flux with E_{max} = 100, 10, 1 TeV and 100 GeV respectively. The black line is the total fluorescence flux for E_{max} = 10 TeV. The flux is assumed to have F_0 = 1 $MeV^{-1}cm^{-2}s^{-1}$ and a spectral index 2.

being F_0 a normalization factor depending on the relevant GRB parameters such as its luminosity and redshift. The flux is assumed to extend from E_{pk}, the so-called synchrotron peak, to the maximum injected energy E_{max}. We set E_{pk} = 100 keV, and E_{max} ranging from 100 GeV up to 100 TeV.

The fluorescence photon flux observed at ground has been calculated taking into account the extinction through the atmosphere. A simple model by Garstang [16], which reproduces the night-sky brightness at several observatories and sites has been used for this purpose. In figure 9 the expected flux at ground is shown.

3.5 Sensitivity at ground

In figure 9 one can see that the fluorescence flux at ground is at most 400 photons $cm^{-2}sr^{-1}s^{-1}$. This value corresponds to a GRB flux constant F_0 = 1 $MeV^{-1}cm^{-2}s^{-1}$.

The detectability of the induced fluorescence flux is primarily limited by the level of the UV background flux at the fluorescence detector site. This flux has been measured at the Auger site [17] and is of the order of:

$$\Phi_{bkgr} \simeq \frac{100}{m^2 \ deg^2 \ \mu s} \simeq \frac{3.3 \ 10^7}{cm^2 \ sr \ s}$$

with a mild dependence on the zenith angle. It is sensible to infer that it is roughly the same in all the sites suitable for fluorescence detection.

Assuming to be able to detect a GRB signal when an extra flux of $\delta \times \Phi_{\mathrm{bkgr}}$ is added up to the background, a signal is detectable if the GRB flux constant F_0 is:

$$F_0 \gtrsim \delta \times \left(\frac{\Phi_{bkgr}}{400 cm^{-2} sr^{-1} s^{-1}} \right) MeV^{-1} cm^{-2} s^{-1} \simeq \delta \times 8 10^4 MeV^{-1} cm^{-2} s^{-1} \tag{2}$$

The lower limit given in eq. (2) applies if the burst duration Δt_{b} exceeds the time window Δt used to measure the background flux. For shorter bursts the GRB signal is diluted into this window and the threshold (2) is raised by a factor of about $\Delta t / \Delta t_{\mathrm{b}}$. The limit on the flux constant is easily converted into a limit on intensity, the fluence $\mathcal{F}$ in the time window Δt.

We used Swift [18] as a reference where fluences are measured in the interval $15 \div 150$ keV. Then we computed the photon intensity from our minimum energy, 100 keV, up to 150 keV. Denoting such intensity by $\mathcal{I}_{100}$ one gets the detectability condition:

$$\mathcal{I}_{100} \gtrsim 0.05 \times \frac{\delta}{\epsilon} \left(\frac{erg}{cm^2 s} \right) \tag{3}$$

where $\epsilon = \min[1, \Delta t_{\mathrm{b}} / \Delta t]$.

¿From the Swift GRB Table [19] we retrieved the fluences $\mathcal{F}$ and T90 durations of 272 GRBs. The corresponding average intensities $\mathcal{I}_{100}$ have been deduced by a simple model of the signal and then fitted by a simple power law:

$$\frac{dN}{d\mathcal{I}_{100}} \propto \mathcal{I}_{100}^{-\beta} \tag{4}$$

getting $\beta = 1.59 \pm 0.07$.

Using eq. (3) and assuming for Swift an effective exposure of $2\pi \times 30 \ \% \times 3$ yr and a duty cycle of the fluorescence detector of 10% one gets the expected event rate as a function of the threshold parameter δ. This is shown in figure 10. It can be recognized that to achieve the sensitivity of detecting at least one event in 10 years one needs a threshold δ not exceeding one percent under the most favourable conditions of current GRB estimates. More realistically one needs δ to be about 1 per mill or better.

A discussion about the ability of reaching such challenging threshold is beyond the aim of the present paper. From eq. (3) we can simply point out what are the minimal requirements for a fluorescence detector aiming to detect GRB signals. These are:

1. capability of detecting very low intensity excesses with respect to the background, in order to get δ of the order of one per mill or even better;

2. wide (possibly full) sky coverage through detector pixels;

3. short sampling period of the photon intensity, in order to get the GRB signal spread out over several time bins;

4. full-time measurement of the light intensity, in order to maximize the number of photons at each sample.
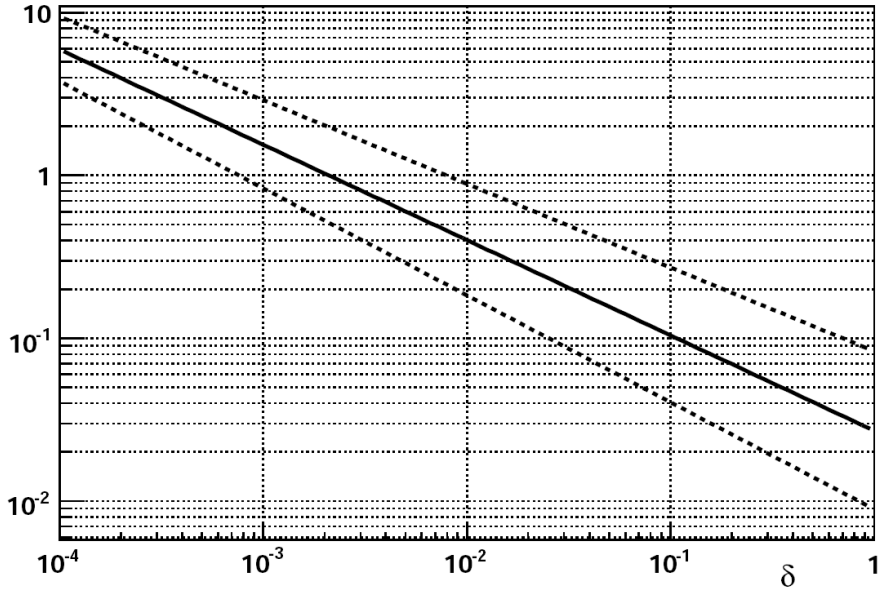
Figure 10: Number of expected GRBs in 10 years from fluorescence detection as a function of the threshold parameter δ. The solid line corresponds to the best fit of β with its one sigma deviation (dashed line), the case $\epsilon = 1$ is assumed.

It can be noticed that the first three requirements are correlated one with each other. In fact the possibility of detecting a true signal and the minimum threshold applicable to data rely on the collective effects that a GRB induces in the FD detector, i.e. the number of pixels jumping at the same time (item 2) and the number of contiguous time bins realizing a minimum pixel majority (item 3). In fact, the higher are such multiplicities the lower is the probability for the detected signal of being generated by random noise. Consequently these conditions allow to set very low thresholds.

Looking at current detectors one can see that only a part of these requirements are fulfilled. In the case of the FD system of the Pierre Auger Observatory [20], requirement (2) is fulfilled because of a very fine pixellation (about 10,000 pixels with 1.5° field of view each) and a coverage of about half of the whole sky. But the other parameters are not adequate for a GRB search. In particular the sky brightness is sampled with a 30 s period, which is too long for signal sequencing. Moreover the light intensity is measured (through ADC variances) in a 6.5 ms time window for each sample, being the monitor system required to detect an intensity increase of 5 % or more [21]. This window allows the collection of a very small fraction (about 2 per mill) of the total signal.

4   List of Publications

1. Status and recent results from the Pierre Auger Observatory. By Pierre Auger Collaboration (J.R.T. de Mello Neto for the collaboration). Dec 2007. 4pp. Presented at International Symposium on Multiparticle Dynamics (ISMD07), Berkeley, California, 4-9 Aug 2007. e-Print: arXiv:0712.3727 [astro-ph]

2. Measurement of cosmic ray energy with the Pierre Auger Observatory. By Pierre Auger Collaboration (Jan Ridky for the collaboration). 2007. 8pp. Prepared for 2nd International Colliders to Cosmic Rays Conference (C2CRO7), Lake Tahoe, California, 25 Feb - 1 Mar 2007. Published in AIP Conf.Proc.928:39-46,2007.

3. Correlation of the highest-energy cosmic rays with the positions of nearby active galactic nuclei. By Pierre Auger Observatory (The Pierre auger Collaboration for the collaboration). FERMILAB-PUB-07-678-A-TD, Dec 2007. 33pp. Temporary entry Submitted to Astropart. Phys. e-Print: arXiv:0712.2843 [astro-ph]

4. Upper limit on the cosmic-ray photon flux above 10**19-eV using the surface detector of the Pierre Auger Observatory. By Pierre Auger Collaboration (J. Abraham et al.). Dec 2007. 28pp. e-Print: arXiv:0712.1147 [astro-ph]

5. Correlation of the highest energy cosmic rays with nearby extragalactic objects. By Pierre Auger Collaboration (J. Abraham et al.). FERMILAB-PUB-07-579-AD-CD-E-TD, Nov 2007. 22pp. Published in Science 318:938-943,2007. e-Print: arXiv:0711.2256 [astro-ph]

6. Physics of astroparticles. S.J. Sciutto (La Plata U.) . 2007. 5pp. Prepared for 1st Latin American Workshop on High Energy Phenomenology, Porto Alegre, Brazil, 1-3 Dec 2005. Published in Braz.J.Phys.37:494-498,2007.

7. The Pierre Auger Observatory and neutrinos. By AUGER Collaboration (Pierre Billoir et al.). 2007. 7pp. Prepared for Workshop on Neutrino Oscillation Physics (NOW 2006), Otranto, Lecce, Italy, 9-16 Sep 2006.
Published in Nucl.Phys.Proc.Suppl.168:225-231,2007.

8. Search for ultrahigh energy photons with the Pierre Auger Observatory. By Pierre Auger Collaboration (M.D. Healy for the collaboration). FERMILAB-CONF-07-518-TD, Oct 2007. Contributed to 30th International Cosmic Ray Conference (ICRC 2007), Merida, Yucatan, Mexico, 3-11 Jul 2007. e-Print: arXiv:0710.0025 [astro-ph]

9. Pierre Auger enhancements: Transition from galactic to extragalactic cosmic ray sources. A. Etchegoyen, D. Melo, A.D. Supanitsky (CNEA, Buenos Aires) , M.C. Medina (CNEA, Buenos Aires & Buenos Aires, CONICET) . 2007. 9pp. Prepared for 12th Mexican School on Particles and Fields and 6th Latin American Symposium on High Energy Physics (VI-Silafae/XII-MSPF), Puerto Vallarta, Mexico, 1-8 Nov 2006.
Published in AIP Conf.Proc.917:210-218,2007. Also in *Puerto Vallarta 2006, Particles and fields* 210-218

10. The accuracy of signal measurement with the water Cherenkov detectors of the Pierre Auger Observatory. By Pierre Auger Collaboration (M. Ave et al.). FERMILAB-PUB-07-681-E, 2007. 5pp. Published in Nucl.Instrum.Meth.A578:180-184,2007.

11. A MC simulation of neutrino showers and their detection with the Pierre Auger Observatory. D. Gora (Karlsruhe U., EKP & Cracow, INP) , M. Roth (Karlsruhe, Forschungszentrum) , A. Tamburro (Karlsruhe U., EKP) . FZKA-7340ZG, Aug 2007. 4pp. FZKA-7340 pp 129-132. Prepared for 30th International Cosmic Ray Conference (ICRC 2007), Merida, Yucatan, Mexico, 3-11 Jul 2007.

12. Comparison of preshower characteristics at Auger South and North. P. Homola, J. Pekala, B. Wilczynska, H. Wilczynski (Cracow, INP) , M. Risse (Wuppertal U.) , Ralph Engel (Karlsruhe, Forschungszentrum) , D. Gora (Cracow, INP & Karlsruhe U., EKP) . FZKA-7340ZB, Aug 2007. 4pp. FZKA-7340 pp 109-112. Prepared for 30th International Cosmic Ray Conference (ICRC 2007), Merida, Yucatan, Mexico, 3-11 Jul 2007.

13. HEAT: Enhancement telescopes for the Pierre Auger Southern Observatory. By Pierre Auger Collaboration (H.O. Klages for the collaboration). FZKA-7340Z, Aug 2007. 4pp. FZKA-7340 pp 101-104.
    Prepared for 30th International Cosmic Ray Conference (ICRC 2007), Merida, Yucatan, Mexico, 3-11 Jul 2007.

14. Qualification tests of the 11000 photomultipliers for the Pierre Auger Observatory fluorescence detectors. K.-H. Becker et al. 2007. 11pp.
    Published in Nucl.Instrum.Meth.A576:301-311,2007.

15. 3D Reconstruction of Extensive Air Showers from Fluorescence Data. By Pierre Auger Collaboration (S. Andringa et al.). FERMILAB-CONF-07-404-A-TD, Jul 2007. 4pp.
    To appear in the proceedings of 30th International Cosmic Ray Conference (ICRC 2007), Merida, Yucatan, Mexico, 3-11 Jul 2007. e-Print: arXiv:0707.4463 [astro-ph]

16. Dark matter halos and the anisotropy of ultra-high energy cosmic rays in the Pierre Auger Observatory. B.B. Siffert, B. Lazarotto, J.R.T. de Mello Neto (Rio de Janeiro Federal U.) , A. Olinto (Chicago U., Astron. Astrophys. Ctr.) . 2007. 4pp. Prepared for 18th Workshop on Hadronic Interactions (RETINHA-18), Sao Paulo, Brazil, 22-24 May 2006. Published in Braz.J.Phys.37:48-51,2007.

17. The UHECR spectrum measured at the Pierre Auger Observatory and its astrophysical implications. By Pierre Auger Collaboration (T. Yamamoto for the collaboration). FERMILAB-CONF-07-088-A-TD, Jul 2007. Contributed to the 30th International Cosmic Ray Conference (ICRC 2007), Merida, Yucatan, Mexico, 3-11 Jul 2007. e-Print: arXiv:0707.2638 [astro-ph]

18. The Pierre Auger Observatory at 10^{18}18-eV. B.R. Dawson (Adelaide U.) . 2007. 4pp. Prepared for 2nd Workshop on TeV Particle Astrophysics, Madison, Wisconsin, 28-31 Aug 2006. Published in J.Phys.Conf.Ser.60:155-158,2007.

19. Measurement of the UHECR spectrum above 10-EeV at the Pierre Auger Observatory using showers with zenith angles greater than 60 degrees. By Pierre Auger

Collaboration (P. Facal San Luis for the collaboration). FERMILAB-CONF-07-089-A-TD, Jun 2007. 4pp. To appear in the proceedings of 30th International Cosmic Ray Conference (ICRC 2007), Merida, Yucatan, Mexico, 3-11 Jul 2007. e-Print: arXiv:0706.4322 [astro-ph]

20. Selection and reconstruction of very inclined air showers with the Surface Detector of the Pierre Auger Observatory. By Pierre Auger Collaboration (D. Newton for the collaboration). FERMILAB-CONF-07-382-A-TD, Jun 2007. To appear in the proceedings of 30th International Cosmic Ray Conference (ICRC 2007), Merida, Yucatan, Mexico, 3-11 Jul 2007. e-Print: arXiv:0706.3796 [astro-ph]

21. Measurement of Aerosols at the Pierre Auger Observatory. By Pierre Auger Observatory (S.Y. BenZvi et al.). FERMILAB-CONF-07-374-A-TD, Jun 2007. 4pp. To appear in the proceedings of 30th International Cosmic Ray Conference (ICRC 2007), Merida, Yucatan, Mexico, 3-11 Jul 2007. e-Print: arXiv:0706.3236 [astro-ph]

22. Constraints on top-down models for the origin of UHECRs from the Pierre Auger Observatory data. D.V. Semikoz (APC, Paris) , Pierre Auger Collaboration . FERMILAB-CONF-07-375-A-TD, Jun 2007. Contributed to 30th International Cosmic Ray Conference (ICRC 2007), Merida, Yucatan, Mexico, 3-11 Jul 2007. e-Print: arXiv:0706.2960 [astro-ph]

23. A search for possible anisotropies of cosmic rays with 0.1<E<10-EeV in the region of the Galactic Centre. By Pierre Auger Collaboration (E.M. Santos for the collaboration). FERMILAB-CONF-07-421-A-TD, Jun 2007. 4pp. Contributed to 30th International Cosmic Ray Conference (ICRC 2007), Merida, Yucatan, Mexico, 3-11 Jul 2007. e-Print: arXiv:0706.2669 [astro-ph]

24. Measurement of the UHECR energy spectrum from hybrid data of the Pierre Auger Observatory. By Pierre Auger Collaboration (Lorenzo Perrone for the collaboration). FERMILAB-CONF-07-087-A-TD, Jun 2007. To appear in the proceedings of 30th International Cosmic Ray Conference (ICRC 2007), Merida, Yucatan, Mexico, 3-11 Jul 2007. e-Print: arXiv:0706.2643 [astro-ph]

25. Search for large-scale anisotropies with the Auger Observatory. By Pierre Auger Collaboration (E. Armengaud for the collaboration). FERMILAB-CONF-07-092-A-TD, Jun 2007. 4pp. To appear in the proceedings of 30th International Cosmic Ray Conference (ICRC 2007), Merida, Yucatan, Mexico, 3-11 Jul 2007. e-Print: arXiv:0706.2640 [astro-ph]

26. Measurement of the UHECR energy spectrum using data from the Surface Detector of the Pierre Auger Observatory. By Pierre Auger Collaboration (Markus Roth for the collaboration). FERMILAB-CONF-07-372-A-TD, Jun 2007. 4pp. Contributed to 30th International Cosmic Ray Conference (ICRC 2007), Merida, Yucatan, Mexico, 3-11 Jul 2007. e-Print: arXiv:0706.2096 [astro-ph]

27. Testing the surface detector simulation for the Pierre Auger Observatory. By Pierre Auger Collaboration (Piera L. Ghia for the collaboration). FERMILAB-CONF-07-380-A-TD, Jun 2007. To appear in the proceedings of 30th International Cosmic Ray Conference (ICRC 2007), Merida, Yucatan, Mexico, 3-11 Jul 2007. e-Print: arXiv:0706.1212 [astro-ph]

28. Hybrid Performance of the Pierre Auger Observatory. By Pierre Auger Collaboration (B.R. Dawson for the collaboration). FERMILAB-CONF-07-371-A-TD, Jun 2007. To appear in the proceedings of 30th International Cosmic Ray Conference (ICRC 2007), Merida, Yucatan, Mexico, 3-11 Jul 2007. e-Print: arXiv:0706.1105 [astro-ph]

29. Ultra high energy cosmic rays and the Pierre Auger Observatory. By Auger Collaboration (M. Unger for the collaboration). 2007. 9pp. Prepared for 2nd Cairo International Conference on High Energy Physics
(CICHEP 2), Cairo, Egypt, 14-17 Jan 2006. Published in AIP Conf.Proc.881:220-228,2007. Also in *Cairo 2006, High energy physics* 220-228

30. The surface detector of the Pierre Auger Observatory. By Pierre Auger Collaboration (J. Ridky for the collaboration). 2007. 5pp.
Prepared for CRIS 2006: Cosmic Ray International Seminar: Ultra-High Energy Cosmic Rays: Status and Perspectives, Catania, Italy, 29 May - 2 Jun 2006.
Published in Nucl.Phys.Proc.Suppl.165:45-49,2007. Also in *Catania 2006, Cosmic ray* 45-49

31. The fluorescence detector of the Pierre Auger Observatory. By Pierre Auger Collaboration (V. Verzi for the collaboration). 2007. 8pp.
Prepared for CRIS 2006: Cosmic Ray International Seminar: Ultra-High Energy Cosmic Rays: Status and Perspectives, Catania, Italy, 29 May - 2 Jun 2006.
Published in Nucl.Phys.Proc.Suppl.165:37-44,2007. Also in *Catania 2006, Cosmic ray* 37-44

32. The Pierre Auger Project: A Model for international science. By Pierre Auger Observatory (Paul M. Mantsch for the collaboration). FERMILAB-PUB-07-068-E-TD, Mar 2007. 8pp.

33. An upper limit to photons from first data taken by the Pierre Auger Observatory. By Pierre Auger Collaboration (Markus Risse for the collaboration). Jan 2007. 8pp. Prepared for 6th Rencontres du Vietnam: Challenges in Particle Astrophysics, Hanoi, Vietnam, 6-12 Aug 2006. e-Print: astro-ph/0701065

References

[1] Recent Results from the Pierre Auger Observatory Subm. to Proc. 2007 Europhysics Conf. on High Energy Physics, July 19 - 25, 2007, Manchester, UK (2007).

[2] M.-P. Véron-Cetty, P. Véron, Astron. Astrophys. 455, 773 (2006).

[3] Correlation of the highest energy cosmic rays with nearby extragalactic objects. By Pierre Auger Collaboration (J. Abraham et al.). Science 318:938-943,2007.

[4] M. Ave et al.:Search for clustering of ultra high energy cosmic rays from the Pierre Auger Observatory, Auger Tech. Note GAP 2008-015.

[5] C. B. Finley and S. Westerhoff, Astropart. Phys. 21 359 (2004).

[6] Abassi R U et al., 2005, Ap. J. 622 910

[7] Alvarez-Muiz J et al., 2003, Phys. Rev. D66 123004 (astro-ph/0209117)

[8] Newton D, J. Knapp and A. A. Watson, 2007, AstropartPhys 26 414

[9] Roth M, Pierre Auger Collaboration: 2007, Proc. 30th ICRC (Mérida), #313

[10] Perrone L, Pierre Auger Collaboration: 2007, Proc. 30th ICRC (Mérida), #316

[11] Watson A A, 1991, Nuclear Physics B (Proc Suppl) 22B 116

[12] R. Caruso et al. [Pierre Auger Collaboration], 29th International Cosmic Ray Conference Pune (2005) 8, 125-128.

[13] US Standard Atmosphere 1976, US Government Printing Office, Washington, DC, 1976.

[14] M. Nagano, K. Kobayakawa, N. Sakaki, K. Ando, Astropart. Phys. 22 (2004) 235.

[15] M. Ave et al. [AIRFLY Collaboration], Astropart. Phys., 28 (2007) 41.

[16] R. H. Garstang, Pub. Astron. Soc. Pacific, 101 (1989) 306.

[17] R. Caruso et al. [Pierre Auger Collaboration], 29th International Cosmic Ray Conference Pune (2005) 8, 117.

[18] N. Gehrels et al, ApJ 611 (2004) 1005.

[19] http://swift.gsfc.nasa.gov/docs/swift/archive/grb_table/

[20] J. Abraham et al. [Pierre Auger Collaboration], Nucl. Instrum. Meth. A523 (2004), 50.

[21] M. Kleifges et al., IEEE Trans. Nucl. Sci., 50, (2003) 1204.

LIBS-X
X ray Laser Induced Breakdown Spectroscopy

A. Reale[a], G. Tomassetti[a], L. Palladino[a], A. Ritucci[a],
A. Gaudieri [a], P. Zuppella[a], P. Tucceri[a], S. Santucci[a], L. Ottaviano[b],
F. Bussolotti[b], S. Piperno[b], M. Rinaldi[b], L. Reale[b], F. Flora[c],
L. Mezi[c], P. Dunne[d], J. Kaiser[e].

[a] Dipartimento di Fisica dell'Università dell'Aquila ,
e g.c. ai LNGS-INFN, Assergi (AQ)Italy
[b] Dipartimento di Fisica dell'Università dell'Aquila, Italy
[c] ENEA, Dip.FIM-FIS-ACC CR -ENEA Frascati, Italy
[d] School of Physics,Univ College Dublin,Belfield,Dublin4,Ireland
[e] Inst of Phys Engineering,Brno Univ of Technology,Brno,Czek Republic

Abstract

The aim of the experiment LIBS-X is the study of the applicability of the technique LIBS(Laser induced breakdown spectroscopy) for trace elements analysis, mainly vegetation samples, in environmental studies using our table top soft X ray capillary discharge laser at 46.9 nm. This laser has been built according a technique initiated by J.J.Rocca at the Univ of Colorado and up to now we used it for some applications as the processing of a dielectic material or the creation of photoluminescent pattern of color centers on the surface of LiF crystals.

In 2007 we achieved a good upgrading of the laser properties so that, as a convenient by-product of our activity, we took profit of the full coherence property of our laser, using it as a interference lithography tool for a complete nanofabrication process of metallic pattern with a periodic structure resolution well below 100nm.

This activity suggested by the performance of our laser, resulted into a partial modification and delay of the original research programs of the 2006 LIBS proposal, which has been anyhow prosecuted by a series of LIBS measurements with a Nd-YAG laser at Brno University.

1   Introduction

Today the detection of the presence of contaminants by means of simple and fast methods, is important because there is an increasing risk to transfer the pollutant in the human body. The presence of heavy metals, which represents a considerable part of the toxicity of the pollution, can be easily detected by LIBS (Laser induced breakdown spectroscopy), even if usually the quantitative evaluation in not of high precision. Our experiment proposes the application to this technique of the soft X-ray capillary laser which has been developed by our group.

The technique consists essentially in the recognition of the fluorescence lines of trace elements in a sample.Such lines are present in the radiation emitted by the hot plasma obtained by focusing a pulsed laser, usually a Nd-YAG on the sample. Usually the focal spot is of the order of $0.1 \div 1.5$ mm. For intensities of the order of Gwatt/cm^2, a single laser pulse causes the evaporation of a small quantity of material from the surface of the sample, few tens of ng producing a plasma which expands rapidly reaching few eV temperatures.

Using our EUV-X ray laser with a shorter wavelength could be very interesting for studying surfaces, thin films and micrometric structures with very high spatial resolution because of the very small diameter focal spot we can achieve (few microns). Correspondly a very high fluence of the order of $10 \div 100$ Gwatt can generate a plasma such that the critical density is about 10^{23} and also the laser can ionize the atoms of the target by a single photo interaction what makes different the mechanism of deposition of the energy from that of conventional plasmas.

Another approach to the use of the laser is Interferometric Lithography(IL) a technique very promising to create nanoscale periodic structures: a spatially coherent light beam is splitted in two beams and by a Lloyd mirror or similar device, the beams interfere on a photo sensitive surface like a photo resist or a LiF crystal. Research in IL are more and more moving towards EUV radiation either using synchrotron radiation or EUV lasers. A lithographic process requires a careful matching of the exposed photoresist with the radiation dose and the control of the lift-off process. We are in conditions, using our tabletop laser - and as a by product of our main activity - to achieve pattern modulation of the PMMA and strips on silicon by metal deposition of Ni and lift-off of the PMMA with resolution much better than 100 nm.

2   Experimental Results in 2007

- Two goals were attained in 2007: the final upgrading of the capillary laser and the transport, reflection and focusing.of the beam inside the ablation chamber for LIBS. The improvement of the experimental set up has been successfully concluded. The capillary laser is presently able to give $\sim 150~\mu$J/pulse ($\pm5\%$) at 0,2 Hz repetition rate, with 5 mrad divergence, 1,7 ns duration time and high spatial coherence. The starting point of our job has been the study on the ablation induced by the laser on different materials. As we have reported in our previous paper [1] focusing measurements of the laser beam both on a SiO_2/Si and LiF target, has been
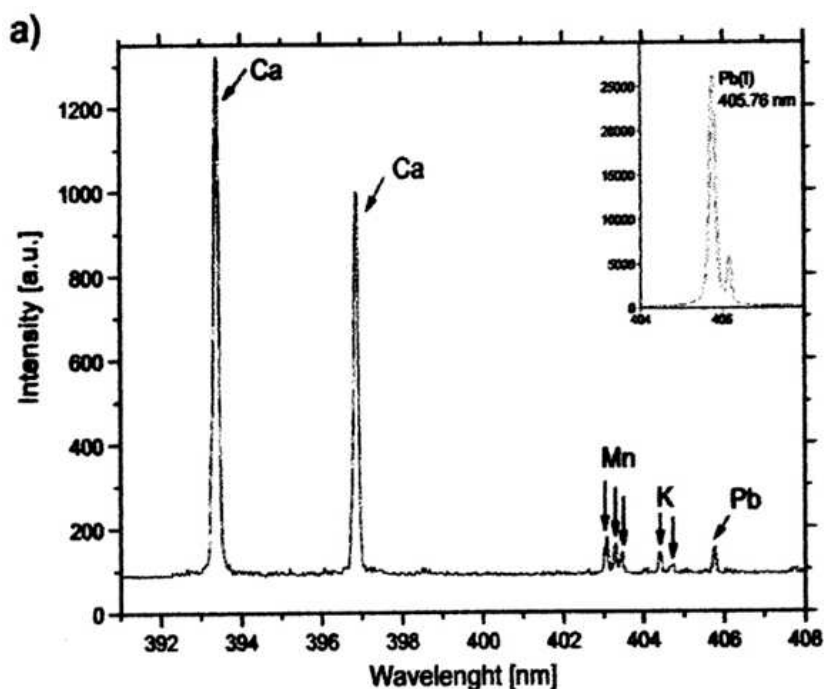
Figure 1: The LIBS spectrum of 10 mM PbAc treated sample obtained using a Nd-YAG laser at Brno Univ In the insert the LIBS spectrum of the lead standard target is shown [2].

operated in a multi-shots regime. The first ablation craters obtained exposing the samples to a 25 laser shots sequence have a 6 μm diameter and 1,5 μm depth.

In order to increase the ablation rate (nm/pulse) and to proceed with the focalization produced plasma fluorescence we are now setting up an optical system based on the use of spherical multilayer mirrors with high nominal reflectivity (60%). The optimization of the system and the experimental measurements in these conditions will be the research activity of the next months.

In meanwhile, LIBS proposal, has been prosecuted by a series of measurements with a Nd-YAG laser at Brno University of Techn. to achieve some direct experience regarding this technique which will be very useful for planning our fluorescence apparatus whose components are being assembled. Concerning the investigation of biological samples as treated leaves or leaf sections by LIBS technique with the Nd:YAG laser[2], in our earlier measurements [3] we demonstrated that in Helianthus annuus species Pb is accumulated mainly in the veins of leafs. In the experiment we performed at Brno we achieved a clear evidence that not only it is possible to recognize the type of pollutant in the leafs of the considered species but also to map the distribution of the pollutant within the sample. We hope to increase the spatial resolution as soon as we will be in conditions of using our laser.

- As reported in the summary, in the second part of 2007 we took profit of the very good coherence property of our laser and we mounted an interference lithography
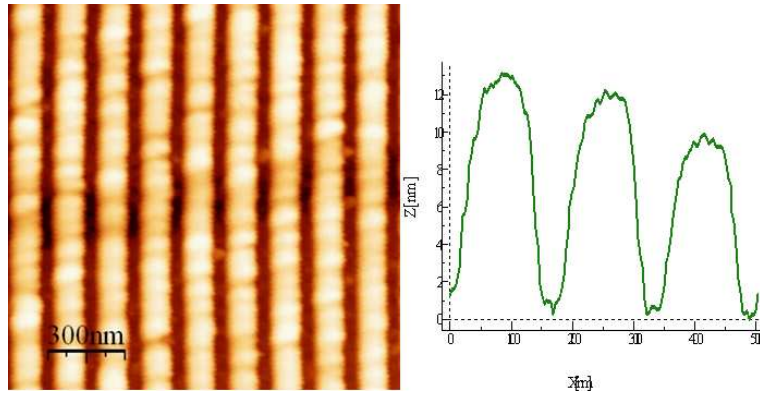
225

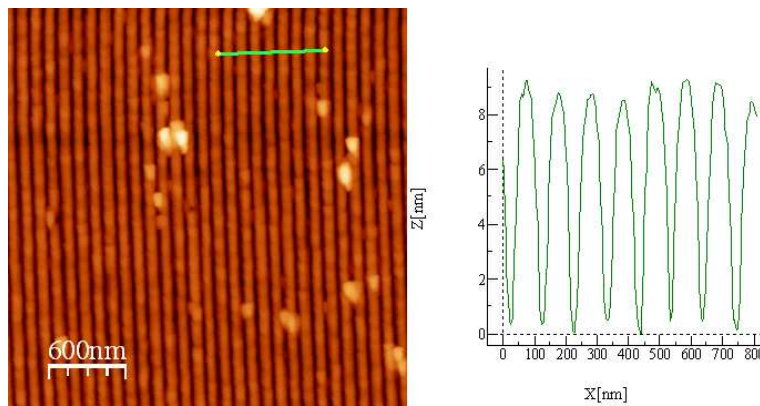Figure 2: 200 nm periodic structures on PMMA.

Figure 3: 100 nm periodic structures on PMMA.

setup.

The laser was used for a lithographic writing procedure on a nanometric scale, using photosensitive polymers as detectors. The best results we got are periodic structures with a critical dimension less than 50 nm (see Fig. 2-3) and about ten nm depth [4]. The potentialities of this technique open new application perspectives in various fields of nanotechnologies. The fabrication of metal gratings on a nanometric scale is expecially interesting in the nanooptics and nanoelectronics fields. The optimization of the lithographic technique of the polymer deposition and of the lift-off process allowed us to get 600 nm metal patterns on a large area(0,5 mm^2) [5]. We are presently optimizing the process in order to attain better resolution.

3   Conclusion

In 2007 we have completed the upgrading of our laser and now we are building the setup for the detection of the fluorescence from the plasma we produce by focusing the laser on a target sample by a curved multilayer mirror. We have to compare our theoretical
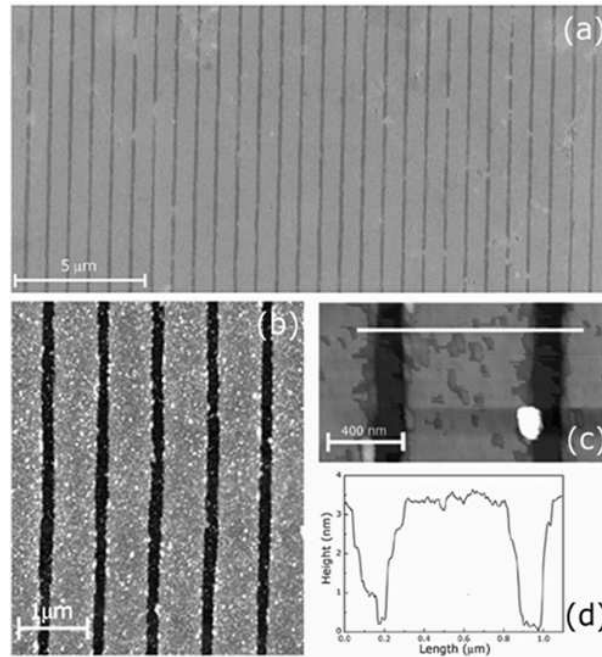
226

Figure 4: Metal deposition on 600nm periodic structure.

predictions with the experimental results on the effective ablated material we can get in single shot with this laser.

As a second research line we have successfully verified that our tabletop laser is well suitable for fabrication of metallic pattern by EUV interferometric lithography with resolution well below 100nm.

References

[1] *Annual Report 2006 of Laboratori Nazionali del Gran Sasso-INFN.* Assergi(AQ),Italy

[2] M.Galiova, J.Kaiser, K.Novotny, O.Samek, L.Reale, R.Malina, K.Palenikova, M.Liska, V.Cudek, V.Kanicky, V.Otruba, A.Poma, A.Tucci-*Utilization of laser induced break down spectroscopy for investigation of the metal accumulation in vegetal tissues.* Spectrochimica Acta Part B,62,(2007)1597-1605

[3] J.Kaiser, L.Reale, A.Ritucci, G.Tomassetti, A.Lai, F. Flora, A. Faenov, T. Pikuz, A. Tucci, A. Poma, M. L.Spanò, L.Mancini, G.Tromba, F.Zanini-*Mapping of the metal intake in plants by large-field-X-ray microradiography and preliminary feasibility studies in microtomography.*

[4] A. Ritucci, A. Reale, P. Zuppella, L. Reale, P. Tucceri and G. Tomassetti*, P. Bettotti, L. Pavesi-*Interference lithography by a Soft X-ray laser beam nanopatterning on photoresist.* J. Appl. Phys. 102, 034313 (2007)

[5] L. Ottaviano, F.Bussolotti, S.Piperno, M.Rinaldi, S.Santucci, F.Flora, L.Mezi, P.Dunne,J.Kaiser, A.Reale, A.Ritucci, P.Zuppella-*Fabrication of metallic nanopatterns using table top extreme ultraviolet laser interferometric lithography.* Plasma Sour. Sci, & Technol. (accepted).

PULEX

F. Antonelli[a], M. Belli[a], M. Pinto[a], O. Sapora[a], E. Sorrentino[a],
G. Simone[a], M. A. Tabocchini[a], L. Conti Devirgiliis[b], C. Carbone[b],
M. Balata[c], L. Ioannucci[c], S. Nisi[c], L. Satta[d]

[a] Istituto Superiore di Sanità, Technology and Health Department,
and INFN-Roma1 Gr,coll. Sanità
[b] Department of Basic and Applied Biology, L'Aquila University
[c] Service of Chemistry,
Cryogenic and Chemical Plants of the INFN - Gran Sasso National Laboratory
[d] INFN - Frascati National Laboratory

Abstract

Pulex is designed as an experiment aimed at investigating the effects of environmental background radiation on metabolism and responses to physical and chemical agents on cultured mammalian cells. The approach used is the comparison between cell cultures grown in the Gran Sasso tunnel, under conditions of reduced background radiation, and other similar cultures grown outside the tunnel. The exploratory phase of the experiment has been concluded and its feasibility demonstrated. The results show several differences in biochemical and radiobiological properties between the two kinds of cultures, and suggest that environmental background radiation can act as a priming dose capable of triggering an adaptive response in living cells.

1 Introduction

The aim of the Pulex experiments (the one whose status is here reviewed is the third in the series) is to understand if there exists a measurable effect of the natural background radiation on living matter. To do so, the experimental method we choose is to culture

the same cellular strain contemporarily inside the Gran Sasso Laboratory, where the background radiation is very low, and in an external laboratory in Roma with "normal" background conditions. All other parameters are as far as possible kept identical for both cultures. If the background radiation acts as a priming dose eliciting an adaptive response subsequent to a challenging dose, the behaviour of the two cultures should differ as time goes by, at least for some biological end-points. The first experiment, or rather a feasibility study, was performed on yeast cells. It was found that after more than 100 generations cells grown inside the Gran Sasso Lab were less efficient in repairing acute damage by genotoxic agents than those cultured in the external laboratory [1]. In the second experiment Hamster cells of the V79 strain were employed, and we addressed several biological end-points. A difference between the internal and the external cultures was observed when they were compared after three and ten months. After three months it was found that apoptosis could be induced by cycloheximide more easily in the cells grown inside the Gran Sasso Lab than in those grown in the external laboratory. After ten months it was found that mutation frequency at the *hprt* locus induced by γ-rays was significantly higher for the culture grown inside the Gran Sasso Lab [2]. Both these findings are consistent with the hypothesis of an adaptive response in the cells cultured in the external laboratory triggered by natural background radiation. It must be noted however, that it cannot be excluded that after many duplications clones with different characteristics have been selected in the two cultures independently of background radiation. This observation implies that a new experiment was needed to disentangle these two possibilities. Therefore we decided to perform a third experiment on the same V79 cells, with two independent cultures both inside the Gran Sasso Laboratory and in the external laboratory. Furthermore, to reduce margins for errors, the external laboratory was also installed at the Gran Sasso Laboratory outside the tunnel. This choice assured a uniform treatment of the four cultures, but the ratio of external/internal background was reduced with respect to the comparison with cultures grown in Roma. In the following we briefly comment on the results obtained for the various biological end-points examined.

2   Micronuclei induction

Chromosome damage, which can be caused by exposure to ionizing radiation, was determined with the cytokinesis-block micronucleus assay [3], in V79 cells either grown inside the Gran Sasso laboratory or in the external laboratory. All the cell cultures were irradiated with 1 Gy of X-rays and the results are reported as the number of induced micronuclei per 2000 binucleated cells. As it is shown in figure 1, after 10 months of culture there is a slightly increases in the normalized number of induced micronuclei with respect to the zero time for both growth conditions and no significant difference is found between the V79 cells grown in the presence of low background radiation and that grown under "normal" background conditions.
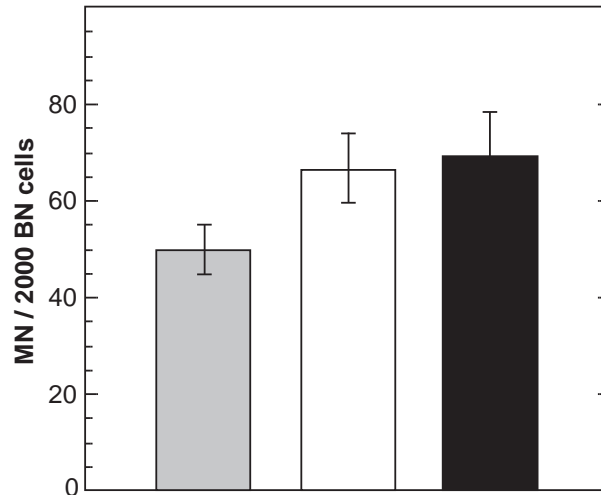
Figure 1: Normalized micronuclei induction by 1 Gy of γ-rays in V79 cells measured at zero time (grey bar) and at 10 months in cultures A and B (values pooled together, white bar) and C and D (values pooled together, black bar).

3 Apoptosis induction

Apoptosis induced by cycloheximide (CHX) treatment was assayed by flow cytometry, analyzing the labelled DNA strand breaks with the TUNEL (Terminal Deoxynucleotide Transferase dUTP Nick End Labeling) assay [4]. All the cultures show an increased sensitivity to the drug with the time, probably dependent on cellular aging. In figure 2 is represented the percentage of apoptotic cells in the different cultures after 3 months of continuous culture under "normal" (A and B) and in low (C and D) background radiation conditions. It can be seen that cells cultured under the Gran Sasso Lab are more sensitive to apoptosis induction than those grown in the external laboratory. This effect, well evident at 3 months, is still maintained after 10 months of culture, even if for the D culture it appears slightly lower (data not shown).

4 Determination of p53 and c-myc expression

Experiments on cells treated with cycloheximide were performed to investigate the expression of proliferation and apoptosis related genes, such as those coding for p53 and c-myc proteins. It was found that the concentration of these two proteins strongly decreased after treatment with cycloheximide, and there are no obvious differences between cells grown inside the Gran Sasso Lab and in the external laboratory, neither after three months, nor after ten months of continuous culture. It is worth noting that after ten months the concentration of P53 after treatment is notably larger in the four cultures than the one measured after three months (data not shown).
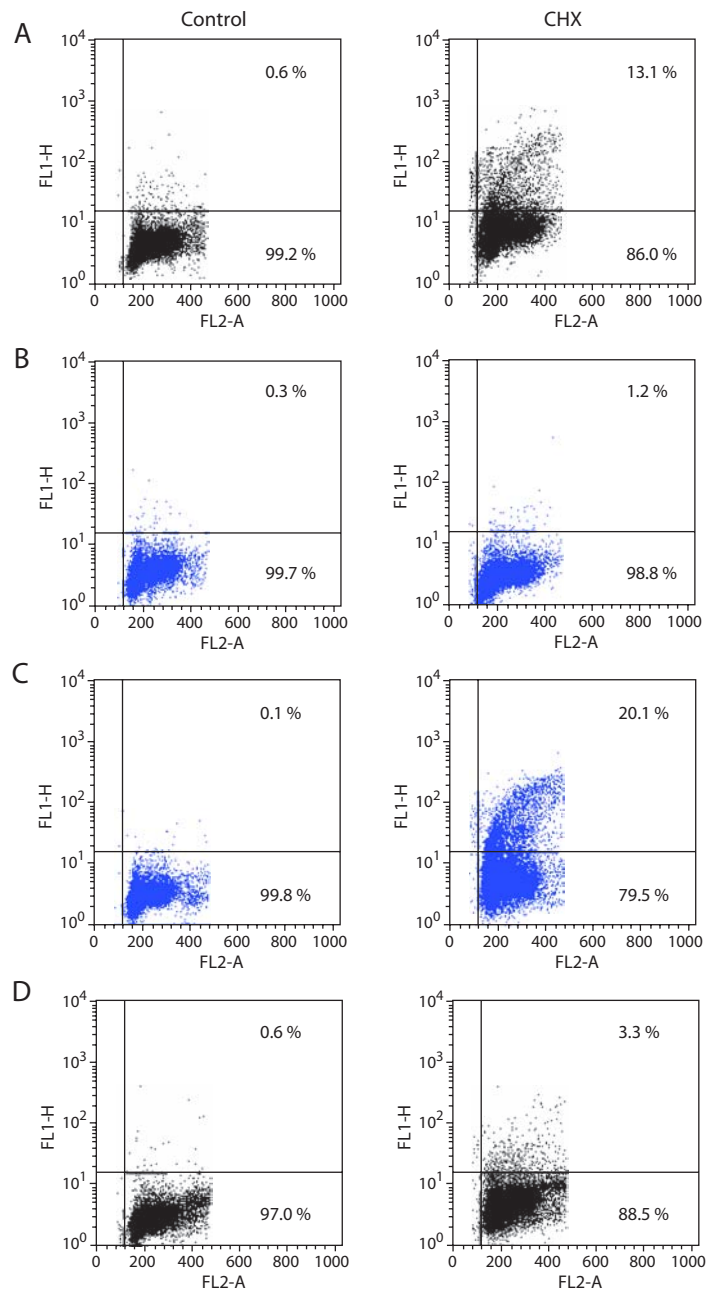
Figure 2: Apoptotic induction by CHX treatment in V79 cells after 3 months of culture in normal background radiation (A and B) and in low background conditions (C and D). Left column: control; right column: CHX treatment. The FL2-A axis represents the amount of cellular DNA stained with iodine propide, while the FL1-H axis represents the extent of DNA apoptotic fragmentation in the analyzed cells measured with the TUNEL assay. The numbers in the upper right boxes represent the percentage of apoptotic cells.
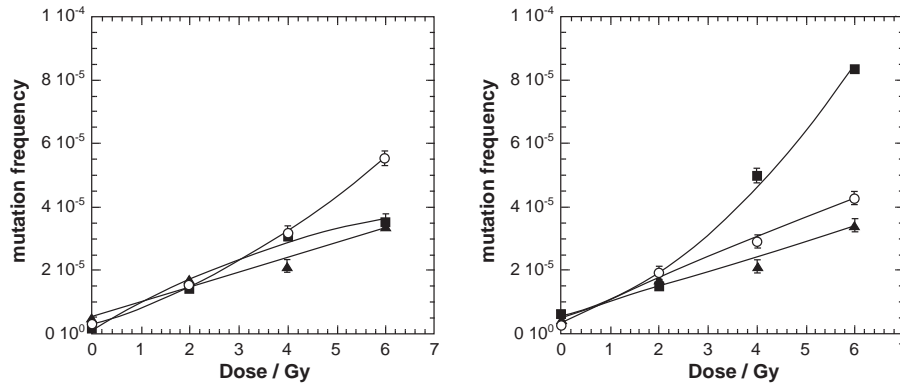
Figure 3: Number of mutants as a function of X-ray dose. Left panel: 3 months of culture; right panel: 10 months of culture. External A and B (○) and internal C and D (■) cultures. The response at zero time (▲) is also reported in both panels for comparison.

5   Mutation induction

To study the mutagenic sensitivity to ionising radiation, at zero time, after 3 months and 10 months all four cultures were exposed to X-rays at doses of two, four and six Gy and mutation induction at the *hprt* genetic locus was measured. The results are presented in figure 3. After 3 months of culture (left panel) the response of the two internal cultures was rather similar, as was that of the two external culture, so that in the figure the average value for each pair of cultures is presented. Also the measurement at zero time is reported. The three sets of data are rather similar, except for the point at 6 Gy for the external cultures, which is a little higher than the other two.

The results at 10 months of culture are reported in the right panel of figure 3, together with the measurement at zero time. Again the responses of the two pairs of cultures were similar, so that in the figure the average value for each pairs is shown. The zero time data are similar to those obtained for the external cultures. For the internal cultures the points at 4 and 6 Gy are significantly higher than the corresponding points of the external culture, indicating an increased radiosensitivity for mutation induction in cells grown in the reduced background radiation environment. It must be noted that an additional pair of cultures were grown in the laboratory at the Istituto Superiore di Sanità (ISS) in Roma, where the dose rate from background radiation is estimated to be larger by a factor of about seven than that in the external laboratory at the Gran Sasso. One of these cultures showed an anomalous response, as its background mutation frequency became larger by an order of magnitude with respect to all other cultures. The response of the second one was similar to that of the other external cultures, except for the point at 6 Gy at 10 months, which is somewhat higher. These data are not shown in figure 3.

6   Enzymatic activity

Antioxidant enzymes are involved in the processing of the reactive oxygen species (ROS), known to be damaging species also induced by radiation. In order to see if there were
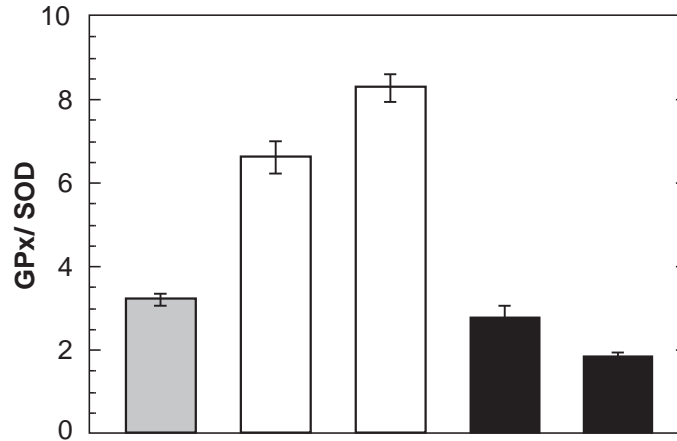
Figure 4: GPx/SOD ratio at zero time (grey bar) and at 10 months in external A and B (white bars) and internal C and D (black bars) V79 cultures.

differences between the two radiation background conditions, the biochemical activities of superoxide dismutase (SOD), catalase (CAT) and selenium-dependent glutathione peroxidase (GPx) were measured in all the V79 cell cultures. The ratios CAT/SOD and GPx/SOD are linked to the scavenging efficiency of cells against ROS. An increase in one or both of these ratios means a high ROS scavenging efficiency, while a reduction means a reduced scavenging efficiency. Our data on the ratio GPx/SOD, shown in figure 4, indicate that after 10 months this ratio increases for the cultures grown in the external laboratory, and strongly decreases for those grown in the internal laboratory. Again, cells cultured in the presence of the "normal" background radiation are more efficient in removing the ROS than those cultured in a reduced background radiation environment.

7   Conclusions

As in our previous studies, this experiment showed several results which are consistent with the hypothesis that the background radiation induces an adaptive response in living matter. In effect, we observed that V79 cells cultured for long time under reduced background radiation conditions became more sensitive and less protected against ionizing radiation. This can be explained by the loss of the adaptive response gained in the presence of the "normal" background. However, it cannot still be excluded that what we observed is due to the casual selection of mutants with such properties capable to mimic the loss of an adaptive response after 10 months inside the tunnel. Nevertheless, this possibility can be given a very low probability, thanks to the design of the described experiment which involved pairs of cultures, so that it is very unlikely that in both sister cultures mutations have occurred which give the same response changes. In order to give an even more firm support for this conclusion, we are presently exploring performing the following tests:

- to extract the cells grown inside the Gran Sasso Lab and culture them in the external

laboratory, together with those already there, to check if, in the presence of the "normal" background radiation, they will be able to recover the "lost" adaptive response;

- to give the cells grown inside the Gran Sasso Lab an acute priming dose first, "equivalent" to that received by the external culture during the conditioning time and then a challenging dose to see if they show an adaptive response similar to that found in the external culture.

References

[1] Satta L, Augusti-Tocco G, Ceccarelli R, Esposito A, Fiore M, Paggi P, Poggesi I, Ricordy R, Scarsella G, Cundari E. *Low environmental radiation background impairs biological defences of the yeast Saccaromyces cerevisiae to chemical radiomimetic agents.* Mut Res (1995) 347: 129-133

[2] Satta L, Antonelli F, Belli M, Sapora O, Simone G, Sorrentino E, Tabocchini MA, Amicarelli F, Ara C, Ceru' MP, Colafarina S, Conti Devirgiliis L, De Marco A, Balata M, Falgiani A, Nisi S. *Influence of a low background radiation environment on biochemical and biological responses in V79 cells.* Radiat. Environ. Biophysics (2002) 41:217-224

[3] Fenech M. *Cytokinesis-block micronucleus cytome assay.* Nature Protocols (2007) 2:1084-1103

[4] Bortner CD, Oldenburg NB, Cidlowski JA. *The role of DNA fragmentation in apoptosis Trends Cell.* Biol (1995) 5: 21-26

LASEX

An X-ray plasma source driven by a Nd:YAG laser for biological and medical applications.

L. Palladino[a,c], T. Limongi[a,b], G. Gualtieri[b], R. Gimenez De Lorenzo[a] and P. Zuppella[a]

a) Physics Department of L'Aquila University

b) Science and Biomedical Technology Department of L'Aquila University

c) INFN, Laboratorio Nazionale del Gran Sasso, Assergi (AQ)

Abstract

The aim of this experiment (2007 first year of the activity) is the realization of an X ray source. The X-rays are produced by a plasma, obtained focalizing an high power Nd:YAG laser beam on a specific target and the experimental layout is presented.

The measures of the characteristics of a custom Nd:YAG high power laser beam (8 J max @ 1064 nm, 5 nsec pulse duration) and a new disposition of the target-lens system in the interaction chamber are discussed.

The aim of this project is the use of the plasma, resulting by the focalization of the laser beam, it will be used as a soft X-ray source or an electron source instead of the hot filament of the standard mammographic X-ray tubes.

1   Introduction

Different applications of soft X rays ($\approx$ 70 eV – 2 KeV) and of hard X-rays ($\approx$ 3 KeV – 25 KeV) in biological [1], in radiobiological [2] and in medical imaging field [3], have encouraged the development of the X ray sources based on the production of plasma.

In this work, the project and realization of a non-traditional X-ray source with energy ranging from about 70 eV to about 20 - 25 KeV is proposed.

The X-rays emission is due to a plasma obtained focalising an high power Nd:YAG laser beam on different targets (Al, Cu, Y or mylar).

Soft X-rays, 70 eV - 2 KeV, are produced by the dynamic expansion of the plasma, while X-rays in an higher energy region (about 25 KeV) are produced by the accelerated electrons of the plasma in an High Voltage potential incident on a target (Mo, Ti, W) for bremmsthralung effects. So, with this experimental set-up a plasma produced by the focalization of a laser beam can be used independently as a source of electrons or of X-ray photons.

This source is characterized by an instantaneous spectral high brightness, by a punctiform dimension (some tens microns, focal laser spot) and by a pulse temporal structure with the same duration of the laser in the whole spectral region.

A new concept of a plasma source interaction chamber is described; the target is not centered in the vacuum chamber, allowing so a more flexible use of the X ray beam in different applications.

This apparatus is under construction in the X-ray Biophysics Laboratory, Physics Department of Aquila University.

2. Experimental Layout

2.1 Nd –YAG Laser system

In figure 1 the layout of the Nd - YAG high power laser system (by Quanta System) used for plasma production is shown. It is composed by an oscillator (Nd - YAG rod (rod#1 in figure 1)), a pre-amplifier (Nd - Glass rod (rod#2 in figure 1)) and two amplifiers (two Nd - Glass rods (rod#3 and rod#4 in figure 1)). The output energies measured at the end of each rod and the other characteristics of the laser, as the repetition rate, are resumed in table 1. With this configuration the energy laser beam and then the power density (Watt/cm^2) on the target can be modulated. The power density is fundamental to determine the plasma temperature, the X-ray emission and plasma ionization. The photon frequency of the output beam (IR @ 1064 nm) can be doubled (green at 532 nm) by a Second Harmonic Generator (SHG in Figure 1). The laser is protected from back-reflections of the laser beam on the target by a Faraday Isolator (FI in Figure 1).

Table 1 - Nd YAG / Nd Glass characteristic

Laser Part	Energy (@1064 nm)	Energy (@532 nm)	Beam Diam. (cm)	Repetition Rete
Oscillator	240 mJ	18 mJ	7.0 mm	1 pulse/sec
+ pre-Ampl.	1.5 J	380 mJ	9.5 mm	1 pulse/min
+ Ampl # 1	5 J	2 J	15 mm	1 pulse/min
+ Ampl # 2	8 J	4 J	25 mm	1 pulse/min

The laser pulse duration is 5 nsec and the measured divergence is 0.8 – 0.9 mrad about 4 times the diffraction limited. In figures 2a e 2b the pattern and densitometry profile of the laser beam in output of the Ampl 1 (ø 15 mm, 5 J @1064 nm) is shown and in figures 2c e 2d the pattern and densitometry profile of the laser beam in output of the Ampl 2 (ø 25 mm, 8 J @1064 nm) is reported.

Nd:YAG / Nd:Glass optical layout

QWP:	Quarter wave plate at 1064nm
HWP:	Half-wave plate @1064nm
L1:	Cylindric Negative lens f = 0.125 dpt, AR@ 1064nm
L2, L4:	Negative lens f = -190mm, diam 25mm, AR@ 1064nm
L3:	Positive lens f = +250mm, diam 25mm, AR@ 1064nm
L5:	Positive lens f = +300mm, diam 25mm, AR@ 1064nm
L6:	Negative lens f = -225mm, diam 25mm, AR@ 1064nm
L7:	Positive lens f = +250mm, diam 25mm, AR@ 1064nm
FI:	Faraday Isolator
SHG:	Second Harmonic Generator Crystal, KDP type II

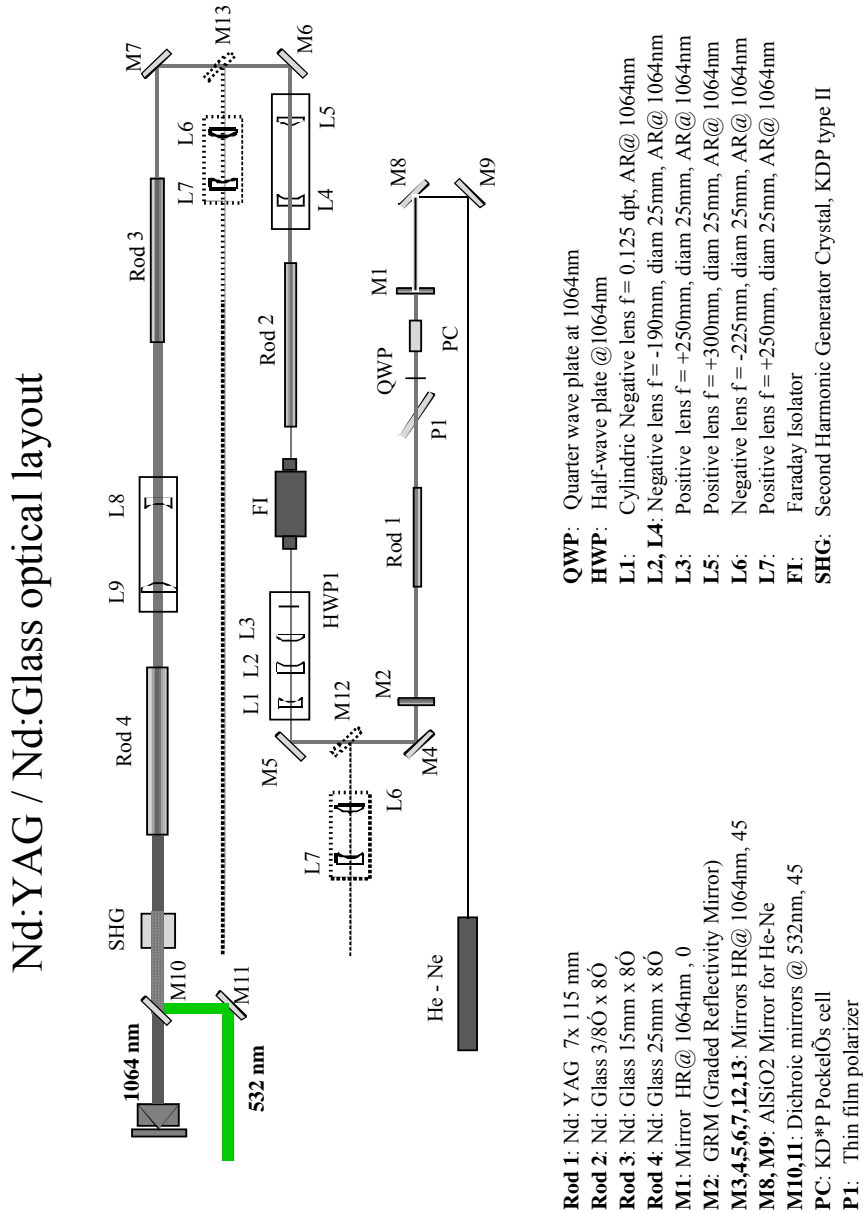|	
Rod 1:	Nd: YAG 7x 115 mm
Rod 2:	Nd: Glass 3/8Ó x 8Ó
Rod 3:	Nd: Glass 15mm x 8Ó
Rod 4:	Nd: Glass 25mm x 8Ó
M1:	Mirror HR@ 1064nm , 0
M2:	GRM (Graded Reflectivity Mirror)
M3,4,5,6,7,12,13:	Mirrors HR@ 1064nm, 45
M8, M9:	AlSiO2 Mirror for He-Ne
M10,11:	Dichroic mirrors @ 532nm, 45
PC:	KD*P PockelÒs cell
P1:	Thin film polarizer

Figure 1 - Nd – YAG/Glass system with the fundamental components described in the legend and reported in the text.

The measures of the dimensions of the focalization spots have been executed using an aspherical triplet lens, 12 cm focal length and 4 cm diameter, for reduce the geometrical aberrations.

The laser beam, at low energy pulses (about 250 mJ at 1064 nm), was focalized on a copper target, the dimension of the spot is about 80 micron, as we can see in the TEM image of the crater shown in figure 3, corresponding at a power density $\approx 10^{12}$ W/cm^2. More accurate measurements of the spot dimension will be executed using a pinhole camera.

2.2   The interaction chamber

In the soft X-ray energy region, the beams are produced by dynamic expansion of the plasma and the relative configuration of the interaction chamber (configuration 1) is shown in figure 4a. The laser beam is focalized by an aspherical triplet lens on a target and the plasma and X-ray photons are emitted in 2π Sr solid angle in opposite direction of the laser beam.

Output AMPL # 1
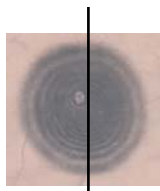
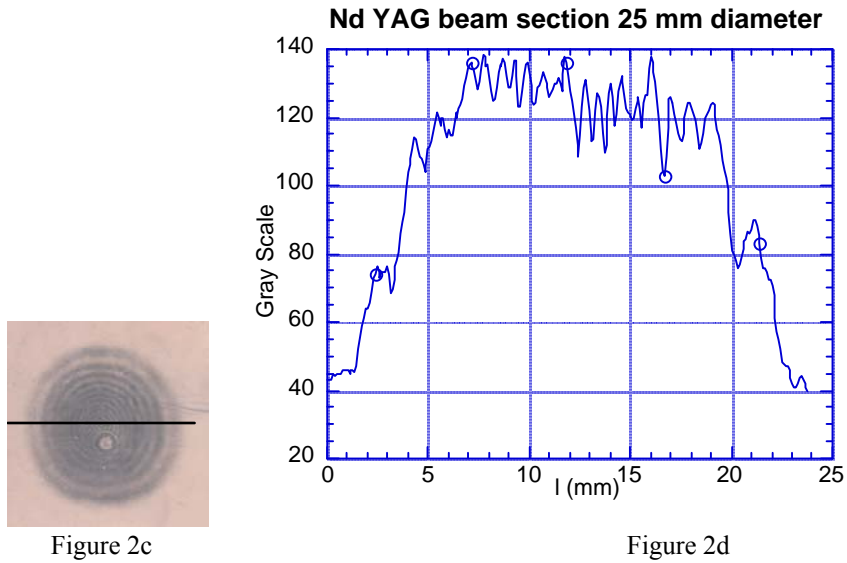Figure 2a   Figure 2b

Output AMP # 2

Nd YAG beam section 25 mm diameter
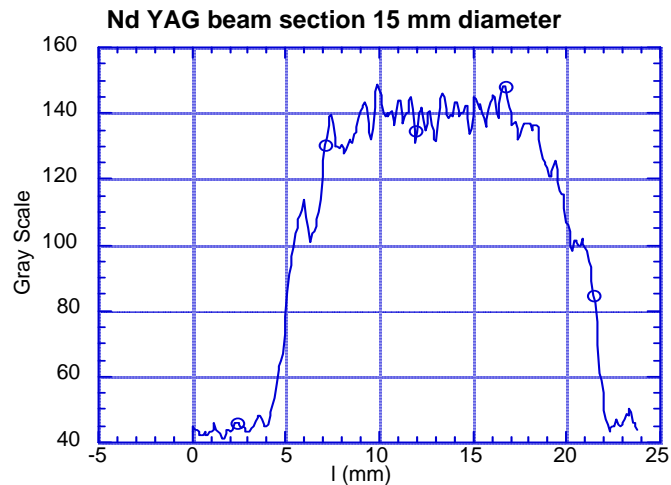
Figure 2c

Figure 2d

Figure 2 – a) the pattern and b) densitometry profile of the laser beam in output of the Ampl # 1 (ø 15 mm, 5 J @1064 nm); c) the pattern and d) densitometry profile of the laser beam in output of the Ampl # 2 (ø 25 mm, 8 J @1064 nm).
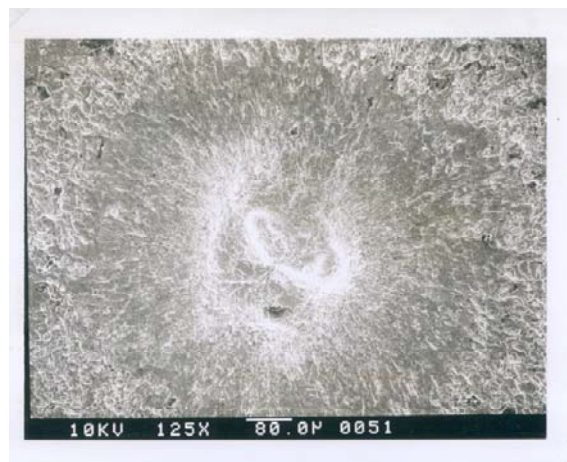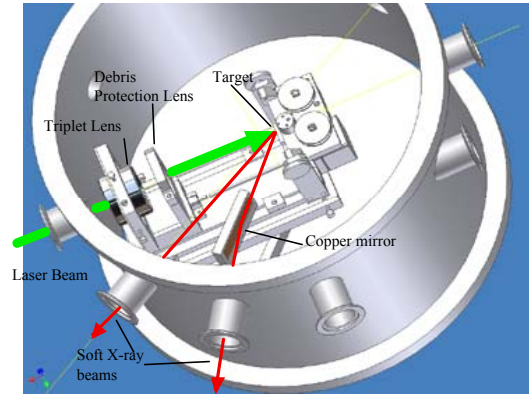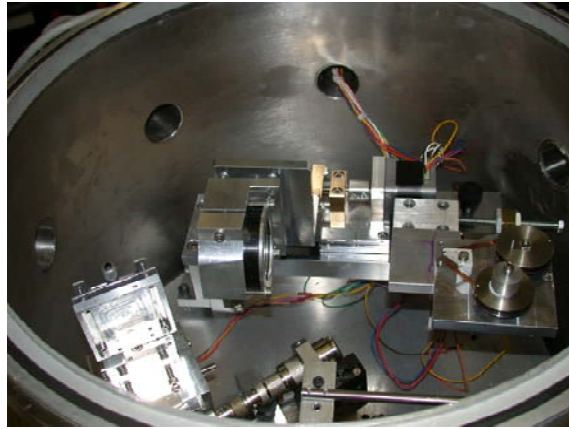

Figure 3 - The TEM image of the crater produced by focaliztion of the laser beam, at low energy pulses (about 250 mJ at 1064 nm), on a copper target. The dimension of the spot is about 80 micron.

Configuration 1

(a

(b

Figure 4 – a) Configuration of the interaction chamber as soft X-ray source (configuration 1). The diameter is 40 cm and can work at p=10^{-3} tor.; b) the mechanical realization

The lens is protected from the debris, produced during the ablation of the target material, by a thin circular glass window.

The position of the lens respect to the target and the renewal of the target, after every ablation, are controlled by computer. It is introduced a new disposition of the target-lens system in the interaction chamber. In particular, it is possible to place the target in different positions respect to the centre of the vacuum chamber. In figure 4b the mechanical realization of the X-ray production system and relative movements of the lens and the target is shown; a mirror or a crystal is used for select the X-ray beams energy intervals. As shown in figure 5, the geometrical relation from φ angle (formed by laser beam direction and X-ray beam direction), θ angle (grazing angle to surface of the mirror or the crystal), l (CS distance in figure 5) and h (CT distance in figure 5) is

$$l = h \sin(\varphi - 2\theta)/\sin(2\theta).$$
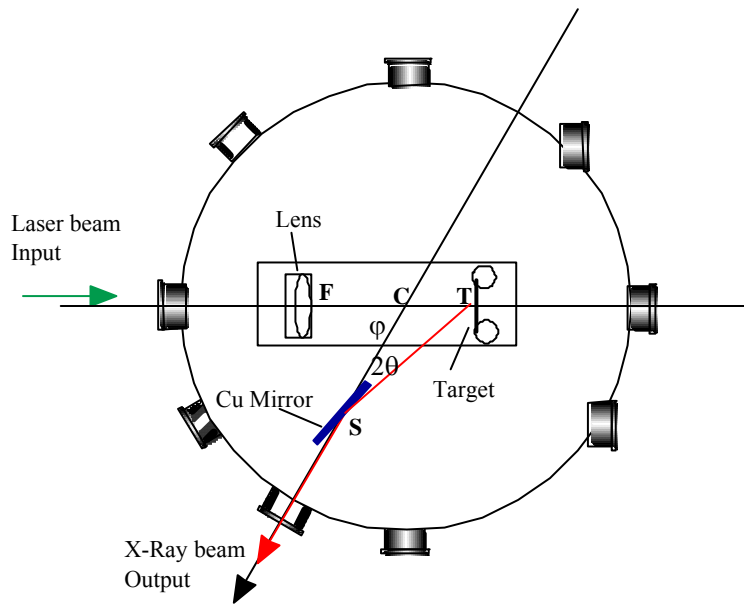
Geometrical relation:

$$l = h \sin(\varphi - 2\theta)/\sin(2\theta).$$

l = CS (distance of the chamber centre – Cu mirror centre)
h = CT (distance of the chamber centre – Target position)

S = Cu mirror centre	φ angle = FCS
C = Chamber centre	θ angle = grazing angle to surface of the Cu mirror
T = Target position	2θ angle = CST

Figure 5 - The geometrical relation from φ angle (formed by laser beam direction and X-ray beam direction), θ angle (grazing angle to surface of the mirror or the crystal), l (CS distance in figure) and h (CT distance in figure) is shown.

The X-rays ranging from $\approx$ 200 eV up to $\approx$ 800 eV are used in several biomedical and X-ray microscopy applications [1]. To select the photons in this energy region a copper mirror at fixed grazing incidence and helium gas at 1 atm are used. In fact, in figure 6a and 6b are shown respectively the copper reflectivity at different grazing angle θ and He transmission (for distance = 0.5 cm and p = 1 atm) [4]. We note that optimal grazing angle for stop the X-ray greater of $\approx$ 900 eV is θ=5 degree and the He absorbs at energy lower of $\approx$ 200 eV realizing a partial monochromatic beam at large band. The X-ray in energy and intensity will be measured by PIN diode solid state detector filtered with microfoils of different

thickness (about 1 micron or sub-microns) and material and by spectrometers based on KAP crystals or mica crystals respectively.
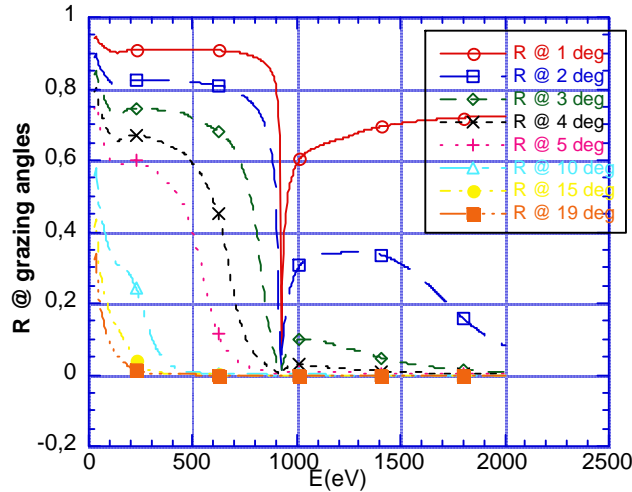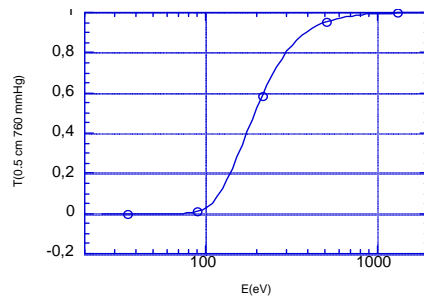

Figure 6a

Figure 6b

Figure 6. (a) The curves of the copper reflectivity at different grazing angles θ. We note that for θ = 5 degree the X-rays with energy greater ≈ 900 eV are absorbed and the reflectivity is about 50%.
(b) The curve of He transmission (for distance = 0.5 cm and p = 1 atm) is shown. We note that the He absorbs at energy lower ≈ 200 eV.

The X-ray of the higher energy region (about 25 KeV) are produced for bremmsthralung effect; the external electrical field is so efficient only for a Debye radius r_D because, as in this case, for long laser pulse duration the plasma reached the Local Thermodynamic Equilibrium (LTE) condition) [5]. While, the non-LTE condition are present only in the first hundreds of picoseconds of the laser pulse duration with plasma density close to solid density [6].

r_D, the characteristic distance at which the plasma screens the external field, is defined as

$$r_D = (kT/ (4\pi\, n\, e^2))^{1/2} = 7.43 \times 10^2\, T^{1/2}\, n^{-1/2}\ cm$$

where T is the plasma temperature in eV and n is the electron density in cm^{-3}. Usually only the electrons localized in the Debye radius are in non equilibrium with the plasma and sensitive to accelerating external fields [7]. Then, the plasma can be considered as an electron source and the current of the electron beam extract from plasma-cathode is, in first approximation, independent from the intensity of the electrical field. So the X-ray energy can be modulate independently from the X-ray intensity. The X-ray energy depends from the High Tension (HT) voltage and the X-ray intensity is related to the plasma conditions such as the plasma temperature and the ionization degree. Referring to the over described experimental set-up, the power density focalized on the target (≈ 80 μm diameter) ranges from $10^{12} - 10^{14}$ W/cm^2 corresponding to laser energy interval from 250 mJ to 8 J (@ 1064 nm) and a plasma temperature of about 100 eV.

The relative configuration of the interaction chamber (configuration 2) is shown in figure 7. Respect to the configuration 1 (figure 4a) the main difference is the application of a HT voltage (30 – 50 KV) from the target on which the laser is focalized (cathode) and the anode (such as metallic materials Mo or W) where are produced X-rays for bremmsthralung effect. A Faraday cup and a Rogowsky loop are used to measure the ionization state of the plasma and the intensity of the electronic current.
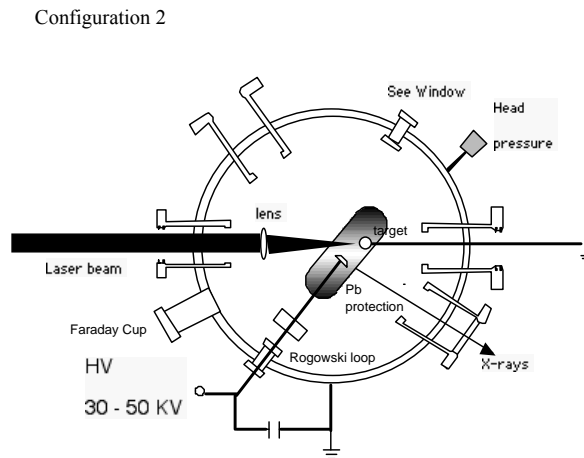
Configuration 2

Figure 7 - Configuration of the interaction chamber as hard X-ray source (configuration 2). The work pressure is p=10^{-7} tor.

3   Conclusion

The characteristics of a Nd–YAG/Glass high power laser and the preliminary power density on a copper target are been measured. The power density is about 10^{12} W/cm^2. More accurate measurements of the focal spot dimensions will be

executed using a pinhole camera. A new mobile disposition of the target-laser system and the mirror/crystal holder put inside of the interaction chamber have been illustrated.

In this project the physical relations from the plasma parameters and the X-ray emission will be studied. An important goal of this apparatus will be the realization of a systems for applications in biomedical field; the possibility of use the plasma as electron source instead of the hot filament in medical X-ray tubes is investigated, in particular, for mammographic imaging.

Acknowledgment

References

[1] T. Limongi, L. Palladino, E. Bernieri, G. Tomassetti, L. Reale, F. Flora, P. Cesare, C. Ercole, P. Aimola and A.M. Ragnelli. *J. Phys. IV France* **2003**, 104, p. 345 – 348.

[2] I.C.E. Turcu, G.J. Tallents, I.N. Ross, A.G. Michette, M.S. Schultz, R.A. Meldrum, C.W. Wharton, D. Batani, M. Martinetti, A. Mauri. *Phys. Med.* Vol. X, N. 3, July-September **1994**, p. 93-99.

[3] P.J. Mallozzi, H.M. Epstein, R.G. Jung, D.C. Applebaum, B.P. Fairand and W.J. Gallagher
Journal of . Applied. Physics 1974, Vol. 45, No. 4, April **1974**, p. 1891-1895.

[4] Calculated from *X-Ray Data Booklet*. Center for X-ray Optics and Advanced Light Source.Compiled and edited by Albert C. Thompson and Douglas Vaughan Lawrence Berkeley National Laboratory - University of California - Berkeley, California 94720 Second edition, January **2001**

[5] F.O'Neill-*Laser Plasma XUV source*-RAL Report, November 1988, RAL-88-101

[6] P. Alaterre, H. Pépin, R. Fabbro and B. Faral

Physical Review A Volume 34, Number 5, November 1986, p. 4184 - 4194.

[7] B. M. Smirnov – Introduction to Plasma Physics – Mir publishers Moscow - 1977

International Conference

L. Palladino, T. Limongi, G. Gualtieri, R. Gimenez De Lorenzo and P. Zuppella
Experimental layout for the realization of an X-ray plasma source driven by a Nd:YAG laser for biological and medical applications.
3th workshop "Plasma Production by laser ablation"(PPLA2007)
14th to 16th June in Scilla, Reggio Calabria, Italy.